



<https://theses.gla.ac.uk/>

Theses Digitisation:

<https://www.gla.ac.uk/myglasgow/research/enlighten/theses/digitisation/>

This is a digitised version of the original print thesis.

Copyright and moral rights for this work are retained by the author

A copy can be downloaded for personal non-commercial research or study, without prior permission or charge

This work cannot be reproduced or quoted extensively from without first obtaining permission in writing from the author

The content must not be changed in any way or sold commercially in any format or medium without the formal permission of the author

When referring to this work, full bibliographic details including the author, title, awarding institution and date of the thesis must be given

Enlighten: Theses

<https://theses.gla.ac.uk/>
research-enlighten@glasgow.ac.uk

MULTIPHOTON RESONANT IONISATION
-APPLICATIONS TO HIGH ENERGY PHYSICS.

Michael Towrie B.Sc.
Department of Physics and Astronomy.
University of Glasgow.

Presented as a thesis for the degree of Doctor of Philosophy
in the University of Glasgow.

February 1987.

ProQuest Number: 10991914

All rights reserved

INFORMATION TO ALL USERS

The quality of this reproduction is dependent upon the quality of the copy submitted.

In the unlikely event that the author did not send a complete manuscript and there are missing pages, these will be noted. Also, if material had to be removed, a note will indicate the deletion.



ProQuest 10991914

Published by ProQuest LLC (2018). Copyright of the Dissertation is held by the Author.

All rights reserved.

This work is protected against unauthorized copying under Title 17, United States Code
Microform Edition © ProQuest LLC.

ProQuest LLC.
789 East Eisenhower Parkway
P.O. Box 1346
Ann Arbor, MI 48106 – 1346

CONTENTS.

CHAPTER 1: INTRODUCTION

1-1: Introduction.	1
1-2: MPI: A historical background.	3
1-3: Theoretical predictions in MPI processes.	5
1-4: Absorption and decay schemes in atoms and molecules.	22
1-5: MPI spectroscopy.	28
1-6: Conclusions.	35

CHAPTER 2: LASER IONISATION, APPLICATIONS TO HIGH ENERGY PHYSICS.

2-1: Introduction.	37
2-2: Ion tracks produced by particles and lasers.	41
2-3: Laser calibration.	48
2-4: Conclusions.	54

CHAPTER 3: APPARATUS.

3-1: Introduction.	55
3-2: The Lasers and optics.	56
3-3: The electronic arrangement.	66
3-4: The Proportional Counters.	68
3-5: Description of seeding and UV spectrometer apparatus.	72
3-6: The Quadrupole Mass Spectrometer.	74

CHAPTER 4: LASER IONISATION WITH DIFFERENT LASERS.

4-1: Introduction.	80
4-2: Results and discussion.	83
4-3: Conclusions.	86

CHAPTER 5: LASER IONISATION IN PROPORTIONAL COUNTERS BY ADDITION OF LOW IONISATION POTENTIAL VAPOURS.

5-1: Introduction.	87
5-2: Results and discussion.	90
5-3: Conclusions.	99

CHAPTER 6: ANALYSIS OF THE BACKGROUND IONISATION IN PROPORTIONAL COUNTERS.

6-1: Introduction.	105
6-2: Wavelength dependence of ionisation between 260nm and 337nm.	106
6-3: Desorption of impurities from counter surfaces.	114
6-4: Investigation of the effect of gas purification on the background laser ionisation in proportional counters.	116
6-5: Conclusions.	117

CHAPTER 7: LASER IONISATION ENHANCEMENT WITH PHENOL, TOLUENE AND OTHER MOLECULES WITH UV RESONANCES AT AROUND 266NM WAVELENGTH.

7-1: Introduction.	119
7-2: Results and discussion.	121
7-3: Conclusions.	128

CHAPTER 8: LASER IONISATION IN A QUADRUPOLE MASS SPECTROMETER.

8-1: Introduction.	133
8-2: Mass analysis.	135
8-3: Conclusions.	142

CHAPTER 9: CONCLUSIONS AND FUTURE.

9-1: Conclusions.	143
9-2: Future.	151

APPENDIX 1: POPULATION RATE EQUATION MODELLING. 160

APPENDIX 2: THE ALEPH TPC. 166

APPENDIX 3: ELECTRONIC ABSORPTION IN BENZENE AND ITS SUBSTITUTES. 172

APPENDIX 4: MPI SPECTROSCOPY OF CAESIUM ATOMS.

A4-1: Introduction.	180
A4-2: Summary of results.	182
A4-3: Conclusions.	187

LIST OF FIGURES.

FIGURE	TITLE	TO FOLLOW PAGE
1-1	Non-resonant N-photon ionisation.	1
1-2	Resonant $N+N'$ -photon ionisation.	1
1-3	Probability factor plotted against ω .	9
1-4	The ionisation dependence of four photon ionisation of potassium.	18
1-5	Angular distribution of photo-electrons for the resonant 2-photon ionisation of sodium atoms.	21
1-6	Potential energy diagram for diatomic molecules.	22
1-7	The Frank-Condon principle.	23
1-8	Autoionisation.	23
1-9	Autoionisation.	23
1-10	Preionisation.	24
1-11	Predissociation.	24
1-12	Dissociation.	25
1-13	Collisional decay.	25
1-14	Molecular absorption and decay processes.	25
1-15	Multi-laser absorption through two intermediate states.	28
1-16	Doppler free absorption.	29
1-17	2-photon ionisation of nitrogen dioxide.	31
1-18	2-photon ionisation of molecules.	31
1-19	The five MPI schemes.	33
2-1	Centroid determination of induced signals on pads.	38
2-2	Energy loss of charged particles.	42
2-3	Ejection energies of δ -electrons.	42
2-4	Range of δ -electrons in argon.	43

2-5	Cutaway view of the TPC 90.	50
2-6	Beam alignment for the TPC 90.	50
3-1	Apparatus for seeding and R2PI experiments.	55
3-2	Four level diagram for the Nd:YAG laser.	56
3-3	Basic layout of the Spectron Nd:YAG laser.	56
3-4	Energy level diagram for the N_2 laser.	57
3-5	Energy level diagram for the XeCl laser.	58
3-6	Unstable Resonator Optics.	58
3-7	Energy level diagram for the dye laser.	59
3-8	Diagram of the EPD Lumonics dye laser.	59
3-9	Diagram of the oscillator cell.	59
3-10	Temporal profile of the Excimer laser.	59
3-11	Dye tuning curves.	61
3-12	Schematic of second harmonic generation.	62
3-13	Ray velocity diagram for KDP crystal.	62
3-14	The variable attenuator.	64
3-15	Electronic arrangement.	66
3-16	Summary of gate generation.	66
3-17	The type 1 counter.	68
3-18	The type 2 counter.	69
3-19	The type 3 counter (caesium counter).	70
3-20	The flow apparatus.	72
3-21	The static fill apparatus.	72
3-22	The UV spectrometer.	72
3-23	The quadrupole filter.	74
3-24	Typical ion trajectories in a quadrupole filter.	74
3-25	Diagram of quadrupole mass spectrometer.	75
3-26	The channeltron SEM.	75
3-27	Electronic apparatus for the mass spectrometer.	75

4-1	Attenuation curve for the Nd:YAG at 1060nm.	82
4-2	Attenuation curve for the Nd:YAG at 530nm.	82
4-3	Attenuation curve for the N ₂ laser.	82
4-4	Attenuation curve for the KrF laser.	82
4-5	Attenuation curve for the AF laser.	82
4-6	Attenuation curve for the XeF laser.	82
4-7	Absorption of UV light in air.	84
4-8	Absorption of UV light in quartz glass.	84
4-9	Ionisation potentials of organic molecules.	84
4-10	Estimated laser fluences required to produce 20IP/cm.	85
5-1	Ionisation versus pressure curve for DMA.	90
5-2	Ionisation versus assumed DMA pressure.	91
5-3	Vapour pressure curve for DMA.	91
5-4	Background and DMA R2PI spectra.	91
5-5	Attenuation curves for DMA at 320nm and 330nm.	92
5-6	Attenuation curves for DMA at 310nm and 266nm.	92
5-7	Vapour pressure curve for DEA.	92
5-8	DEA seeding by the flow method.	93
5-9	Ionisation versus vapour pressure for DEA.	93
5-10	Vapour pressure curve for TMAE.	94
5-11	Vapour pressure curve for TEA.	95
5-12	R2PI spectrum for TEA.	95
5-13	Attenuation curve for TEA.	95
5-14	Effect of TMA on the counter gain.	96
5-15	R2PI spectrum for TMA.	96
5-16	Graph of ionisation versus nominal pressure of TMA.	96
5-17	R2PI spectrum for naphthalene.	97
5-18	Attenuation curve for naphthalene.	97
5-19	Attenuation curve for TMPD.	98

6-1	Wavelength dependence of the background ionisation in a type 1 counter.	106
6-2	Wavelength dependence of the background ionisation in a type 1 counter after cleaning and baking.	106
6-3	Background R2PI spectra between 266nm and 278nm.	107
6-4	Attenuation curve for the background ionisation.	107
6-5	UV spectrum of impurities in cold trap.	110
6-6	Difference between solvent and gas phase UV spectra.	111
6-7	Background R2PI and UV absorption spectra of phenol.	111
6-8	Background ionisation of the type 2 counter.	111
6-9	Background R2PI spectrum between 262nm and 269nm for the type 2 counter.	111
6-10	Background R2PI and UV absorption spectrum of toluene.	112
6-11a	R2PI spectrum of toluene.	112
6-11b	Background R2PI spectra.	112
6-12	Comparison between two R2PI spectra taken 10 hours apart.	112
6-13	Background subtracted R2PI spectrum.	113
6-14	Background R2PI spectrum for the type 3 counter.	113
6-15	Static and Flow mode, R2PI spectra for the type 2 counter.	114
6-16	Effect of heating the counter on the ionisation.	114
6-17	Effect of the gas purification system on the ionisation.	116
7-1	Lutidine UV absorption spectrum.	119
7-2	Vapour pressure curve for phenol.	121
7-3	R2PI spectrum of phenol.	121
7-4	R2PI spectra for a type 2 counter before and after introduction of a length of plastic pipe.	122
7-5	Flushing toluene from a counter.	123
7-6	R2PI of diethyl-phthalate.	124
7-7	Vapour phase UV spectra for Mesitaldehyde.	125
7-8	R3PI spectrum of acetaldehyde.	126

7-9	R2PI and UV spectra of DMA.	129
7-10	R2PI and UV spectra of TEA.	129
7-11	R2PI and UV spectra of TMA.	129
7-12	UV absorption spectra of TMAE.	129
8-1a	Laser induced mass spectrum for TEA.	136
8-1b	Electron bombardment mass spectrum for TEA.	136
8-2	Signal delay time versus mass for the mass spectrometer.	137
8-3	Laser induced mass spectrum for phenol and DMA.	138
8-4	Laser induced mass spectrum for phenol.	138
8-5	Fragmentation pattern of phenol.	141
8-6	Fragmentation pattern of phenol at lower laser fluence.	141
8-7	Fragmentation pattern of toluene.	141
8-8	Fragmentation pattern of toluene at lower laser fluence.	141
9-1	The Time of Flight Mass Spectrometer.	153
9-2	Dependence of sputter yields on primary ion energy.	155
9-3	Variation of sputter yields on different noble gases.	155
9-4a	Collision induced ionisation.	156
9-4b	Field induced ionisation.	156
9-4c	Autoionisation.	156
9-5	The poschenrieder TOF mass spectrometer.	158
9-6	The reflectron TOF mass spectrometer.	158
A1-1	Schematic diagram of $N+N'$ -photon ionisation of molecules.	160
A1-2	PRE model calculation for MPI of typical molecule.	165
A1-3-13	The effects of varying parameters in the PRE equation for R2PI.	165
A2-1	Cutaway view of the ALEPH TPC.	166
A2-2	Pad geometry of the ALEPH TPC.	166

A2-3	Wire plane configuration of the ALEPH TPC.	166
A2-4	Projection of track on wire plane.	167
A2-5	Projection of track on wire plane with $\underline{E \times B}$ effect.	167
A2-6	Projection of track on pad plane.	169
A2-7	ALEPH TPC beam transport system.	170
A3-1	Schematic diagram of the benzene molecule.	172
A3-2	Energy levels of the benzene molecule.	172
4A-1	R2PI spectrum of caesium at a laser fluence of $7.2\mu\text{J}/\text{mm}^2$	182
4A-2	Effect of increasing laser fluence on linewidth.	182
4A-3	R2PI spectrum of caesium at a laser fluence of $0.8\mu\text{J}/\text{mm}^2$	182
4A-4	Laser line broadening effects (laser fluence of $8\mu\text{J}/\text{mm}^2$).	183
4A-5	Laser line broadening effects (laser fluence of ($1.18\text{mJ}/\text{mm}^2$)).	183
4A-6	Laser line broadening effects.	183
4A-7	6s to 8p transitions at a laser fluence of $1.19\mu\text{J}/\text{mm}^2$	183
4A-8	6s to 8p transitions at a laser fluence of $23.8\mu\text{J}/\text{mm}^2$	183
4A-9	6s to 8p transitions at a laser fluence of $7\text{mJ}/\text{mm}^2$	183
4A-10	6s to 9p transitions at a laser fluence of $155\mu\text{J}/\text{mm}^2$	183
4A-11	6s to 9p transitions at a laser fluence of $8.5\text{mJ}/\text{mm}^2$	183
4A-12	R2PI spectrum of caesium at a laser fluence of $1\text{mJ}/\text{mm}^2$	184
4A-13	R2PI spectrum of caesium at a laser fluence of $6.3\text{mJ}/\text{mm}^2$ UV and $18.3\text{mJ}/\text{mm}^2$ fundamental.	185
4A-14	MPI spectrum of caesium at laser fluences of $2.8\text{mJ}/\text{mm}^2$ UV and $12.7\text{mJ}/\text{mm}^2$ fundamental.	185
4A-15	R3PI spectrum of caesium at a laser fluence of $53\text{mJ}/\text{mm}^2$	186

LIST OF TABLES.

TABLE	TITLE	PAGE
4-1:	Laser ionisation produced by a variety of lasers.	82
5-1:	Properties of additives.	102
5-2:	General properties of additives.	103
5-3:	Ionisation of additives.	104
6-1:	Impurities in a counter gas at CERN (Boerner(1985)).	118
7-1:	Summary of additives discussed in Chapter 7.	130
7-2:	Summary of additives studied for laser calibration.	131
7-3:	Ionisation potentials, R2PI and UV cross-sections for seeding compounds.	132

PREFACE.

The work summarised in this thesis was carried out in the Physics and Astronomy department of the University of Glasgow between October 1983 and September 1986.

Multiphoton ionisation of molecules in gases has found a use in High Energy Physics, where laser induced ion tracks have been used to simulate particle tracks in large gas-filled Multi-Wire Proportional Chambers (MWPC's). The simulated tracks are used to calibrate the MWPC's. Laser calibration is to be incorporated into the ALEPH TPC (a type of gas filled MWPC) at CERN. Before laser calibration can be put to full use, some questions must be answered:

- 1) What type of laser would be best for laser calibration purposes?
- 2) Can the ionisation be controlled by adding low ionisation potential molecules to the counter gas, and what additive would be best for the job?
- 3) What are the impurities responsible for the background ionisation observed in many chambers when UV laser light is passed through them?

The experimental work described in this thesis was performed to find answers to these questions.

Chapter 1 contains a brief introduction to the theoretical aspects of multiphoton ionisation. Also, a brief historical review is given, with a summary of some general applications for multiphoton ionisation.

In Chapter 2, with particular reference to the ALEPH TPC, the author provides a review of much of the work carried out in laser calibration to date. Also described in Chapter 2 are the fundamental

differences between the production of ion tracks by high energy particles and by lasers. The type of laser track best suited for calibration purposes is also discussed.

The study of ionisation in proportional counter gas with various lasers was carried out prior to the author joining the RIS Group at Glasgow. The author's interpretation of the results is given in Chapter 4. From the results of these experiments it was thought that the best type of laser for calibration of MWPC's would be one with a short pulse duration ($<10\text{ns}$) in the near UV ($\sim 300\text{nm}$).

Seeding low ionisation potential molecules into chamber gas, as a method for ionisation control, is described in Chapter 5. Some of the molecules have also been studied by other authors, whose results are discussed.

Background ionisation produced by near UV lasers has been observed in many chambers. The ionisation was thought to be caused by the 2-photon ionisation of molecular impurities with low ionisation potentials. Background resonant 2-photon ionisation (R2PI) spectra were produced for a typical chamber gas. Two background impurities, phenol and toluene, were identified by comparison of these spectra with UV absorption spectra. Another author reported the presence of a series of organic compounds in chamber gas. A table of these compounds is given at the end of Chapter 6. Experiments described in Chapter 6 also show that the impurities were outgassing from the walls of the chambers or from plastic flow lines used to carry the chamber gas. Also in Chapter 6 is a summary of the effect of the gas purification system (proposed for the ALEPH TPC) on the background ionisation. This work was carried out by Dr D.T. Stewart, S.L.T. Drysdale and A.P. Land. (They also carried out experiments on the effect of toluene on the purification system. This work is summarised in chapter 7).

Chapter 7 describes experiments where toluene and phenol are used

as seeding agents. Several other molecules with strong UV resonances around 266nm were also studied, as well as Acetaldehyde, a molecule with absorption resonances around 360nm.

Chapter 8 describes attempts to identify further impurities in chamber gas. Samples of impurities trapped from chamber gas were analysed by laser ionisation in a quadrupole mass spectrometer. The low sensitivity of the apparatus meant that no impurities could be detected. Laser induced fragmentation patterns were produced for phenol and toluene. The importance of these spectra is explained in Chapter 9. Gas analysis using the quadrupole mass spectrometer and the interpretation of the R2PI was carried out solely by the author.

Much of the experimental work involving proportional counters was carried out with the help of other members of the RIS Group at Glasgow.

The work carried out allowed answers to be found for the questions posed earlier:

1) The best type of lasers for laser calibration are short pulse duration ($<10\text{ns}$), with a diffraction limited laser beam and single mode output at wavelengths of between 200nm and 340nm (preferably closer to 200nm). The laser should also have a long lifetime and good pulse to pulse reproducibility.

2) Two seeding agents gave promising results. TMA at 100ppm gave 10^4 ion pairs/cm for a laser fluence of $1\mu\text{J}/\text{mm}^2$. Other authors have indicated that at a concentration of 100ppm TMA increased the lifetime of the counter by three fold. Unfortunately TMA has a very unpleasant odour which even at ppb level is unbearable. Toluene on the other hand did not have this problem. At 266nm and with a laser fluence of $1\mu\text{J}/\text{mm}^2$, 6ppm toluene gave ionisation of 10^4 ion pairs/cm. Long term effects of toluene are still to be studied but in the short term it has no effect

on the gain properties of proportional counters or on the purification system proposed for the ALEPH TPC.

3) Two impurities, phenol and toluene, were positively identified. There are strong reasons to believe that further substituted benzene impurities are present in chamber gas.

These conclusions are discussed further in Chapter 9.

Also of interest at Glasgow is the development of a sensitive time of flight mass spectrometer for the analysis of trace elements in bulk samples. Resonant multiphoton ionisation is to be used as an element selective ion source. A description of this work is also given in Chapter 9. Preliminary studies on the resonant ionisation of elemental caesium are described in appendix 3. Caesium is to be analysed by resonant ionisation mass spectroscopy. The author spent some time gathering and interpreting caesium multiphoton spectra.

There are four appendices, the first deals with population rate equations, the second gives a description of the ALEPH TPC, the third is on molecular UV absorption and a fourth is on the multiphoton ionisation of caesium.

PUBLICATIONS

Laser Induced Ionisation in Proportional Counters Seeded with Low Ionisation Potential Vapours.

K.W.D. Ledingham, C. Raine, K.M. Smith, A.M. Campbell, M. Towrie, C. Trager and C.M. Houston.

Nucl. Instr. & Meth. 225 (1984) 319.

Wavelength Dependence of Laser Induced Ionisation in Proportional Counters.

K.W.D. Ledingham, C. Raine, K.M. Smith, M.H.C. Smyth, D.T. Stewart, M. Towrie and C.M. Houston.

Nucl. Instr. & Meth. A241 (1985) 441.

Detection of Phenol in Proportional Counter Gas by Two-photon Ionisation Spectroscopy.

J.W. Cahill, C.M. Houston, K.W.D. Ledingham, C. Raine, K.M. Smith, M.H.C. Smyth, D.T. Stewart and M. Towrie.

CERN - EP/85-198 (December 1985).

Detection of Phenol in Proportional Counter Gas by Two-photon Ionisation Spectroscopy.

M. Towrie, J.W. Cahill, K.W.D. Ledingham, C. Raine, K.M. Smith, M.H.C. Smyth, D.T. Stewart and C.M. Houston.

J. Phys. B: Atomic and Molecular Physics. 19 (1986) 1989.

Detection of Toluene in Proportional Counter Gas by Resonant Two-photon Ionisation Spectroscopy.

S.L.T. Drysdale, C.M. Houston, K.W.D. Ledingham, C. Raine, K.M. Smith, M.H.C. Smyth, D.T. Stewart and M. Towrie.

CERN -EP/86-28 (February 1986).

Detection of Toluene in Proportional Counter Gas by Resonant Two-photon Ionisation Spectroscopy.

S.L.T. Drysdale, K.W.D. Ledingham, C. Raine, K.M. Smith, M.H.C. Smyth, D.T. Stewart, M. Towrie and C.M. Houston.

Nucl. Instr. & Meth. (To be published)

Investigation of the Effect of Gas Purification on the Background Laser Ionisation in Proportional Chambers.

S.L.T. Drysdale, A.P. Land, K.W.D. Ledingham, C. Raine, K.M. Smith, M.H.C. Smyth, D.T. Stewart, M. Towrie and C.M. Houston.

ALEPH 86-30 (distr. TPC-CAL) (1986)

Investigation of the Effect of Toluene on the Gas Purification System Proposed for the ALEPH TPC.

S.L.T. Drysdale, K.W.D. Ledingham, C. Raine, K.M. Smith, M.H.C. Smyth, D.T. Stewart, M. Towrie and C.M. Houston.

(To be published).

Applications of Resonant Ionisation Spectroscopy to Accelerator Based High Energy Physics.

K.W.D. Ledingham, J.W. Cahill, S.L.T. Drysdale, C. Raine, K.M. Smith, M.H.C. Smyth, D.T. Stewart, M. Towrie and C.M. Houston.

"R.I.S. - 86", Swansea (1986) (to be published)

Detection of Cs Atoms by Two-photon Resonance Ionisation Spectroscopy.

K.W.D. Ledingham, C. Raine, K.M. Smith, M.H.C. Smyth, D.T. Stewart, M. Towrie and C.M. Houston.

Proc. SPIE - Int. Soc. Opt. Eng. ("Laser Applications in Chemistry and Biophysics") 620 (1986).

Multiphoton Transitions in Caesium Vapour.

C.M. Houston, S.L.T. Drysdale, K.W.D. Ledingham, C. Raine, K.M. Smith, M.H.C. Smyth, D.T. Stewart and M. Towrie.

"R.I.S. - 86", Swansea (1986) (To be published).

The Potential of Resonant Ionisation Mass Spectroscopy for Detecting Environmentally Important Radioactive Nuclides.

M.H.C. Smyth, S.L.T. Drysdale, R. Jennings, K.W.D. Ledingham, D.T. Stewart, M. Towrie, C.M. Houston, M.S. Baxter and R.D. Scott.

"R.I.S. - 86", Swansea (1986) (To be published).

ACKNOWLEDGEMENTS.

I would like to thank: Dr Kenneth Ledingham, my supervisor, for his help and advice throughout the period of my studies; Christine Houston and Michael Smyth, my fellow research students, for their help in running many of the experiments carried out; Dr D.T. Stewart, Dr K.M. Smith, Dr C. Raine and Mr J. Cahill for helpful discussions and suggestions and for Dr Raine's very considerable assistance in setting up data taking and processing programs and electronics; Professor I. Hughes for his interest and support; T. McCanny and A. Seath for technical support and advice and my thanks also to Anne Campbell and Michael Smyth who kindly proof read much of this thesis.

Finally I would like to thank SERC for their financial support.

CHAPTER 1

SECTION 1-1: INTRODUCTION.

The Multi-Photon Ionisation (MPI) of atoms, or molecules, is a very recent field of research, made possible by the advent of high power lasers.

MPI processes will be defined as the simultaneous absorption of two or more photons of light by an atom or molecule (system). The total additive energy of the photons must be greater than the ionisation potential, E_{ip} , of the system. For example figure 1-1 shows a schematic diagram of a N-photon ionisation process with a monochromatic light source; $N > 2$ and $Nh\nu > E_{ip}$ ($h\nu$ is the energy of a photon). When no resonances occur between the photons and intermediate states of the system, the ionisation is called a N-photon non-resonant MPI process. Figure 1-2 is a schematic for an N-photon resonant MPI process. N_R ($N_R > 1$) photons excite the system into an intermediate real state and a further N_I ($N_I > 1$) photons subsequently ionise the system.

As early as 1931 Gopert-Mayer predicted theoretically the possibility of two-photon absorption. More than 30 years later MPI was actually observed, in the form of a spark, at the focal point of a Ruby laser (Maker et al 1964). Since then, with the increase of laser output powers and a greater selection of available wavelengths, research has expanded into diverse fields, for instance atomic and molecular spectroscopy, mass spectroscopy, isotope separation, laser induced fusion, gas breakdown studies and laser ablation. In fact, wherever high powered lasers interact with matter, MPI processes will occur, and indeed may even become the predominant mechanism at very high powers (Bunkin and Prokhurov 1964).

Figure: 1-1 Non-resonant N-photon ionisation.

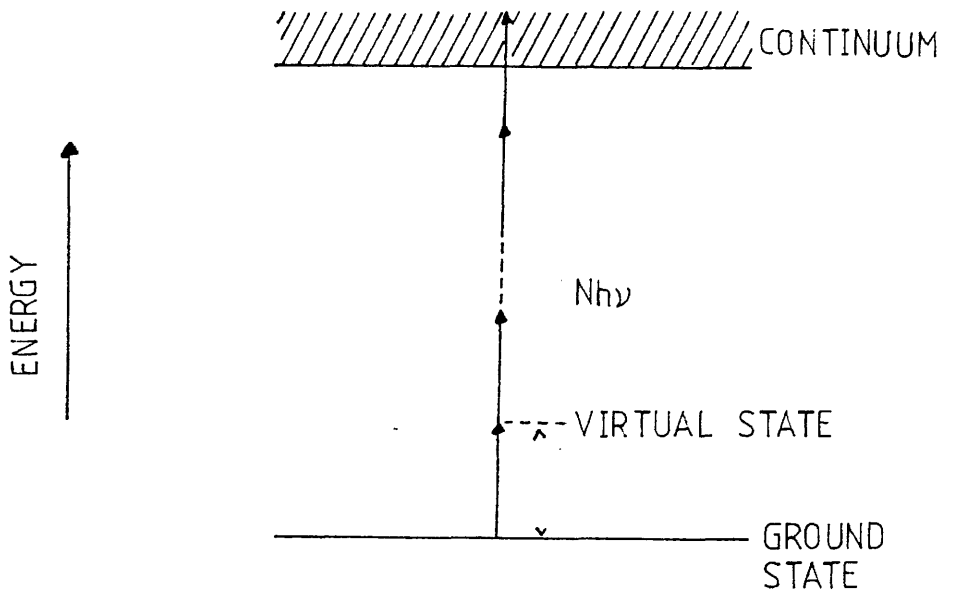
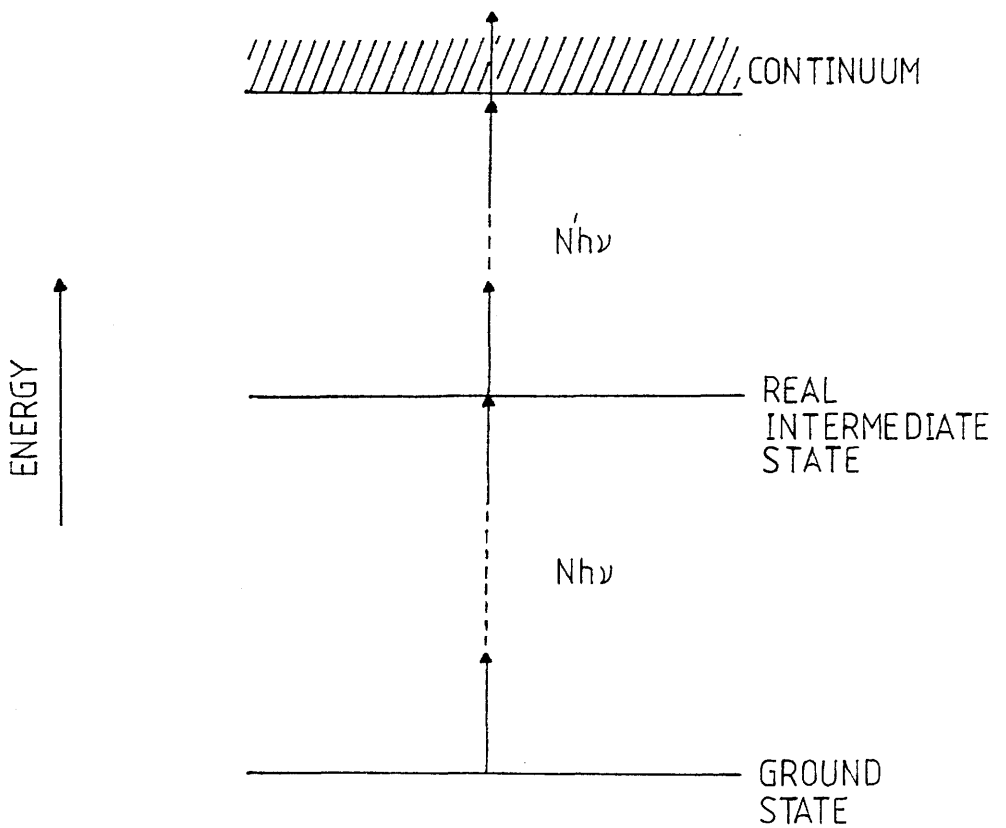


Figure: 1-2 Resonant N+N'-photon ionisation.



Ultra-sensitive detection techniques for counting small numbers of electrons and ions produced by MPI give an alternative method for the analysis of low concentrations of atoms or molecules in bulk samples.

In addition, MPI is fast becoming very important in the field of High Energy Physics (H.E.P.), where laser induced ion tracks are being used to simulate particle tracks in gas filled particle detectors.

There was a need for a greater understanding of the mechanisms involved in, and methods for control of, the ionisation in detector gases. These problems have been studied by the Laser Ionisation Group in the Department of Physics and Astronomy at the University of Glasgow. This thesis reports on some general theory and practice in MPI. Further, in connection with the ALEPH experiment at CERN, a review is given on calibration of gas filled particle detectors with laser induced ion tracks. Results for experiments on laser ionisation control and on the identification of the constituents responsible for the ionisation are given. Finally conclusions are drawn that have some import for MPI studies in general.

SECTION 1-2: MPI-A HISTORICAL BACKGROUND.

The ability to produce multi-photon absorption is a fairly recent development. Not until the advent of high power (high flux) lasers could multi-photon absorption be demonstrated experimentally, although in 1931 Gopert-Mayer predicted the process theoretically.

In 1961 two-photon absorption in quartz was observed by Franken et al. The first MPI was detected by Maker et al in 1964 in the form of a spark at the focal point of a Ruby laser.

MPI of xenon atoms was reported by Voronov and Delone (1966), and also by Agnosti et al in 1968.

Early MPI was restricted mainly to the non-resonant ionisation of noble gases by Ruby lasers but the development of tunable dye laser allowed expansion into the field of resonant MPI. Resonant MPI studies were reported by Bjorkholm and Liao (1974) on metal atoms, Collins et al (1973) on dimers such as Cs_2 and Andreyev et al (1977) on polyatomic molecules such as formaldehyde.

MPI was first demonstrated as a spectroscopic tool in 1975 (Johnson et al (1975)) with work on the NO molecule and by Petty et al (1975) on the I_2 molecule. Detection of Cs_2^+ ions, produced by MPI, in a mass spectrometer was first observed in 1972 (Held et al (1972)) followed in 1976 with work by Grannemann et al on Cs_2 , Rb_2 and RbCs ; Heldman et al (1977) on Na_2 and BaCl and Herrman et al (1977) on metallic clusters, such as K_n and Na_n . Mathur et al (1978) achieved the selective MPI of different isotopes of the Li_2 molecule.

The first resonant MPI of polyatomics was demonstrated in 1977 by Andreyev et al with formaldehyde. Then in conjunction with mass analysis in supersonic cooled jets, the MPI spectra for several organic polyatomic molecules were produced by Johnson (1976), Vaida et al (1978), Parker et al (1976, 1978), Neiman et al (1978), Robin et al

(1978), Berg et al (1978) and Turner et al (1978).

Dissociation of molecules under intense laser light was demonstrated in experiments on the MPI of benzene and transbutadiene in a mass spectrometer (Zandee et al (1978) and Zandee and Bernstein (1979 a,b)). Extensive fragmentation of the molecules was observed. C^+ ions were detected which corresponded to the multi photon absorption of more than 9 photons! (28eV).

From 1980 onwards research into and the study of MPI in atoms and molecules has expanded rapidly. It would be pointless here to review all of this work. Instead a short review and discussion on the theory and modelling of MPI processes shall be given. Then some of the techniques used in MPI studies shall be listed with reference to some authors.

SECTION 1-3: THEORETICAL PREDICTIONS IN MPI PROCESSES.

The application of time dependent quantum theory to MPI has helped explain, at least qualitatively, many of the experimental observations made to date. This section contains a brief description of perturbation theory taken to first order. The theory is used to model single photon absorption in atoms and molecules. The modelling of MPI processes by this method is very much more complicated, but the basic mathematical techniques are the same.

A summary is given on effects predicted by perturbation theory, the primary difficulties in its use as a model for real systems and comparisons of some theory and practice.

PERTURBATION THEORY TAKEN TO FIRST ORDER.

Quantum mechanics uses the wave nature of particles in bound states to study the physical properties of a system as a whole. The wave function $\Psi(t)$ for a particle in a bound state must satisfy the Time-dependent Shrodinger equation:

$$i\hbar \frac{d}{dt} | \Psi(t) \rangle = \hat{H} | \Psi(t) \rangle$$

Where \hat{H} is the Hamiltonian of the system, and is an operator defining the energy of the particle.

Only in a very few simple systems can an exact solution for the wavefunctions be found, although many complicated problems are often 'close' to the exactly solvable problems. Perturbation theory is used as a basis for building mathematical models for more complicated cases. It builds an approximate solution for the complex system by taking the exact solutions as a starting point.

The perturbation method always begins with a Hamiltonian for the problem which is given as the sum of two terms:

$$\hat{H} = \hat{H}_0 + V \quad 2$$

where the unperturbed Hamiltonian \hat{H}_0 is the energy operator for the solvable case. V is a perturbation to the system and must be small relative to \hat{H}_0 .

Time-dependent perturbation theory allows the study of changes in non stationary states with time. Solutions to these problems can lead to information on transitions between states in the presence of a radiative field.

Perturbation theory relies on only a small disturbance to the system. This enables approximations to the solutions by expanding the exact wavefunctions (eigenfunctions) in terms of a 'smallness' parameter, μ . Equation 1 is now written:

$$\hat{H} = \hat{H}_0 + \mu V \quad 3$$

μ is a dimensionless label used to keep track of the terms in the expanded series and can be put to 1 to give back equation 2.

For the completely general case. The unperturbed eigenfunctions Ψ_n^0 satisfy the equation:

$$\hat{H}_0 \Psi_n^0 = i\hbar (\delta \Psi_n^0 / \delta t) \quad 4$$

Ψ_n^0 are written in the form:

$$\Psi_n^0 = \Psi_n e^{-itE_n/\hbar}$$

where the exponential term is the time-dependent factor usually associated with the stationary state functions Ψ_n . Also:

$$\hat{H}_0 \Psi_n = E_n \Psi_n \quad 5$$

where E_n are the energy eigenvalues of the states Ψ_n . To obtain a solution Ψ to equation 1, the expansion theorem is used. Ψ is written in terms of the known unperturbed eigenfunctions Ψ_n^0 which form the basis set for Ψ :

$$\Psi = \sum_n C_n(t) \Psi_n^0 \quad 6$$

$C_n(t)$ are the time-dependent expansion coefficients taking into account the time-dependency of V . Equation 6 can be interpreted as a mixing of all the states in the system where $|C_n(t)|^2$ is the probability of the system being in a state Ψ_n^0 at a time t . Substituting 6 into 1 gives

$$\sum_n C_n (\hat{H}_0 + \mu V) \Psi_n e^{-itE_n/\hbar} = \sum_n (C_n E_n + i\hbar \dot{C}_n) \Psi_n e^{-itE_n/\hbar} \quad 7$$

The first terms on the right and left sides cancel since $\hat{H}_0 \Psi_n = E_n \Psi_n$. Multiplying 7 on both sides by Ψ_n^* (the complex conjugate of Ψ_n) and using:

$$\int \Psi_m^* \Psi_n \delta t = \begin{cases} 0 & m \neq n \\ 1 & m = n \end{cases}$$

gives in ket/bra notation:

$$\mu \sum_m C_m \langle \Psi_n^0 | V | \Psi_m^0 \rangle = i\hbar \dot{C}_n$$

By the usual procedure in perturbation theory, C_m is set as a power series of μ :

$$C_n = C_n^{(0)} + \mu C_n^{(1)} + \mu^2 C_n^{(2)} + \dots \quad 9$$

Substituting 9 into equation 8 and equating coefficients of μ gives:

$$dC_n^{(0)}/dt = 0 \quad 10$$

$$i\hbar (dC_n^{(1)}/dt) = \sum_m C_m^{(0)} \langle \Psi_n^0 | V | \Psi_m^0 \rangle \quad 11$$

$$i\hbar (dC_n^{(2)}/dt) = \sum_m C_m^{(1)} \langle \Psi_n^0 | V | \Psi_m^0 \rangle \quad 12$$

To solve equation 11 the initial conditions of the system are needed.

Suppose that the system is initially in a state k , then

$$C_k^{(0)} = 1 \quad C_m^{(0)} = 0 \quad 13$$

Substituting 13 into 11 gives:

$$C_n^{(1)} = (i\hbar)^{-1} \int_0^t \langle \Psi_n^0 | V | \Psi_m^0 \rangle dt \quad 14$$

$t = 0$ is the point at which the perturbation to the system is 'switched on'.

The perturbation theory is now said to be calculated to first order in μ . For a 'first order' process the quantity $|C_n^{(1)}|^2$ represents the probability of a transition occurring to a state n from the state k of the system in a time T .

A system perturbed by a sinusoidally varying field can be treated by the Harmonic perturbation approximation given below:

$$V(r,t) = V(r) \cos \omega t \quad 15$$

Solving for $C_n^{(1)}$ gives:

$$C_n^{(1)} = \frac{\langle \Psi_n | V(r) | \Psi_k \rangle}{2\hbar} \left[\frac{e^{i(\omega_{nk} - \omega)T} - 1}{\omega_{nk} - \omega} + \frac{e^{i(\omega_{nk} + \omega)T} - 1}{\omega_{nk} + \omega} \right] \quad 16$$

where:

$$\omega_{nk} = (E_n - E_k) / \hbar$$

Therefore when $\omega = \omega_{nk}$ then the transitions shall become appreciable. Suppose $\omega \approx \omega_{nk}$ then the transition probability $|C_n^{(1)}|^2$ can then be written:

$$|C_n^{(1)}|^2 = |\langle \Psi_n | V(r) | \Psi_k \rangle|^2 \frac{\sin^2 1/2 (\omega_{nk} - \omega)T}{\hbar (\omega_{nk} - \omega)^2} \quad 17$$

Figure 1-3 shows the factor:

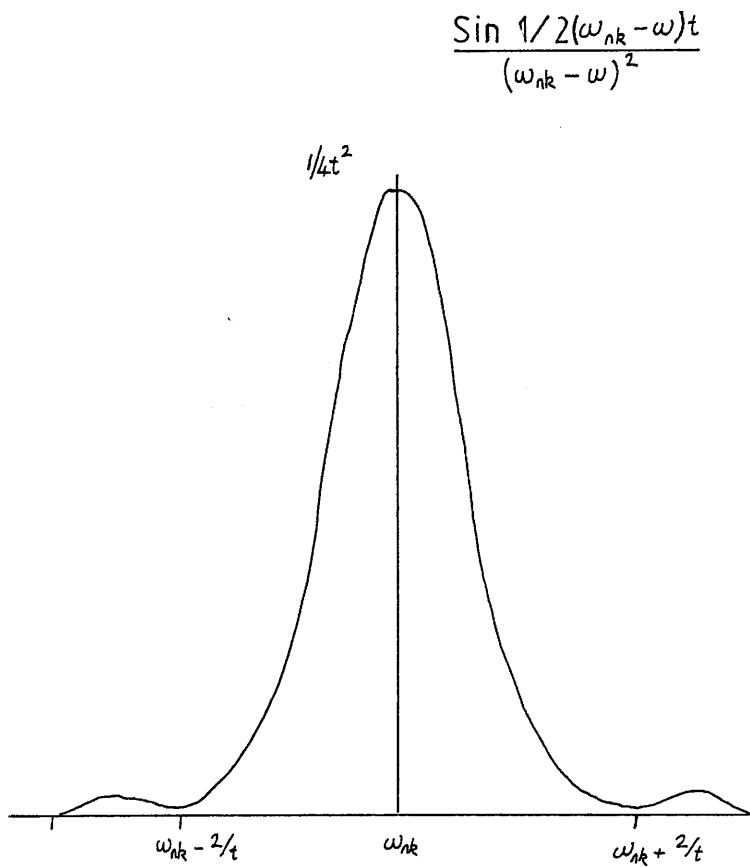
$$\sin^2 1/2 (\omega_{nk} - \omega)T / (\omega_{nk} - \omega)^2$$

plotted as a function of ω . At around $\omega = \omega_{nk}$ a resonance is observed. The FWHM of the peak is equal to $1/T$. The probability of transitions occurring between states n and k are appreciable between $\omega - 1/2T$ and $\omega + 1/2T$. The equivalent energy range can be written $\Delta E \sim \hbar/T$. T is regarded as the duration of the pulse Δt , so:

$$\Delta E \Delta t \sim \hbar$$

This is the energy-time uncertainty relation.

Figure: 1-3 Probability factor plotted against ω .



ABSORPTION OF ELECTROMAGNETIC RADIATION BY ATOMS.

The proper treatment of the absorption of electromagnetic radiation by a system requires quantisation of the radiation field (Heitler (1954); Louisell, (1973) and Sargent et al (1974)). Although good results can be obtained by regarding the field as a classical perturbation.

An electromagnetic wave, like a photon, has an oscillating electric field. Generally the wavelength of the wave is much larger than the size of the system being perturbed (typical values are 200nm and 1nm respectively). Therefore to first approximation the change in the electric field across the system can be neglected. The system then 'sees' an oscillating electric field, described by equation:

$$\underline{E} = \underline{E}_0 \cos \omega t \quad 18$$

E_0 is approximately constant. The energy of interaction between the field and a slow moving electron (when magnetic effects can be neglected) is $-e \cdot \underline{E} \cdot \underline{r}$, where \underline{r} is the position vector for the electron. The interaction can be treated as a harmonic perturbation. Putting $V = -e \cdot \underline{E} \cdot \underline{r}$ into equation 24 gives the transition probability of a transition between states Ψ_g and Ψ_f :

$$|C_n^{(1)}|^2 = e^2 E_n^2 | \langle \Psi_f | \underline{r} | \Psi_g \rangle |^2 \frac{\sin^2 1/2 (\omega_{fg} - \omega)t}{3\hbar (\omega_{fg} - \omega)} \quad 19$$

The factor of 1/3 comes from an averaging over all orientations of the vector \underline{E} corresponding to unpolarised radiation. From equation 19 it can be seen that a resonance will occur when the electric field has a frequency of ω_{fg} , i.e. when the energy difference between the states Ψ_g and Ψ_f equals the energy of the photon.

The energy flux is given by:

$$I = 1/2 \epsilon_0 E^2 c \quad 20$$

But because in most practical applications the wave consists of a range of frequencies, $\Delta\omega$, much broader than the resonant peak depicted in figure 1-3, the total transition probability must be obtained by summing over $\Delta\omega$. The frequencies form a continuum, so the total energy flux is replaced by the energy flux per unit frequency interval, denoted by $I(\omega)$, where $I(\omega)$ is defined as the intensity of the radiation.

Putting these replacements into equation 19 leads to:

$$|C_n^{(1)}|^2 = 2e^2/\epsilon_0 \hbar c \int_{\Delta\omega} \left[I(\omega_{fg}) |\langle \Psi_f | \underline{r} | \Psi_g \rangle|^2 \frac{\sin^2 1/2 (\omega_{fg} - \omega)t}{(\omega_{fg} - \omega)^2} \right] d\omega \quad 21$$

To a good approximation the slowly varying functions in ω can be replaced by their values at ω_{fg} and removed from the integral. The transition probability then becomes

$$|C_n^{(1)}|^2 = 2e^2/2\epsilon_0 \hbar c \left\{ I(\omega_{fg}) |\langle \Psi_f | \underline{r} | \Psi_g \rangle|^2 \int_{\Delta\omega} \frac{\sin^2 1/2 (\omega_{fg} - \omega)t}{(\omega_{fg} - \omega)^2} d\omega \right\} \quad 22$$

The integral is carried out by assuming $\Delta\omega$ extends from $-\infty$ to ∞ . Its solution is then $\pi t/2$. The transition rate, $W = |C_n^{(1)}|^2/t$ can then be written as:

$$W = \pi e^2 I(\omega_{fg}) |\langle \Psi_f | \underline{r} | \Psi_g \rangle|^2 / 3\epsilon_0 \hbar c \quad 23$$

In this approximation equation 23 also applies to the stimulated emission of light from a system.

The perturbation theory described so far gives the probability of a transition occurring between two bound states. In a photoionisation

process the transition is between bound states and a continuum of states above the ionisation potential of the system. The perturbation theory described before will be adapted to model the simplest case.

THE PHOTOELECTRIC EFFECT.

The simplest photoionisation process is a transition between a single bound state and the continuum states of a system. The transition probability for this process is found by summing the transition probabilities for all of the states in the continuum. Instead of calculating just $|C_n^{(i)}|^2$ the sum over all available states must be taken:

$$\sum_n |C_n^{(i)}|^2 \longrightarrow \int_{-\infty}^{+\infty} |C_n^{(i)}|^2 \rho(\omega_{nk}) d\omega_{nk} \tag{24}$$

$\rho(\omega_{nk})$ is the density of the states in the continuum (the number of states per unit frequency interval $d\omega_{nk}$). $|C_n^{(i)}|^2$ is sharply peaked around $\omega_{nk} = \omega$ and generally ρ and $(\Psi_n | V | \Psi_k)$ are slowly varying functions of ω , therefore to a good approximation equation 24 can be simplified to:

$$\begin{aligned} & \langle \Psi_n | V | \Psi_k \rangle \rho(\omega) / 4\hbar^2 \left\{ \frac{\sin^2 1/2 (\omega_{nk} - \omega)t}{[(\omega_{nk} - \omega)/2]^2} d\omega_{nk} \right\} \\ & = \pi |\langle \Psi_n | V | \Psi_k \rangle|^2 \rho(\omega) / 2\hbar^2 \end{aligned} \tag{25}$$

and so the transition rate is:

$$W = \pi |\langle \Psi_n | V | \Psi_k \rangle|^2 \rho(\omega) / 2\hbar^2 \tag{26}$$

This is called Fermi's Golden Rule.

PERTURBATION THEORY IN MPI.

A description of perturbation theory taken to first order has been given. MPI cannot be modelled by first order perturbation theory; the theory must be extended to higher orders in μ . For instance two-photon ionisation processes can be modelled by solving equation 15 to find $C_n^{(2)}$. This calculation was made for the general case by Lin et al (1984). An N order MPI process would require the solution of the perturbation theory taken to N th order in μ .

The following section discusses some results of perturbation theory relating to MPI, and reviews comparisons made between theory and practice.

TRANSITION PROBABILITY OF AN N-PHOTON NON-RESONANT PROCESS.

One of the fundamental problems in the application of quantum mechanics to complex systems is that an exact knowledge of the wavefunctions describing the system can not be obtained. Exact functions can only be obtained for hydrogen like systems. More complex systems must be described by approximations to the true wavefunctions.

Theoretical work by Goldberger and Watson (1964); Messiah (1965) and Bebb and Gold (1966), showed that for N-photon non resonant processes the transition probability per unit time, W_{fg} , for a transition from an initial state g to a final state f (in the ionisation continuum) is given by

$$W_{fg} = \hat{\sigma}_n I^N \quad 27$$

$\hat{\sigma}_n$ is called the generalised cross-section for the ionisation process (in

units of $\text{cm}^{2N} \text{sec}^{-N-1}$). I is the average flux of photons in photons/ cm^2/sec .

A three photon process has a cross-section given in 'Ultra sensitive Laser Spectroscopy' (Kliger D.S.(1983)).

$$\sigma_3 \propto \sum_i \sum_j \frac{\langle \Psi_f | \underline{r} \cdot \underline{e} | \Psi_i \rangle \langle \Psi_i | \underline{r} \cdot \underline{e} | \Psi_i \rangle \langle \Psi_i | \underline{r} \cdot \underline{e} | \Psi_g \rangle}{(E_i - 2h\nu_L - E_g)(E_i - h\nu_K - E_g)}$$

Ψ_g and Ψ_f are the ground and final states, Ψ_i and Ψ_j are the intermediate virtual states. Virtual states are formed due to perturbations in the system which 'mix' all of the real states of the system together and can be represented by:

$$\Psi(\text{virtual}) = \sum_k C_k \Psi_k$$

The C_k represent the relative magnitudes of the contributions from each state. The values $h\nu$ and $\underline{r} \cdot \underline{e}$ in equation 28 are the laser photon energy and the electric dipole term respectively. The factors in the denominator are weighting factors governed by the difference in energy between the real and virtual states.

Typical values for 1,2 and 3-photon ionisation cross-sections for atoms and molecules are 10^{-16} - 10^{-22}cm^2 , 10^{-48} - $10^{-57} \text{cm}^4 \text{sec}$ and $10^{-80} \text{cm}^6 \text{sec}^2$ (Chin and Lambropoulos (1984)).

Conventional light sources have intensities of not much more than 10^{15} photons/ cm^2/sec . At these intensities MPI is highly improbable. To produce significant ionisation for even two-photon ionisation the intensity must be of order $\geq 10^{20}$ photons/ cm^2/sec (Lambropoulos (1976)).

Often, when using pulsed lasers, the total energy of the pulse is quoted. The total energy of the pulse is given by:

$$E = IT \times (2 \times 10^{-16}) \quad \text{J} \qquad 29$$

E is in joules and T is the pulse duration. The total energy of the pulse in terms of photons/cm² is called the fluence of the laser, the fluence is given by:

$$F = IT$$

30

In the time T (the duration of the pulse) the total number of ions produced is found from equation 27 to be:

$$I_{\text{ion}} = \int_0^T \omega_{fg} dt = \omega_{fg} T$$

for a square pulse. Therefore the total ionisation intensity is proportional to the Nth power of fluence, in an N-photon non-resonant process.

The expression for W_{fg} in equation 27 becomes invalid when resonances or near resonances between bound states occur. The perturbation must be adapted to include resonant shifts and line widths of the states.

EFFECTS OF RAPID FLUCTUATIONS IN LASER INTENSITY WITH TIME.

Measurements of the generalised cross-sections for an N-photon process in atoms have been attempted (Chin et al (1969); Held et al (1972a); Bakos et al (1970); Fox et al (1971); Evans and Thonemann (1972) and Grannemann and van der Wiel (1975)). All were found to be greater than the values predicted by perturbation theory. The discrepancy was thought to be the oversimplification of using an average intensity for the calculation of the transition rate. In reality a laser pulse is never homogeneous in time. The fluctuations must be taken into account. For an N-photon non-resonant process the total

ionisation can be given by the following relation

$$I_{\text{ion}}(r,t) \propto \int_V \int_t I^N(r,t) \, d\mathbf{r}^3 \, dt$$

$I(r,t)$ is the intensity as a function of space and time. The integral is taken over the interaction volume V and the duration of the pulse T . For $N=1$ the intensity of the laser can be averaged but for $N>1$ the ionisation produced will be greater than the theory predicts when the average intensity of the pulse is used.

The function can often be split into two parts, a temporal dependence and a spatial dependence:

$$I(r,t) = I(r) \times I(t)$$

Errors in the generalised cross-section can then be calculated under different spatial and temporal conditions. For instance, in an N photon MPI process, a temporal dependence consisting of random gaussian fluctuations (like chaotic non-coherent light) gives a factor of $N!$ greater ionisation than the value estimated by using the average intensity of the pulse.

High powered lasers often have many modes in their outputs and can be considered to approximate chaotic light. Some of the discrepancies between theory and practice may then be attributed to this effect. (strong spatial fluctuations will also lead to discrepancy).

Laser pulses cannot generally be considered completely chaotic or coherent but are somewhere in between. In these cases a model of the spatial and temporal structure of the pulse has to be made. An experiment by Krasinski (1974) demonstrated this effect. Using a continuous laser in single and multi-mode, considered coherent and chaotic respectively, it was found that in a 2-photon process the ratios

of the coherent to chaotic ionisation was somewhere between 1.86 and 1.52. The expected value of 2 was not obtained because a laser can never be perfectly coherent or chaotic. A similar experiment by Lecompte et al (1974,1975) produced 11! times more ionisation between multi-mode and single mode operation of a Nd:YAG laser. They were looking at the 11-photon MPI of xenon.

Temporal effects have also been treated by Brody (1957), Hundley et al (1967) and Carusotto et al (1970).

RESONANT EFFECTS IN MPI.

Resonant effects are common in MPI, especially in large order (large N) MPI processes where transitions into the dense bound states just below the continuum are likely. Resonances in molecules are also quite likely due to dense regions of vibrational and rotational states in the electronic states. Calculations incorporating resonant effects were carried out by Goldberger and Watson (1964), Lambropoulos (1974) and Mower (1966). The calculations led to some interesting results. For example ac Stark effects are predicted, where changes in the laser intensity of near resonance light can pull or push the state into, or further from, resonance.

Stark effects are caused by the influence of the electromagnetic fields, in the laser beam, on the atomic levels of the system (Sobelman (1979)).

Ac Stark effects in MPI were first observed by Abella (1962) using a ruby laser tuned to a 2-photon resonance in caesium. Dye lasers offering large continuous wavelength selectivity and low bandwidths greatly simplified this type of study. Further studies in resonant behaviour have been made by M.Lambropoulos et al (1973) and more recently ac Stark effects were studied by Otis and Johnson (1981).

RESONANT SATURATION EFFECTS.

In the absence of resonances or near resonances the expected ionisation rate behaviour is proportional to the N th power of the laser intensity, in an N order MPI process. For low order MPI processes and fairly low laser powers this type of behaviour has been observed (Delone et al (1972), Held et al (1971, '72a, 72b) and M.Lambropoulos et al (1973)).

The light intensities required to produce appreciable ionisation in a non-resonant N -photon process would tend to saturate a similar, but resonant, N -photon resonant MPI process. Saturation of MPI process is characterised by a drop in the expected laser intensity dependence. Figure 1-4 shows a typical resonant saturation effect. At relatively low laser intensity, off resonance, the expected I^4 dependence for 4-photon non resonant MPI is observed. A slight adjustment in the laser wavelength brought it into three photon resonance with subsequent ionisation by a fourth photon. Then, for considerably lower intensities than for the non-resonant case, an $I^{1.5}$ dependence was observed.

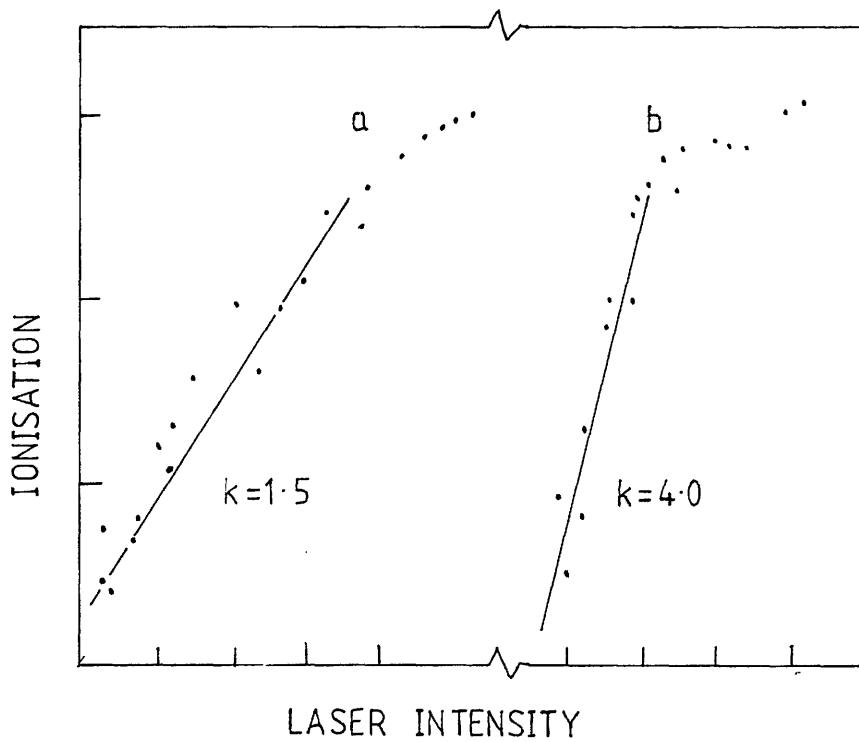
IONISATION RATE DEPENDENCY ON LASER FLUX NEAR RESONANCE.

In a non-resonant N -photon MPI process the ionisation rate is generally proportional to I^N . On resonance this can change to $I^{N'}$ ($N' < N$). Near resonance the intensity dependence can be raised or lowered by ac Stark effects. Stark effects are intensity dependent and can raise or lower the energy levels of wavefunctions of a systems. As a result the resonance can be pulled closer to or further from the perturbing frequency.

A raising of the intensity dependance to I^6 was demonstrated by Held et al (1973). They used a near 3-photon resonance in the 4-photon

Figure: 1-4 The ionisation dependence of four photon ionisation of potassium.

- a) On a 3-photon resonance to the 4f level (Delone et al (1972))
- b) Non-resonant (Delone et al (1972)).



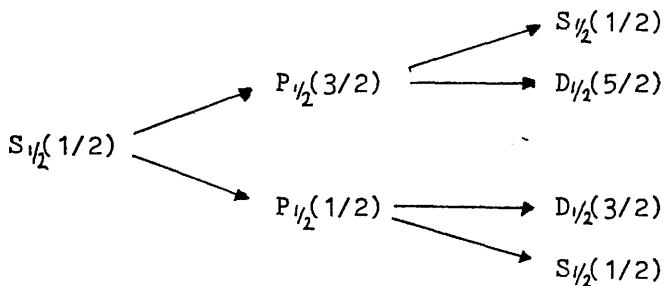
ionisation of caesium.

ANGULAR MOMENTUM AND POLARISATION EFFECTS.

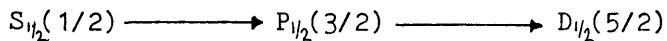
In the interaction of a photon with an electron, in addition to changing its energy, its angular momentum, L , or spin, S , will also change (Sakurai (1967)). A photon of light has an intrinsic angular momentum of 1 (in units of $\frac{h}{2\pi}$). By momentum conservation, the angular momentum of an electron must change by 1 when it absorbs a photon. In an MPI process more than one photon is absorbed, the angular momentum will change by 1 with each successive photon. The sign of the change is dependent on the polarisation of the absorbed light.

A quantitative view of angular momentum changes in MPI processes is given by Sobelmann (1979). For linearly polarised light the selection rules for the absorption of a photon is given by $\Delta J = \pm 1, 0$ (J is the total angular momentum for a system) and $\Delta M = 0$ (M labels the orientations of orbitals in the system). For circularly polarised light $\Delta J = \pm 1, 0$ and $\Delta M = \pm 1$, + for right and - for left circularly polarised light.

Using the hydrogen model, the allowed transition quantum states from an initial state $S_{1/2}(1/2)$ are:



for linearly polarised light and:



for circularly polarised light.

As a result of the different paths available to, and the differences in, the transition strengths of both MPI processes, the overall transition probabilities will be different.

Experiment has shown (Fox et al(1971) and Kogan et al (1971)) that for low order MPI processes in caesium, the transition rates for circularly polarised light are greater than for linearly polarised light. For higher order processes, linearly polarised light will generally yield much higher rates. This is borne out theoretically by Lambropoulos (1972a,b), Gontier and Trahin (1973), Klarsfeld and Maquet (1972, 1974), Reiss (1972), Mizuno (1973), Jacobs (1973), Lambropoulos and Teague (1976) and Teague and Lambropoulos (1976a,b).

The emergence of multi-photon absorption by lasers has been of great benefit to spectroscopists, who can now study previously forbidden transitions in atoms and molecules. For example a $S_{1/2}(1/2)$ to $S_{1/2}(1/2)$ transition, by absorption of a single photon is not allowed, but is 2-photon allowed (as long as the light is linearly polarised).

Appendix 4 summarises some results of the 2 and 3-photon ionisation of caesium. (the work was carried out by the RIS group at Glasgow University and is detailed by Ledingham et al (to be published)).

ANGULAR DISTRIBUTIONS IN ELECTRONS EMITTED IN MPI PROCESSES.

Studies of angular distributions of the electrons emitted in an MPI process have been carried out by Lambropoulos (1972b), Jacobs (1973), Lambropoulos and Berry (1973), Mizuno (1973), Arnous et al (1973) and Gontier et al (1975a,b,c).

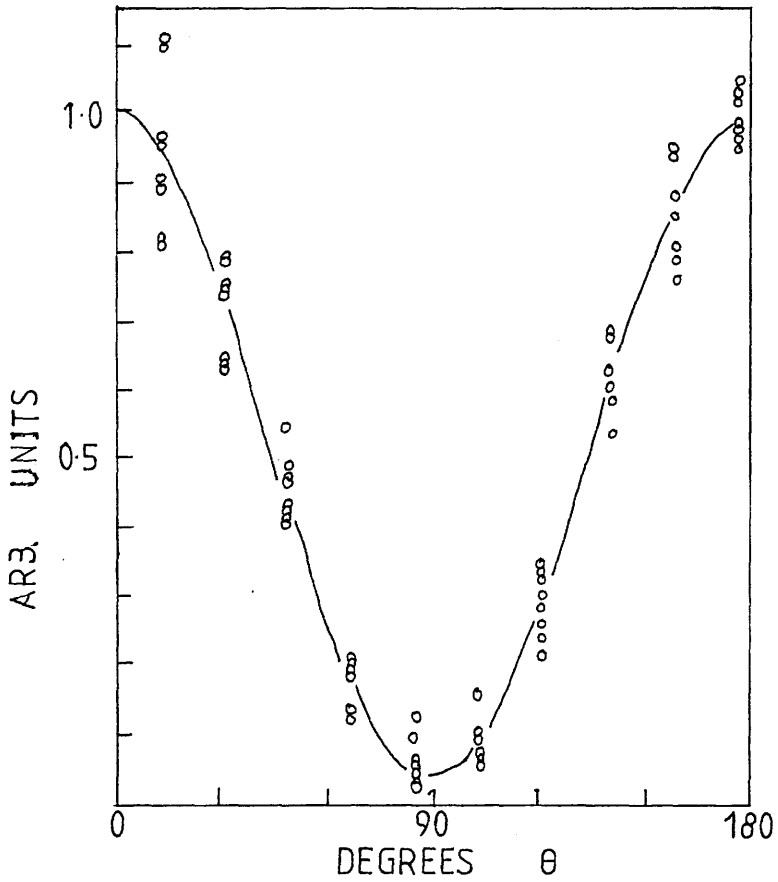
Generally photoelectron angular distributions are dependent on the real bound and continuum state wavefunctions for a system. Study of photoelectron distributions leads to information on the orbital structure of a system (Leuchs and Walther (1984)). For instance photoelectron distributions, from excited intermediate states of atoms, have been studied by MPI.

A typical distribution, obtained by Duncanson et al (1975) is shown on figure 1-5. The results were obtained from the 2-photon resonant ionisation of Sodium via its $3P_{3/2}$ state, using linearly polarised light.

More recently, angular distributions have been studied by Compton et al (1984a,b) and Geltman and Leuchs (1985).

Figure: 1-5 Angular distribution of photo electrons for the resonant 2-photon ionisation of sodium atoms.

Experimental angular distribution of photoelectrons in resonant 2-photon ionisation of sodium atoms via the $3P_{3/2}$ intermediate state. The solid line is a fit to data and is indistinguishable from theory. (Duncanson et al (1975)).



SECTION 1-4: ABSORPTION AND DECAY SCHEMES IN ATOMS AND MOLECULES.

In the previous section, the resonant and non-resonant MPI processes were modelled on the interaction of a monochromatic radiation field with a valence electron of the system. The inner core of orbitals were said to be left undisturbed. The main absorption and decay schemes available to the system were then taken to be stimulated absorption and emission, and spontaneous emission of photons. For some systems, like atoms, a model of this type is often sufficient to explain much of their behaviour. For more complicated systems like polyatomic molecules the model generally breaks down. A reason for this is that polyatomic molecules have many added degrees of freedom resulting in the availability of a range of absorption and decay routes. For instance radiationless transitions between rotational and vibrational levels can greatly effect absorption and decay processes in molecules.

In this section alternative ionisation channels available to atoms and molecules shall be summarised. Absorption processes in molecules are conveniently depicted by energy level diagrams.

Perturbation techniques can yield reasonably good approximations to the energy levels of small molecules (Murrell (1963)). For larger molecules the perturbation treatment becomes too complicated. Instead an analogy is made between the energy levels of diatomic and polyatomic molecules. Diatomic molecules have energy levels dependent on one coordinate, the interatomic distance. Diatomic energy levels can be represented by energy level diagrams very similar to the harmonic oscillator problem (Atkins (1978)) (see figure 1-6). The potential well represents the energy (an electronic level) of a state of the molecule. Vibrational and rotational energy levels are depicted by horizontal lines in the potential well. At energies above E_D , the vibrational and rotational levels are no longer discrete and the internuclear distance

Figure: 1-6 Potential energy diagram for diatomic molecules.

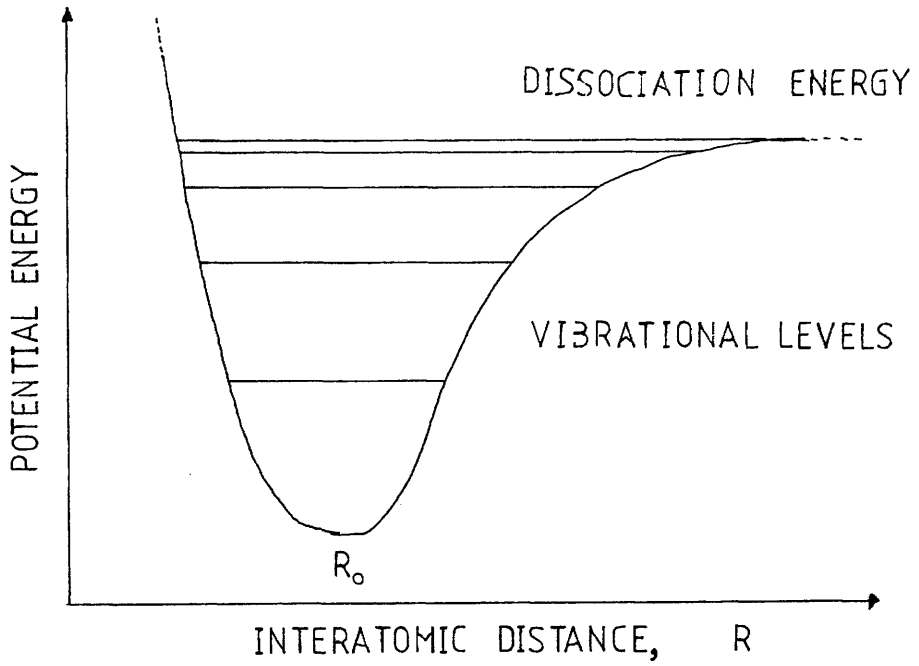
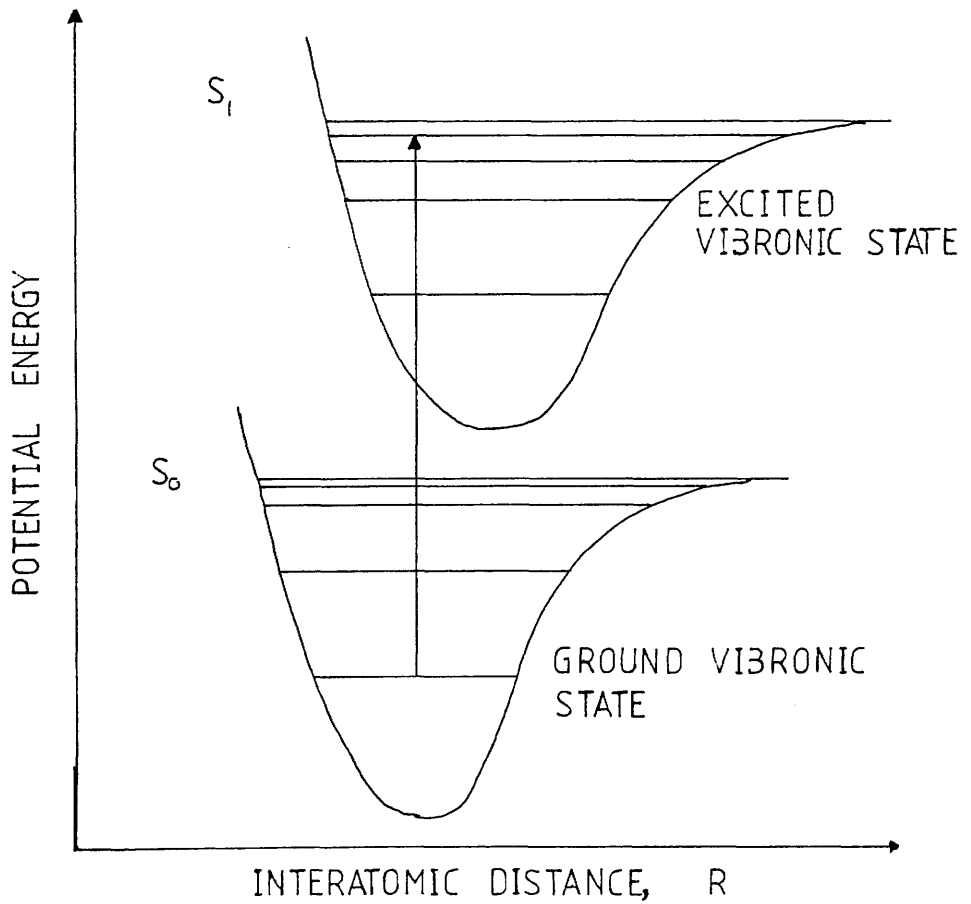


Figure: 1-7 The Frank-Condon principle.



can become infinite. This is equivalent to saying that the molecule has dissociated. E_p is defined as the dissociation energy of the state.

The configuration and therefore the potential energy, of polyatomic molecules, is a function of its many nuclear coordinates. In schematic diagrams depicting the energy levels of polyatomics it is assumed that the configuration of the state is described by only one coordinate along the horizontal axis (in the same way as the diatomic molecule). The electronic states of the molecules are often labelled according to their electronic spin value, S representing a singlet state and T a triplet state.

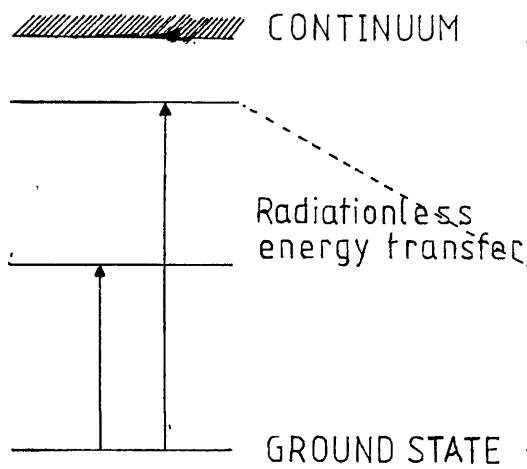
In molecules a transition between states occurs much more rapidly than the rate at which they can change their internuclear configuration. This is called the Franck-Condon principle (Franck (1926) and Condon (1928)) and is used as a basis for the study of transitions in molecular systems. Figure 1-7 demonstrates the principle. A transition is depicted by a vertical line from a lower vibrational level of S_0 to excited vibrational levels of S_1 , which have the same configuration coordinates.

AUTOIONISATION AND PREIONISATION.

With sufficiently high intensity lasers it is possible to excite more than one valence electron from its ground state. Equally it is possible to excite an electron from a state below the valence level of the system. Energetically this type of excited system can be in an overall bound state with an energy greater than the single ionisation potential energy of the system. (see figure 1-8a and 1-9a). If atomic and molecular states were totally discrete with no interactions between them then the system would eventually de-excite by spontaneous emission of two photons. But this is not the case. In many electron/nuclea[^]

Figure: 1-9 Autoionisation.

a



b

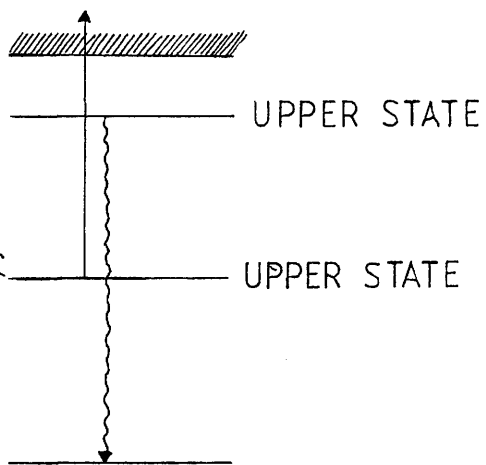
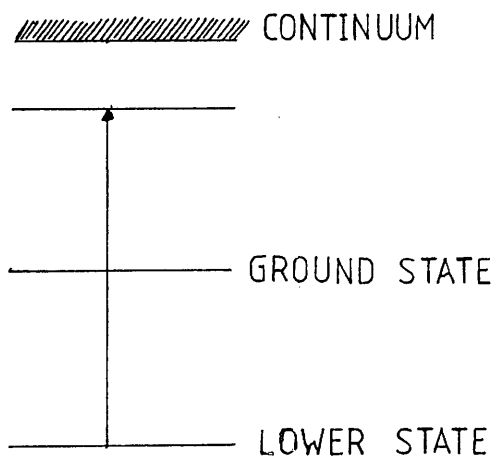
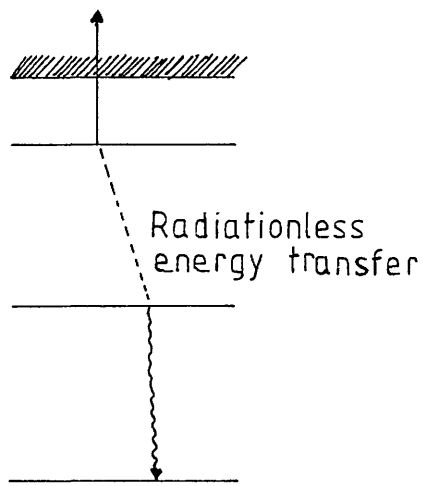


Figure: 1-8 Autoionisation.

a



b



systems, perturbations to an electron occur through interactions with nearby electrons and by nuclear configurational changes (vibrations). The result of the perturbations is a mixing of the states of the system.

A mixing between the excited state and the continuum can lead to a radiationless transition between the states leaving the system ionised. Effectively the process involves an energy transfer between two electrons, without the absorption or emission of a photon, exciting one into the continuum and de-exciting the other to a lower state. A radiationless transition process of this type, that leads to ionisation, is called autoionisation. Figure 1-8b and 1-9b show two types of autoionisation process.

Autoionisation causes apparent resonant structure in the ionisation continuum (Lambropoulos and Zoller (1984), Jungen and Dill (1980) and Tagaki and Nakamura (1981)). Autoionisation also occurs in molecules. If an upper stable state of the molecule lies adjacent to an ionic state then a radiationless transition between them may occur. In molecules this process is called preionisation, it is depicted the energy level diagram in figure 1-10.

PREDISSOCIATION AND DISSOCIATION.

Predissociation of molecules in laser light is similar to autoionisation in atoms. It involves a radiationless transition between states. The molecule will predissociate if a transition occurs between a bound electronic state and a vibrational state above the dissociation energy of a nearby electronic state, or from a bound state to a nearby unstable electronic state. A schematic diagram of both predissociation mechanisms is given in figure 1-11. Predissociation has been studied by Steinfeld and Houston (1978) and Lin and Fujimura (1979).

Dissociation of a molecule occurs when the absorption of light

Figure: 1-10 Preionisation.

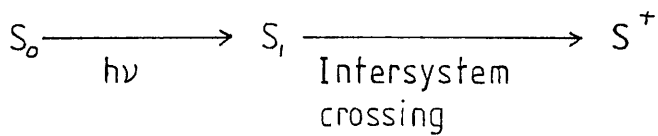
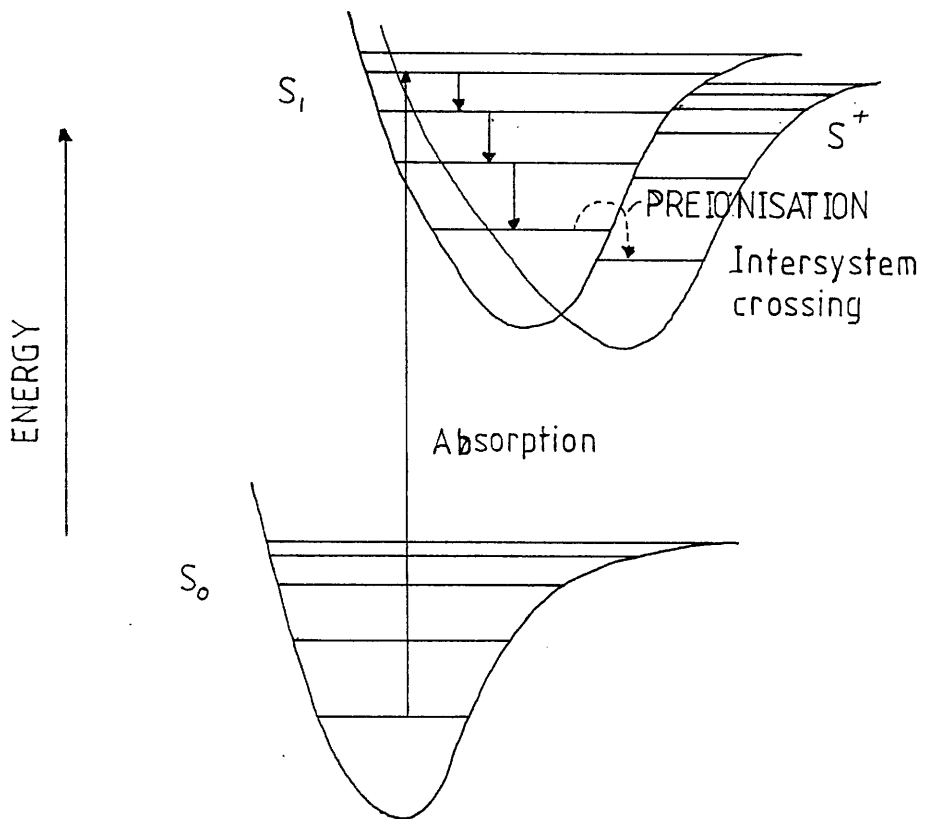
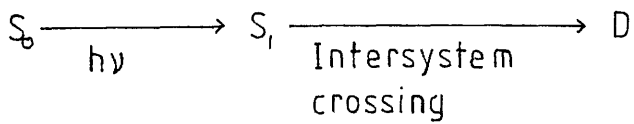
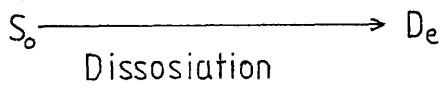
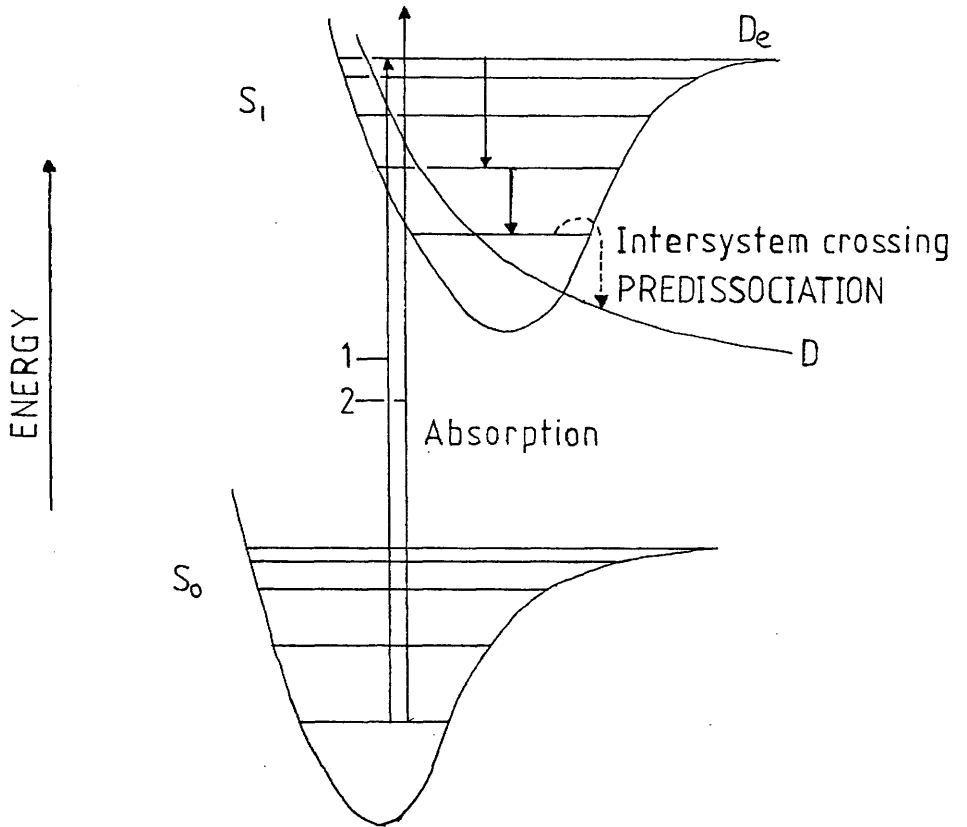


Figure: 1-11 Predissociation.



excites it directly into a vibrational level above E_D of one of its electronic states. A dissociative transition can originate from any electronic bound state of the neutral molecule or from bound ionic states of the molecule (see figure 1-12).

Dissociation (photofragmentation) is generally studied by MPI in a mass spectrometer. A brief review of studies of this type is given in the next section.

COLLISIONAL DECAY.

Molecules in liquids or gases, at close to atmospheric pressure, undergo frequent collisions with surrounding molecules. During collisions molecules can transfer energy to neighbouring atoms or molecules. The energy is derived from, or given to, the molecule by radiationless transfer between its states. (It can also receive translational kinetic energy; this does not change the internal state of the molecule). For a molecule in an excited state a collision can result in a radiationless de-excitation into lower state. Collisional decay is shown schematically on figure 1-13. Collisional processes may also lead to the further excitation of an already excited molecule. This is demonstrated in a paper by Rothberg et al (1981), where atoms in excited states, just below their ionisation potential, were ionised by collisional excitation.

Figure 1-14 shows schematically many of excitation and decay processes in the 4-photon MPI of a molecule. The scheme is applicable to a completely general N-photon process. It includes stimulated absorption and emission, spontaneous emission, fluorescence, phosphorescence, dissociation, predissociation and collisional decay.

Figure: 1-12 Dissociation.

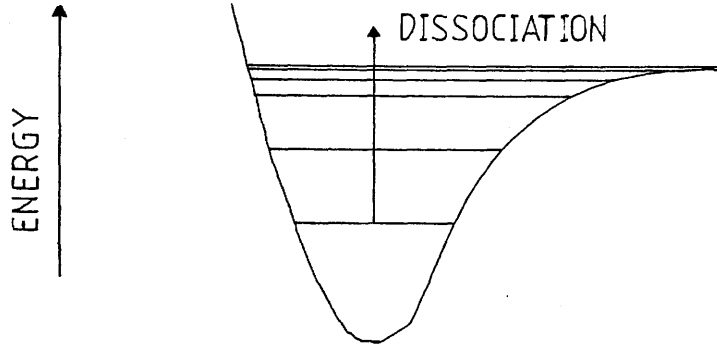


Figure: 1-13 Collisional decay.

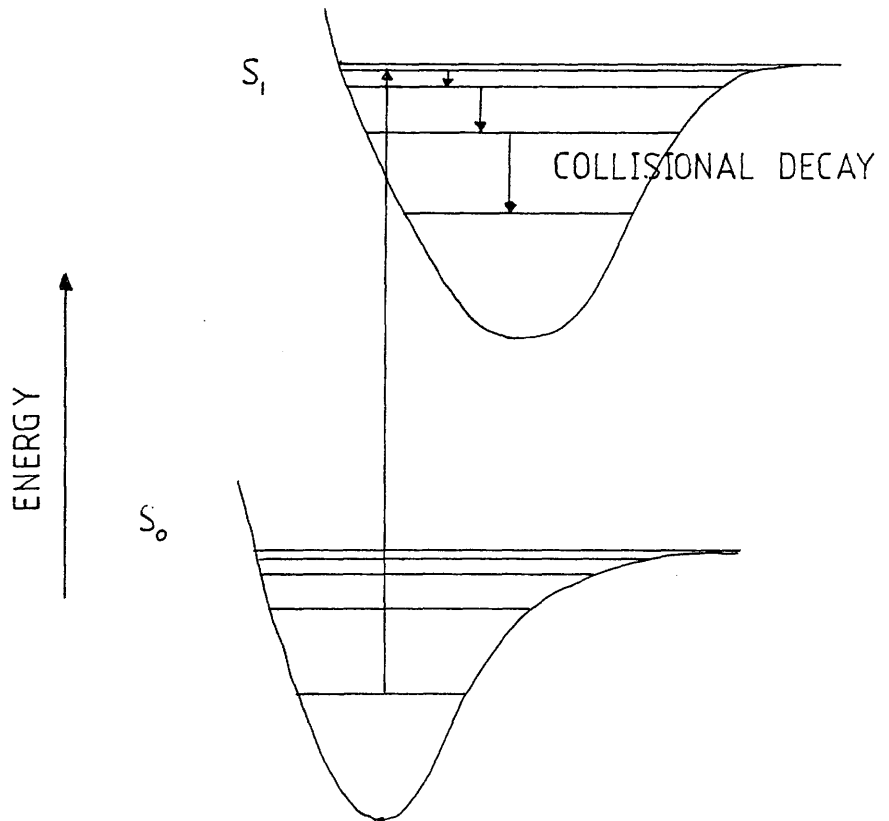
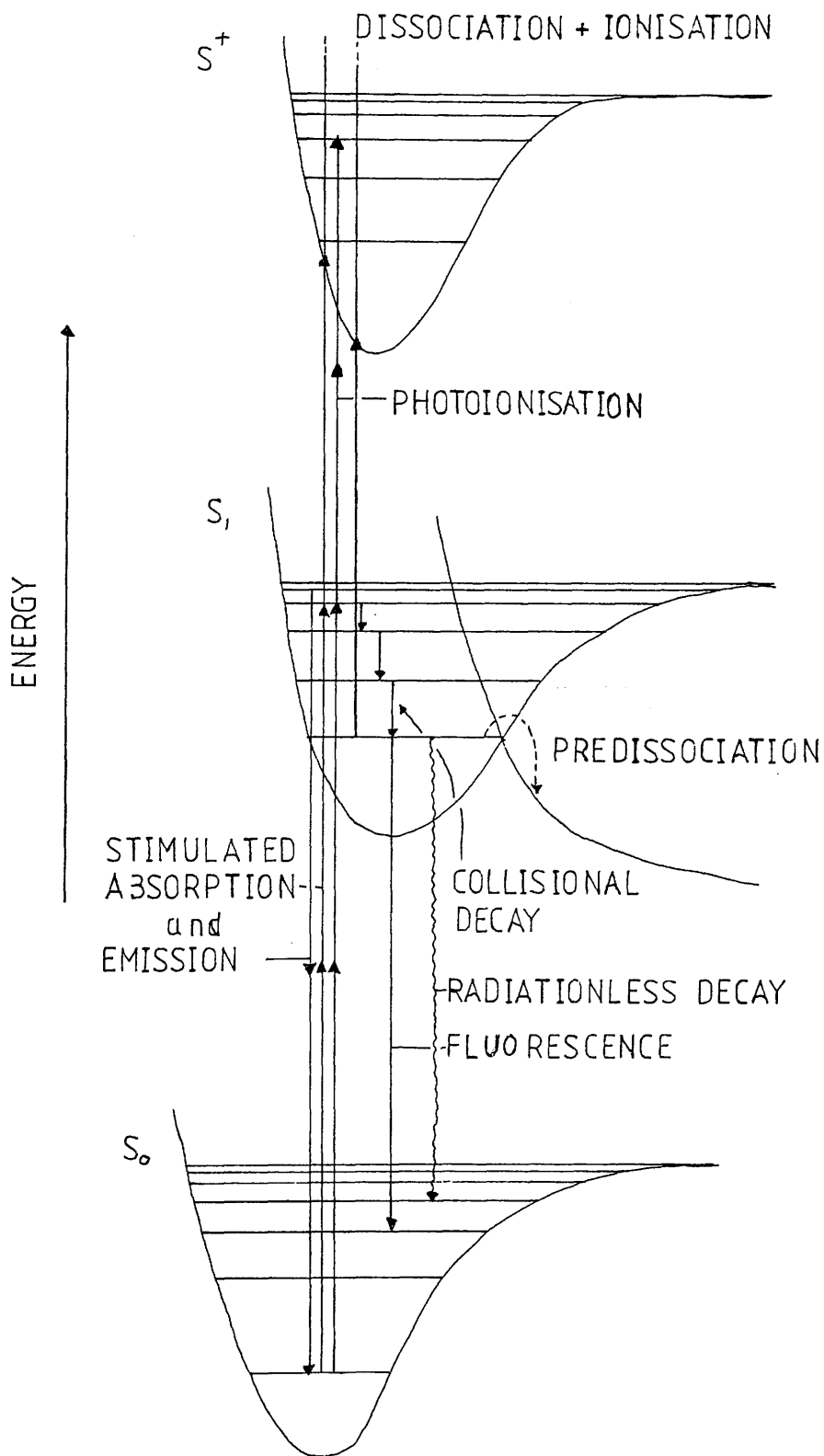


Figure: 1-14 Molecular absorption and decay processes.



COLLISIONAL BROADENING.

Now supposing an isolated excited molecule has a natural excited lifetime τ before spontaneous decay occurs. By the Heisenberg uncertainty principle the energy of the state cannot be measured to better than

$$\Delta E = \hbar / \tau$$

A typical value for τ is 10^{-8} secs, giving a value of 10^{-16} J for ΔE . Collisional decay of molecules leads to a shortening of the states natural lifetime leading to a greater uncertainty in its energy. This effect is called collision broadening.

For a gas medium at STP the collision rate is typically of the order 2×10^{10} secs⁻¹. In each collision the state of the molecule is changed so the lifetime of the excited state is reduced to 5×10^{-11} secs. Corresponding to an uncertainty of $\Delta E = 2 \times 10^{-24}$ J in the energy of the state. In gases collision broadening is generally of the same order of magnitude as processes like Doppler shifting and laser induced line broadening. For molecules in liquids it can become the dominant line broadening effect

LASER INDUCED LINE-BROADENING.

Line broadening effects stem from the need to use high power lasers for MPI. Laser broadening is caused by three effects:

- 1) Saturation effects due to strong laser focussing, increasing as a result the levels of background ionisation.

2) Power broadening effects: At sufficiently high laser powers a system that has been excited into an intermediate resonant level may very rapidly be further excited. The natural lifetime of the state is effectively shortened and, as for collision broadening, the energy of the intermediate state becomes less well defined.

3) Stark effects: The stark effect pulls states into resonance. Effectively this will constitute a broadening of the state.

SECTION 1-5: MPI SPECTROSCOPY.

MPI with wavelength tunable lasers has given greater scope to the field of analytical spectroscopy. For example, many atomic and molecular transitions are found in the deep UV. Monochromatic sources with outputs in this region are rare, but the same transitions can be spanned by multi-photon absorption of light at wavelengths easily obtained with lasers. Below are listed examples of spectroscopic techniques for which MPI is put to use. (MPI of some molecules is reviewed in a paper by Antonov et al (1984)).

SINGLE PHOTON FORBIDDEN STATES STUDIED WITH MPI.

Before the development of high powered tunable lasers, the study of the atomic and molecular energy levels by photon absorption was limited to single photon processes. As a result only transitions with an angular momentum change of $\Delta J = \pm 1$ or 0 could be excited, but in a N-photon absorption process ΔJ can take values up to $\pm N$. Therefore transition into states forbidden by single photon absorption could then be studied (see for example appendix 4).

MULTI-LASER EXPERIMENTS.

A multi-laser experiment involves the use of different laser output wavelengths to excite a system through more than one resonant intermediate level. Figure 1-15 represents a two-colour MPI scheme. Two resonant intermediate states are sequentially excited before a third photon ionises the system.

This method is very useful for the study of intermediate state

Figure: 1-15 Multi-laser absorption through two intermediate states.

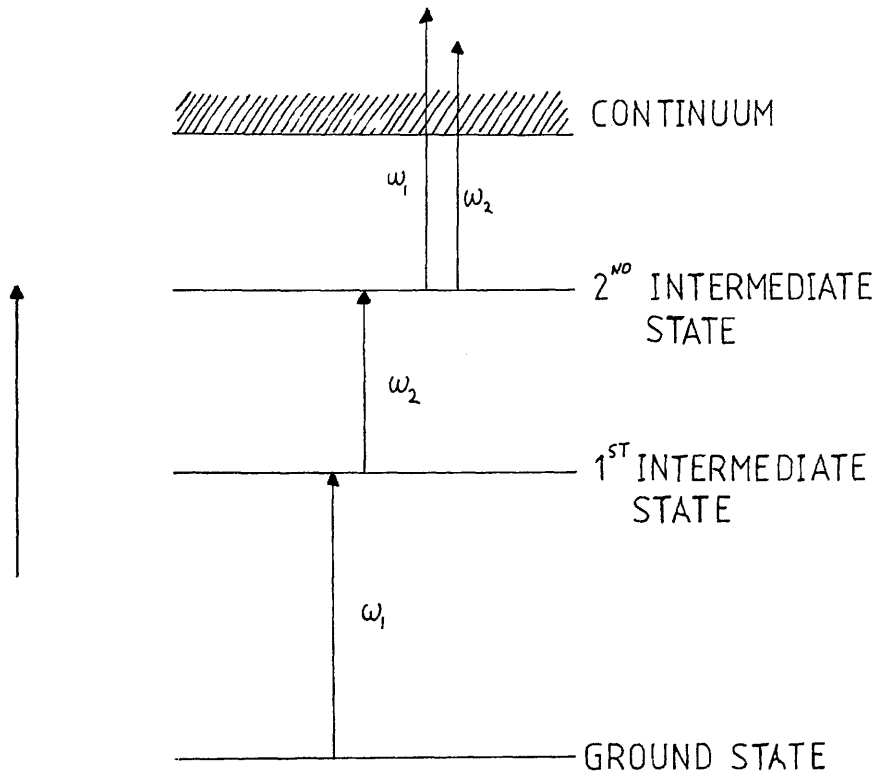
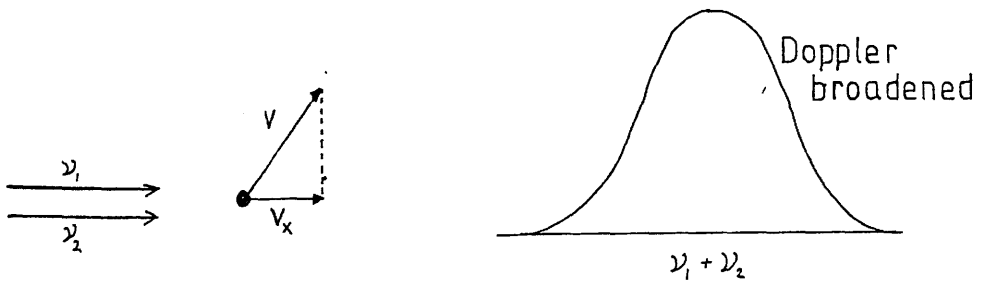
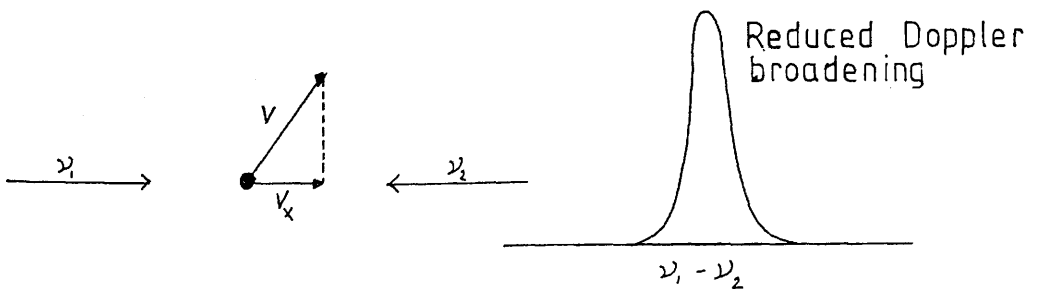


Figure: 1-16 Doppler free absorption.

a)



b)



lifetimes. For the scheme above the intermediate lifetime of the first state would be studied by varying the degree of delay between the first laser and the second. The population of the first intermediate state is then related to the ionisation yield. Work in this field has been carried out by Boesl et al (1980), Glowacki et al (1980), Hopkins et al (1981) and Antonov et al (1978).

By a similar delaying technique the kinetics of photochemical reactions have also been studied. (Baggett (1985))

DOPPLER FREE SPECTROSCOPY.

MPI offers an alternative to conventional forms of Doppler free analysis. Previous to MPI, Doppler free spectroscopy was generally carried out in molecular beams. This involved the cooling of samples by adiabatic expansion of a carrier gas doped with the sample to be analysed. Analysis was limited by the low densities of sample in molecular beams. Using MPI techniques, Doppler free spectroscopy can be carried out with samples at room temperature and pressure in any concentration.

Figure 1-16 gives a schematic representation of a MPI Doppler free process. Figure 1-16a shows the effective Doppler broadening due to a system travelling at a velocity v_x in the direction of the beam. The shift in frequency is given by:

$$\Delta\nu = (\nu_1 + \nu_2) v_x / c \quad 33$$

ν_1 and ν_2 are the frequencies of the absorbed photons. For two laser pulses travelling in opposition, the Doppler shift equation would be written as:

$$\Delta\nu = (\nu_1 - \nu_2) v_x / c \quad 34$$

When $\nu_1 = \nu_2$ then Doppler effects are eliminated. For an example of Doppler free MPI refer to Sansonetti and Lorenzen (1984).

RESONANT 2-PHOTON IONISATION.

The simplest MPI process involves the absorption of a single photon of light into a resonant intermediate state, with subsequent ionisation by a second photon of the same wavelength. Experimentally, resonant two photon ionisation (R2PI) often proves more attractive than resonance enhanced MPI (REMPI). This is mainly because intensity required to produce R2PI is considerably less than for REMPI, since REMPI, unlike R2PI, must undergo transitions through virtual states. Often strong focussing of the laser light is necessary to produce REMPI. Focussing produces a very small interaction volume, and so for low density samples very small ion counts may result. Also intensity variations and saturation effects in focussed beams can make quantitative analysis of atoms and molecules by REMPI very difficult. R2PI on the other hand often needs no focussing at all, allowing greater interaction volumes and well defined beam profiles for quantitative analysis.

Many molecules have ionisation potentials of around 10eV, therefore UV lasers are generally required for molecular R2PI. A second requirement is that the intermediate state of the system has an energy of greater than half of its ionisation potential.

The first step in a R2PI process is precisely that of a single photon absorption process. R2PI along with an ion or electron detection system can prove a very much more sensitive alternative to absorption and fluorescence techniques, especially if sample concentrations are very low or fluorescence and absorption efficiencies are very poor. The reason for this is that ion/electron collection efficiencies can

approach 100% but photon collection is only about 5% efficient.

Since the first step in the R2PI process is the same as a one photon absorption process, it would be reasonable to suppose that R2PI spectra and one photon electronic absorption spectra would look similar. For this to be the case three conditions would have to be met.

1) Saturation of the first step must be avoided since this would tend to flatten out resonant structure.

2) The cross-section of the intermediate to continuum state transition should be wavelength independent over the region of interest.

3) The intermediate state should not decay faster to lower levels than the transition rate into the continuum.

Antonov et al (1977) produced an R2PI spectrum for nitrogen dioxide. Resonances at visible wavelengths were first excited and subsequently ionised by the 7.7eV output of a hydrogen laser. The nitrogen dioxide ionisation potential was exceeded by 0.8eV in this scheme. Figure 1-17 shows the R2PI and electronic absorption spectra for nitrogen dioxide. At least to first order they resemble one another. The same characteristic was observed for toluene (Murakami et al (1981)) and aniline (Brophy and Rettner (1979)).

Molecular systems are free to undergo vibrational and vibronic transitions. Figure 1-18 shows three simple mechanisms for 2-photon ionisation of molecules:

A. Is 2-photon ionisation through excited vibrational states of the molecule in its ground, S_0 , electronic state.

Figure: 1-17 2-photon ionisation of nitrogen dioxide.

Antonov et al (1977).

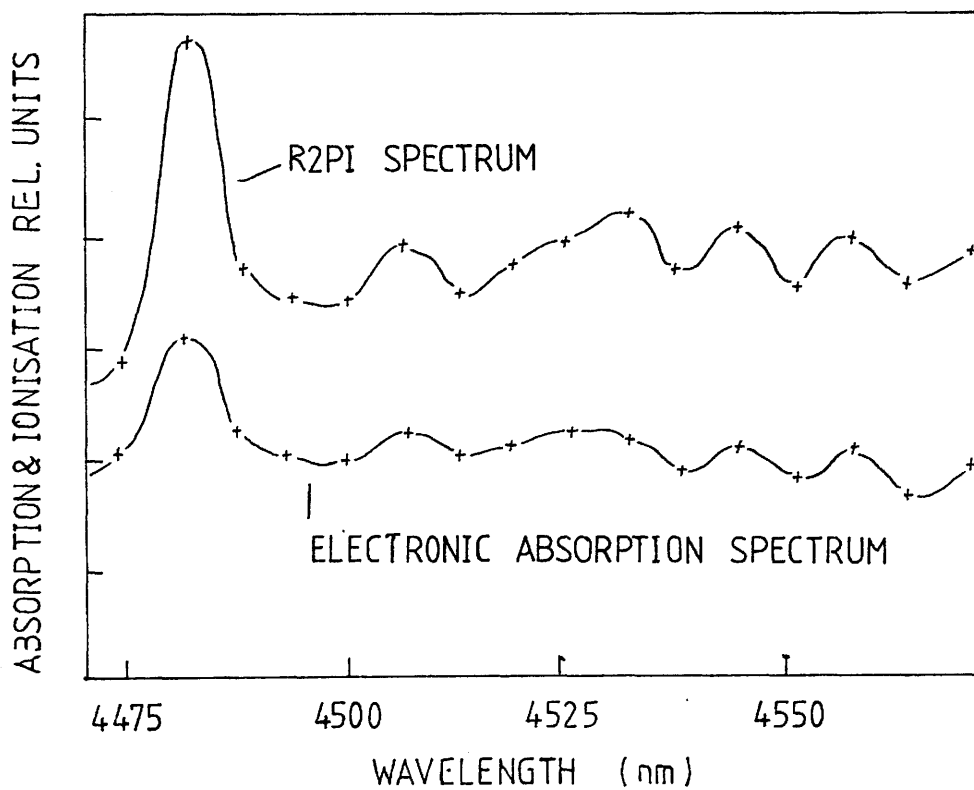
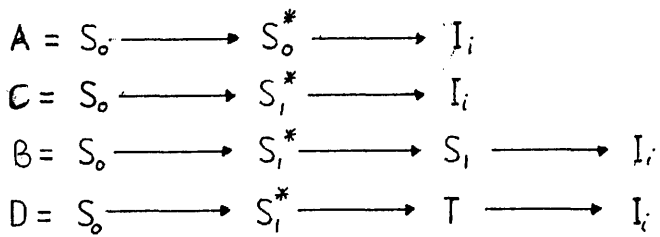
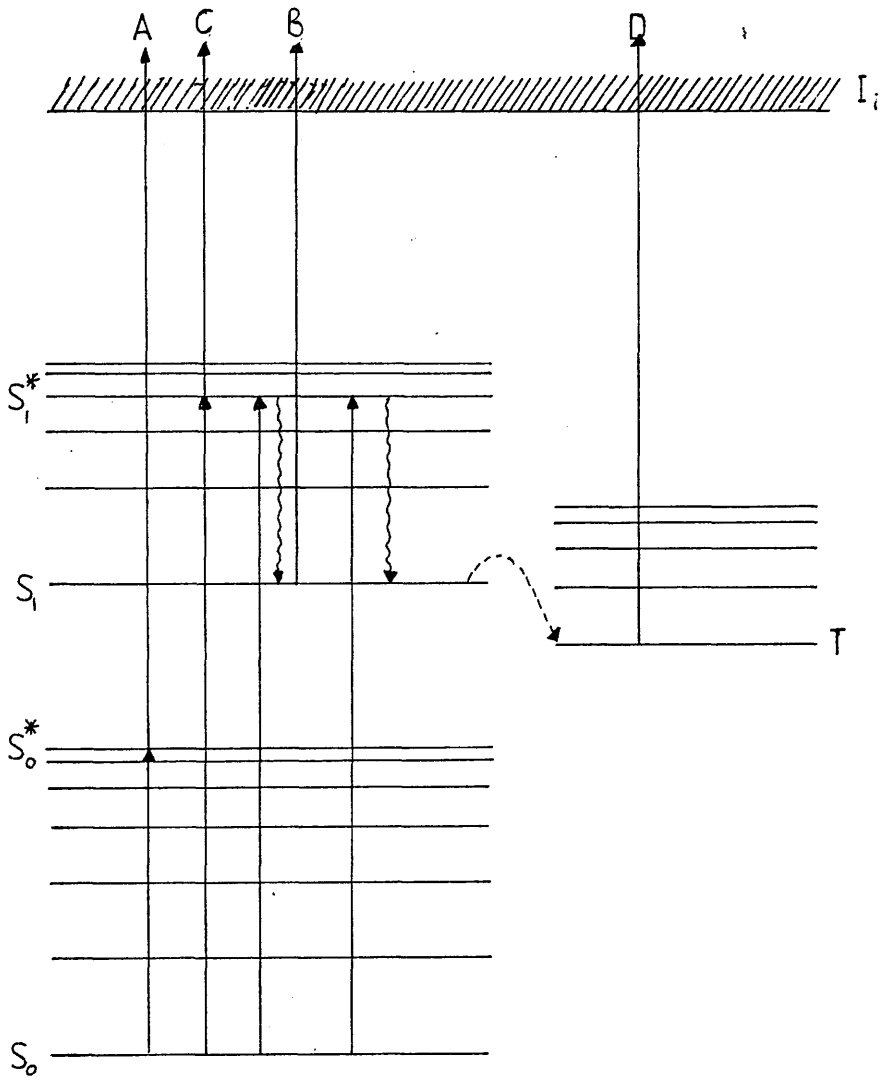


Figure: 1-18 2-photon ionisation of molecules.



B. The first photon excites the molecule into excited vibrational states of the first intermediate electronic level. The molecule then relaxes to the ground vibrational state before subsequent ionisation by a second photon.

C. This is direct ionisation through an excited vibronic level.

D. This process involves a radiationless transition between the S state and a neighbouring triplet, T, state.

Typical excited state lifetimes are 10^{-10} - 10^{-12} secs for vibrational levels, and 10^{-8} secs for electronic levels (Collisional processes may shorten these lifetimes). Ionisation by schemes B and D are much more likely than schemes A and C because the intermediate level is much longer lived than the vibrationally excited states.

Absorption coefficients for molecules are commonly given by the molar extinction coefficients, ϵ_{ν} ; the cross-section in cm^2 is:

$$\sigma_e = 3.8 \times 10^{-21} \epsilon_{\nu}$$

The lifetimes of the states are given by:

$$\tau \approx (0.5 - 1.0) \times 10^{-14} \epsilon_m^{-1}$$

ϵ_m is the extinction coefficient at the maximum of the band considered.

Typical values for molecular cross-sections are $\sigma = 5 \times 10^{-19} \text{cm}^2$.

In appendix 1, a population rate equation (PRE) model is used to describe a two photon ionisation process with monochromatic light. Boesl et al (1981), using a similar model, obtained ionisation cross-sectional data for benzene, thiophene, naphthalene, toluene and aniline.

MPI MASS SPECTROMETRY.

Mass spectrometers offer mass selectivity in a sample of ions produced by MPI and also they can detect very low ion yields. These properties have made them very attractive for the study of photofragmentation processes in molecules and for the analysis of samples by resonant or non resonant MPI combined with mass separation.

Most MPI mass spectrometry is carried out using time of flight systems (TOF). These allow complete mass spectra to be recorded on a pulse to pulse basis, making data collection very efficient.

Other types of mass spectrometer are used, such as singly focussed magnetic and quadrupole mass spectrometers (Agnosti et al (1971), Zacharius et al (1981) and Reilly et al (1980)).

Mass spectrometers have been used to study multilaser experiments, fragmentation patterns in molecules, intensity effects, photoelectron spectroscopy and van der Waals effects in low temperature molecular beams. A review of work carried out with mass spectrometers has been given by Gobeli et al (1985), summarising experiments on molecular systems and metallic clusters in molecular beams.

ISOTOPIC MASS ANALYSIS

All atomic species in the periodic table can be resonantly ionised by multi-photon absorption of laser light. All, except helium and neon, can be ionised by one of five laser ionisation schemes proposed by Hurst et al (1979). Figure 1-19 shows the five MPI schemes.

SCHEME 1

This involves the absorption of two monochromatic photons through a resonant intermediate state.

SCHEME 2

Scheme 2 is the resonant absorption of a frequency doubled photon with subsequent ionisation by a photon of the fundamental light.

SCHEME 3

This is a two-laser scheme, involving resonant absorption between three levels with ionisation by the absorption of a further photon from one or other of the lasers.

SCHEME 4

Scheme 4 is another three-photon scheme but this time using frequency doubled light to excite the first level.

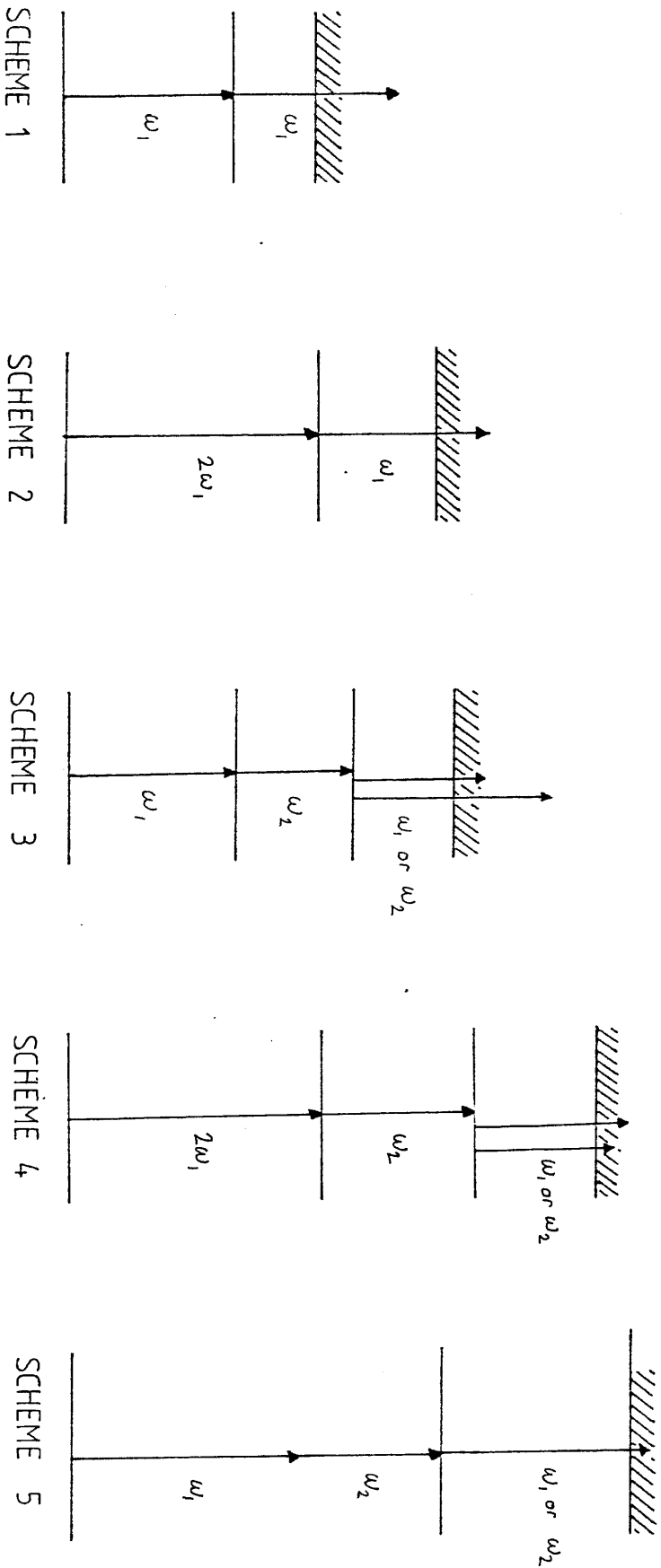
SCHEME 5

Scheme five has a two-photon absorption through a virtual intermediate state with subsequent ionisation by the absorption of a third photon.

Each atomic species in the periodic table has characteristic energy levels associated with their wavefunctions. Atoms can therefore be preferentially ionised by tuning the ionising lasers onto resonances specific to them.

Resonant MPI of this type in conjunction with mass spectroscopy allows very sensitive measurement of isotope ratios in bulk solids containing many atomic species. Resonant MPI with mass spectroscopy (RIMS) is being developed as a sensitive analytical tool for quantitative determination of trace impurities in bulk material.

Figure: 1-19 The five MPI schemes.



SECTION 1-6: CONCLUSIONS.

Resonant and non-resonant MPI processes in simple systems have been modelled successfully using perturbation theory. For many electron and polyatomic systems, perturbation theory becomes more qualitative since approximations to the wavefunctions of the systems have to be made. A fundamental result for all unsaturated N photon MPI processes, involving ionisation is that the ionisation rate is given by

$$W_{fg} = \hat{\sigma}_{fg} I^N$$

where $\hat{\sigma}_{fg}$ is the generalised cross-section for ionisation process and I is the flux of the laser beam. The same flux dependence will also hold for a resonant N-photon MPI process as long as saturation and Stark effects are avoided.

All systems can be ionised by multi-photon processes with any laser of sufficient intensity, although in chemical analysis, resonant MPI of atoms is generally more desirable since it offers atomic selectivity. Photoionisation of atoms is a common MPI scheme, but others are available, such as multiphoton autoionisation and excitation to a state just below the continuum followed by collisional excitation. Molecular systems, with their added degrees of freedom, have many excitation and decay channels available to them. Formation of a polyatomic molecular ion with high flux lasers is often accompanied with fragmentation of the molecule. The process of fragmentation in molecules is studied by MPI in mass spectrometers. Experimental work in Multiphoton absorption and ionisation was reviewed by Baggott (1985).

MPI resonant spectroscopy has several properties that have made it attractive to spectroscopists:

a) Ion and photoelectron detection techniques can be very efficient and therefore sample concentrations need not be very large.

b) Resonances in the far UV can be studied by multi-photon absorption between states.

c) Doppler free spectra can be produced for samples at room temperature by resonant absorption of two photons travelling in opposing directions.

d) Single photon forbidden transitions can be studied by multi photon absorption.

Resonant two photon ionisation spectra are analogous to single photon spectra under certain conditions. R2PI's main advantage over absorption spectroscopy is its greater sensitivity.

A description of multi-photon ionisation of caesium is given in appendix 4, Chapter 9 gives a short description of a TOF mass spectrometer to be built at Glasgow, for the analysis of isotopic samples. MPI has found an application in high energy particle physics. Ion tracks produced by laser ionisation have been used for the calibration of gas filled multi-wire proportional counters. Chapter two gives a brief review of laser calibration work carried out in connection with the ALEPH experiment at CERN and a list of problems that were still to be solved before laser calibration could be put to full use.

A description of the ALEPH TPC (a type of gas filled multi-wire proportional chamber) is given in appendix 2.

APPLICATIONS TO HIGH ENERGY PHYSICS.SECTION 2-1: INTRODUCTION.

Laser induced ionisation of low ionisation potential molecules in gases has found practical uses in the simulation of particle tracks in large multiwire proportional counters (MWPC's).

MWPC's were initially conceived between 1967-1968 (Charpak et al 1968) for the study of elementary particle interactions in high energy physics (HEP). Their use has now spread into the field of applied physics, such as nuclear medicine and vacuum UV light detection in astronomy.

MWPC's are often purpose built for a particular experiment. They may have fundamentally different geometries. Although the following chapter concentrates on the laser calibration of time projection chambers (a type of MWPC), laser calibration can be used for any type of MWPC.

Comprehensive studies of MWPC's have been given by Sauli (1977) and Sadoulet (1980). In principle MWPC's detect ion tracks produced by the interaction of high energy particles and light, with a neutral gas medium. Electrons from the ion tracks drift towards an array of proportional wires. The points of origin of electrons in an ion track may be determined by the time of arrival and the magnitudes of signals induced by the electrons on small metallic plates (called pads) placed close to proportional wires.

The drift velocities of electrons, through commonly used MWPC gas mixtures, are well documented (Sauli (1977)). The distance, z , travelled by the electron in a direction normal to the pads can be

calculated from their drift velocity and time of arrival at the pads. For some MWPC's z may be calculated from the time between the passage of a high energy particle of interest and the arrival, at the sense wires, of the first electron from the track. Alternatively z may be estimated from the position in time of the centroid of the induced signal on the pads. This method requires the use of fast analogue to digital converters and data storage, where the induced signal on a pad is recorded at fixed time intervals (see figure 2-1).

The x and y coordinates of the ion track (lying in the pad plane) are determined from the positions of the sense wires and pads, on which the signals are induced. Greater positional accuracy is obtained by the calculation of the centroid of signals induced on adjacent pads.

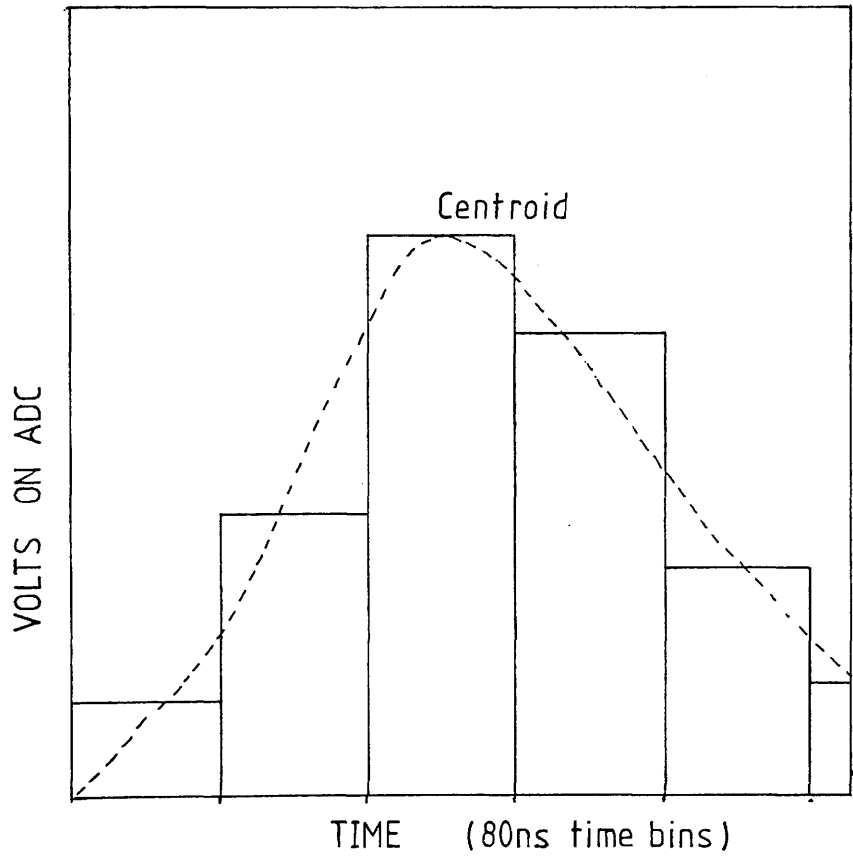
A short description of the ALEPH TPC is given in appendix 2, showing the pad geometry and the orientation of the laser calibration tracks.

In section 2-2 the fundamental principles behind ion track production are discussed. Track production by high energy charged particles, high energy photons and lasers are all treated separately.

Calibration of the MWPC's has always been a non-trivial task involving time consuming statistical analysis of many tracks produced by cosmic rays and charged particles. Calibration with ionisation tracks produced by ultra violet (UV) lasers has been shown to have several advantages over statistical methods. Laser tracks have good resolution over several metres, with none of the multi-scattering events sometimes observed with charged particles. The position of the track is very clearly defined in space and time with no curvature in a magnetic or electric field (imitating tracks produced by particles with infinite momentum). Electron drift velocity and angle can be calculated as functions of gas constituents, pressure and temperature. The effects of varying the electric and magnetic field strengths, the distance from the

Figure: 2-1 Centroid determination of induced signals on pads.

Histogram shows the time development of the signals on the pads.



sense wires and the ionisation density along the track, can also be measured. Accurate corrections can be made for geometric effects, such as wire displacements due to gravitational and electrostatic forces and construction tolerances.

In addition, probably the most important benefit of using laser calibration is that the instabilities in the system, both electrical and mechanical, can be monitored on line during an experiment. One firing of the laser should produce significant data for the calibration of the MWPC, although it is relatively simple to fire the laser more than once and by statistical analysis calculate the position of the track to greater accuracy. Previous calibration methods involved lengthy statistical analysis of many events, making on line calibration almost impossible.

Space charge effects, diffusion of electrons and the speed of the MWPC electronics limits the resolution of the MWPC, that is the minimum distance for which two nearby tracks can be separated. Two track studies, with low density particle beams would need very long data acquisition times to build up sufficient data to be statistically significant. With high density particle beams, corrections to the calculation of their positions are required due to difficulties in localising the tracks, and from interference from unwanted tracks. The ease of directing laser tracks makes them particularly useful for two-track studies. Only one firing of the laser should be necessary to produce sufficient two-track separation data.

Variation of the laser intensity allows the study of pulse height effects, but as yet the control over the intensity of the ionisation is not sufficient to allow the calibration of the counter for dE/dX measurements.

It should be pointed out that the laser calibration is not a test of the capability of an MWPC to detect particles but of its capability

in reconstructing the original position in the MWPC of a charge track. Improvements in MWPC's are continually being made by, for instance, the incorporation of electronics capable of very fast analysis and data transfer. These improvements are very expensive, so it is very important to ensure a good understanding of the system at the prototype stage. Laser calibration is an ideal tool for this job.

A brief historical review relating to the calibration of time projection chambers (TPC's) is given in section 2-3.

SECTION 2-2: ION TRACKS PRODUCED BY PARTICLES AND LASERS.

The two processes of ionisation by particle track interactions and laser interactions, are fundamentally different, although in many respects the resulting tracks are very similar. Track formation by particles is summarised below.

The detection of high energy charged particles in MWPC's is based on the electromagnetic interaction between the particle and the atoms and molecules of the counter gas. The interactions take the form of Coulomb, Bremsstrahlung, Čerenkov and transition radiations, although in gas filled MWPC's only Coulomb interactions play a significant role.

ENERGY LOSS DUE TO ELECTROMAGNETIC INTERACTIONS.

Béthe and Bloch obtained an expression for the differential energy loss per unit length (dE/dX) for a particle, which is written as follows:

$$\frac{dE}{dx} = -K \frac{Z\rho}{A\beta^2} \left\{ \ln \frac{2mc^2\beta^2 E_m}{I^2(1-\beta^2)} - \beta^2 \right\} \quad 2-1$$

where $k=2\pi N z^2 e^4/mc^2$ Z is the nuclear charge of the gas, z is the particle charge, A is the atomic mass number of the medium, ρ is the density of the medium, e is the charge on an electron, β is the velocity of the particle (in units of the velocity of light, c), m is the mass of an electron and I is the effective ionisation potential of the medium. E_m represents the maximum energy transferable to the system, in a single interaction, and is found from two-body kinematics to be:

$$E_m = 2mc^2\beta^2 / (1 - \beta^2) \quad 2-2$$

Equation 2-1 shows that the energy loss is related only to the incoming

particle velocity, not to its mass. Figure 2-2 shows the energy loss for various charged particles. After an initial sharp drop the energy loss reaches a constant value at around $\beta=0.97$ c, and slowly increases again as $\beta \rightarrow 1$ (relativistic rise). The region of constant loss is defined as the minimum ionising region, which is a common situation in HEP.

The interaction often results in the ejection of an electron from the atom or molecule. These ejected electrons are called δ -rays. They can assume any energy E up to E_m . The approximate expression for the probability of an electron receiving an energy E is (Sauli (1977));

$$P(E) = KZ\rho X / A\beta^2 E^2 \quad (E_0 \ll E_m) \quad 2-3$$

where X is the thickness of the detector. From this the expression for the number of electrons produced between an energy E_0 and E_m is calculated to be;

$$N(E) = \int_{E_0}^{E_m} P(E) dE = W (1/E_0 - 1/E_m) \approx W / E_0$$

where

$$W = KZ\rho X / \beta^2 A$$

Figure 2-3 shows the calculations for the number of δ -electrons ejected with energies $\geq E_0$ as a function of E_0 up to the maximum E_m for 1 GeV/c protons.

Consideration of the kinematics of the interaction also leads to the result:

$$\cos^2\theta = E / E_m \quad 2-4$$

where θ is the angle that δ electrons are ejected from the direction of travel of the ionising particle. From this it is seen that δ -rays with $E/E_m \leq 0.001$ will be emitted perpendicular to the incident track. δ -

Figure: 2-2 Energy loss of charged particles.

in air

Energy loss per unit length, from equation 1, for different particles. At energies above 1GeV/c all particles lose about the same amount of energy (minimum ionising energy) (Sauli (1977)).

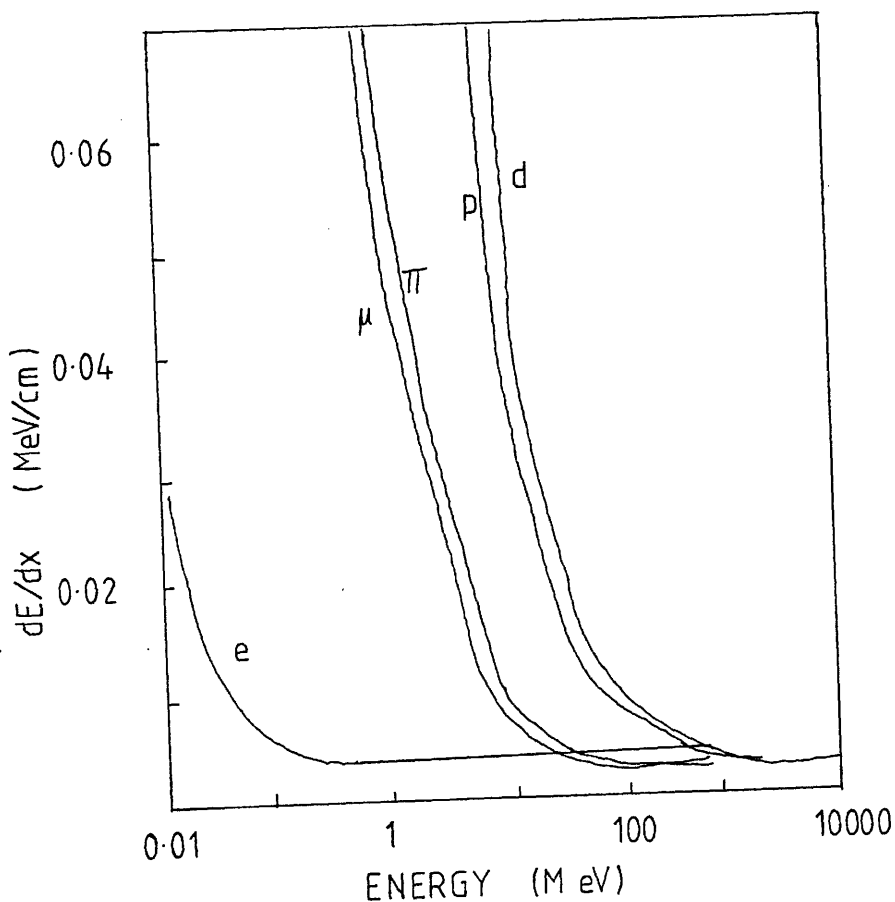
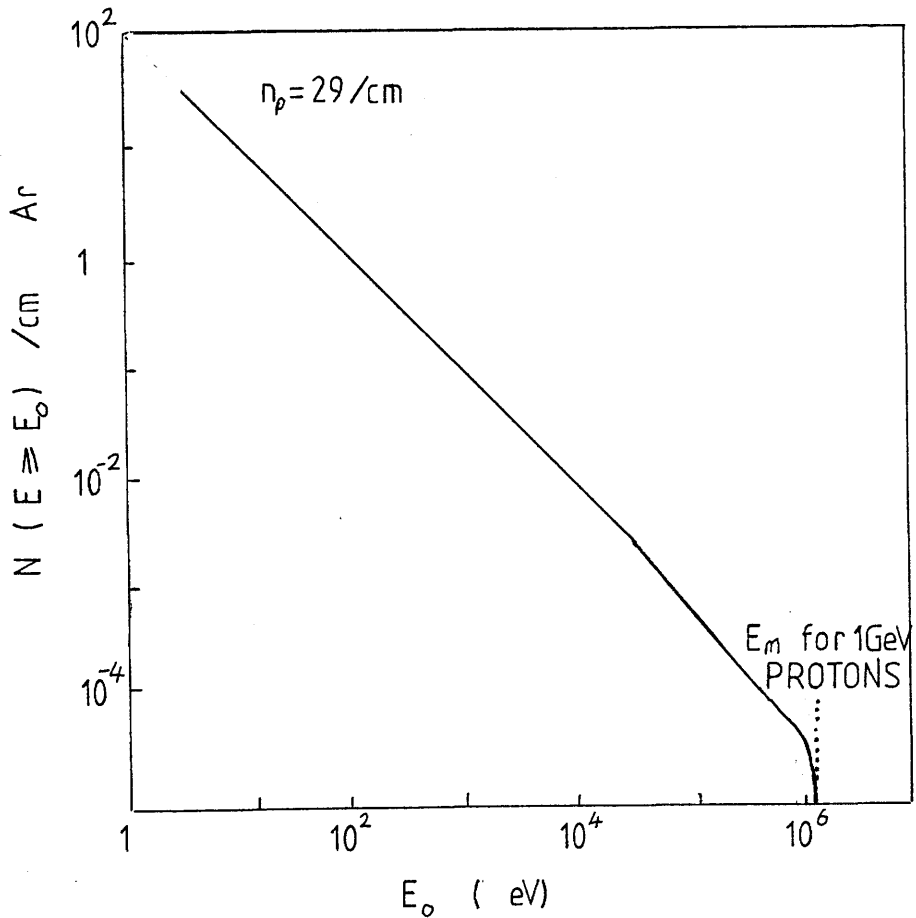


Figure: 2-3 Ejection energies of δ -electrons.

Number of electrons ejected with energies $> E_0$, As function of E_0 calculated from equation 2-2. The average number of primary ionising collisions are 29/cm. (Sauli (1977)).



electrons produced by interactions with charged particles will travel, through the gas medium, a distance which is dependent on the δ -electrons starting energy. For energies up to a few hundred KeV the range R_p , is to a good approximation;

$$R_p \approx 0.71E^{1.72} \text{ g cm}^{-1}$$

(Kobetich and Katz 1968)

(where E is in MeV).

Figure 2-4 gives the range of δ -electrons in argon at standard temperature and pressure, as a function of energy. From these results it is seen that, for a 1GeV proton, only 1 in 3×10^3 δ -electrons ejected have an energy of greater than 3KeV. δ -electrons around this energy have a range of approximately 100 μ m. They are ejected perpendicular to the track and produce a cluster of secondary electrons whose centre of gravity is displaced to the side of the track. This limits the accuracy of the MWPC to somewhere between 20 and 30 μ m.

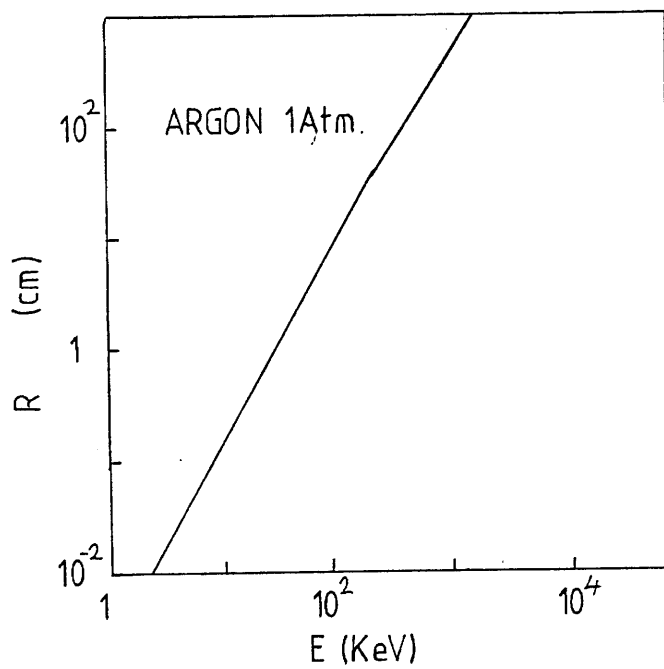
The absorption of a high energy particle therefore leaves a trail of δ -electrons, which in turn undergo interactions with the surrounding atoms and molecules. The ejection of secondary electrons from these atoms and molecules can occur if the energy of the δ -electron is greater than the ionisation potential of the medium. The total number of electrons produced by the absorption of a particle can be written as:

$$n_p = \Delta E / W_i$$

where ΔE is the total energy loss of the particle in the gas volume considered and W_i is the effective average energy to produce one ion pair. Production of a δ -electron and an ion is called a primary ionisation of the gas and n_p is the number of electrons produced in the primary ionisation. For example a minimum ionising particle in 70-30% argon/methane produces a total of 124 ion pairs/cm although the number

Figure: 2-4 Range of δ -electrons in argon.

Range R_0 of electrons in argon as a function of energy (Kobetich and Katz (1968)).



of primary ion pairs produced per centimetre is only 34. Thus the average distance between primary ion pairs is about 300 μ m and each primary electron produces an average of 4 secondary electrons. Therefore tracks produced by charged particles do not form a continuous line of ion pairs but a series of clusters of differing size.

The spatial distribution of the ion pairs puts a limit on the time resolution of MWPC's. For a typical case where the electron drift velocity is 5cm/sec the FWHM of the time distribution of the ion track is about 5nsec.

ABSORPTION OF PHOTONS.

MWPC's will detect photons ranging in energy from a few eV up to hundreds of KeV. Again, as for charged particles, it is the electromagnetic interaction of the photons with the atoms and molecules of the gas that forms the basis for their detection. Instead of producing an ion trail like charged particles, the photon is usually involved in only a single interaction. The type of interaction is dependent on the energy of the photon. For energies up to a few KeV the dominant process is photoelectric conversion. For energies of a few hundred KeV Compton scattering takes over, and for higher energies electron-positron pair production is dominant. No more shall be said about the detection of photons in this respect, except that the absorption of x-ray photons from an Iron 55 source was used as the basis for the calibration of the proportional counters in the experiments described later. Photoelectric conversion of the 5.9KeV Mn 55 x-rays produces an electron with approximately the same energy. This can be treated as a δ -electron which produces a total number of secondary electrons given by;

$$n_T = \Delta E / W_i$$

where ΔE is the energy of the photon (= energy of the photoelectron) and n_{τ} for Iron 55 is approximately 227 ion pairs in 90-10% argon/methane gas, using $w_i = 26\text{eV}$ for P10 gas (Melton et al (1954)).

TRACKS PRODUCED BY THE MPI OF COUNTER GASES BY LASERS.

Electrons ejected from atoms and molecules in an MPI process usually will have energies less than the energy of the photon in the beam. Typical energies^{from MPI} are about 3 eV. Ejected electrons rapidly lose this energy to the medium through collisions, leaving them in thermal equilibrium with the medium. A consequence of this is that any preferred angular distribution of the electrons ejected from the atoms or molecules (through polarisation effects described in chapter 1-4) is rapidly eliminated by collisions. Also, unlike charged particles, laser ionisation does not produce high energy γ -rays, so that clustering effects are not expected.

For calibration purposes it would be preferable to have narrow laser induced ion tracks with constant ion densities of around 5x minimum ionising density (i.e. 500 ion pairs/cm).

Particle tracks are around 30 μm wide. Laser tracks as narrow as this cannot be sustained for more than a few centimetres due to diffraction effects. Fortunately laser induced ion tracks a few millimetres wide are adequate for laser calibration. Diffraction limited laser beams, of around 1mm in diameter, can be maintained over many metres (Sadoulet (1981)). The divergence of a diffraction limited laser beam is given by the equation:

$$r(x) = r(0) \left[1 + \left(\lambda x / \pi r(0)^2 \right)^2 \right]^{1/2}$$

where $r(0)$ is the radius of the beam waist, x is the distance travelled

by the beam and λ is its wavelength. From this it can be seen that the divergence of the laser beam increases with increasing wavelength.

An example of the effect that this may have on the ion density distribution along a laser induced track, is given below. Assume that two diffraction limited laser beams, with wavelengths of 250nm and 1000nm respectively, are used to ionise molecules with an ionisation potential of 9eV. This would require 2 photons at 250nm and 8 photons at 1000nm. From equation 1-27 the dependence of the ionisation on the fluence of the 250nm and 1000nm laser beams would be F^2 and F^8 respectively.

Laser beams of 250nm and 1000nm wavelength with radii both of which have a radius at $r(0)$ of 1mm would diverge over 10m to radii of 1.3mm and 3.3mm respectively. This would produce a drop in ionisation density by factors of about 1.7 and 2×10^7 respectively.

ATTENUATION OF THE LASER LIGHT BY ABSORPTION IN THE GAS.

If the MPI process is resonant, the ionisation may also be affected by attenuation of the beam due to absorption in the gas.

For instance, in a two photon ionisation process, the absorption of light per unit length is given by:

$$I = I_0 e^{-\alpha N x}$$

where σ is the single photon absorption *cross-section*, (with typical values of around $5 \times 10^{-19} \text{ cm}^2$ for molecules (UV Atlas of Organic Molecules (1966))), N is the number of absorbing molecules per unit volume and x is the distance of travel through the medium. In MWPC's the ionisation detected with lasers of around 300nm wavelength was thought to be caused by the two photon ionisation of low concentrations of impurities in the gas. The concentration of the absorbing molecules was thought to

be <1ppm. Using this value, the intensity of the beam after travelling 10m would be reduced by 2%. In a non-saturation 2-photon process this would constitute a drop in ionisation of 4%.

DIVERGENCE AND ABSORPTION: A SUMMARY.

Divergence and absorption of laser beams used for calibration of MWPC's is not a problem provided the laser induced ionisation remains well within the dynamic range of the detector electronics. The problem of divergence would be minimised by using diffraction limited short wavelength, single mode lasers.

To minimise absorption effects the concentration of molecules, capable of absorbing the laser light, must be kept low (say <1ppm).

SECTION 2-3: LASER CALIBRATION.

At the European Organisation for Nuclear Research (CERN) a large electron-positron (LEP) collider is being constructed. At the centre of the detector, built for the ALEPH experiment, is a Time Projection Chamber (TPC). A TPC is a form of gas filled MWPC and is to have a laser calibration system incorporated into it. This section contains a brief history of laser calibration studies in connection with ALEPH, and a review of work carried out in the TPC 90 (a prototype for the ALEPH TPC). A description of the ALEPH TPC is given in appendix 2.

HISTORY OF LASER CALIBRATION.

The following is a brief history of laser calibration studies in connection with ALEPH, DELPHI, OPAL, L3, UA1 and SLAC. In 1979, laser ionisation tracks were produced in counter gas mixed with a small concentration of Nickelocene. The Nickelocene, (a low ionisation potential molecule with absorption resonances around 337nm) was ionised by focussing the output of a N₂ laser with a pulse length of 0.5ns and a wavelength of 337nm (Anderhub et al (1979, 1980)).

In 1980 Bourotte and Sadoulet observed laser ionisation with and without a low ionisation potential additive (this time diethylaniline, DEA). They used the 0.5ns pulse length, 337nm wavelength output of a focussed N₂ laser and the 15ns pulse length, 266nm wavelength unfocussed output of a quadrupled Nd:YAG laser. The mechanism for the ionisation of the gas, when no additive was present, was attributed to the two-photon ionisation of low ionisation potential hydrocarbon impurities in the gas. Rockwood et al (1979) had already observed that organic impurities were responsible for background ionisation in some MPI studies.

Hilke (1980) discussed the formation and applications of laser induced ion tracks in counter gases.

From 1982 onwards, work continued on the calibration of MWPC's with lasers and on laser construction. In 1982 Desalvo and Desalvo made measurements of the laser induced ionisation in argon/ethane counter gas. Gushchin et al (1983) carried out work on the simulation of particle tracks with N_2 lasers by the addition of low ionisation potential vapours to the counter gas. In 1982 Brozzi et al published work on the calibration of the $p\bar{p}$ UA-1 collaboration central detector. Tracks were produced by low divergence N_2 lasers. They indicated, through the dependence of ionisation on laser fluence, that the ionisation was most likely to be due to the double-step (2-photon) ionisation of low ionisation potential impurities. Cochet et al (1982) came to the same conclusion later in the year. Double track and saturation effects were reported by Va'vra (1982) using an N_2 laser. However he reported periodic downtimes in his electronics systems due to radio frequency noise generated across the spark gap of the N_2 laser. He concluded, that N_2 lasers may not be suitable for long term monitoring of large experiments.

In 1983 Desalvo used both a slightly focussed and strongly focussed N_2 laser for the measurement of electron drift velocity, gain, charge diffusion and single electron diffusion in MWPC's. Using a two-stage low divergence focussed N_2 laser, small, localised electron clusters were produced (Guo et al 1982). Timing properties and dead region effects in a MWPC were studied on a submillimetre scale utilising these electron clusters.

Raine et al (1983) reported on ionisation in a proportional counter induced by a variety of lasers. In 1983 Konijn and Hartjes measured the straightness of a N_2 laser induced track to an accuracy of $\sigma \sim 10\mu\text{m}$. 60ppm DEA was added to the counter gas. Drift angles and

drift velocities of electrons were measured experimentally, from tracks produced by a UV laser, by Becker et al (1983). The results compared well with theory. Markiewicz et al (1983) reported on laser induced ionisation tests in the UA-1 MWPC. Using a prototype N_2 laser they observed variations in the levels of ionisation in the gas for a set laser fluence. Over two days the ionisation decreased by a factor of 4. The straightness of the laser tracks were measured to better than $200\mu m$

In 1984 Haissinski et al reported on the determination of longitudinal and transverse diffusion of a single electron. Single electrons were produced at a pin hole in a metal sheet by photoionisation with a N_2 laser. Marrocchesi and Ragusa (1984) reported experimental results from a small prototype of the PISA time projection chamber. They used N_2 laser tracks to study detector pad geometry, pad response functions and the resolution of the detector for straight or nearly straight tracks (stiff tracks).

Some further work, reported at the 1986 Wire Chamber Conference, was the measurement of the straightness of a laser track to an accuracy of $35\mu m$ over 1.6m. This work was carried out using a quadrupled Nd:YAG with a 266nm output. Biagi and Booth (1986) carried out point scans using a sharply focussed N_2 laser in a streamer tube. They measured electron drift velocities close to the sense wires.

Much of the laser calibration work carried out up to 1986 was reviewed in a paper presented by Hilke at the 1986 Wire Chamber Conference (Hilke (1986)).

LASER CALIBRATION IN THE TPC 90 AND THE ALEPH TPC.

The TPC 90 was built as a test model for the ALEPH TPC. During its lifetime the TPC 90 has had several changes of design. A cutaway view of one version of the TPC 90 is shown in figure 2-5

Figure: 2-5 Cutaway view of the TPC 90.

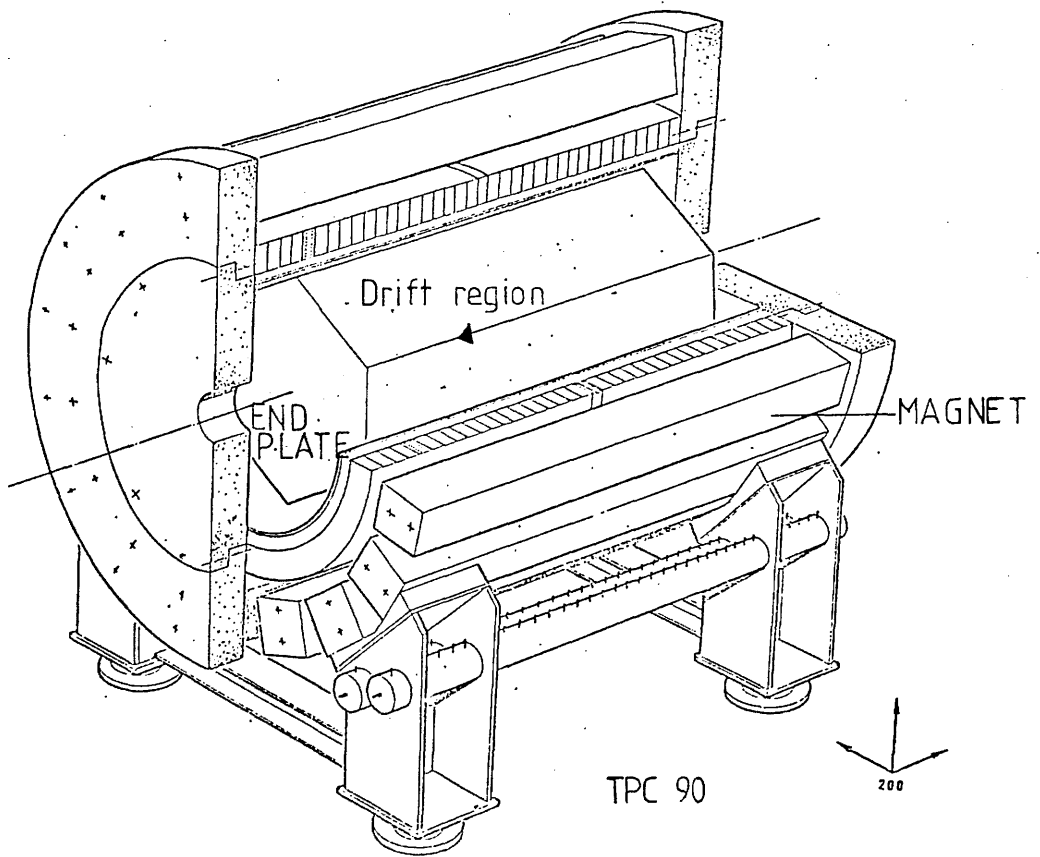
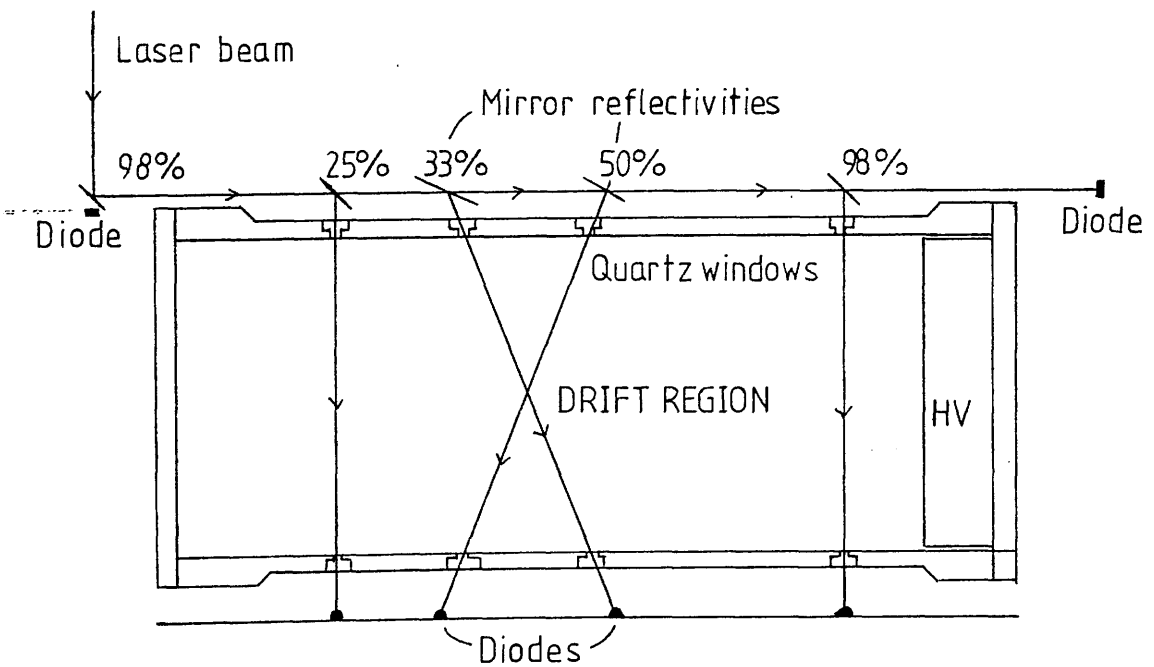


Figure: 2-6 Beam alignment for the TPC 90.



The TPC 90 has a drift length of 1.5m and a diameter of 0.8m. A high voltage is placed at one end of the chamber to form an electron drift region. The detector plane is hexagonal in shape with diameter of 0.75m. The sense wires are arranged similarly to those in the ALEPH TPC and it has 8 rows of pads each $8 \times 8 \text{mm}^2$ in size. It can be operated continuously with magnetic fields up to 7 kGauss or up to 12 kGauss in a pulsed mode. The counter gas is at atmospheric pressure.

Figure 2-6 shows the beam alignment for the TPC 90 laser calibration system. Lasers used for the laser calibration experiments were of three types, N_2 , Krypton Fluoride excimer and quadrupled Nd:YAG lasers.

A short review of the work carried out to date on the laser calibration of the TPC 90 is given below.

In 1984 Price used laser induced ion tracks to study electric field distortions in the TPC 90. He measured the deviation from straightness of tracks passing over 8 pad rows, parallel to the pad plane. The deviations were explained by distortions in the drift field due to a gating grid voltage 'mismatch'.

Further work on field inhomogeneities was carried out by May et al (1984) who reported on the analysis of laser runs in the TPC, and in particular on the systematic displacements of the measured coordinates of the laser tracks. Benetta et al (1985) measured magnetic and electric field inhomogeneities in the TPC 90 using a N_2 laser and compared actual track displacements with calculated displacements for a given magnetic field. Amendolia et al (1986a) reported on wire gain and track distortions near the ALEPH TPC sector edges. A large reduction in the distortions was achieved by the addition of two field correcting strips.

In 1984 the Glasgow group reported on laser studies undertaken with an excimer laser. An Oxford KX2 excimer laser filled with krypton

and fluorine produced a beam with a power of $650\mu\text{J}/\text{cm}^2$ at 249nm wavelength output. They analysed crossed tracks, and variations in the ionisation on beam intensity and brought attention to the problem of beam reflections off the quartz windows in the TPC90 field cage. Reflected beams colliding with the TPC walls produced large photoelectric signals.

Rolandi (1984) measured the statistical density of ionisation along a particle track in the TPC 90 by two separate methods, by pad response function measurements and by the comparison of peak heights for two neighbouring sense wires. He observed a discrepancy between the statistical number of electrons and the average number of electrons detected on the wires. The results indicated that some kind of clustering of the ionisation along the track was occurring. Later, work carried out by Blum et al (1986) suggested that laser induced ion tracks produced little or no clustering. In this work $\underline{E} \times \underline{B}$ effects close to the detector sense wires were studied. By varying the angle ψ , the effective drift angle, a reduction in the $\underline{E} \times \underline{B}$ effect of particle ion tracks was observed, although no change was brought about for the laser induced tracks. Declustering of the tracks by diffusion of electrons in the gas was thought to be responsible. Laser ion tracks did not show this behaviour. A MOPA A400 N_2 laser was used in the experiment.

Richstein and Rolandi (1984) measured the diffusion coefficient and mean free path of electrons, in 90-10% argon/methane gas (P10 gas). They did this by studying the behaviour of the pad response function (PRF), with a varying magnetic field. The expected decrease in diffusion with an increased magnetic field was observed. Richstein (1986) measured the transverse drift diffusion coefficients and mean collision times of electrons in different gases. Ion tracks were produced by a quadrupled Nd:YAG. He also calculated the drift velocities of the electrons in the various gases.

Peisert (1985) reported on two-track resolution of the TPC using 2 crossed laser tracks. Tracks in the xz plane could be resolved if their time separation exceeded 300ns (1.5 cm) whilst tracks 9mm apart in the xy plane could be resolved.

Amendolia et al (1986b) reviewed work carried out in the TPC 90.

Experiments have been carried out in the TPC 90 in connection with seeding of low concentrations of low ionisation potential vapours into the counter gas. An enhancement in the ionisation over background was expected and it was hoped to achieve some control of the ionisation. Seeding work was initiated after encountering problems like those observed in the UA-1 central detector, where Markiewicz et al (1983) observed variations in the levels of ionisation from day to day for a set laser fluence. A discussion of the seeding experiments carried out in the TPC 90 is left until chapter 5.

SECTION 2-4: CONCLUSIONS

Laser induced ion tracks can be used for the accurate calibration of MWPC's. Tracks produced by lasers are not a test of the capability of the MWPC to detect particles but rather of its capability to reconstruct the point of origin of formation of an ion track.

To this end, ionisation along the track should not be strongly variant and should be well defined in space and time. These conditions can best be met by a diffraction limited laser pulse of short wavelength (about 250nm) and pulse duration ($< 25\text{ns}$). (Reasons prohibiting the use of much shorter wavelength lasers are given in chapter 4). Many calibration experiments have been carried out, most of these with short wavelength lasers, ($< 337\text{nm}$). A problem commonly encountered was a lack of control and reproducibility of the laser ionisation levels. This led to the demand for a method of ionisation control and for a clearer understanding of the underlying processes involved in the ionisation observed in MWPC's. Ionisation control could be approached in two ways: by changing the laser fluence to maintain a constant ionisation level or by the addition of low ionisation potential vapours to the counter gas.

Results from the study of several low ionisation vapours are given in chapter 5.

SECTION 3-1: INTRODUCTION.

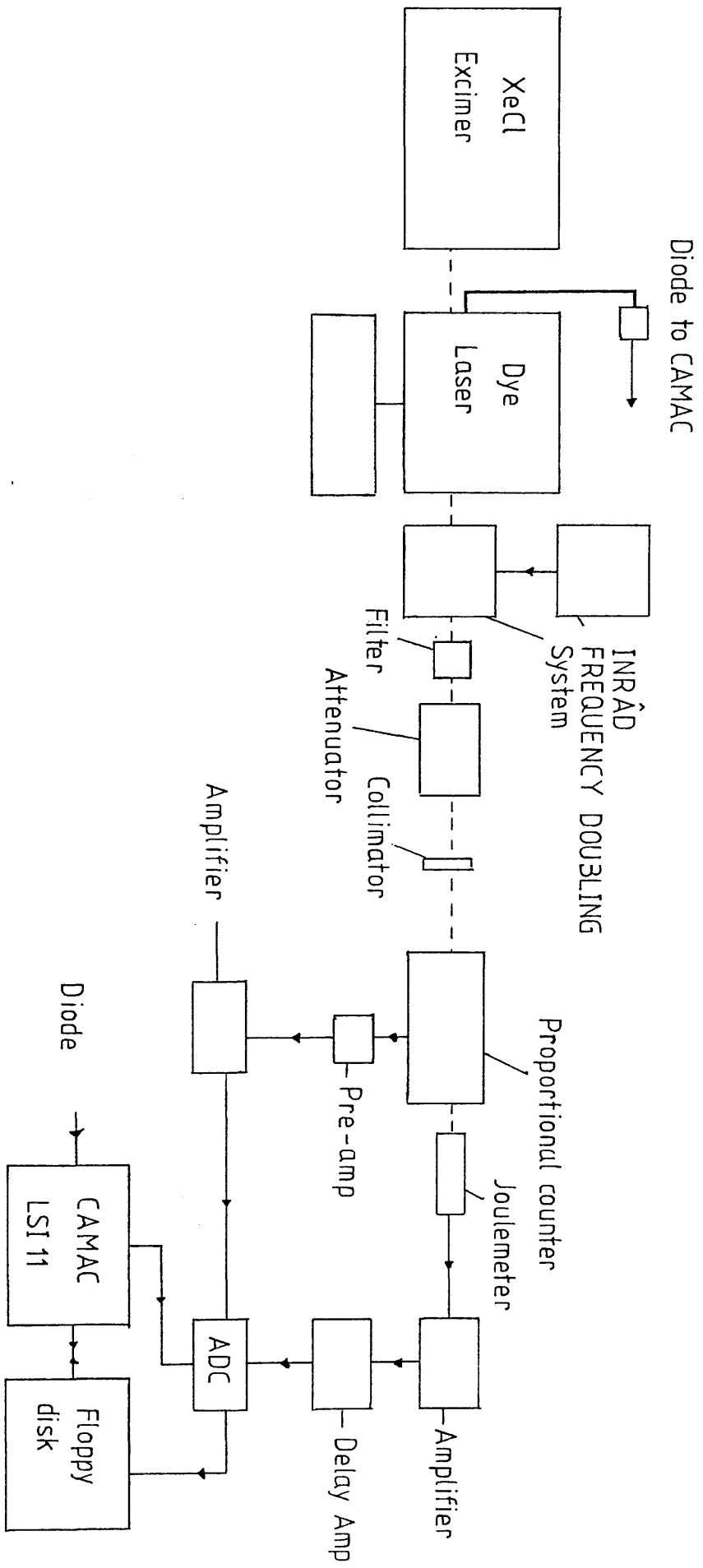
Summarised below are the optical and electronic arrangements used in the analysis of the P10 counter gas by laser ionisation and in the use of additives as a method of ionisation control.

An excimer pumped dye laser provides continuous wavelength coverage between 520nm and 680nm. This light was frequency doubled, to cover the wavelength range of 260nm to 335nm. Doubled light was separated from the fundamental light by one of two methods, dispersion through a quartz prism or absorption of the fundamental in quartz filters. Before passing into the counters the beam was collimated to $1 \times 1 \text{mm}^2$. After passing through the counter, the beam intensity was monitored by a joulemeter.

Signals from the joulemeter and proportional counter were both amplified and delayed so that their peak positions were coincident, with magnitudes well within the dynamic range of the analogue to digital converter (ADC). The ADC was used to digitise the signals. A data acquisition system recorded simultaneously onto a floppy disk digitised signals from the joulemeter and counter. Normalisation and statistical analysis of the data was carried out by an IBM computer. Figure 3-1 shows the experimental apparatus.

The following sections describe individual pieces of apparatus in more detail. Table 3-4 gives a list of the lasers used in experiments described in chapter 4. The quadrupole mass spectrometer is described in section 3-6

Figure: 3-1 Apparatus for seeding and R2PI experiments.



THE NEODYMIUM LASER.

The Neodymium laser is termed a "solid state laser". Its active medium consists of an isotropic crystal of $Y_2Al_5O_{12}$ (Yttrium-Aluminium Garnet:YAG) with Neodymium (Nd) replacing about 1% of the Yttrium.

The Neodymium:Yttrium-Aluminium Garnet (Nd:YAG) laser is a 'four level' laser (refer to figure 3-2). Level 1 lies well above the ground state and is essentially unpopulated when in thermal equilibrium with its surroundings ($N_1 = 0$, where N_1 is the population of level 1). Population inversion is forced between levels 2 and 1 by optical pumping with a flash lamp. Laser action occurs between these levels, at a wavelength of 1060nm.

A property of the crystal structure is the removal of degeneracy in the upper states of the Nd^{3+} ion, called crystal field splitting. Also there is a homogeneous broadening of these states due to vibrations in the crystal lattice. As a result, the absorption spectrum for Nd is diffused, giving it a broad absorption band. Flash-lamps such as krypton filled arc-lamps have output wavelengths overlapping the Nd:YAG absorption band and as a result are an efficient means of optical pumping for the Nd:YAG.

There follows a description of the general characteristics of the Nd:YAG laser used in experiments described later.

The diagram in figure 3-3 shows the basic layout of the Spectron Laser type SL2Q+SL3A. It consists of a flash-lamp pumped oscillator region, followed by a flash-lamp pumped amplifier region. The fundamental light is quadrupled from 1060nm to 266nm by passing through two successive KDP doubling crystals (see second harmonic generation, in

Figure: 3-2 Four level diagram for the Nd:YAG laser.

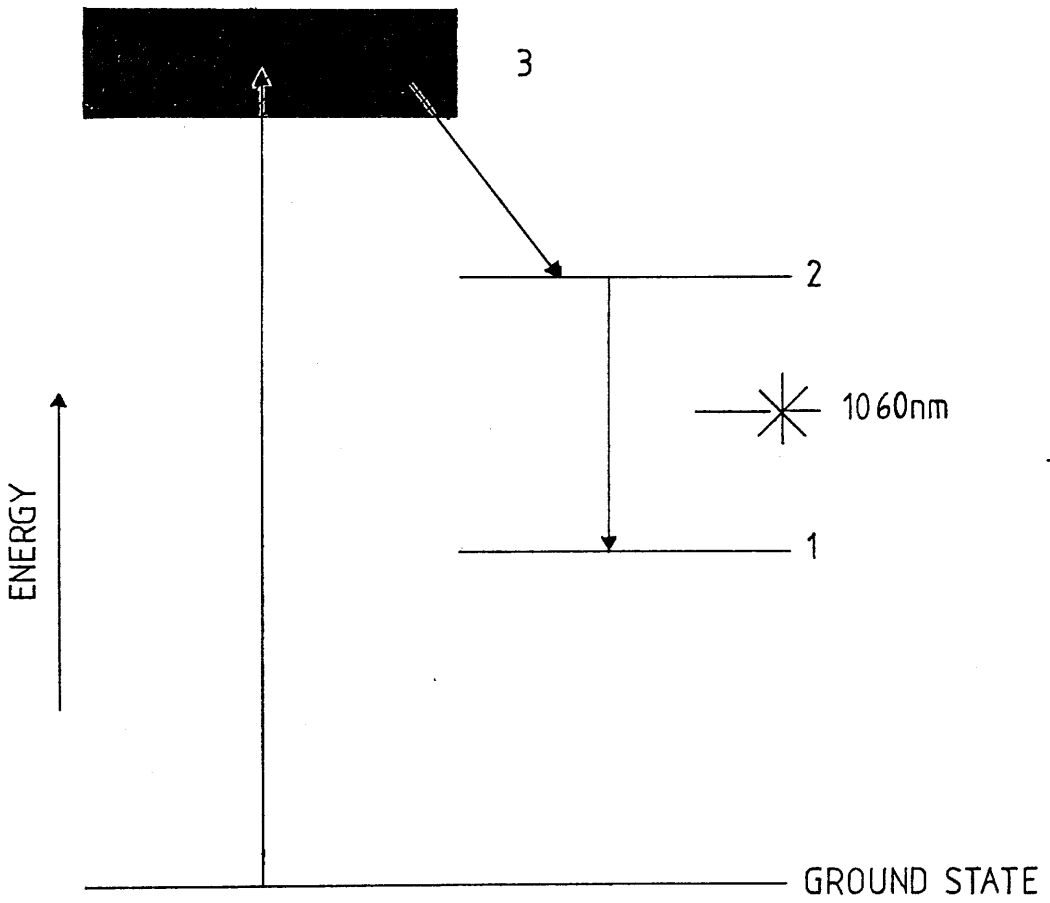
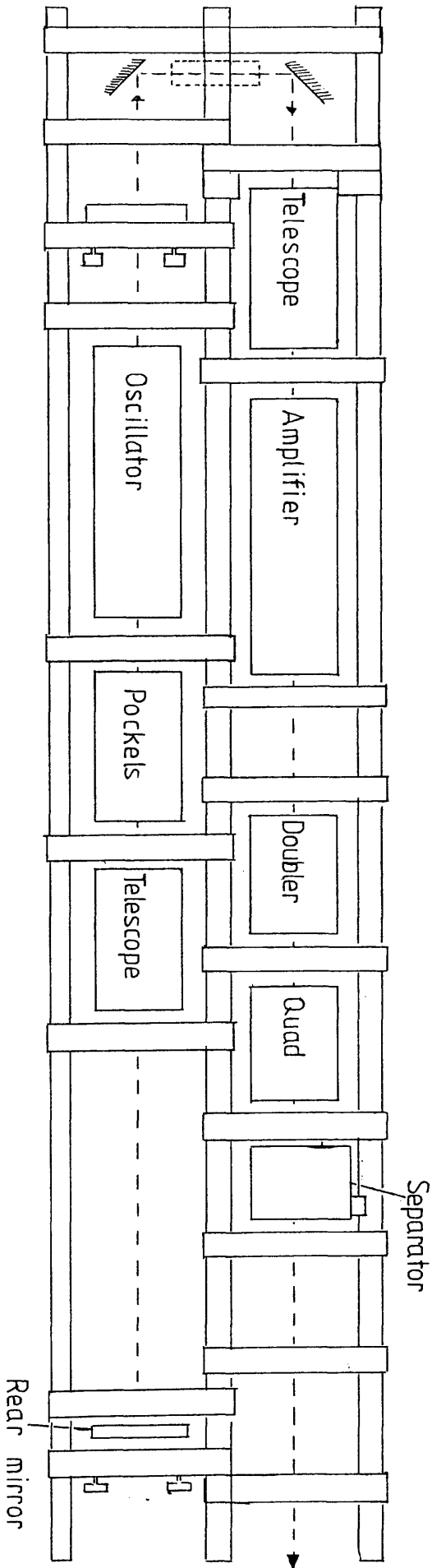


Figure: 3-3 Basic layout of the Spectron Nd:YAG laser.



this section).

The laser repetition rate was optimally 10Hz. The output power of the laser was maximally 50mJ at 266nm with a beam cross-section of approximately 25mm^2 . The laser beam was linearly polarised and multi-mode with a pulse duration of 15ns.

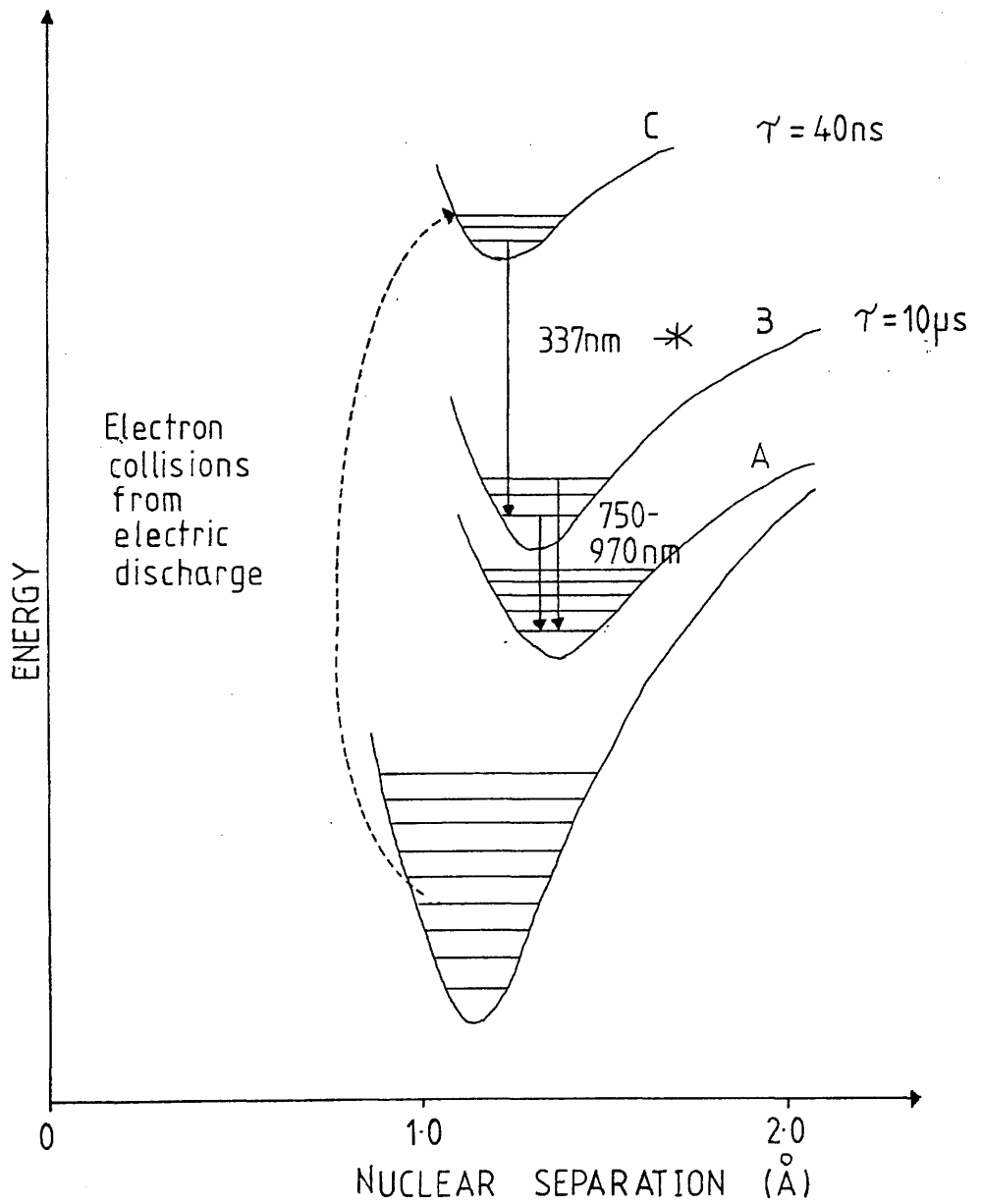
THE NITROGEN LASER.

The nitrogen (N_2) laser has a pulsed output, with a duration of $<5\text{ns}$ and a wavelength output of 337nm. Lasing action occurs between an upper state C (figure 3-4) of short lifetime ($\sim 40\text{ns}$), and a lower state B, of long lifetime ($\sim 10\mu\text{s}$). As a consequence of the lifetimes, the laser action cannot be maintained for longer than the excited state lifetime. During the lasing process there is a rapid increase in the population of the lower states. These can then reabsorb stimulated light, causing rapid drop in optical gain and eventual termination of the laser action.

A Lumonics TE-860-3 laser was used in experiments described later. The Lumonics laser excites the N_2 with a very rapid discharge from a thyratron. Low divergence unstable resonator optics are used, allowing laser light to escape from the optical cavity after only a very few passes through the laser medium. The use of unstable optics minimises reabsorption losses. Specifications of the N_2 laser are given in table 3-1

Some earlier experiments were carried out using a Model LN 100 PRA (Photochemical Research Associates Inc.) Nitromite nitrogen laser with a pulse duration of 300ps and peak output of $60\mu\text{J/pulse}$.

Figure: 3-4 Energy level diagram for the N₂ laser.



THE EXCIMER LASER.

Excimer lasers are capable of producing powerful pulses of laser light at UV wavelengths. This quality makes them particularly useful for pumping dye laser systems.

Excimer lasers operate by the production of excited diatomic molecules by an electrical discharge through a gas medium containing a mixture of noble gases and halogens. The excited molecule (Excimer) remains bound as a result of an attractive potential minimum. Figure 3-5 shows the potential energy curve for the excited molecular state of XeCl (curve B). In its ground state the molecular potential is mainly repulsive (curve A) with a very shallow van der Waals minimum of depth less than the thermal energy, kT , of the molecule at room temperature. Ground state molecules are therefore unstable and rapidly dissociate (10^{-11} - 10^{-12} s).

The population inversion required for laser action is between the upper bound state and the lower dissociating state.

The Lumonics TE-860-3 excimer laser was filled with a Xenon and Chlorine gas mix, with a lasing wavelength of 308nm.

The cavity of the excimer laser had unstable resonator optics (see figure 3-6). Normally a laser has stable optics where the light makes many passes through the lasing medium before passing out of the optical cavity. However the optical gain of the XeCl laser is very large, so that only a very few passes are necessary, allowing unstable resonator optics to be used. They also have very low divergence and can handle very high powers. Some experiments were carried out with unstable resonator optics in place, but, when used to pump the dye laser a slightly divergent beam is preferable and so the stable optics were installed.

The specifications for the XeCl laser are given in table 3-2.

Figure: 3-5 Energy level diagram for the XeCl laser.

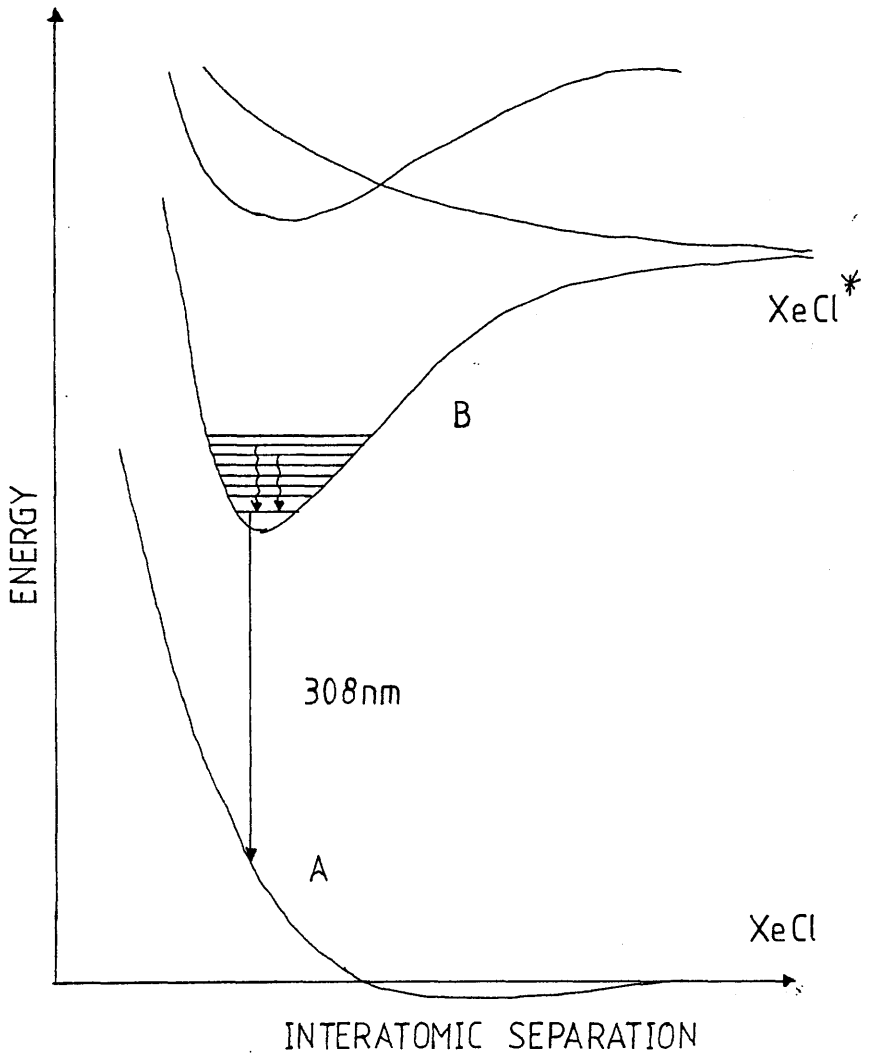
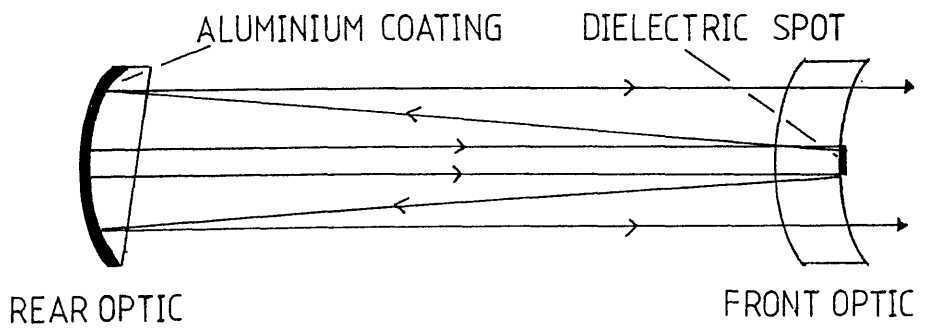


Figure: 3-6 Unstable Resonator Optics.



THE DYE LASER.

Dye lasers are popular because of their broad spectral tunability in the visible and near-visible spectral region.

Dye molecules are dissolved in transparent solvents. Radiation from near UV lasers is used to excite molecules from their ground vibronic state, S_0 , to higher lying vibronic levels of the first excited state, S_1 (see figure 3-7). Through collisions these rapidly fall (10^{-11} - 10^{-12} s) by radiationless transitions into the lowest vibrational level, v_0 , of the excited state. Sufficient irradiation causes a population inversion between v_0 in S_1 and the higher lying vibrational levels, v_R , of S_0 . The states v_R have negligible population at room temperature due to their very small Boltzmann factors ($\exp\{-E(v_R)/kT\}$). The v_R (S_0) levels are rapidly depopulated by collisional decay. The laser action proceeds when the optical gain of the transition $v_0(S_1) \longrightarrow v_R(S_0)$ exceeds the overall losses of the system.

Losses in the system are a combination of resonator losses (absorption, diffraction and scattering of the light in the windows, mirrors etc) and absorption losses in the dye medium. Predissociation, thermal decay and intersystem crossing to neighbouring triplet states are all loss processes. Losses are reduced by rapid removal of dye molecules from the interaction region by flowing.

The EPD-330 Lumonics laser consists of an oscillator region and an amplifier stage with appropriate beam steering optics for the excimer pump laser. (see figure 3-8).

A solution containing the dye is circulated through an oscillator cell, over a knife edge. The 'rectangular' excimer laser pulse is focussed through a cylindrical lens into the oscillator cell. Maximum population occurs close to the pump entrance window along the focal line of the lens (see figure 3-9).

Figure: 3-7 Energy level diagram for the dye laser.

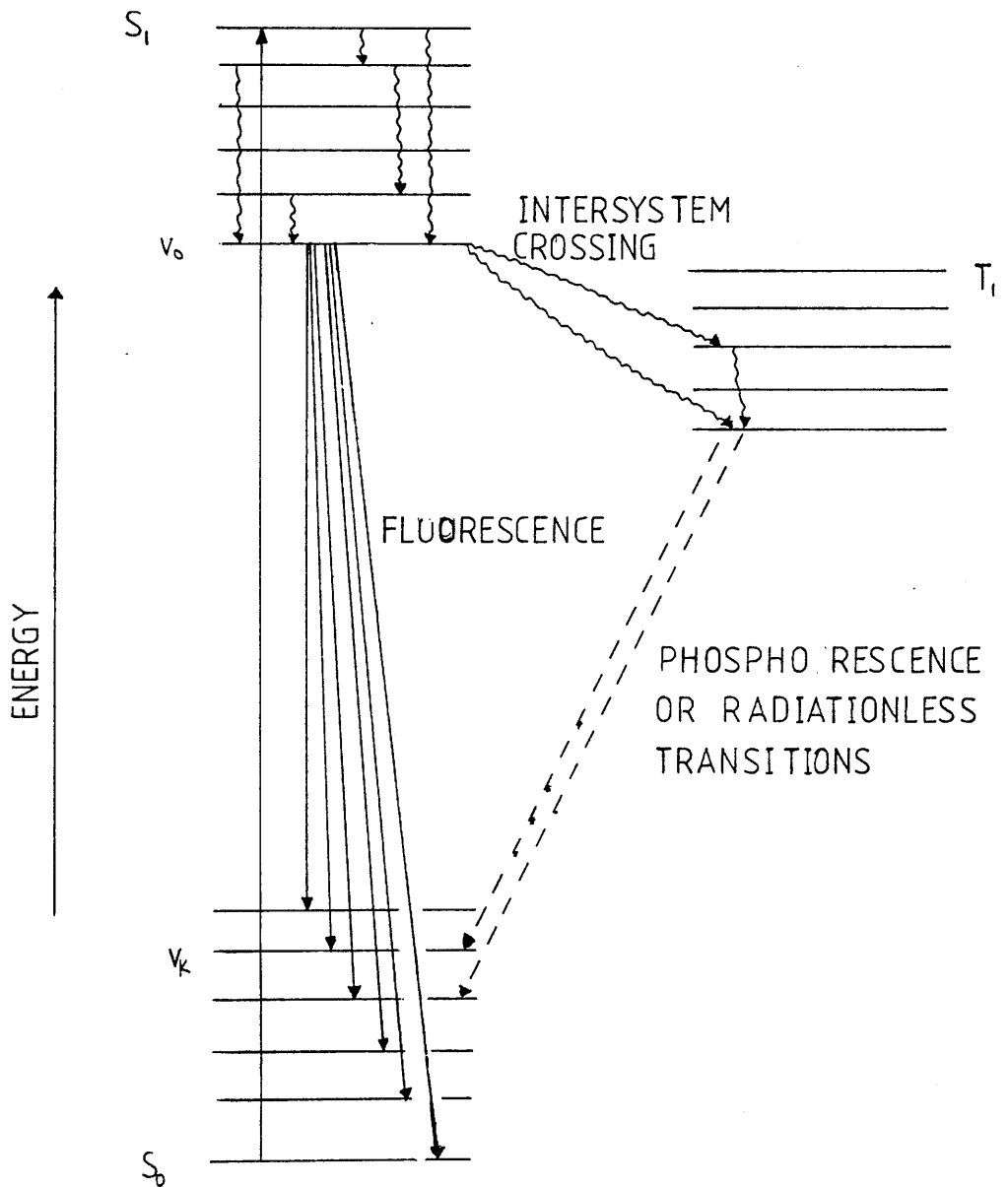
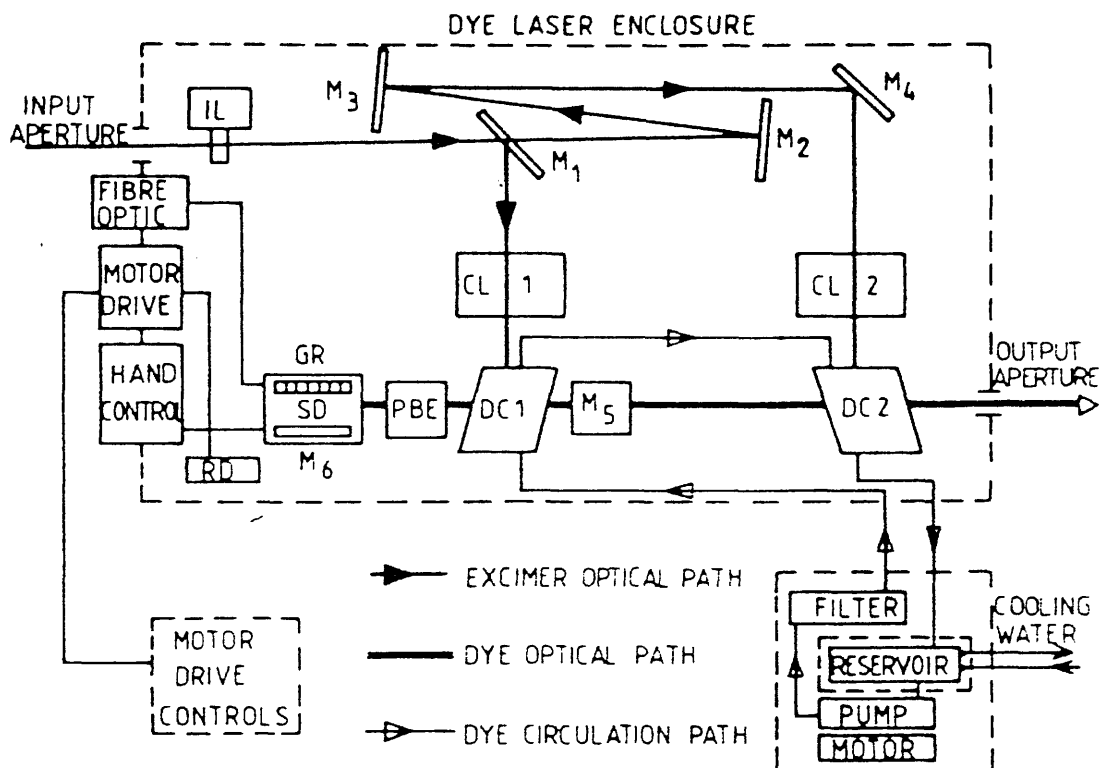


Figure: 3-8 Diagram of the EPD Lumonics dye laser.



- | | | | | |
|-------|--|--------------------|----------------|---------------------|
| KEY : | CL 1,2 | CYLINDRICAL LENSES | M ₅ | OUTPUT COUPLER |
| | DC1,2 | DYE CELLS | PBE | PRISM BEAM EXPANDER |
| | GR | GRATING | RD | READOUT |
| | IL | INTERLOCK | SD | SINE DRIVE |
| | M ₁ -M ₄ -M ₆ | REFLECTORS | | |

OPTICAL SCHEMATIC OF THE LUMONICS
EPD - 330 DYE LASER

Figure: 3-9 Diagram of the oscillator cell.

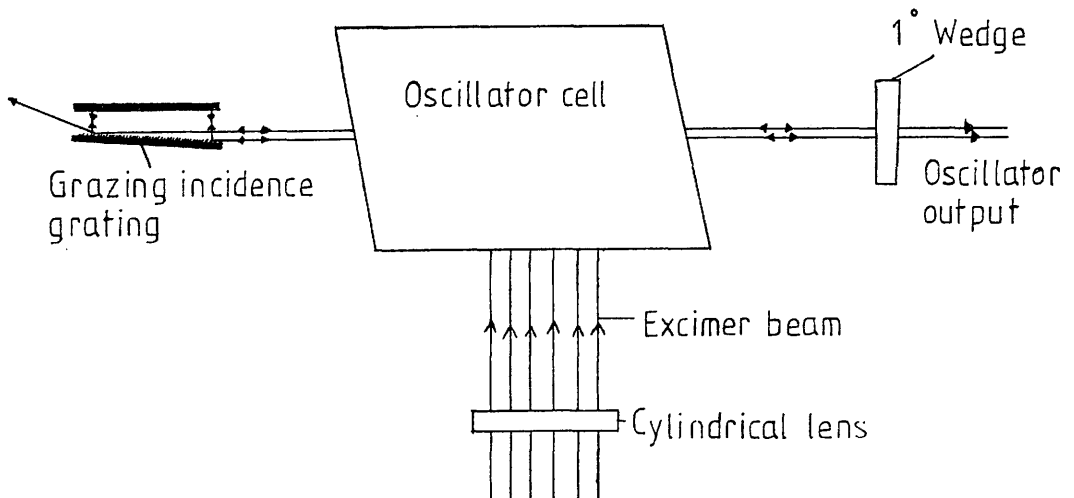
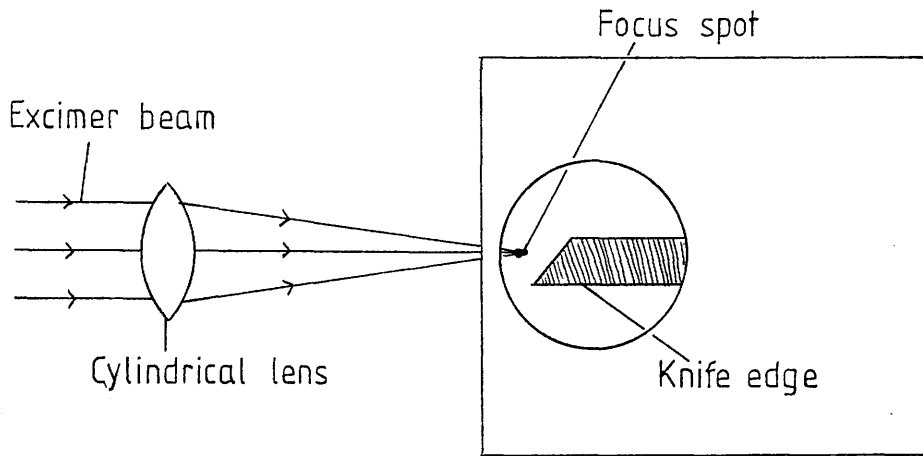
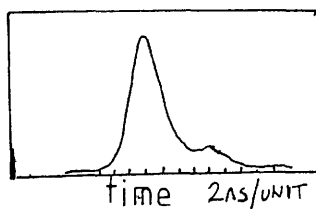


Figure: 3-10 Temporal profile of the Excimer laser.



Wavelength tuning is provided by a grazing incidence grating and a reflecting mirror, M_6 , which has fine angular control. The grating has 2400 lines per millimetre and the light is incident at a grazing angle of 85° to the normal of the grating. Using a fixed angle grating means that the illumination of the grating is over a fixed number of grooves. This results in only a very small variation of the linewidth for different wavelengths. At best the linewidth is 0.003nm. An output coupler, M_5 , with a 1° wedge forms the rest of the oscillator cavity.

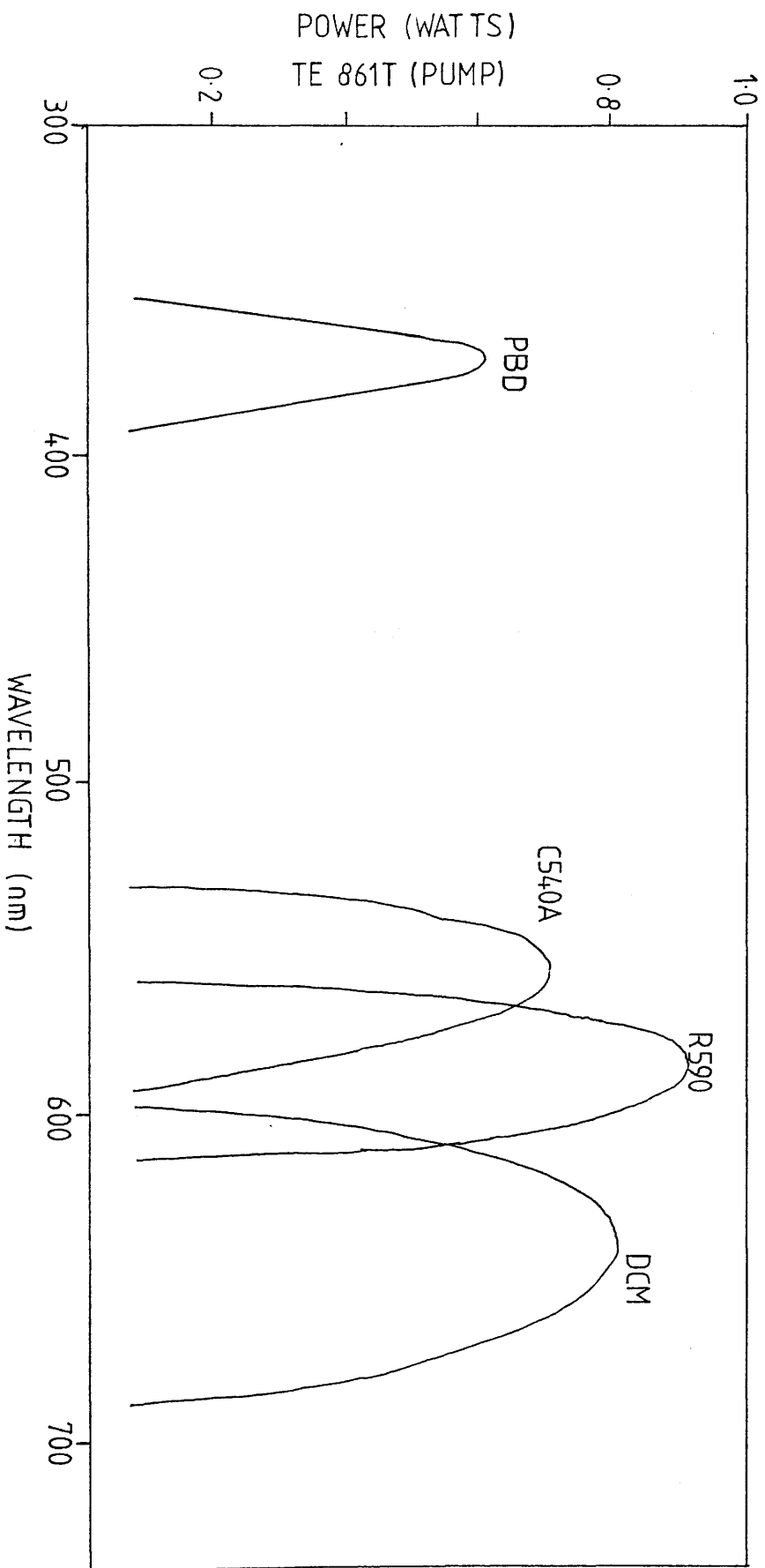
A percentage of the light from the excimer laser is used to optically pump the dye in the amplifier cell. Laser light from the oscillator then passes through the optically excited dye. By stimulated emission the oscillator beam is amplified. Amplification of the laser light outside the oscillator region reduces ablation damage to the delicate grating.

The output of the dye laser has, in general, a resolution of 0.03nm or better and a temporal intensity profile which, because of the high pumping rate, follows the temporal profile of the excimer laser (see figure 3-10). The specifications of the laser are given in table 3-3.

THE DYES.

Coumarin 540A, Rhodamine 590 and DCM dyes were used to cover the spectral range between 520nm and 680nm. PBD covered the range between 358nm and 386nm. The table below gives more information on the dyes. For the full names of these dyes refer to Maeda (1984).

Figure: 3-11 Dye tuning curves.



LASER DYE	LASING MAXIMUM (nm)	WAVELENGTH RANGE (nm)	SOLVENT	CONCENTRATION (molar x 10 ⁻³)
PBD	367	358-386	ETHANOL/ TOLUENE	4
C540A	550	521-605	METHANOL	2
R590	585	566-610	METHANOL	15
DCM	637	602-686	METHANOL	10

Figure 3-11 shows the tuning curves for the dyes .

THE DOUBLING CRYSTALS.

Interaction between the electric field of a light wave and a dense medium, such as glass or crystal, induces dipoles within the material. The induced dipole per unit volume, P, is given by:

$$P = \chi E$$

3-1

Where χ is the polarisability, and is a property of the material. E is the electric field strength of the light. Induced dipoles oscillate with the same frequency as the original wave, but not necessarily with the same phase. The dipoles themselves induce radiation at their oscillation frequencies. As light travels through a medium it will interfere with the dipole induced light. The effect of the interference is an apparent reduction in the velocity of the wave front by a factor n, the refractive index of the medium. The magnitude of the velocity reduction is a function of the original wave frequency.

Equation 3-1 above, is true for most cases, but in very intense electric fields (produced in laser beams), P is no longer proportional

to E. The induced dipole moment per unit volume must then be written in the form:

$$P = X_1 E + X_2 E^2 + X_3 E^3 + \dots \quad 3-2$$

where X_2 and X_3 are called the non-linear polarisabilities. For an incident field of the form $E = A \sin \omega t$, using $\cos \omega t = 1 - 2 \sin^2 \omega t$ and $3 \sin \omega t - 4 \sin^3 \omega t = \sin 3 \omega t$ equation 3-2 is obtained:

$$P = X_1 A \sin \omega t + 1/2 X_2 A^2 - 1/2 X_2 A^2 \cos 2 \omega t - 1/4 X_3 A^3 \sin 3 \omega t + \dots \quad 3-3$$

Non-linear polarisabilities are dependent on the polarisation of the electric field and the optical axis of the crystal. The $2 \omega t$ and $3 \omega t$ terms represent dipole moments per unit volume induced in the medium with oscillation frequencies two and three times the original wave frequency.

SECOND HARMONIC GENERATION (FREQUENCY DOUBLING).

Figure 3-12 gives a schematic diagram of second harmonic generation in a medium. The direction of propagation is in the z direction and the initial length of the material is l. The second harmonic radiation, dE , generated in a slab of material of width dz at a position z is given by:

$$dE^{(2)}(z) \propto P^{(2)}(z) dz \quad 3-4$$

$P^{(2)}(z)$ is the dipole moment per unit volume produced at a frequency 2ω . From equation 3-2 it can be seen that $P^{(2)}(z)$ is proportional to the square of the intensity of the electric field, so:

$$dE^{(2)}(z) \propto e^{2i(k_1 z - \omega t)} dz \quad 3-5$$

Figure: 3-12 Schematic of second harmonic generation.

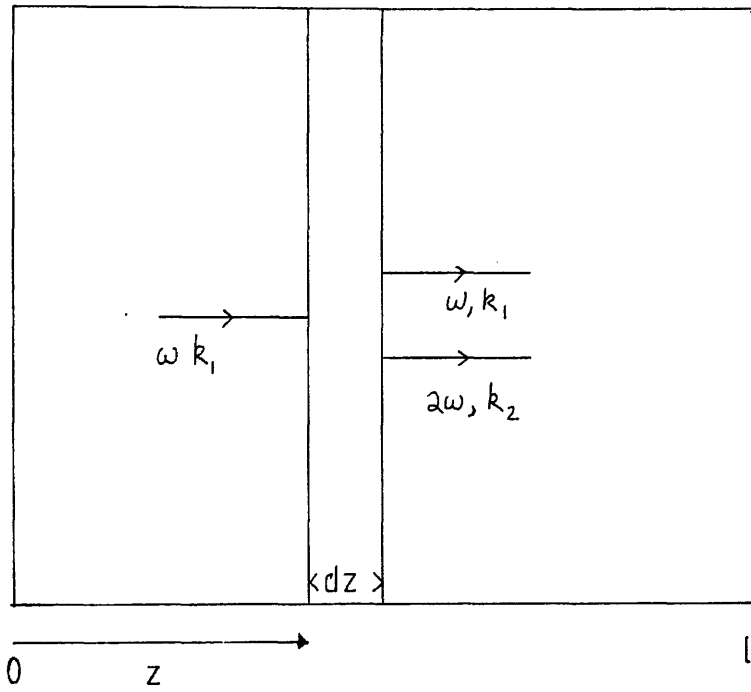
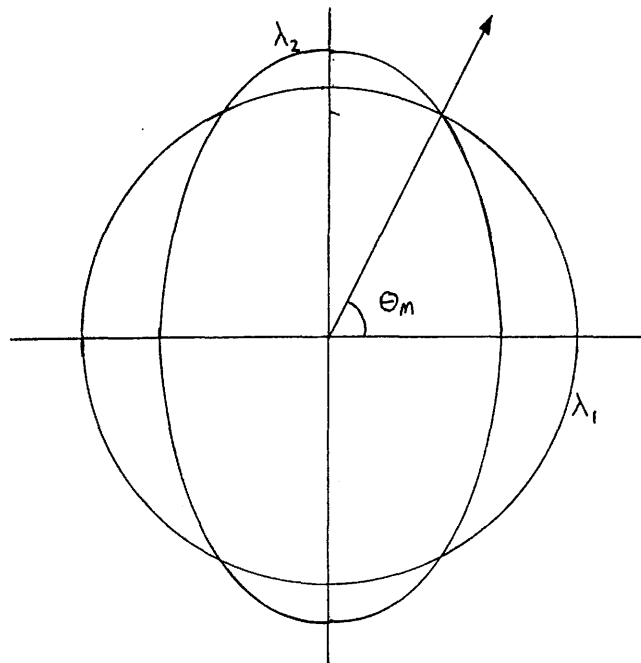


Figure: 3-13 Ray velocity diagram for KDP crystal.



The second harmonic polarisation has a wavenumber $2k_1$ and a frequency 2ω associated with it. Second-harmonic radiation induced by the dipole oscillations will not have a wavenumber of $2k_1$ because of dispersion, since $k_1 = 2\pi n_1/\lambda$. The second harmonic radiation will propagate with a wavenumber $k_2 \neq 2k_1$. The value of $dE^{(2)}(l)$ ($x=l$), for radiation initially produced at a slab located at z is given by:

$$dE^{(2)}(l) \propto dE^{(2)}(z) \cdot e^{ik_2(l-z)} dz \quad 3-6$$

where $\exp(ik_2(l-z))$ is a phase factor. Combining equations 3-5 and 3-6 gives:

$$dE^{(2)}(l) \propto e^{i(2k_1 - k_2)z} \cdot e^{i(k_2 l - 2\omega t)} dz \quad 3-7$$

This then integrates to give:

$$dE^{(2)}(l) \propto \sin(2\pi\Delta n l/\lambda) / (2\pi\Delta n/\lambda) \quad 3-8$$

where λ is the vacuum wavelength of the incident radiation and $\Delta n = n_2 - n_1$, n_2 and n_1 are the respective refractive indices of the second harmonic and incident radiation. When the argument of the sine is equal to $\pi/2$ or $l = \lambda/4\Delta n$ then $E^{(2)}(l)$ is maximised. l is sometimes called the coherence length of the second harmonic radiation and for ordinary materials is generally less than a few micrometres.

In crystals such as potassium dihydrogen phosphate (KDP) l can be quite large. For a KDP crystal the velocity of the incident ray is not a function of the crystal orientation (represented by a sphere in figure 3-13). The second harmonic radiation, on the other hand, does have an orientation dependent velocity of propagation. The second harmonic rays are called extraordinary rays (represented as a wave ellipsoid in figure

At certain orientations, the wave ellipsoid and wave sphere intersect (θ_m). At these orientations the propagation velocities, and therefore the refractive indices of the original and second harmonic rays are almost the same. In this orientation the rays are said to be phase matched. Phase matched rays can have quite large coherence lengths (a few centimetres), since $\Delta n = n_1 - n_2 \rightarrow 0$.

Using the principle of phase matching, the production of second harmonic radiation can become very efficient, say 15%-20% conversion for incident radiation at a power density of $100\text{MW}/\text{cm}^2$.

KDP doubling crystals were used to cover the wavelength range from 260nm to 335nm. The crystals, crystal mountings and automatic frequency tracking apparatus were supplied by Interactive Radiation Inc. (INRAD). At the time the experiments reported in this thesis were carried out, the automatic tracking facility in the INRAD system was inoperative. As a result the orientation of the KDP crystal was adjusted manually.

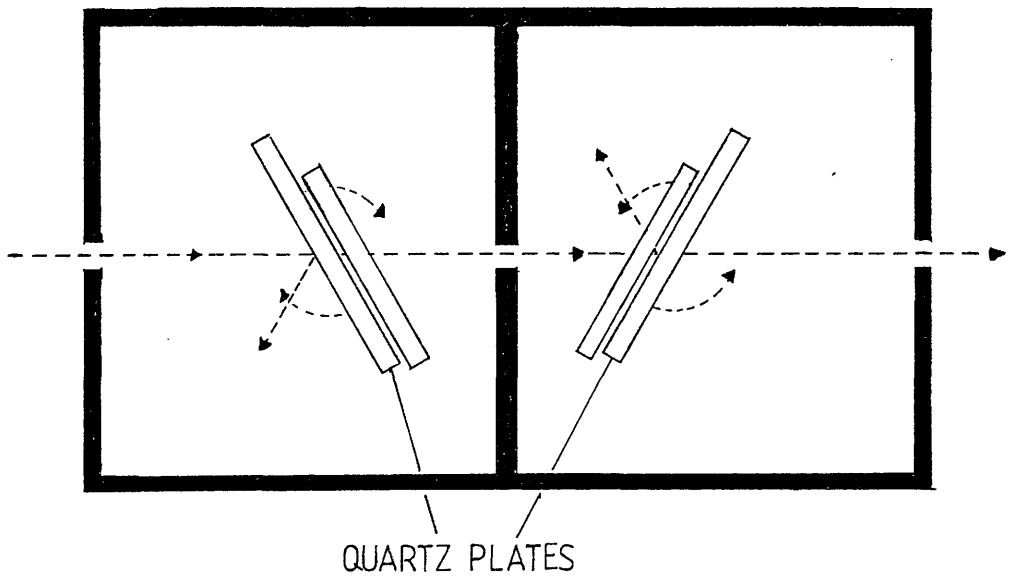
THE MEASUREMENT AND CONTROL OF THE LASER INTENSITY.

The pulse to pulse fluence of the laser was monitored with a Molelectron J3 pyroelectric joulemeter. The molelectron J3 is a calibrated fast response detector. Over the spectral range of 200nm to 700nm it has a voltage response of 2.47mV per μJ . The joulemeter is capable of measurement rates of 4KHz.

Where necessary the laser intensity was controlled by a NRC (Newport corporation) Model 935-5 variable attenuator (see figure 3-14). With this, the light could be attenuated by between 20% and 99.9%.

In principle its operation is very simple. The laser beam is passed through four inclined quartz plates. Part of the light is reflected and part transmitted. The amount of light transmitted is a

Figure: 3-14 The variable attenuator.



function of the angle of inclination of the plates to the laser beam. The transmission is controlled by varying the angle of the quartz plates. The relative positions of the plates removes displacements of the beam caused by refractive effects.

LASER SAFETY.

Light emitted by lasers is generally very intense and as a result can be hazardous in a number of ways. Care must always be taken to avoid looking directly into a laser beam. Different laser wavelengths can cause eye damage in different ways. UV light below 300nm can 'sunburn' the cornea and the skin. At longer wavelengths the light will be partially transmitted through the cornea where it will be absorbed in the lens. This can cause cataract or opacity of the lens. Visible and near-infrared radiation, up to 1400nm, is transmitted to the retina where it is focussed to a spot which can cause photochemical or thermal damage. Between 1400nm and 3000nm the radiation will penetrate the lens and may cause cataracts.

The lasers described in section 3-2 were all class IV, which produce dangerous levels of radiation even from diffuse reflections. Intense radiation from a class IV laser can also cause thermal damage to any solids in the beam path. This problem was observed for the fundamental 1060nm output of the Nd:YAG laser described earlier.

Personnel operating class IV lasers must wear appropriate safety goggles to filter out stray radiation. Class IV lasers must also be interlocked to avoid accidental exposure to unauthorised personnel entering a laser facility.

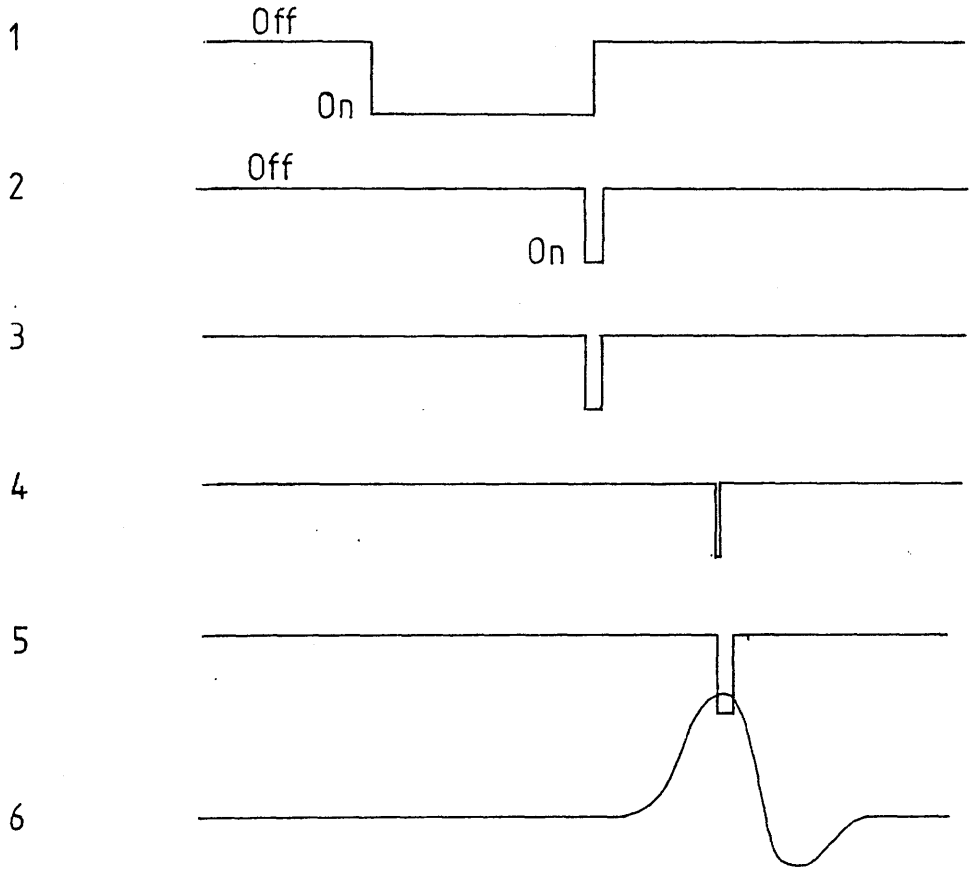
SECTION 3-3: THE ELECTRONIC ARRANGEMENT.

The signals from the joulemeter and proportional counter were measured simultaneously using a voltage sensitive analogue to digital convertor (ADC). The ADC had 7 channels with 11 bit resolution over a 2 volt dynamic range. A timing reference signal for gating the ADC was provided by directing a portion of the laser pulse down an optical fiber onto a photodiode.

The digitised signals were stored event by event on floppy disk and displayed on line in bidimensional and one dimensional histograms. Figure 3-15 shows the electronic arrangement used to produce the timing gate for the ADC. The gate generation is summarised below, with reference to figure 3-16.

- 1) The LSI-11 computer signifies readiness to accept data by switching on the gate generator with a NIM pulse from the output register.
- 2) The photodiode reference signal is passed through an octal discriminator.
- 3) 1 and 2 are fed into a coincidence unit. When both are ON a NIM pulse is generated. This stops the gate generator (1) and after adaption becomes the gate pulse.
- 4) Signal 3 is delayed about 4 μ s to coincide with the peak positions of the input signals to the ADC (6).
- 5) The gate is only 10ns wide after delaying. A gate generator extends this to 600ns, the operating width of the ADC.

Figure: 3-16 Summary of gate generation.



6) Input signals from the joulemeter and the proportional counter.

The output from 5 is also used to signify the end of an event. This pulse is delayed by more than 80 μ s to allow the ADC to make its conversion. Also 5 is passed through an octal discriminator to make it compatible with a NIM/TTL convertor. A TTL signal is needed to interrupt the LSI-11.

SECTION 3-4: THE PROPORTIONAL COUNTERS.

Many of the studies into laser ionisation of counter gases were carried out in single wire proportional counters filled with 10% methane 90% argon (P10) counter gas at 760torr.

A proportional counter gives a direct means of detecting electrons ejected by the laser ionisation of atoms or molecules. The basic properties of proportional counters are the same as those for MWPC's. A review of their operation was given by Sauli (1977).

Throughout experimentation the counter design was modified. This was to provide easier access for cleaning, or to cut down on the quantity of plastics, rubbers and resins incorporated in their construction. The modifications resulted in three types of counter.

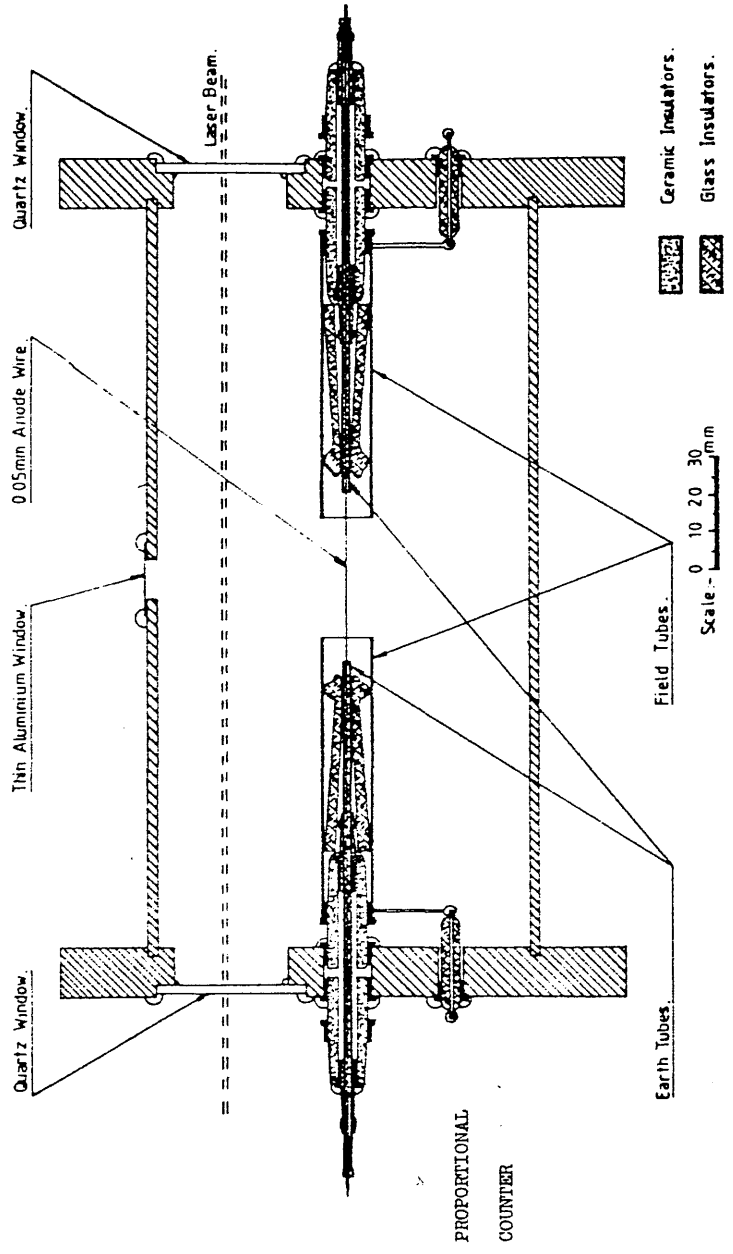
THE TYPE 1 COUNTER (SEE FIGURE 3-17).

The type 1 counter was used in early seeding experiments (see chapter 5) and for the first background laser ionisation spectra. It consists of an outer stainless steel casing 24cm long and 10cm in diameter. Stainless steel end plates were made vacuum tight by clamping them onto indium o-rings. The end plates provided support for the field correcting tubes, anode wire and electrical feedthroughs. These were insulated from the end plates and from each other by glass or ceramic insulators and were held rigidly in place with torr seal epoxy resin.

Wires carrying the high voltages were connected to the field tubes with soft solder joints. A 3cm gap between the field tubes in the centre of the counter provided the active collection region of the counter.

3cm diameter quartz windows allowed laser light at wavelengths

Figure: 3-17 The type 1 counter.



between 260nm and 670nm to pass parallel to the anode wire approximately 3cm above the active region. The windows absorbed <5% of the laser light at wavelengths between 260nm and 670nm.

A thin aluminium window directly above the active region allowed the transmission of soft x-rays into the counter. These were used to calibrate the counter.

Metallic surfaces in the counter were smoothed by rubbing them with fine emery paper. This reduced the surface area in contact with the counter gas reducing the amount of impurities desorbed from the surfaces into the counter gas. Gas inlets sealed with vacuum valves were placed at each end of the counter.

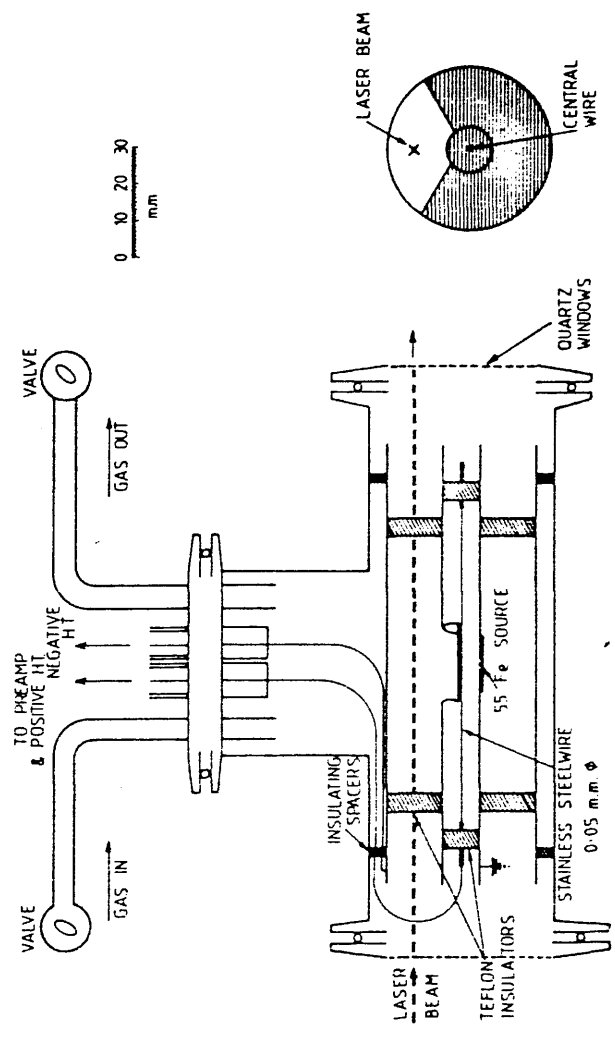
Operating volts were supplied by two high voltage power supplies. The anode wire was made earthy and the inner earth tubes were earthed. The optimum ratio for the volts on the casing and the field tubes were found to be 1.7:1.0. This gave the best resolution for Fe55 x-rays.

THE TYPE 2 COUNTER (SEE FIGURE 3-18).

The body of the type 2 counter consisted of a Dural T-piece. Stainless steel end plates sealed by viton o-rings were clamped onto the T-piece. The clamps were quick release, providing easy access into the counter. The T-piece acted only as a vacuum tight container for the counter proper.

The counter itself consisted of a 5cm diameter stainless steel field tube insulated from the T-piece by nylon screws. Inner field tubes were held at the centre of the outer field tube by teflon spacers. Further teflon spacers were used to hold the sense wire. High voltage feedthroughs supplied high volts to the counter. Electrical connections inside were made with teflon coated stainless steel wires clamped in place.

Figure: 3-18 The type 2 counter.



PROPORTIONAL COUNTER

A small hole bored through the inner field tube gave passage to Fe55 x-rays, which were used to calibrate the counter. A larger rectangular cut out of the inner field tube provided an active collection length of 2cm.

Gas and high volts were passed through the upper end plate of the T-piece. 3cm diameter quartz windows allowed the passage of laser light parallel to the wire axis. Care was taken that the laser beam did not strike insulator and field tube surfaces.

This counter, in contrast to the type 1 counter, had high volts on the sense wire, supplied through the bias of a preamplifier. The inner field tube was earthed and negative volts were placed on the outer tube.

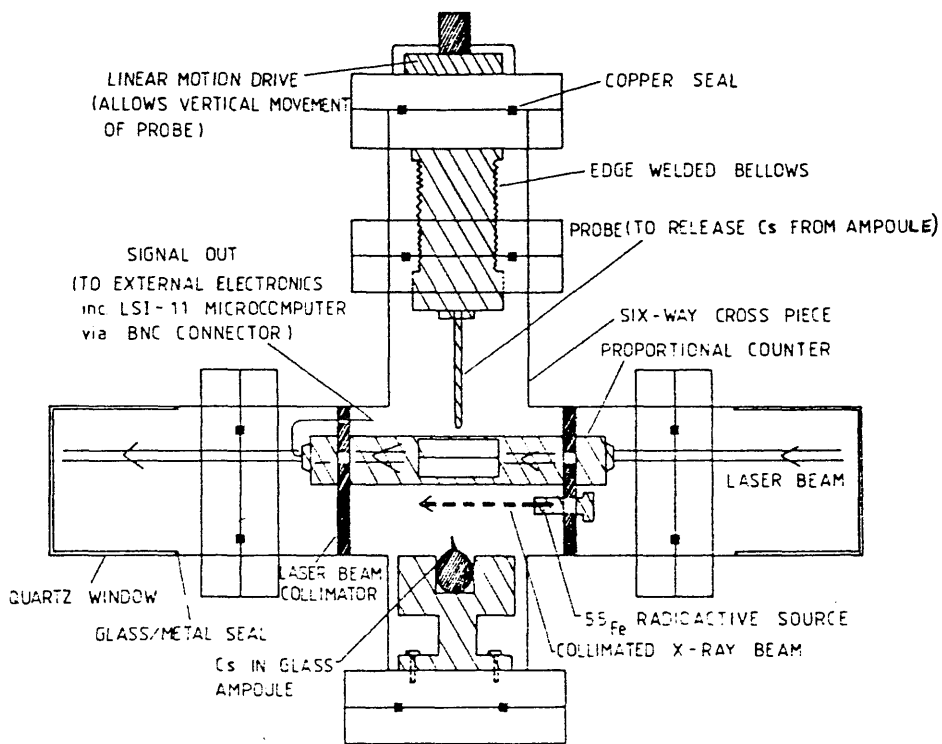
THE TYPE 3 COUNTER (SEE FIGURE 3-19).

The type 3 counter was designed for the study of the resonant MPI of alkali metal vapours. Alkali metals react rapidly with many of the impurities present in counter gases, such as oxygen, water and large organic molecules. To reduce this loss of alkali atoms the type 3 counter was constructed of high vacuum components only. These were composed of stainless steel, ceramics, glass, copper and viton. Viton was used as a seal in an Edwards valve. A cold trap was placed between the Edwards valve and the counter to avoid contamination of the alkali metal by any organic molecules the seal may have desorbed.

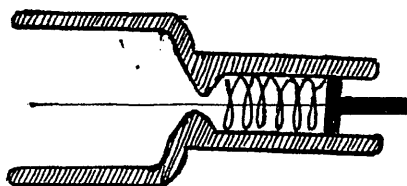
The vacuum tight chamber was built around a stainless steel 6-way piece. On two legs, vacuum tight quartz windows were placed, on the other legs, a sample holder, a linear drive and electrical feedthroughs.

The proportional counter was of the same design as that used in the type 2 counter, except, the spacers were made of glass instead of teflon. Tension on the sense wire was maintained by a coil spring

Figure: 3-19 The type 3 counter (caesium counter).



CAESIUM CHAMBER MARK 3 STAINLESS STEEL DESIGN



SPRING TENSIONING ARRANGEMENT

arrangement also shown in figure 3-19. Two metal plates were used to hold the counter in place. Imbedded into one of these was an Fe55 x-ray source used for the calibration of the counter. Two 5cm diameter holes through these plates allowed the passage of laser light 2cm above the active region of the counter. Light could not impinge directly on the sense wire.

SECTION 3-5: DESCRIPTION OF SEEDING AND UV SPECTROMETER APPARATUS.

Two methods were used for adding controlled concentrations of seeding vapour to the proportional counter gas. For one method the seeding sample was held in a temperature controlled bath, while counter gas flowed over its surface. At low flow rates ($\sim 100\text{ml}/\text{min}$) the partial pressure of seeding agent in the counter gas remained close to its saturated vapour pressure value. Figure 3-20 shows the flow apparatus used for seeding by the flow method.

Some seeding experiments were carried out by the static seeding method. This involved filling an evacuated proportional counter with a small amount of seeding agent. The counter was then filled to 760torr with argon methane counter gas and sealed. The apparatus required for the static fill method is shown in figure 3-21. The pressure of the seeding agent was monitored on an MKS Baratron.

The MKS Baratron Model 90 measures the differential pressures on two sides of a taut metal membrane. Two insulating discs support capacitive electrodes. Different pressures on each side of the membrane displace the membrane. The displacement is measured from the resulting change in the capacitance of the capacitors.

The dynamic range of the Baratron is from 10^{-5} to 1000torr with an accuracy of $\pm 0.05\%$.

Experiments were carried out to determine both the saturated vapour pressure and the vapour phase UV spectrum for several seeding agents. Vapour pressures were measured on the Baratron using apparatus similar to that depicted in figure 3-21. UV spectra were obtained from a Beckmann UV Spectrophotometer using vapour samples held inside a Hellma 10cm quartz spectrometer cell.

The Beckman Spectrophotometer U.V. 5270 has double and single beam recording. A double monochromator gives a resolution of better

Figure: 3-20 The flow apparatus.

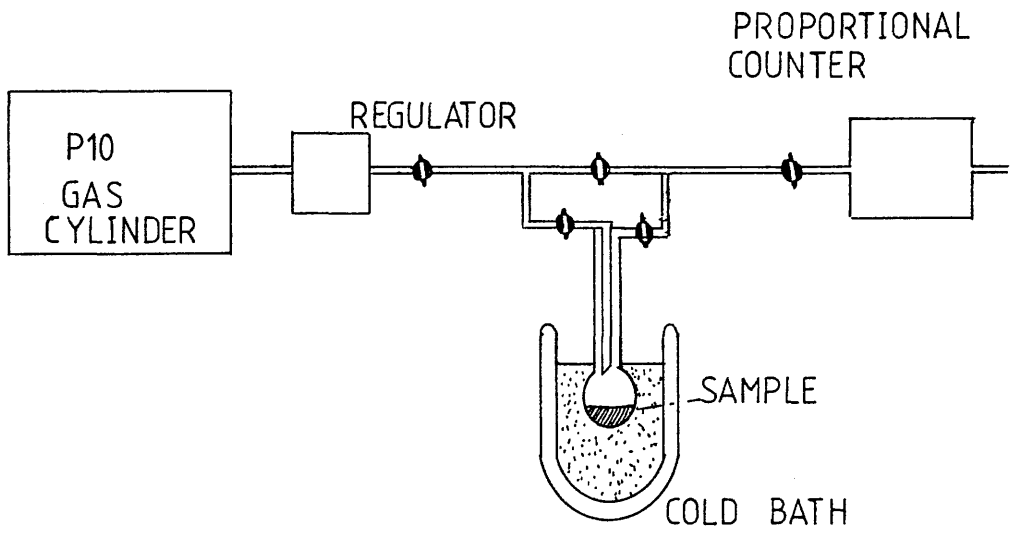


Figure: 3-21 The static fill apparatus.

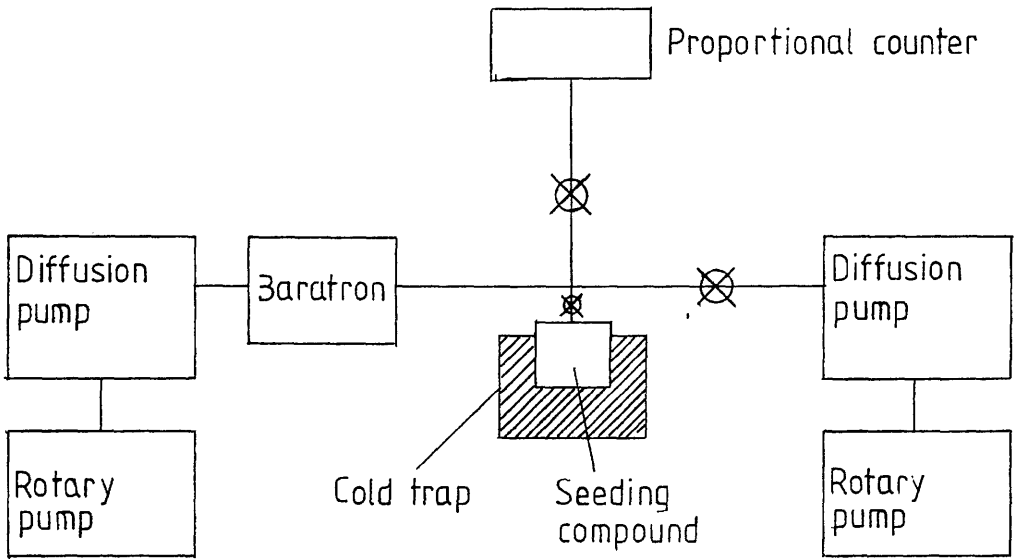
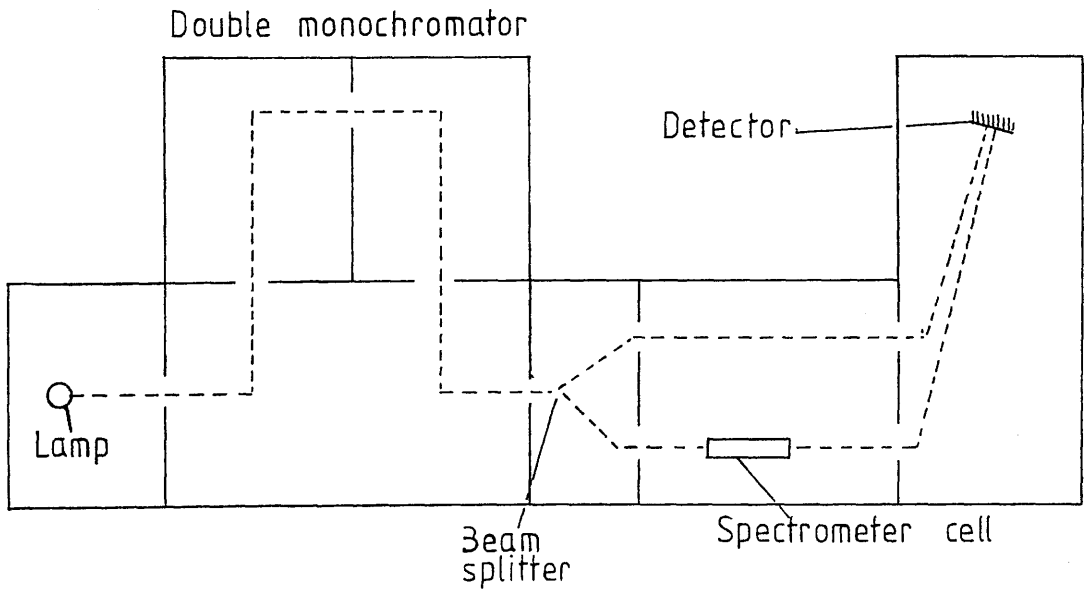


Figure: 3-22 The UV spectrometer.



BECKMAN[®] UV SPECTROPHOTOMETER

than 0.05nm between 190nm and 800nm with a wavelength accuracy of ± 0.1 nm. Stray radiation noise is $< 0.001\%$. A deuterium lamp gave a UV output between 190nm and 350nm. Figure 3-22 gives a schematic diagram of the UV Spectrophotometer.

SECTION 3-6: THE QUADRUPOLE MASS SPECTROMETER.

A quadrupole mass spectrometer was used for the analysis of proportional counter gas by resonant ionisation mass spectroscopy. Laser induced fragmentation spectra were also taken with this system.

The basic operating principle of the quadrupole mass spectrometer is given by the Mathieu equations. These equations of motion describe the trajectories of ions moving through two fields produced by a direct current (DC) modulated by a radiofrequency (RF).

The quadrupole is made up of four steel bars each positioned on the corner of a square. A DC and RF potential of positive sign is placed on two diametrically opposing bars while potentials of the same magnitude but opposite sign are placed on the other two bars (see figure 3-22). This constitutes the quadrupole filter.

An accelerated particle entering the filter will begin to oscillate in RF-DC field in a manner which is both dependent on its charge to mass ratio, m/e , and the RF/DC ratio. (Typical ion trajectories are depicted in figure 3-23). For every value of these ratios only one ion mass can pass through the filter to impinge on the collector. Other ion masses will have trajectories of greater periodicity. They hit the quadrupole bars where they are discharged. By variation of the RF/DC ratio single values of m/e can be chosen. A typical quadrupole has a resolution of 1000.

The quadrupole mass spectrometer, used in the experiments described in chapter 8, was a V.S.W. Mass Analyst with a mass range of 0-200AMU. It comprises an ion source, ion focussing optics, quadrupole filter and two detectors (see figure 3-24, this figure also shows the position of the sample inlet nozzle used in some experiments). Adjustments to the operating voltages and currents could be made, and measured, by the control system for the quadrupole

Figure: 3-23 The quadrupole filter.

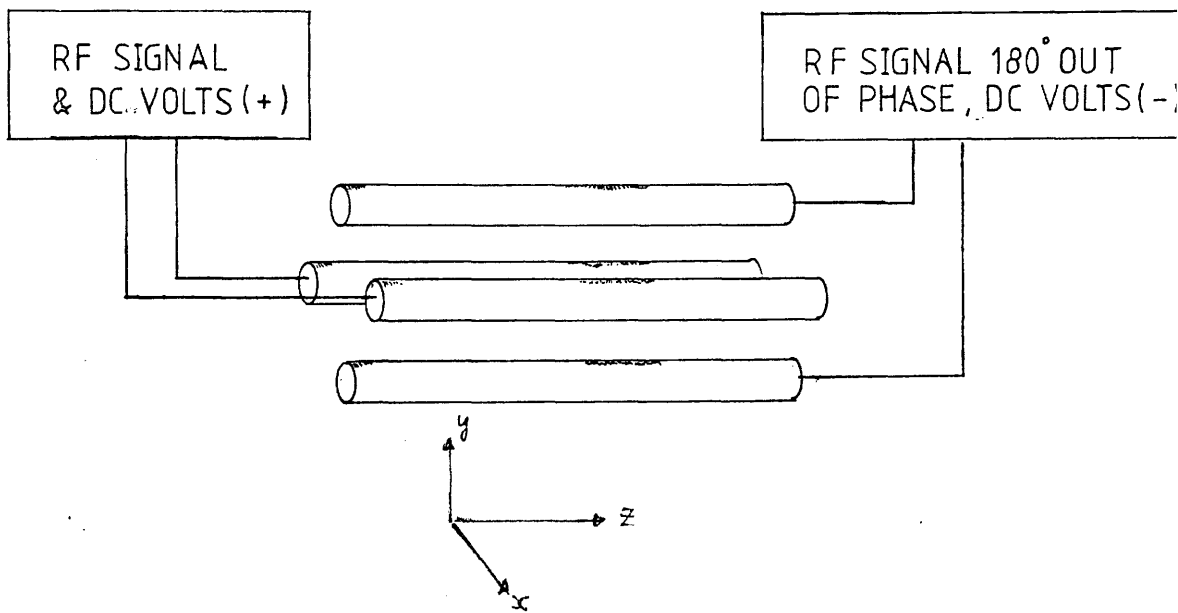
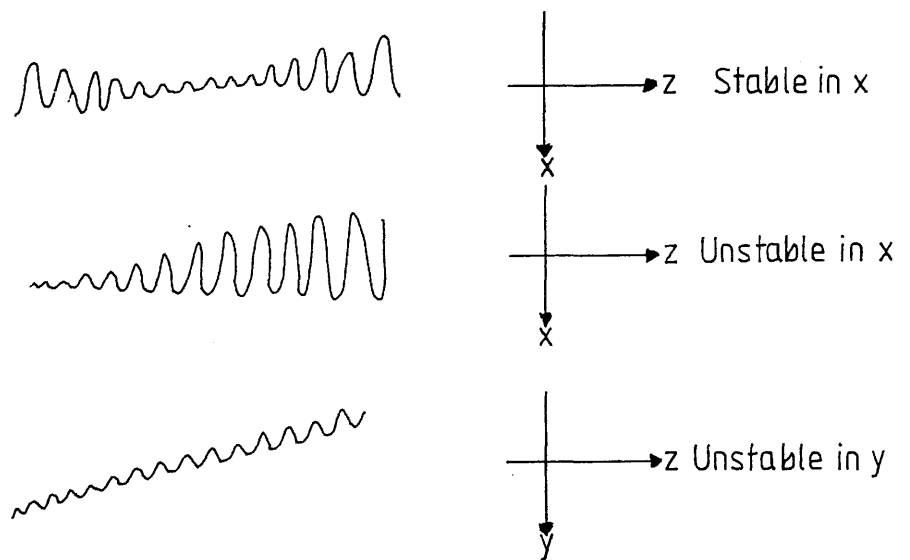


Figure: 3-24 Typical ion trajectories in a quadrupole filter.



Ions in the ion source could be produced in two ways, either by electron bombardment or laser ionisation. A hot wire filament provided a source of electrons. Ports were cut through the ion source to allow the passage of laser light.

Three electrodes accelerated and focussed ions before they passed into the quadrupole filter. Ions transmitted through the filter were detected either by a Faraday detector or a secondary electron multiplier (SEM). The Faraday detector is simply a metal plate upon which the ions impinge. When using electron bombardment the currents detected are small (10^{-8} A to 10^{-15} A). A sensitive amplifier is used before displaying the current signal.

The SEM was mounted off the centre line of the filter axis to reduce unwanted noise from neutral particles. Ions hitting the entrance of the SEM produce an avalanche of secondary electrons. The SEM is a Galileo 4771 dynode electron multiplier (Channeltron) (see figure 3-25). It has a gain range between 10^3 and 3×10^6 and at high gain should be capable of single ion detection. In electron bombardment mode the output from the SEM is DC and must be amplified with a current amplifier before display. The signal from the SEM induced by laser ions are pulsed, it is therefore better to use a charge amplifier.

While in use as a laser ionisation mass spectrometer the filament current had to be switched off. Unfortunately the mass spectrometer control system was designed to handle DC signals from a current amplifier. This meant that the signals from the charge amplifier had to be analysed on the electronic apparatus described in section 3-3. Figure 3-26 shows the electronic arrangement of the mass spectrometer when set up for laser ionisation.

Figure: 3-25 Diagram of quadrupole mass spectrometer.

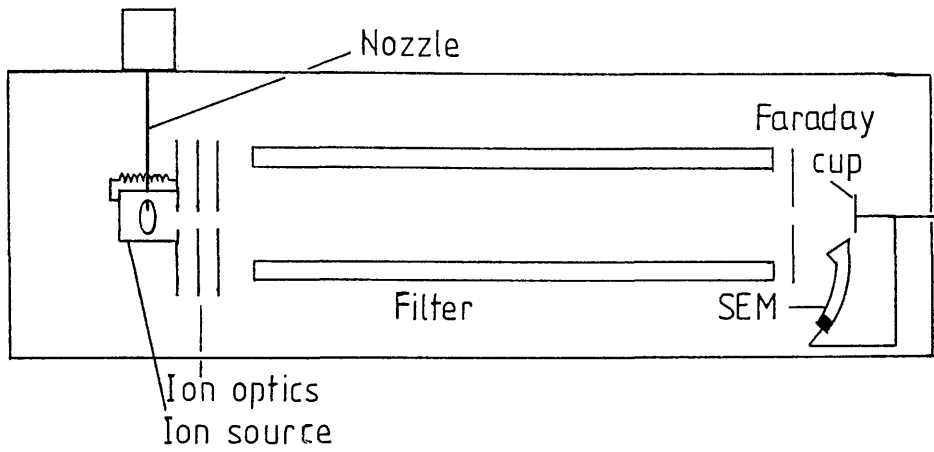


Figure: 3-26 The channeltron SEM.

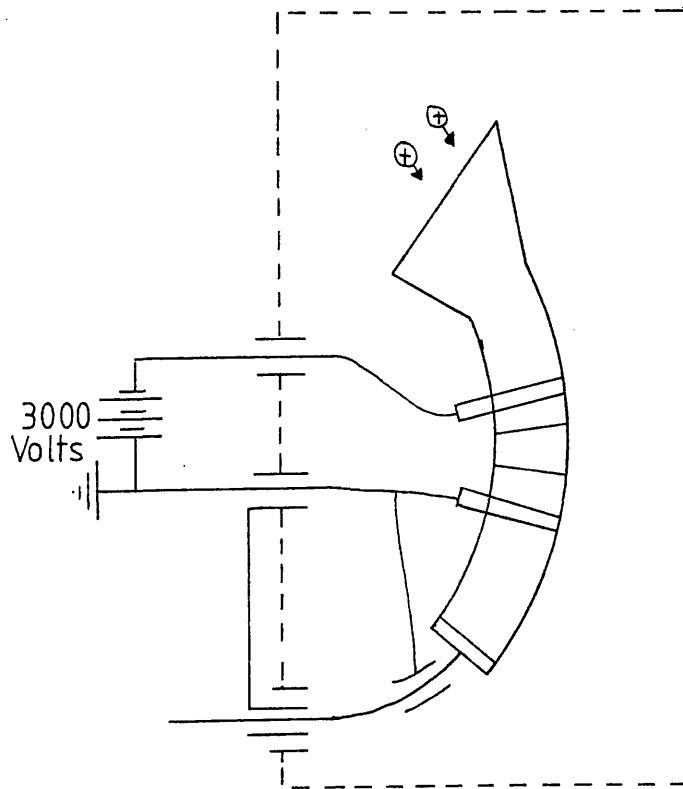


Figure: 3-27 Electronic apparatus for the mass spectrometer.

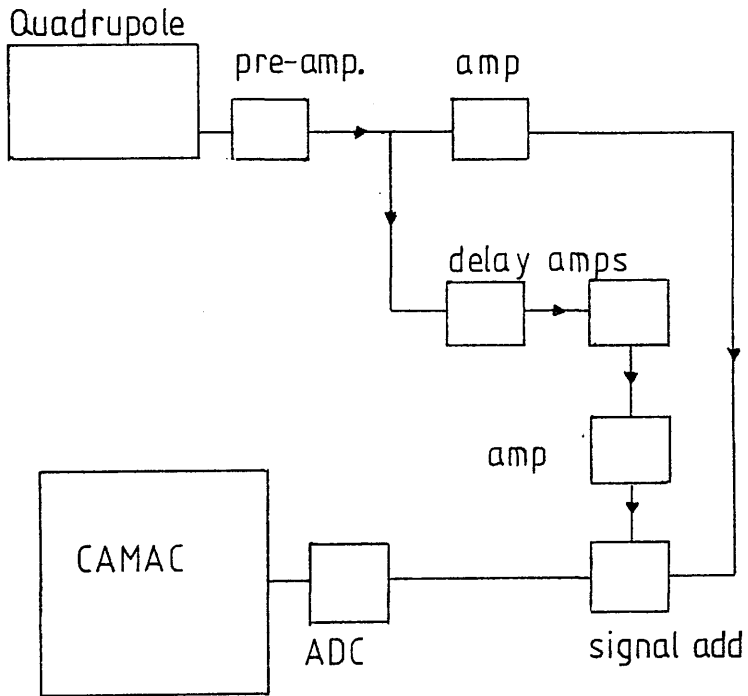


TABLE 3-1: SPECIFICATIONS OF THE N₂ LASER.

LUMONICS SERIES TE-860-3	EXCIMER LASER
TE-86 1M	THYRATRON SWITCHED
WAVELENGTH	337nm
MAX REPETITION RATE	80 pps
AVERAGE POWER	0.2Watts at 50pps
MAXIMUM PULSE ENERGY	7mJ
PULSE WIDTH (FWHM)	4ns
BEAM CROSS-SECTION	10x20mm ²
BEAM DIVERGENCE	Not Measured.
PULSE TO PULSE REPRODUCIBILITY	± 5%

TABLE 3-2: SPECIFICATIONS OF THE XeCl EXCIMER LASER.

LUMONICS TE-860-3	EXCIMER LASER
TE-86 1M	THYRATRON SWITCHED
WAVELENGTH	308nm
MAX REPETITION RATE	80 pps
AVERAGE POWER	5Watts at 65pps
MAXIMUM PULSE ENERGY	80mJ
PULSE WIDTH (FWHM)	10ns
BEAM CROSS-SECTION	8x12mm ²
BEAM DIVERGENCE	2.4x6mR
PULSE TO PULSE REPRODUCIBILITY	± 3%

TABLE 3-3: DYE LASER SPECIFICATIONS.

LUMONICS EPD-330	DYE LASER
TUNING RANGE	320-950nm
MAX AVERAGE POWER	1.2watts (~12% Efficiency)
LINE WIDTH STANDARD	0.003nm (320-730nm)
MAX PULSE WIDTH	6ns
SPECTRAL PURITY	>99%
AMPLITUDE STABILITY	± 3%
BEAM DIAMETER	1x2mm ² Typical
BEAM DIVERGENCE	<1mR (full angle)
POLARIZATION	>95% Vertical
WAVELENGTH ACCURACY	± 0.5nm
WAVELENGTH RESETABILITY	± 0.01nm
WAVELENGTH STABILITY	± 0.01nm

TABLE 3-4: LASER USED IN THE EXPERIMENTS DETAILED IN CHAPTER 4.

NAME	ABBREVIATED NAME	WAVELENGTH (nm)	PULSE DURATION. (ns)
XENON CHLORIDE EXCIMER.	XeCl	308	10
XENON FLUORIDE EXCIMER	XeF	351	14
KRYPTON FLUORIDE EXCIMER	KrF	249	16
ARGON FLUORIDE EXCIMER	ArF	193	14
NITROGEN	N ₂	337	0.5
NEODYMIUM:YTTRIUM- ALUMINIUM GARNET	Nd:YAG	1060	25
	Nd:YAG	530 (Doubled)	25
	Nd:YAG	355 (Tripled)	25
	Nd:YAG	266 (Quadrupled)	25
DYE LASER		494	6

CHAPTER 4

LASER IONISATION WITH DIFFERENT LASERS.

SECTION 4-1: INTRODUCTION.

As described in chapter 2-2, lasers suitable for laser calibration of MWPC's must have a short pulse duration (~ 10 nsecs), a low beam divergence, stable outputs and must produce ionisation levels not strongly dependent on laser fluence. The ion track produced by the laser will then be well defined in space and time, giving accurate calibration of the counter.

Low divergence for most lasers can be obtained with the appropriate choice of optics inside and outside the laser cavity. However, imperfections in the optics and diffraction effects mean that the laser must diverge to some extent. As a result there will always be a variation in the spatial and temporal cross-sections of the laser beam as a function of position in the MWPC. However, a small divergence is acceptable in cases where the ionisation has a weak dependence on laser fluence and the position of the track is measured from the 'centre of gravity' of the ion track. In unsaturated MPI processes with order $N \geq 2$ the ionisation yield is very strongly dependent on the divergence of the beam. Even beams with low divergence produce tracks showing large variations in ionisation intensity, making calibration more difficult.

Weak ionisation dependence on laser fluence shall be defined as a laser ionisation process which has a squared, or less than squared, dependence on laser flux. A weak dependence can be achieved in one of two ways: by a single or two-photon ionisation process; or by saturation of a higher order MPI process. Therefore in principle any laser with

a short pulse duration and stable output could be used for laser calibration.

A study was made of the ionisation intensities and properties of a variety of lasers with output wavelengths between 193nm and 1060nm. A 30cm quartz lens was used to focus the beams into the centre of a type 1 proportional counter. Log/log plots of ionisation versus laser fluence were drawn for some of the laser outputs giving some indication as to the order, N , of the MPI process. The results are summarised in the table below.

TABLE 4-1 LASER IONISATION PRODUCED BY A VARIETY OF LASERS.

LASER TYPE	OUTPUT WAVELENGTH (nm)	PULSE DURATION (ns)	PULSE ENERGY (mJ/mm ²)	LASER INDUCED IONISATION (IP/cm)	LOG/LOG PLOT
Nd:Glass	1060	25	1500	20	fig 4-1
Nd:Glass	530	25	150	1.5×10^4	fig 4-2
Nd:Glass	350	25	7.4	1.1×10^4	
Nd:Glass	266	25	0.05	1.2×10^5	fig 4-3
N ₂	337	0.5	0.14	505	
XeCl	308	6	0.5	8.5×10^6	fig 4-4
KrF	249	16	0.05	8.5×10^5	
AF	193	14	0.05	1.1×10^7	fig 4-5
Coumarin 307 dye	494	6	6.3	600	fig 4-6
XeF	351	14	20	6.5×10^5	

Figure: 4-1 Attenuation curve for the Nd:Glass at 1060nm.

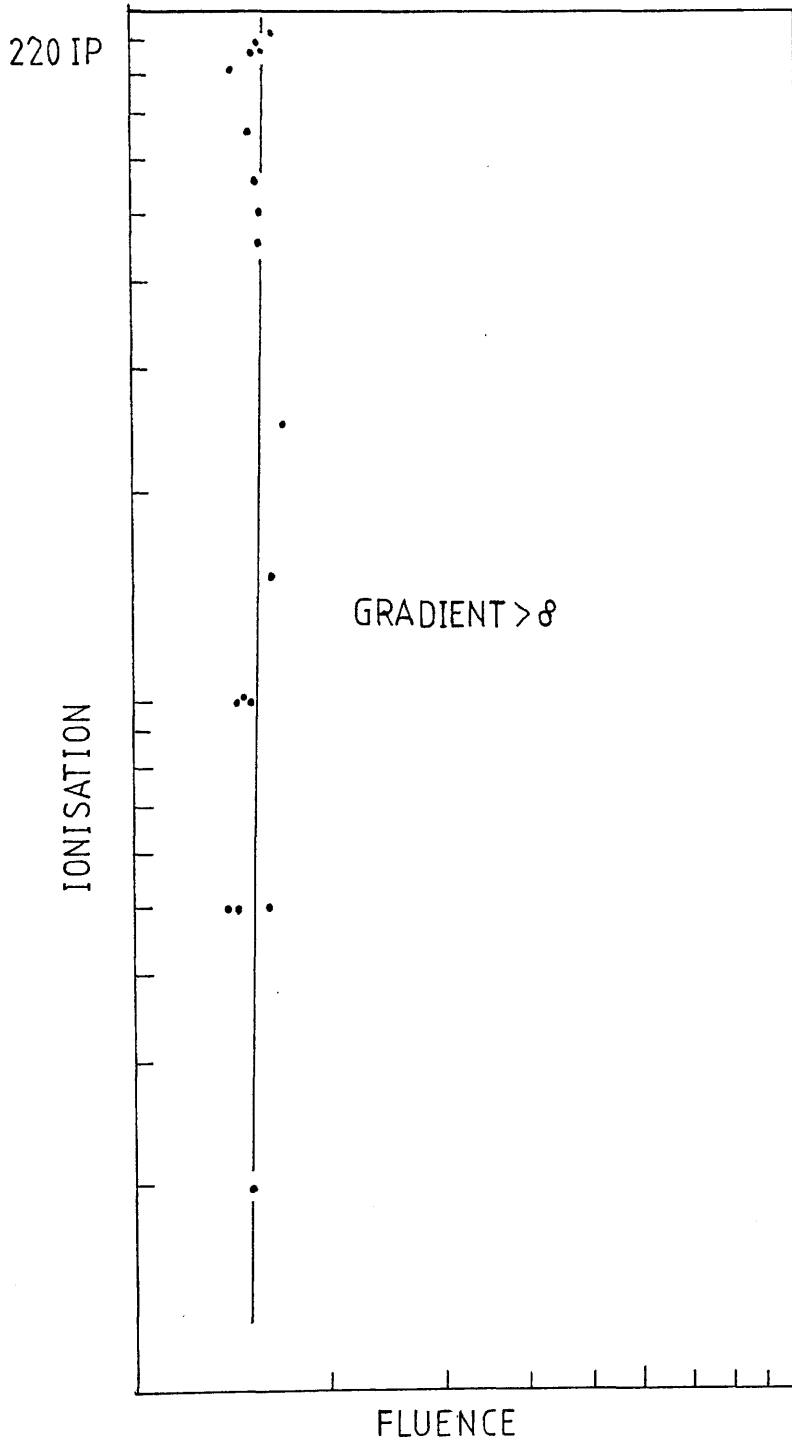


Figure: 4-2 Attenuation curve for the Nd:Glass at 530nm.

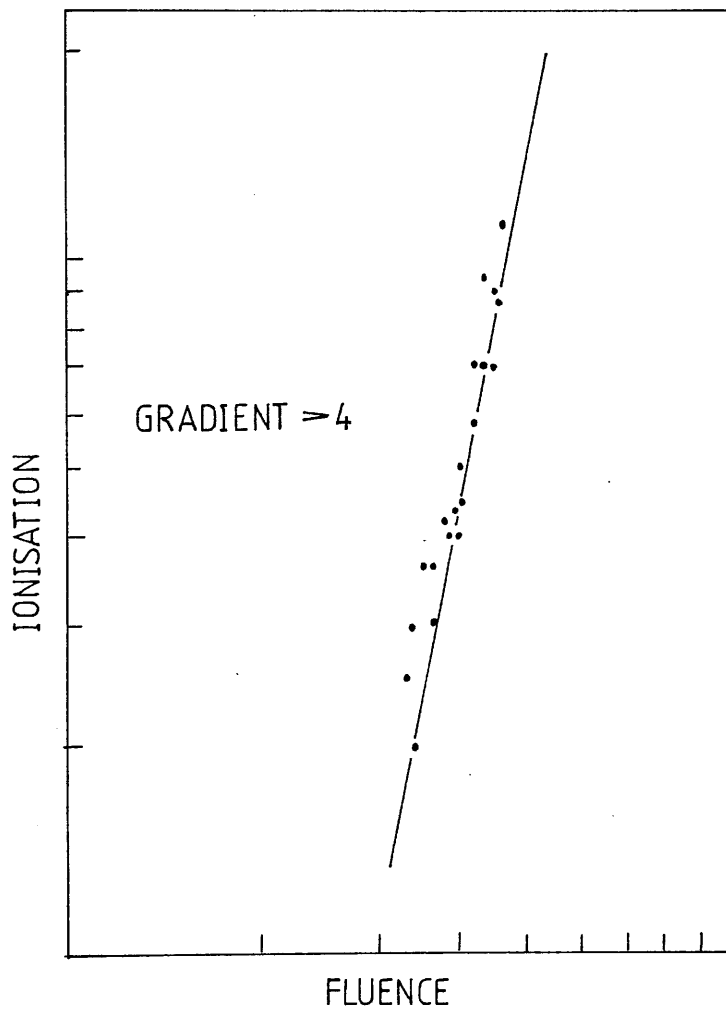


Figure: 4-3 Attenuation curve for the N₂ laser.

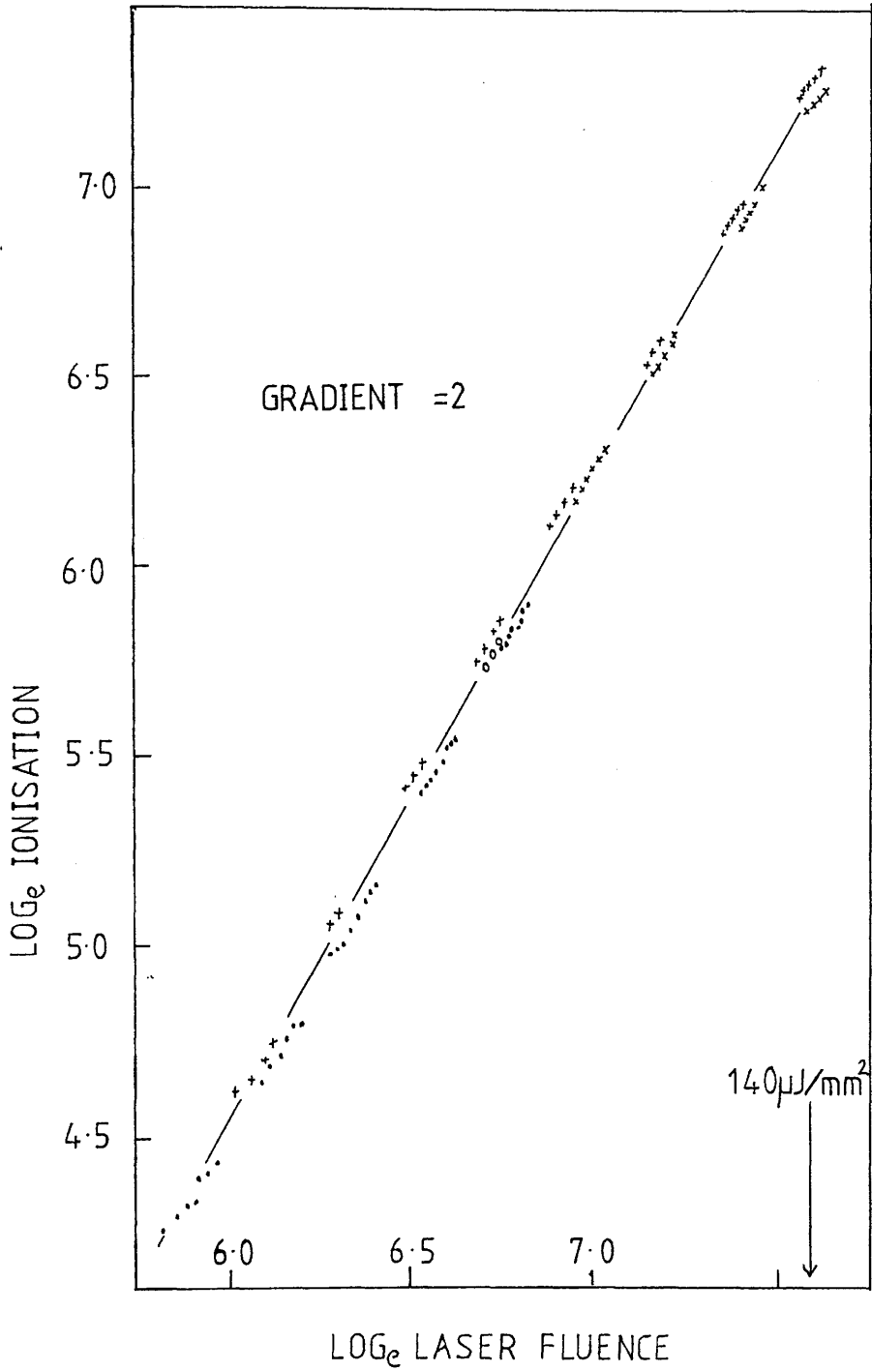


Figure: 4-4 Attenuation curve for the KrF laser.

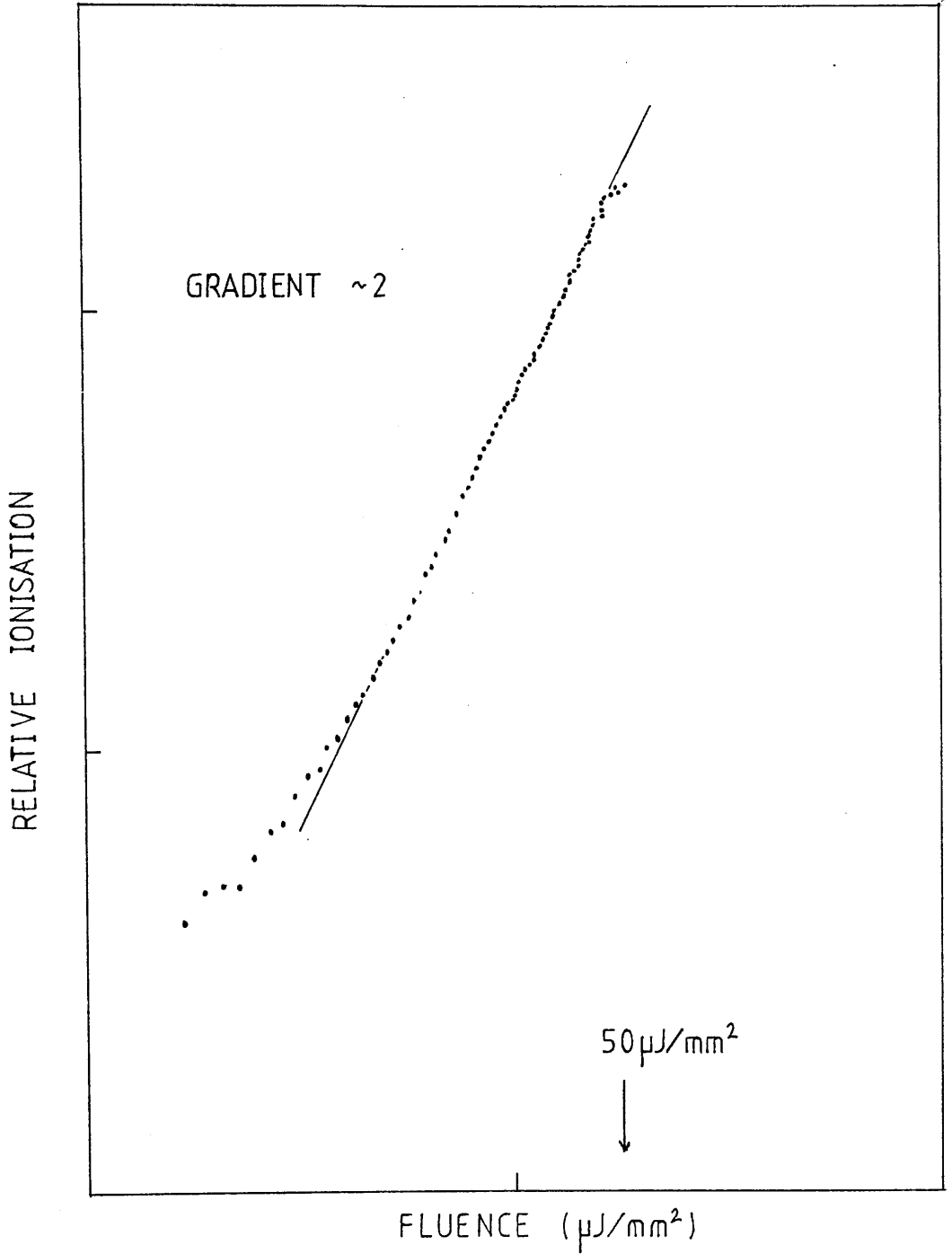


Figure: 4-5 Attenuation curve for the AF laser.

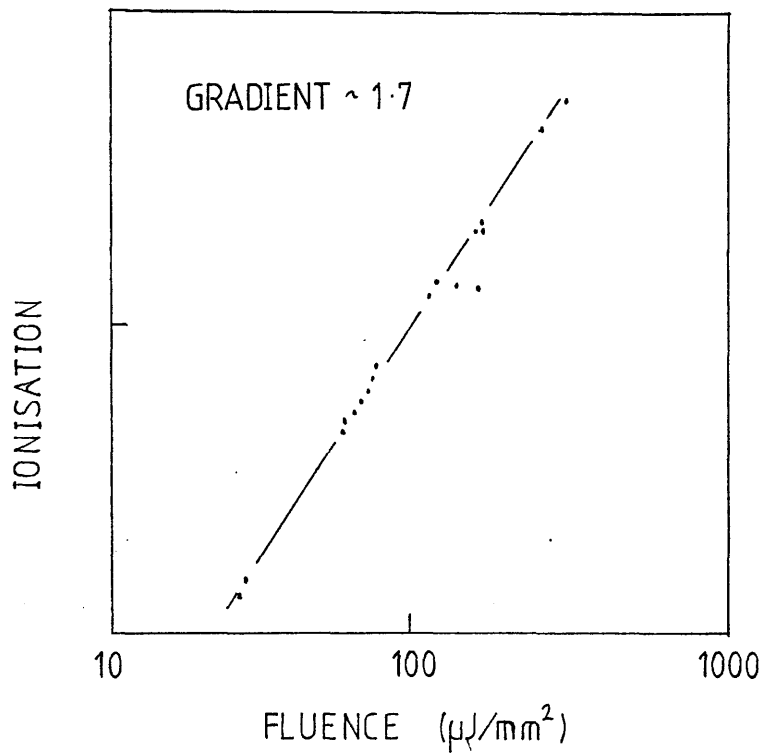
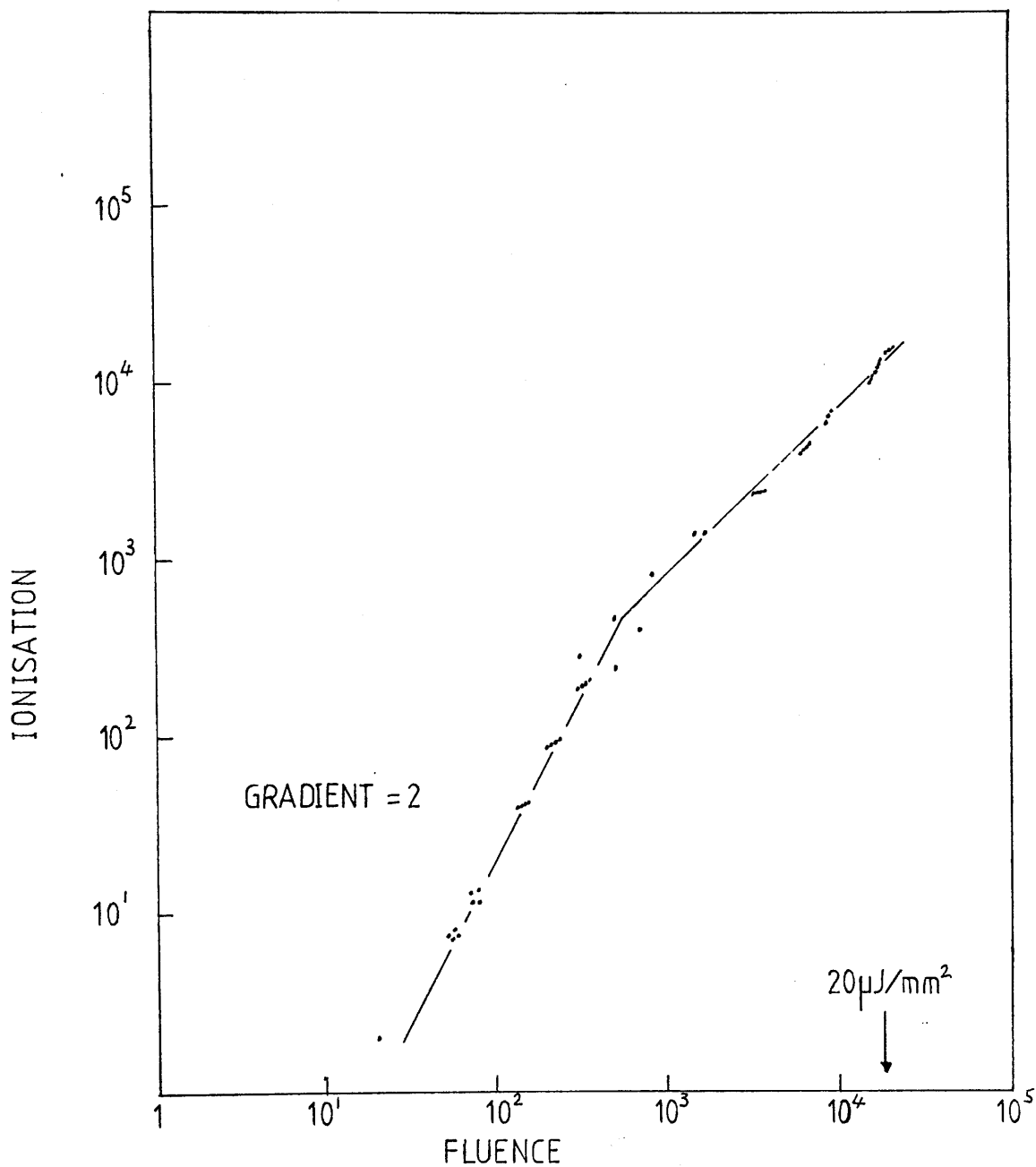


Figure: 4-6 Attenuation curve for the XeF laser.



SECTION 4-2: RESULTS AND DISCUSSION.

As the wavelength of the laser increases the order N of the MPI process increases. The value of N is characterised by the gradients of the log/log plots of ionisation versus laser fluence. For instance at 1060nm and 266nm the gradients of the log/log plots were ≥ 8 and 2 respectively. This indicates that the orders of the MPI processes in each case were $N \geq 8$ and $N=2$ respectively.

At 1060nm, a fluence of over 1.5 J/mm^2 produced only 20IP/cm, but at 266nm, a laser fluence of only $50 \mu\text{J/mm}^2$ was sufficient to produce 10^5 IP/cm. This difference reflects the large decrease in the probability of ionisation occurring as the order of the MPI process increases.

At the fundamental Nd:Glass output of 1060nm a laser fluence of 1.5 J/mm^2 gives a gradient of ≥ 8 . For this laser to be used for calibration its fluence would have to be increased until the ionisation was strongly saturating. The Nd:Glass at this wavelength would require optics capable of withstanding high powers for long periods of time, and the adoption of stringent safety precautions to avoid injury to personnel or damage to sensitive equipment from stray laser light. These problems would be considerably reduced if the output frequency from the same Nd:Glass were quadrupled. At the 266nm quadrupled Nd:Glass wavelength the MPI process is 2-photon, giving it a quadratic dependence on laser fluence at low powers. At higher laser fluences the ionisation would increase to saturation and becomes independent of the laser fluence.

From table 4-1 it may be concluded that for wavelengths greater than 494nm the order of the MPI process is greater than 2. Thus, high fluences would be required to saturate the MPI process leading to problems in beam handling, as described previously for the Nd:Glass laser at 1060nm.

On the other hand, a laser of very short wavelength would need very low fluences to produce ion tracks (assuming single photon ionisation were possible). This would be advantageous, but problems still occur. Short wavelength lasers below 200nm are comparatively rare and tend to be gas filled excimer lasers with short working lifetimes and require frequent gas refills. In addition, the absorption of light in air and quartz glass windows becomes significant at wavelengths less than 200nm. These effects are illustrated in figures 4-7 and 4-8. These latter problems occurred with the 193nm output of the Argon Fluoride excimer laser where 60% of the light was absorbed by the windows of the counter. Thus there is a lower wavelength limit of about 200nm set for laser calibration purposes.

Between the AF laser output of 193nm and the 337nm output of the N laser the ionisation process was 2-photon (found from the gradients of the log/log plots). In this region an increase in ionisation was observed as the wavelength decreased (see table 4-1). It was found that, after quadratic normalisation to a laser fluence of 0.05mJ/mm^2 , the difference in the ionisation between the N_2 and AF outputs was nearly a factor of 10^5 .

Appendix 1 shows that the ionisation is not dependent on the pulse duration, T, when the laser fluence is low. Therefore the differences in pulse duration of the two lasers does not account for the difference in the ionisation levels.

There are at least two possible mechanisms which could explain this difference. If the impurities in the counter gas had wavelength dependent ionisation cross-sections or if the distribution of ionisation potentials of the impurities was weighted towards shorter wavelength, then more molecules would be ionised at shorter wavelengths. Figure 4-9 gives the ionisation potentials of a number of organic molecules listed in the Handbook of Chemistry and Physics (1986). A greater number of

Figure: 4-8 Absorption of UV light in quartz glass.

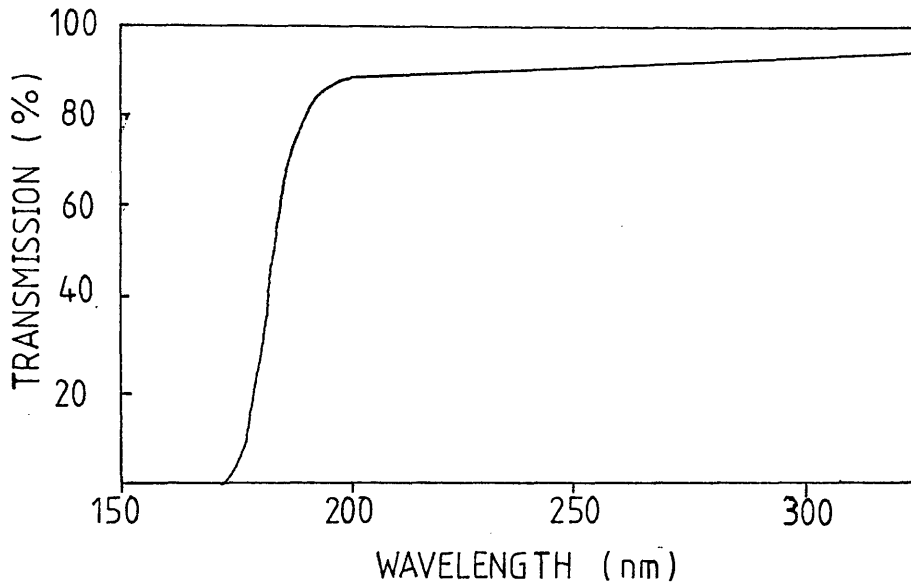


Figure: 4-7 Absorption of UV light in air.

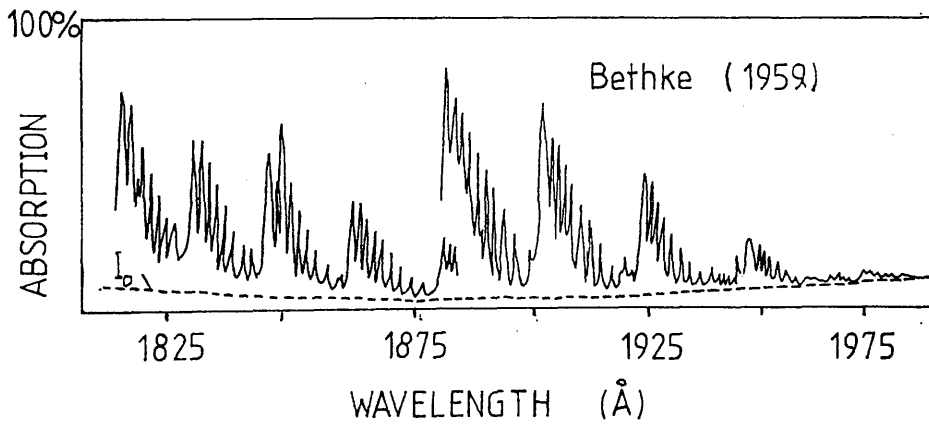
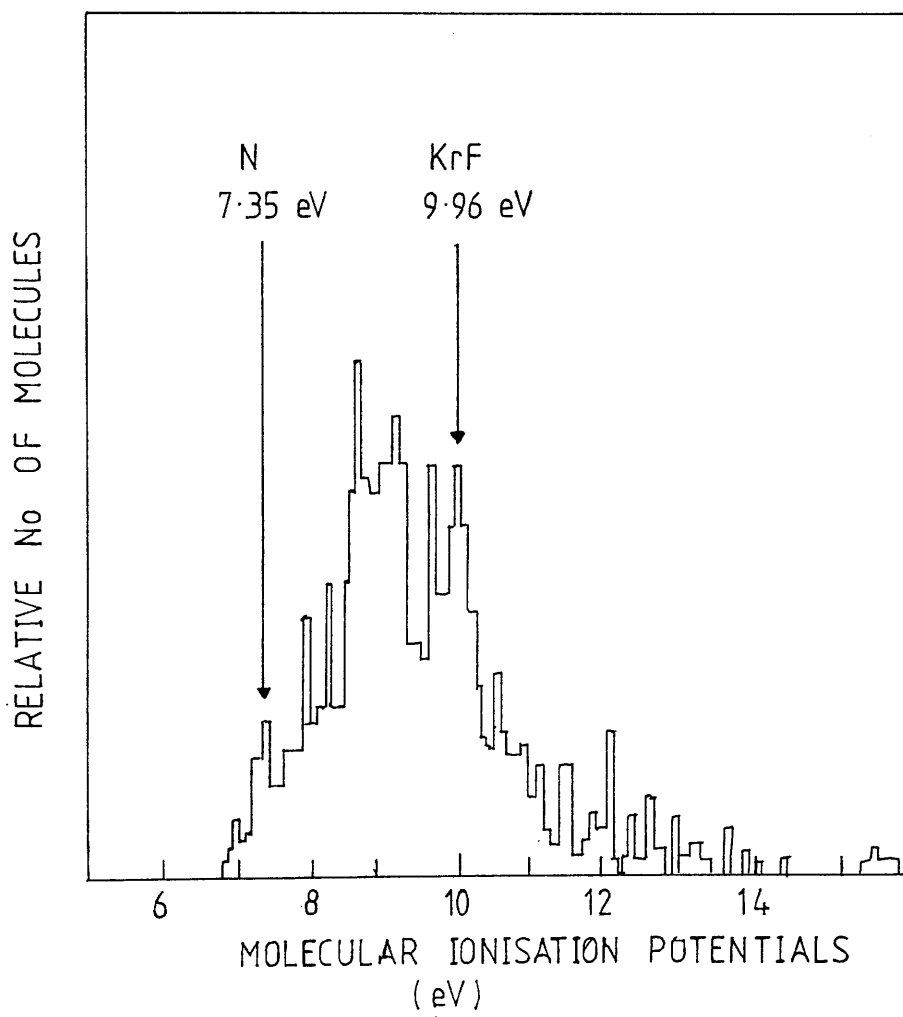


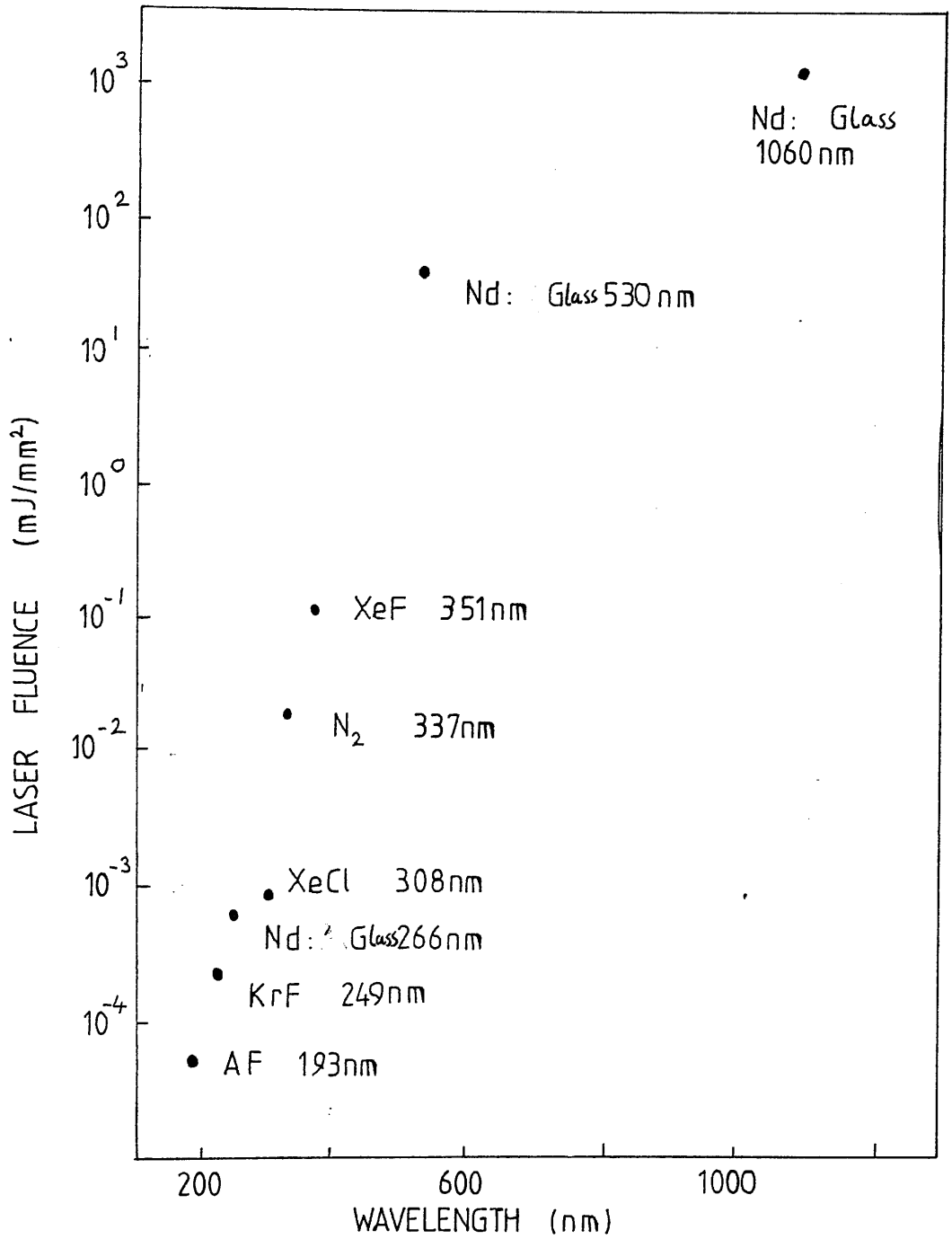
Figure: 4-9 Ionisation potentials of organic molecules.



molecules can be ionised at shorter wavelengths.

The ionisation probability drops rapidly as the order of the MPI process rises. Figure 4-10 gives a rough estimate of the laser fluence that would be required to produce 20IP/cm for each laser output. The calculation is made by normalising the data on table 4-1 assuming the order of the MPI process to be the gradients of the log/log plots for each output, and also assuming a T^2 dependence of ionisation on the laser flux. Rate equation modelling predicts a squared dependence in T for an MPI process well away from saturation (see appendix 1). The figure shows the increasing powers required to ionise the gas as the output wavelengths increase.

Figure: 4-10 Estimated laser fluences required to produce 20IP/cm.



SECTION 4-3: CONCLUSIONS.

The laser ionisation was observed to be strongly dependent on the wavelength of the output. Lasers with wavelengths greater than 350nm required the absorption of more than two photons to produce ionisation. Therefore unless used at high fluences where saturation of the MPI process occurred they would not be suitable for laser calibration.

Below 350nm the ionisation process is two-photon. The ionisation potentials of the impurities in the counter gas responsible for the laser ionisation at 350nm must have ionisation potentials of less than 7.1eV. As argon and methane have ionisation potentials of 16eV and 12eV respectively, they cannot be responsible for the ionisation at this wavelength. These results indicate the presence of low ionisation potential impurities in the counter gas.

LASER IONISATION CONTROL IN PROPORTIONAL COUNTERS
BY ADDITION OF LOW IONISATION POTENTIAL VAPOURS.

SECTION 5-1: INTRODUCTION.

The ability to produce controllable and reproducible levels of laser ionisation is important for the study of space charge effects in MWPC's, such as in two-track studies. More fundamentally, ionisation control may be necessary in some cases simply to produce ionisation above the detection threshold of the MWPC. Variations in laser ionisation intensity by factors of 3 and 7 were reported for the TPC 90 and in a counter at Dortmund (Blum (1984)). In the UA-1 detector (Marciewicz et al (1983)) a fall in ionisation by a factor of 4 occurred over a day. Shortly after, the ionisation fell below the detection limit of the system.

The ionisation could be controlled in one of two ways: either by the adjustment of the ionising laser intensity, or by the addition of a laser ionisable compound (seeding compound) to the counter gas. Ionisation control by the variation of the laser intensity may not be possible in some cases, for instance when even the maximum intensity of the laser produces no detectable ionisation. Then the second method of control must be adopted.

Seeding compounds most commonly studied are organic molecules with low ionisation potentials. Efforts have already been made to obtain ionisation control by the addition of low concentrations of organic vapours to counter gas es. (Anderhub et al (1979, 1980), Bourotte and Sadoulet (1980), Cochet et al (1982), Guo et al (1982), and Gushchin et

al (1983)). None of the additives were recommended for seeding into the ALEPH TPC since their long term effects on the detector properties were unknown.

For the reasons given in chapter 4, UV lasers with wavelengths of around 300nm are the most likely candidates for the laser calibration of gas filled counters. For the direct single photon ionisation of an additive, using photons of around 300nm wavelength, the additive must have an ionisation potential of less than about 5eV. Very few molecules with ionisation potentials as low as this exist and those that do tend to be chemically unstable. Many metallic atoms have ionisation potentials of around 4eV, but free atomic metals are generally reactive and would be rapidly adsorbed onto metallic surfaces in the MWPC, or would be lost in oxidation reactions with impurities like O₂ in the gas.

The problem of chemical reactivity is reduced if higher ionisation potential molecules are used for seeding. At near UV wavelengths two-photon ionisation of molecules with ionisation potentials of around 8eV has already been demonstrated.

Another alternative would be to go a step further and use three photons to ionise molecules with ionisation potentials of around 12eV. Since quenching gases in MWPC's have ionisation potentials in this region, at first sight, this would appear to be a very tempting method, since it would require no seeding. It unfortunately demands the use of a very intense UV laser and expensive beam handling facilities.

The two-photon ionisation of seeding compounds appeared to be the best option. The seeding compounds tested and discussed in this chapter were chosen, over many other possible candidates, for no very powerful reasons. Di-ethylaniline (DEA) and Tetrakis-(dimethylamino) ethylene (TMAE) had already been studied as seeding agents in counters (Anderson et al (1981)), so these were again studied along with a similar molecule to DEA, Di-methylaniline (DMA). Trimethyl- and triethyl-amine (TMA and

TEA) were chosen for their very high vapour pressures (TMA is a gas at room temperature) and for their apparent molecular simplicity. N,N,N',N'-Tetramethyl-p-phenylene diamine (TMPD) had a very low ionisation potential which it was hoped would give a large enhancement in ionisation for very low seeding concentrations. Naphthalene was chosen for its low ionisation potential but also because it was a familiar and reasonably harmless compound. (Naphthalene is the major constituent in moth balls).

The above compounds were studied in small proportional counters filled with 90-10% argon/methane (P10) counter gas. The effects on the laser ionisation levels for various seeding concentrations and for set laser fluences, were studied. Effects on the counter properties were also studied, such as undesirable changes in counter gain and resolution. Since excessive sticking of seeding compounds to the counter surfaces could affect the counter lifetime, the ease of removal from the counter after seeding was also studied.

SECTION 5-2: RESULTS AND DISCUSSION.

Experimental results for and the discussion of each seeding compound will be given in turn. The results are summarised in tabular form at the end of the section. Additional information on the properties of these molecules is also given.

Fluctuations in the laser fluence by as much as 30% were observed. In a non-saturating 2-photon process this constitutes 60% fluctuations in the laser ionisation intensity. Laser fluence and ionisation were both recorded pulse by pulse allowing normalisation of the ionisation to a specific laser fluence for each event. For a non-saturating 2-photon process the ionisation must be quadratically normalised. In all of these experiments the ionisation process was taken to be non-saturating.

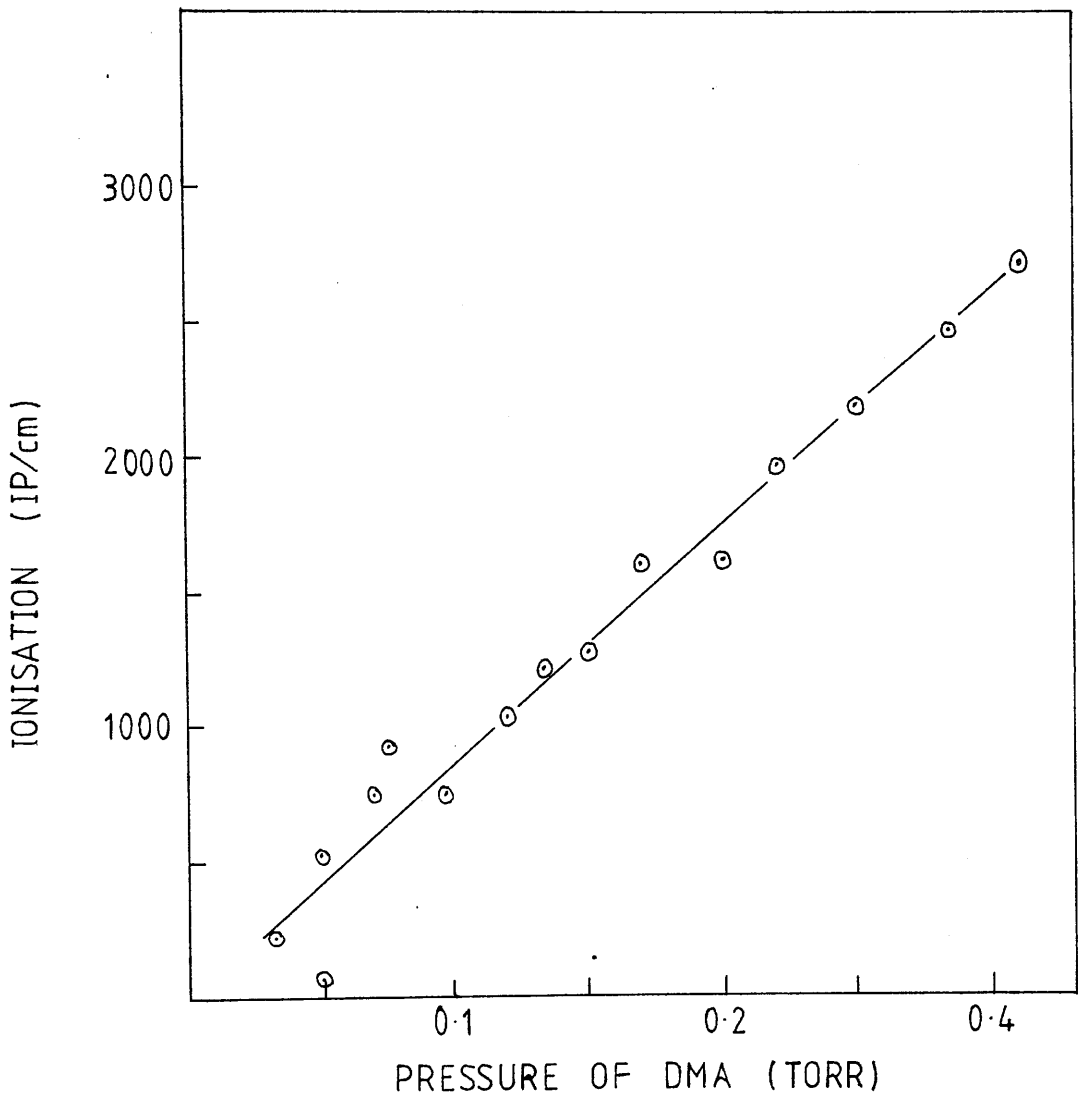
N,N,-DIMETHYL-ANILINE (DMA).

An MKS Baratron was used to measure the pressure of DMA introduced into an evacuated type 1 proportional counter (the static fill method). The laser ionisation was measured for a range of partial pressures of DMA between 0.04 and 0.3 Torr in P10 gas at 760 Torr.

Figure 5-1 shows the ionisation versus pressure curve produced by an unfocussed N_2 laser with a fluence of about $14\mu\text{J}/\text{mm}^2$ and a pulse duration of 5ns. The ionisation was quadratically normalised to $14\mu\text{J}/\text{mm}^2$. A linear dependence between ionisation and the pressure of DMA in the counter was observed.

DMA was introduced into a counter at 0.3Torr which was then filled to 760Torr with P10 gas. With this pressure of DMA the counter resolution and gain were not affected (measured from the Fe 55 x-ray ionisation spectra). After isolation for a week, little deterioration

Figure: 5-1 Ionisation versus pressure curve for DMA.



of the counter resolution was observed, although the laser ionisation intensity dropped by a factor of 2.

The ease with which DMA could be removed from the counter was measured in the following way. An evacuated type 1 counter was filled with a known low pressure of DMA then filled to 760Torr with P10 gas. The ionisation was measured at a known laser fluence. The counter was then evacuated to 380 Torr and refilled with fresh P10 gas to 760Torr and the ionisation for the same laser fluence was recorded. This procedure was repeated several times. After each pump out and refill the pressure of DMA in the counter was assumed to have dropped by half. Figure 5-2 shows ionisation intensity at a set laser fluence versus assumed DMA pressure. The non-linear dependence indicated that DMA had been adsorbed onto the counter walls and was subsequently outgassing back into the P10 gas (Ledingham et al (1984)). After pumping out for a few minutes, most of the DMA was removed from the counter.

The 337nm output of the N_2 laser at a laser fluence of $14\mu J/mm^2$ produced approximately 1700IP/cm in P10 mixed with 260ppm DMA.

The ionisation dependence of DMA on wavelength was studied using the frequency doubled light from a dye laser. DMA was introduced into P10 gas by passing the gas at 250ml/min over a sample of DMA held at $0^\circ C$ in a cold bath. At this temperature the saturated vapour pressure of DMA is 0.06 torr (see figure 5-3). Careful measurements of flow rates and loss of mass of the DMA sample showed that the actual pressure of the DMA was closer to 0.036torr

The wavelength was stepped between 264nm and 332nm. A gap in the spectra, at around 308nm, appears due to laser inefficiency near the edges of the dye tuning curves. The laser fluence was set at around $14\mu J/mm^2$ and the ionisation then quadratically normalised, pulse by pulse, to a fluence of $1\mu J/mm^2$. Figure 5-4 shows both the background and DMA 2-photon ionisation spectra. Between 264nm and 310nm the ionisation

Figure: 5-2 Ionisation versus assumed DMA pressure.

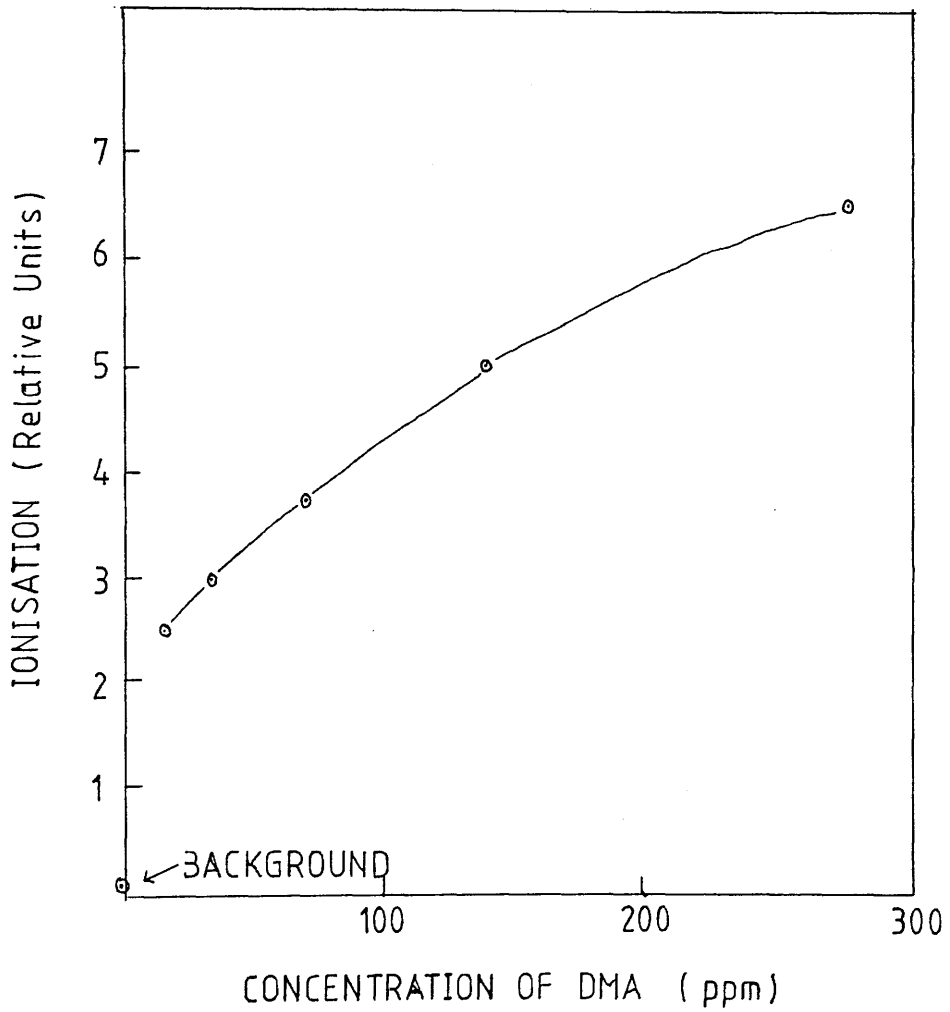


Figure: 5-3 Vapour pressure curve for DMA.

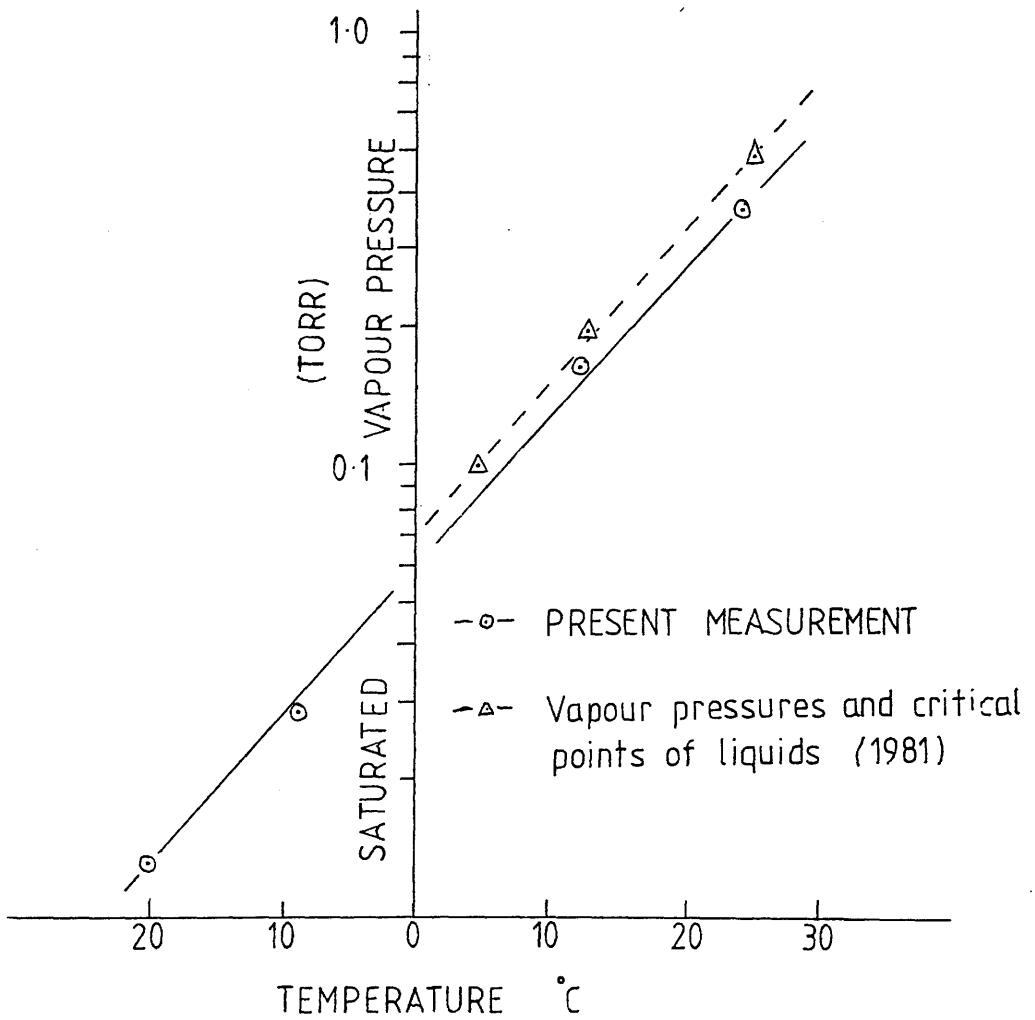
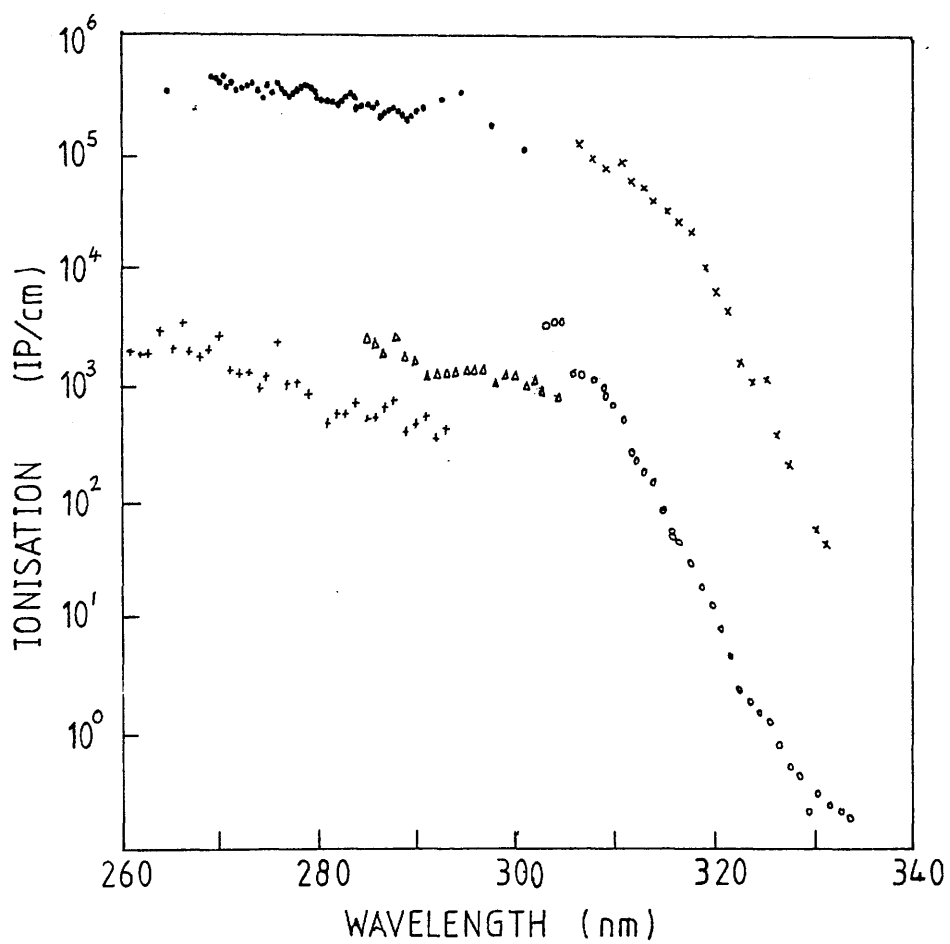


Figure: 5-4 Background and DMA R2PI spectra.



was fairly constant but then fell by 3 orders of magnitude between 310nm and 332nm.

The ionisation observed at 266nm with a laser intensity of $12\mu\text{J}/\text{mm}^2$ was 3×10^7 IP/cm for DMA at a concentration of 260ppm. This was over 4 orders of magnitude greater than the ionisation observed for the same concentration of DMA ionised by the N_2 laser with a $14\mu\text{J}/\text{mm}^2$ pulse.

One reason for the flattening off of the 2-photon spectrum below 310nm may be explained, in part, by the apparent saturation of the ion signal from the counter. Figures 5-5 and 5-6 show attenuation curves of laser ionisation versus laser fluence. At 320nm and 330nm the dependence is quadratic and therefore non-saturating but at 310nm and 266nm the ionisation is seen to be strongly saturated at laser fluences of around $10\mu\text{J}/\text{mm}^2$.

Saturation of the 2-photon ionisation process was thought unlikely, since that would mean that most of the DMA molecules, in the beam interaction volume, would have had to have been ionised. However calculations showed that only a millionth of the DMA molecules in the interaction region had been ionised.

The saturation was attributed to the effects of space charge building up near the sense wire of the proportional counter. For electron densities of up to $10^7 \text{e}/\text{cm}$ on the wire these effects are minimal, but beyond $10^7 \text{e}/\text{cm}$ the counter becomes non proportional. Even before amplification near the wire, DMA was producing ionisation levels close to, or greater than, $10^7 \text{e}/\text{cm}$.

DIETHYL-ANILINE (DEA).

Diethyl-aniline is chemically very similar to DMA, although it has a slightly lower ionisation potential and a vapour pressure 1/3 that of DMA (see figure 5-7).

Figure: 5-5 Attenuation curves for DMA at 320nm,1 and 330nm,2.

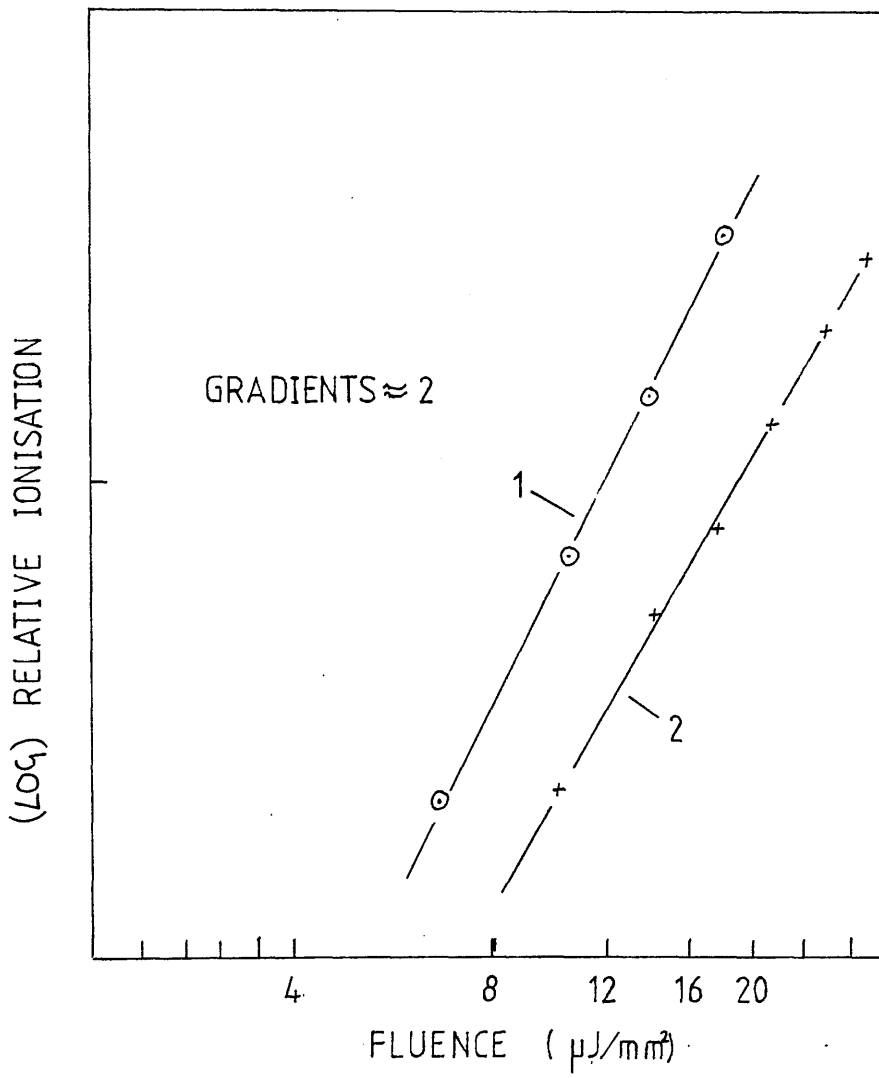


Figure: 5-6 Attenuation curves for DMA at 310nm,¹ and 266nm,².

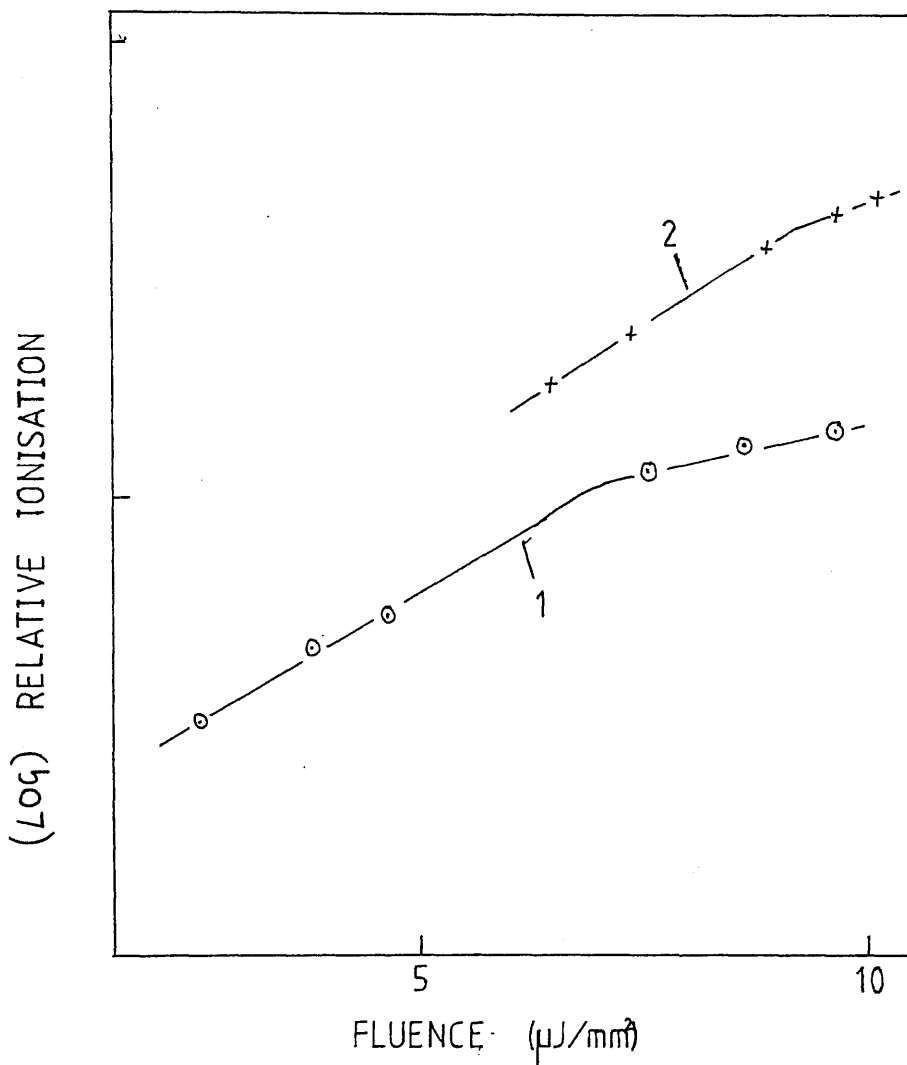
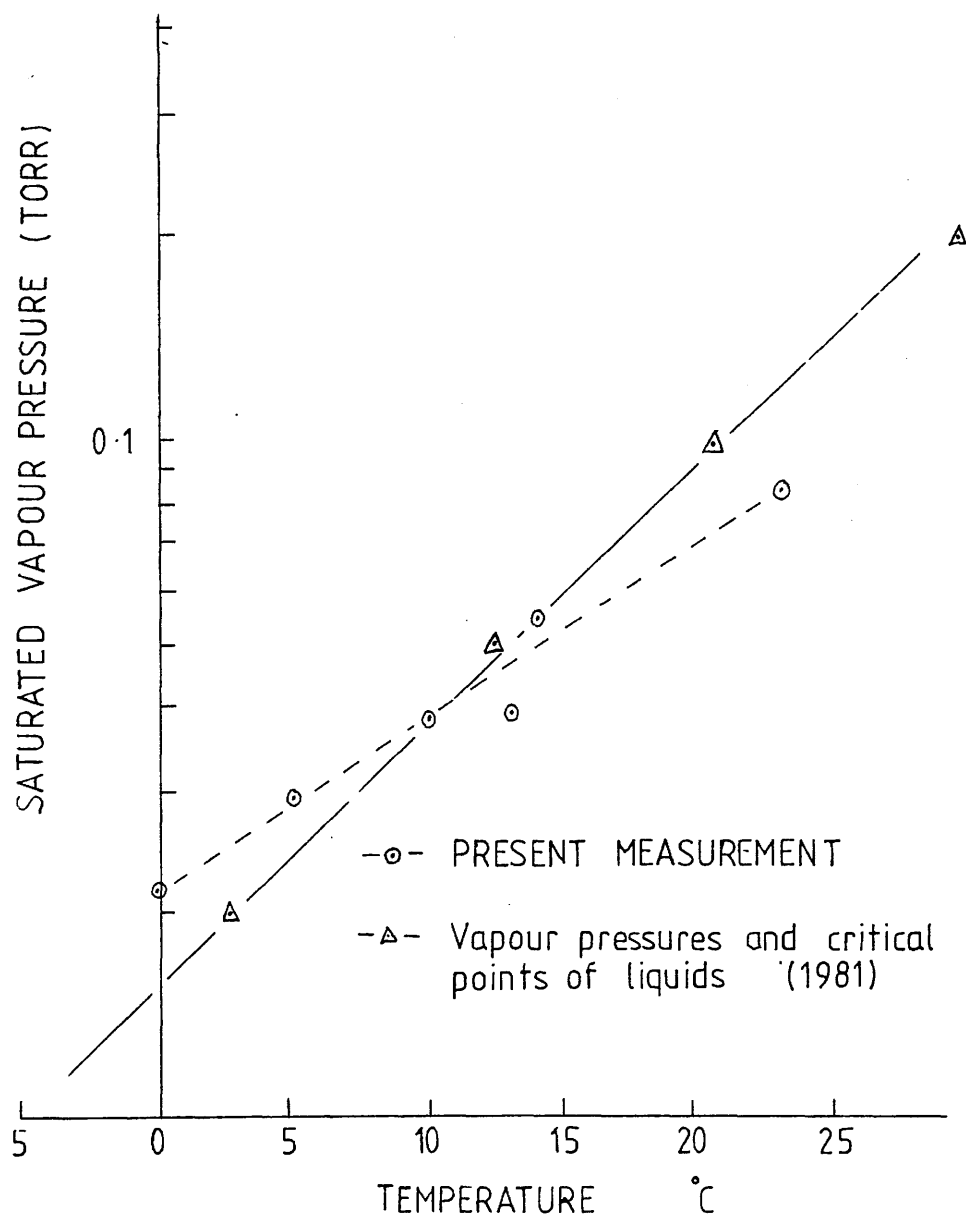


Figure: 5-7 Vapour pressure curve for DEA.



Adsorption and subsequent outgassing of DEA from the counter walls made the static filling of the counters an unreliable method for introducing DEA into the counter. Instead the DEA was introduced by flowing P10 gas at both 50ml/min and 250ml/min over a sample of DEA held at temperatures between 0°C and 21°C. Figure 5-8 shows the increase in ionisation of DEA as its concentration builds up with time in the counter. The first part of each curve is the background ionisation in the counter when the P10 gas flow was bypassing the DEA sample. Gas flow was then switched to pass over the DEA sample and an exponential rise in ionisation was observed. The rise was consistent with a very rapid distribution of the seeding vapour throughout the counter volume. After a time the ionisation reached a steady state. At flow rates of 50ml/min and 250ml/min the steady state ionisation levels were the same, indicating that at least to first order, the concentration of DEA in the P10 gas was independent of flow rate. The ionisation in each case is proportional to the vapour pressure for temperatures between 0°C and 21°C (see figure 5-9).

Measurement of the flow rate and mass loss at 21°C indicated that the partial pressure of DEA in the P10 gas was about 30% of the saturated vapour pressure of DEA. A cooling down of the surface of the DEA sample by evaporative heat loss accounted in part for the discrepancy between the observed partial pressure of DEA and the saturated vapour pressure.

DEA at a concentration of 33ppm gave ionisation of about 1800IP/cm with a N₂ laser at a fluence of 14μJ/mm² and wavelength of 337nm. The 2-photon ionisation cross-section is very similar to that of DMA, but DEA proved to be much more sticky and because of this no more work was carried out with it.

Figure: 5-8 DEA seeding by the flow method.

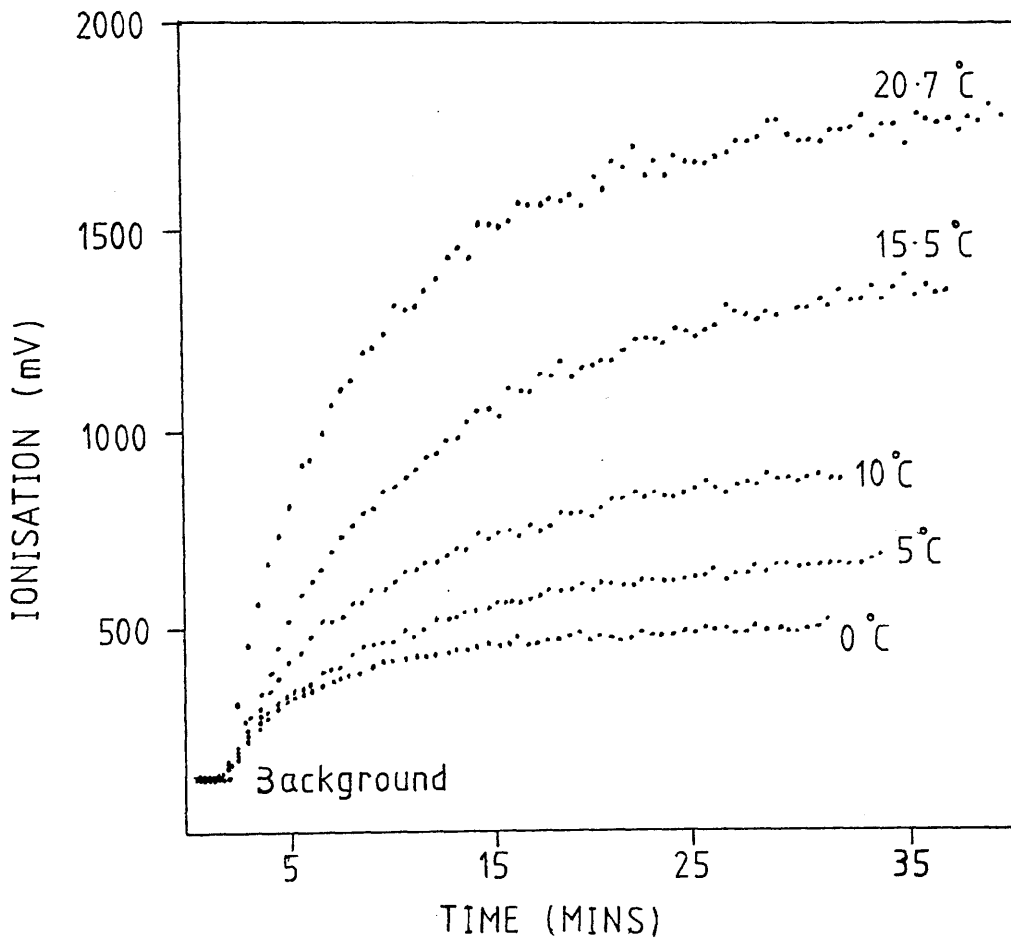
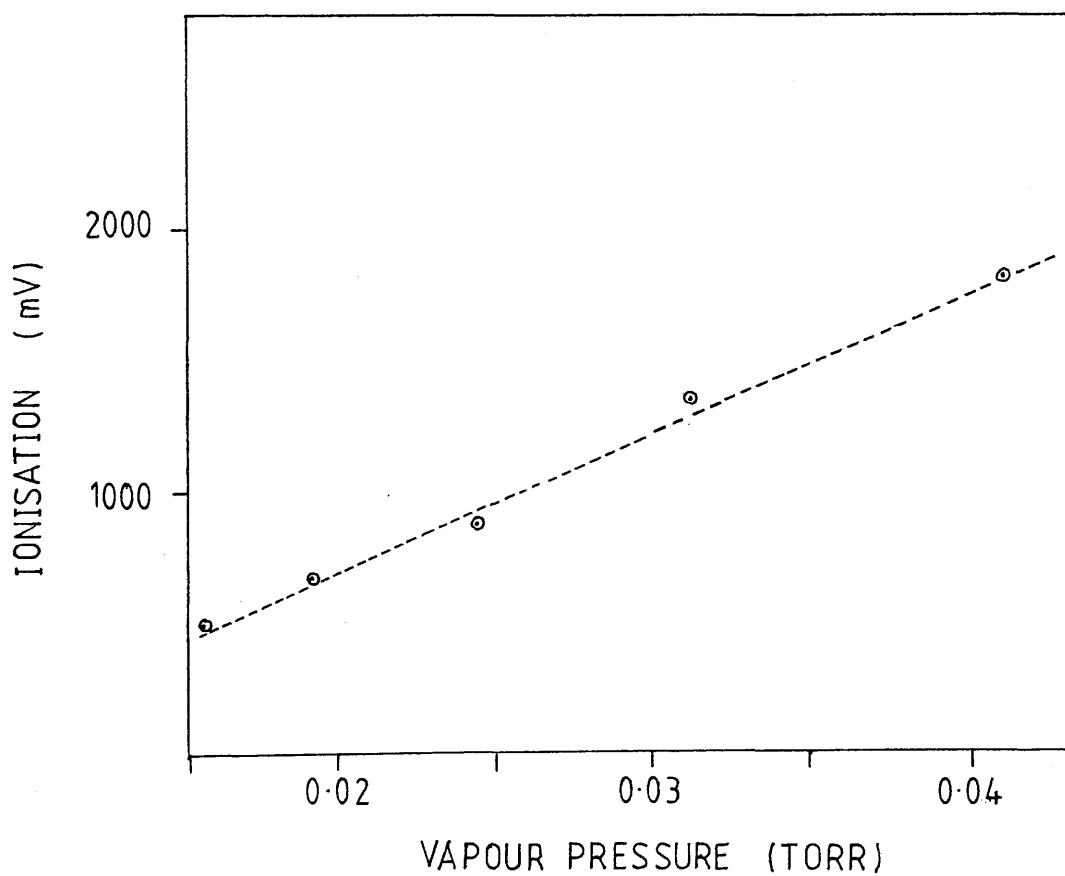


Figure: 5-9 Ionisation versus vapour pressure for DEA.



TETRAKIS (DIMETHYLAMINO) ETHYLENE (TMAE).

With its very low ionisation potential TMAE was potentially a seeding vapour of great promise. Considerable work (Anderson et al (1981)) has already been carried out on a group of tetraaminoethylenes, of which TMAE was one. These were introduced into photoionisation proportional scintillation chambers. Anderson et al described problems arising from TMAE seeding. All the surfaces in the chamber rapidly became photosensitive implying adsorption of TMAE onto the chamber walls. Also, depending on the type of surface and its temperature, it was found to take many hours to remove TMAE from the chambers by pumping with a diffusion pump.

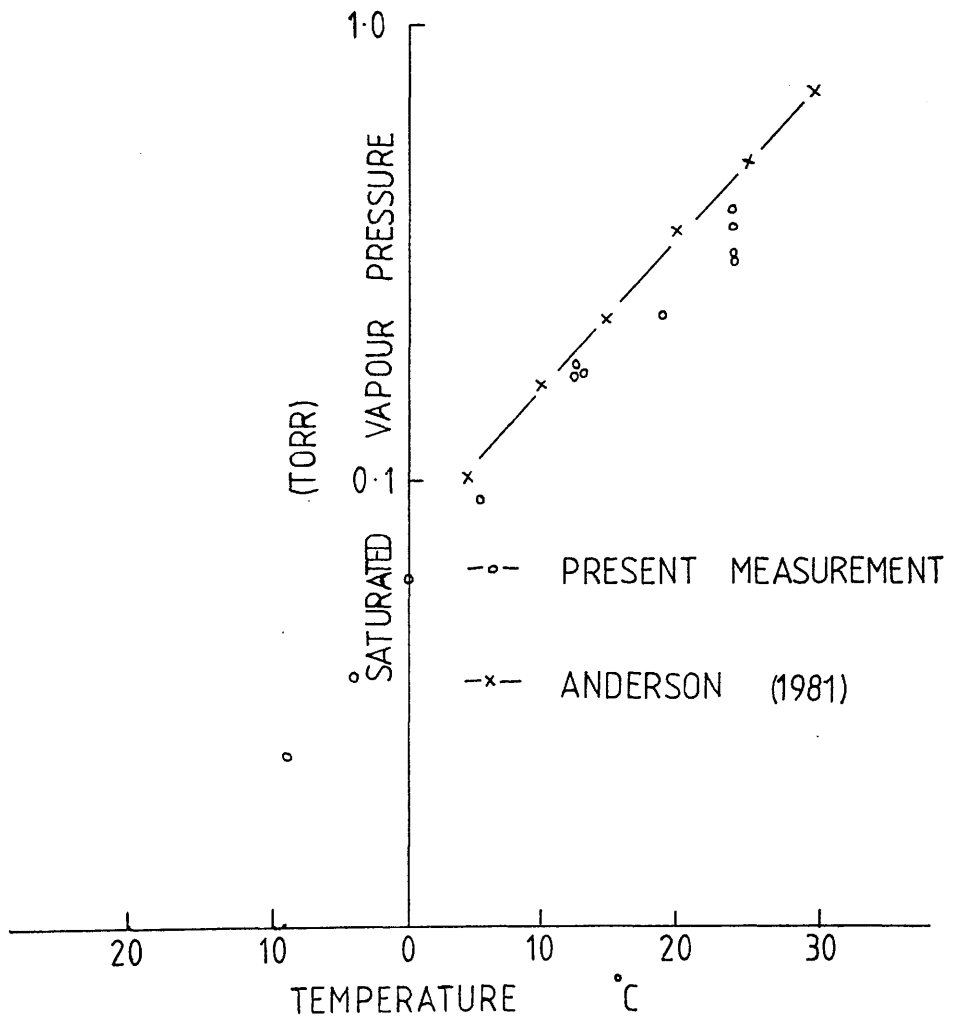
Experiments with TMAE confirmed these problems. TMAE at its saturated vapour pressure at -10°C (figure 5-10) was introduced into a type 1 counter under vacuum. Very high ionisation levels were produced and only after considerable pumping did the ionisation return to the original background level.

A fairly reproducible measurement of laser ionisation of TMAE was obtained when P10 gas was flowed over a sample of TMAE held at between -40°C and -30°C (TMAE is solid at these temperatures). By a linear extrapolation of the saturated vapour pressure versus temperature graph the concentration of TMAE in the P10 gas was estimated to be about 10^{-3} torr. The ionisation produced by the N_2 laser at $1\mu\text{J}/\text{mm}^2$ was about 5×10^3 IP/cm.

TMAE proved very difficult to handle reliably. Even with flowing techniques it seemed to stick to the counter surfaces. An additional problem with TMAE was its reactivity. In contact with air it oxidises to form compounds that may not be ionised by two photons at 337nm.

Although it has been used successfully as a photoionising vapour in MWPC's designed to detect and localise UV photons (Charpak and Sauli

Figure: 5-10 Vapour pressure curve for TMAE.



(1984) and Sauli (1986), TMAE is not recommended as a seeding agent for the ALEPH TPC.

TRIETHYLAMINE (TEA).

Triethylamine was introduced into a type 1 counter by the flow method. P10 gas flowing at a rate of 250ml/min was passed over a sample of TEA held at temperatures between -22°C and 0°C . This procedure resulted in seeding concentrations of between 10ppm and 10^4 ppm (found from the vapour pressure of TEA in this region, figure 5-11).

A N_2 laser with a fluence of $14\mu\text{J}/\text{mm}^2$ gave no measurable ionisation above the 40-60IP/cm considered to be background, although with a concentration of 1.5torr TEA, the gas gain of the counter increased considerably. This effect was also observed in MWPC's with 1.5% TEA in the counter gas (Sauli (1986)).

A pressure of 1.5torr TEA was maintained by flowing P10 gas over a sample of TEA held in a cold bath at -20°C . With a laser fluence of $8\mu\text{J}/\text{mm}^2$ a 2-photon spectrum for TEA was taken between 264nm and 290nm in 1nm steps (figure 5-12) The data was quadratically normalised to a laser fluence of $1\mu\text{J}/\text{mm}^2$. Figure 5-13 shows an approximately quadratic dependence of ionisation with laser fluence at 266nm.

TEA does not show evidence of ionisation at wavelengths greater than 280nm. This explains why no ionisation was observed in TEA with the N_2 laser at 337nm. Below 280nm the ionisation increased until at 276nm it reached 2×10^5 IP/cm. It remained roughly at this value down to 264nm.

At 2000ppm (1.5 torr) TEA the gas gain increased by a factor of

Figure: 5-11 Vapour pressure curve for TEA.

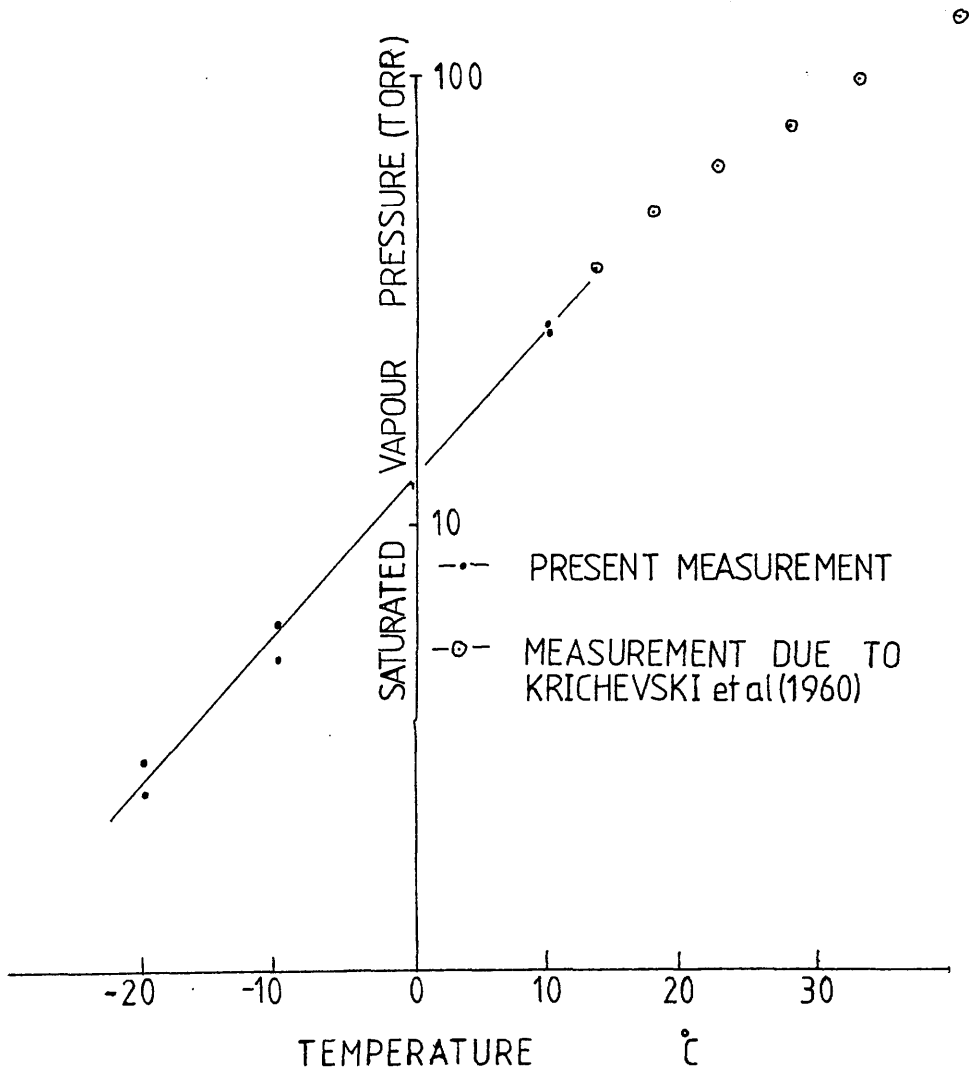


Figure: 5-12 R2PI spectrum for TEA.

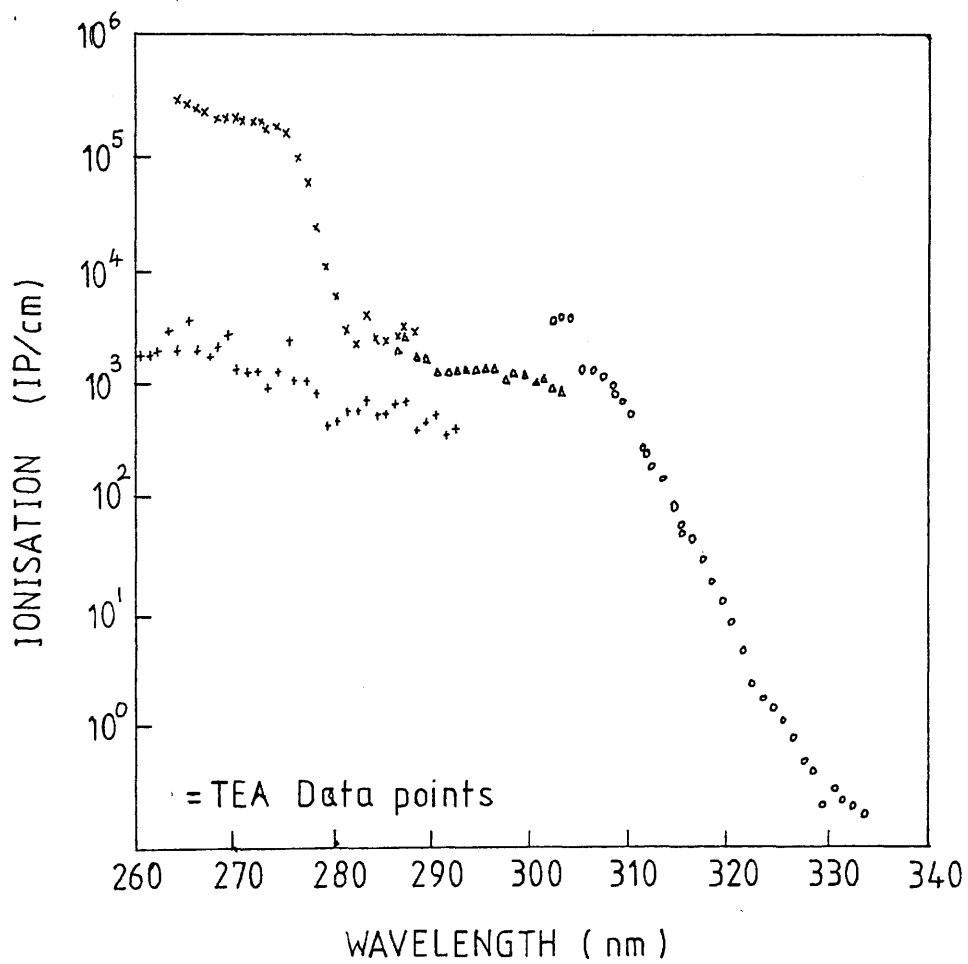
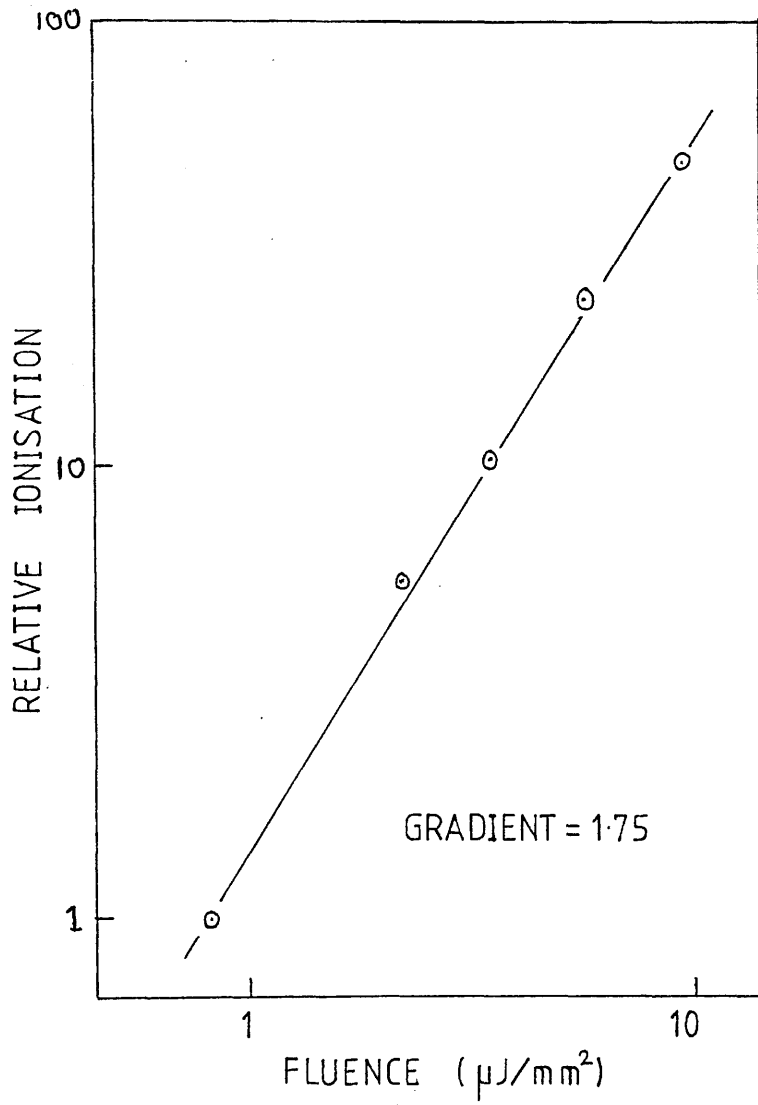


Figure: 5-13 Attenuation curve for TEA.



six over that for pure P10 gas. This change is not seen in the data since the number of ion pairs produced by laser ionisation is calculated using the x-rays from an Fe 55 source.

TEA did not appear to be very sticky and could easily be removed from the counter by flushing with clean P10 gas. TEA has not been dismissed as a possible seeding agent for calibration purposes.

TRIMETHYLAMINE (TMA).

TMA, unlike all the other seeding compounds is a gas at room temperature. At a partial pressure of 10Torr, (measured on the MKS Baratron) TMA was introduced into an evacuated type 2 counter which was then filled to 760 torr with P10 gas. A doubling of the counter gain was observed with this concentration of TMA, but below 5×10^2 ppm there appeared to be no appreciable effect on the counter gain (see figure 5-14).

A 2-photon spectrum between 266nm and 300nm in steps of 1nm was taken for TMA. The ionisation was quadratically normalised from about $0.8 \mu\text{J}/\text{mm}^2$ to $1 \mu\text{J}/\text{mm}^2$. The 2-photon ionisation of TMA rises continuously from background at 298nm down to 266nm (figure 5-15).

At 266nm, the normalised background subtracted ionisation level for TMA at 10torr is 5.7×10^5 IP/cm. Extrapolation gives a corresponding ionisation of 130IP/cm at $1 \mu\text{J}/\text{mm}^2$ and 3ppm TMA. This is very close to the figure of 160IP/cm reported by Hubricht et al (1985).

Figure 5-16 gives a graph of ionisation versus nominal pressure of TMA. The data was produced in a similar way to the "stickiness" test adopted for DMA. The ionisation only deviates very slightly from a straight line and then only in the region where background ionisation becomes significant. From this it was concluded that TMA is not sticky.

TMA has been introduced into the TPC 90 (Blum et al (1984)), at a

Figure: 5-14 Effect of TMA on the counter gain.

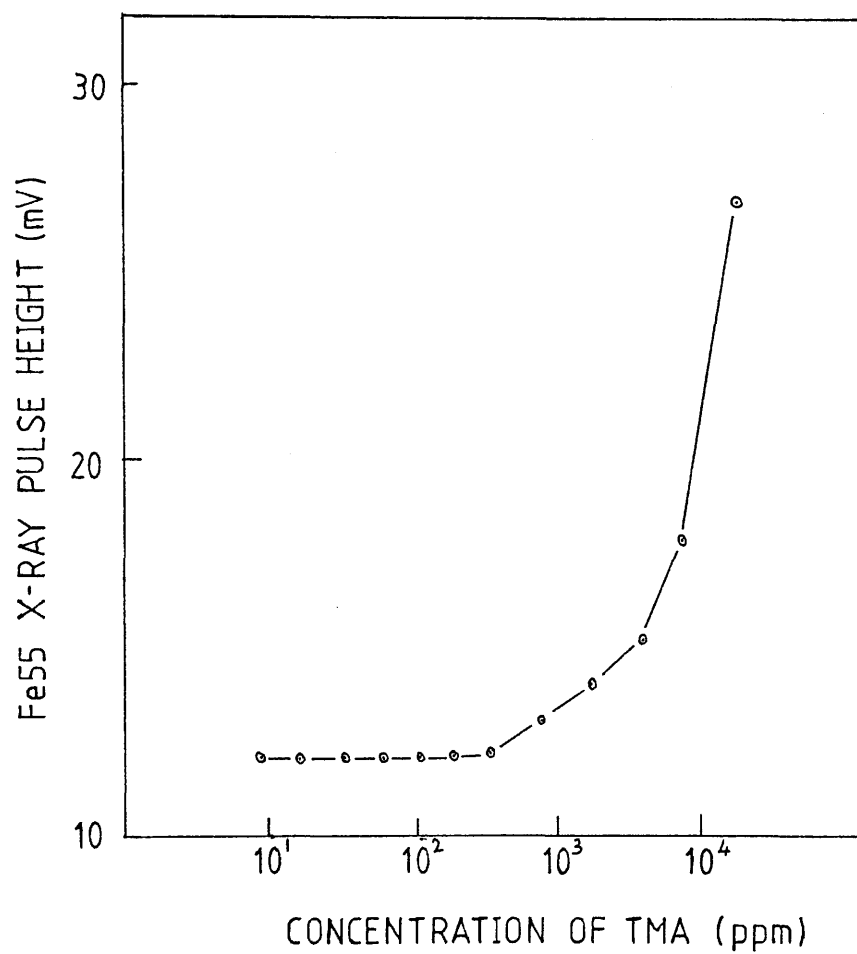


Figure: 5-15 R2PI spectrum for TMA.

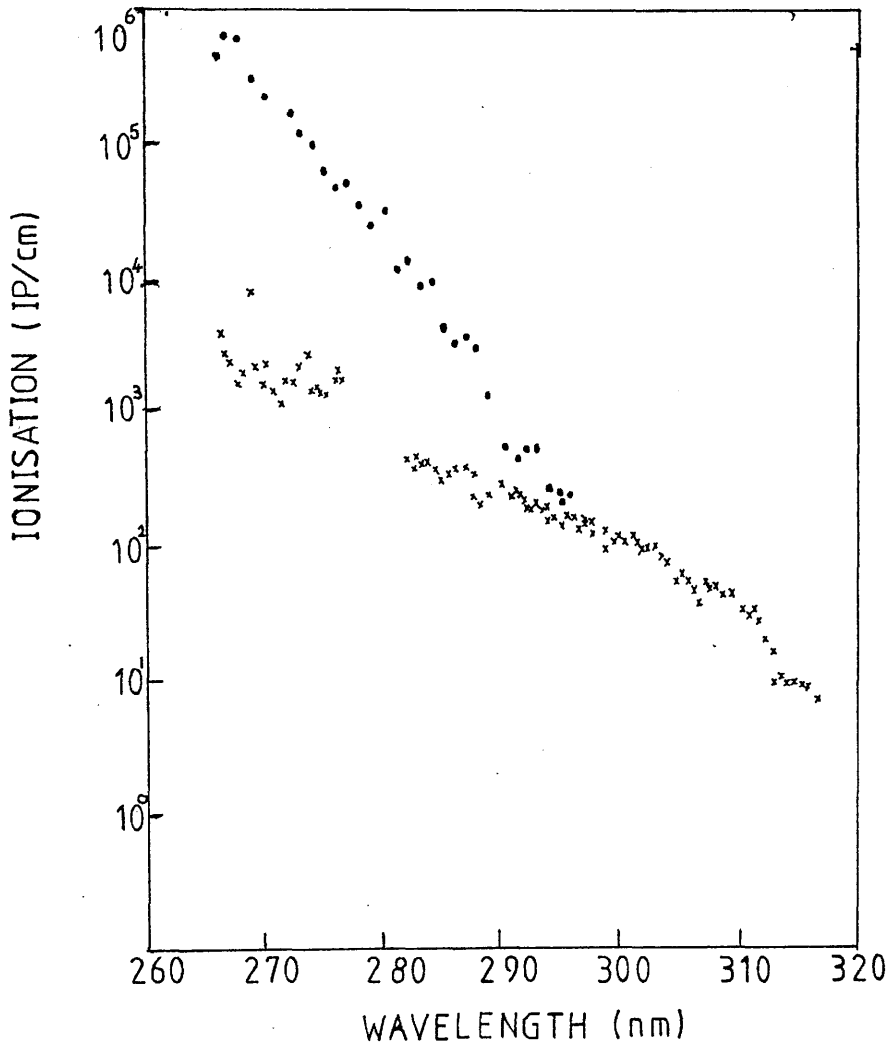
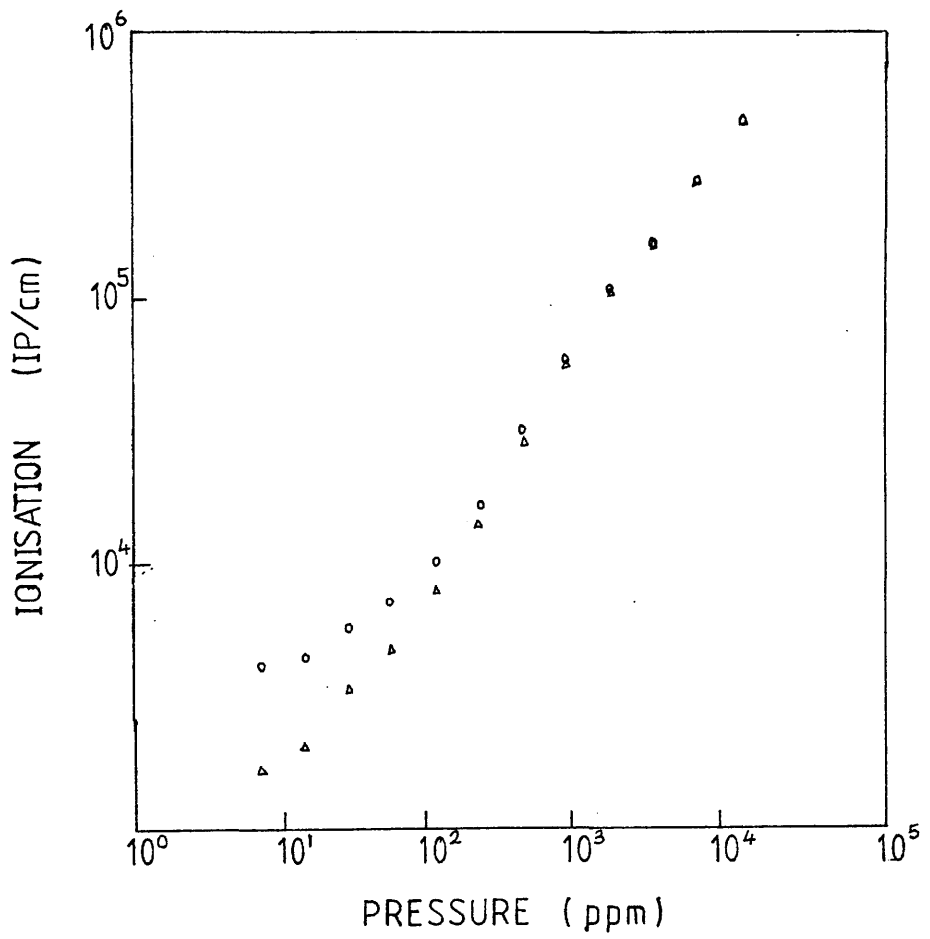


Figure: 5-16 Graph of ionisation versus nominal pressure of TMA.



concentration of 30ppm. They observed an ionisation of 420IP/cm for a quadrupled Nd:YAG (266nm) at a fluence of $1\mu\text{J}/\text{mm}^2$.

Also Dortmund looked at the effect of TMA on the counter lifetime. They defined the lifetime of the counter as the time taken for the resolution of the counter, measured with an Fe55 source, to increase to 30%. TMA doped at 100ppm into the counter gas actually gave a three fold increase in lifetime over that of the unseeded counter.

NAPHTHALENE.

P10 gas flowing at a rate of 100ml/min was passed through a sample of crystalline naphthalene at room temperature. At this temperature the vapour pressure of naphthalene would not be greater than 0.05torr, the saturated vapour pressure of naphthalene at 21°C (Handbook of Chemistry and Physics (1986)).

The 2-photon ionisation spectrum of naphthalene taken between 272nm and 300nm in steps of 0.1nm (see figure 5-17), displays fairly constant ionisation between 272nm and 280nm and then a drop of over two orders of magnitude between 280nm and 300nm. The laser fluence was fixed at about $4\mu\text{J}/\text{mm}^2$. At 274nm the ionisation begins to saturate at this fluence (see figure 5-18). This was attributed to a build up of space charge in the counter.

A 2-photon ionisation spectrum of naphthalene taken by Frueholz et al (1980) displayed resonant fine structure at wavelengths around 280nm. Structure is apparent in the spectrum depicted in figure 5-17, but is washed out to some extent due to the saturation of the proportional counter.

UV absorption data (Atlas of Spectral data and Physical constants for organic compounds (1975)) show that naphthalene has structure at around 270nm. Very similar absorption cross-sections are quoted for UV

Figure: 5-17 R2PI spectrum for naphthalene.

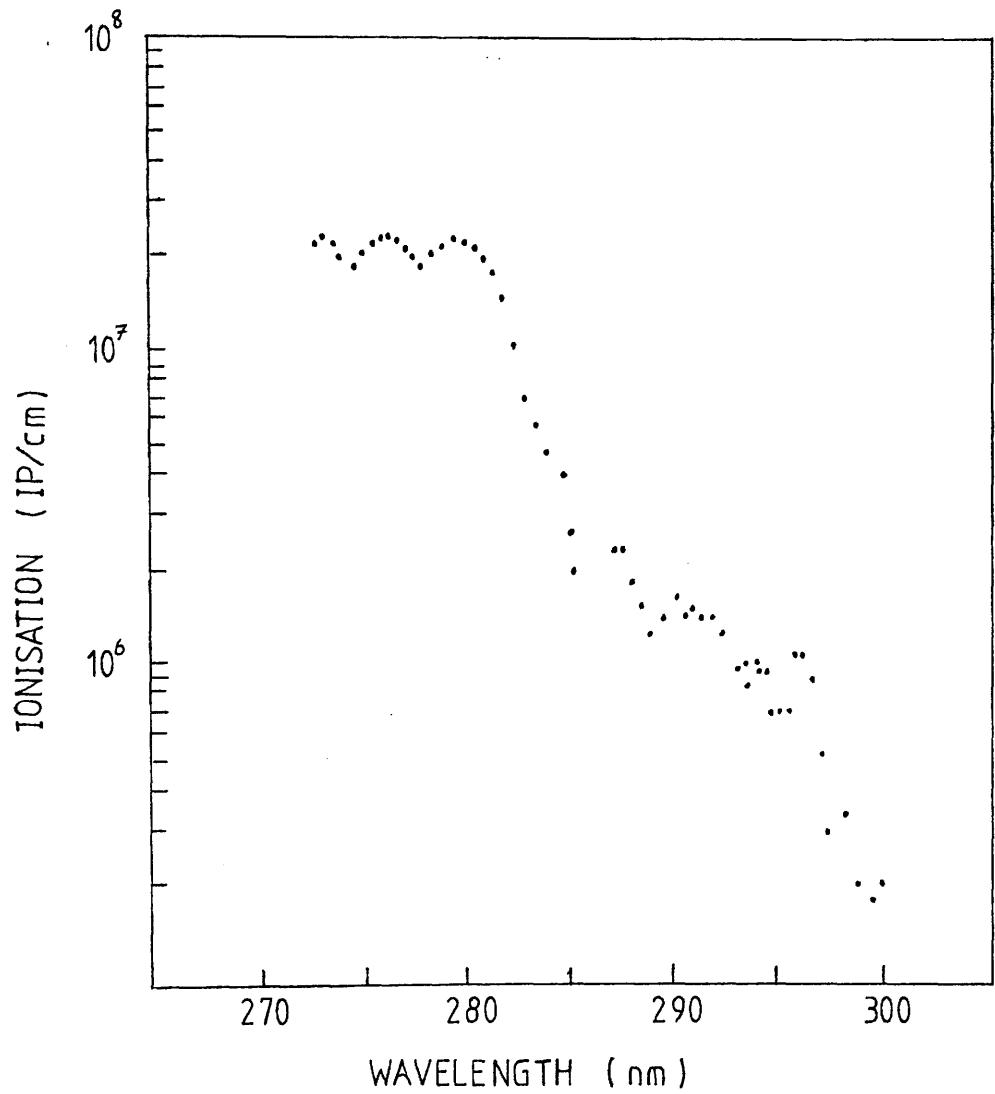
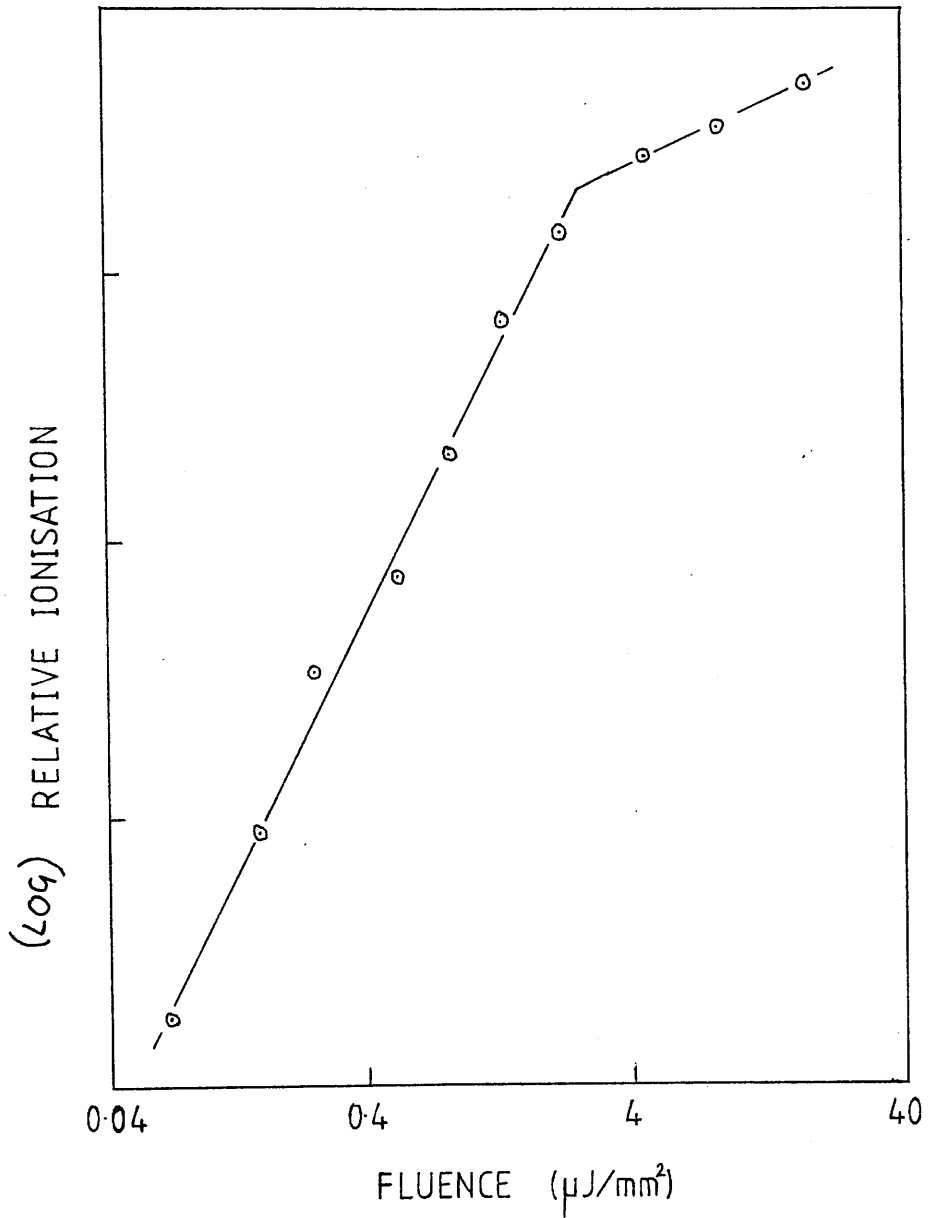


Figure: 5-18 Attenuation curve for naphthalene.



light at 275nm and 266nm.

The 2-photon spectrum did not cover the 266nm wavelength of the quadrupled Nd:YAG, but since naphthalene is still resonant at 266nm, it may be assumed that the ionisation will not differ greatly from the value at 274nm.

At the concentrations of naphthalene used in this experiment it proved difficult to clean the counter by pumping it out after seeding. Hubricht et al (1985) carried out seeding experiments with Naphthalene and also found it sticky but had no apparent difficulty in removing or controlling it. They measured an ionisation level of 1.4×10^7 IP/cm at 37ppm of naphthalene at a laser fluence of $1 \mu\text{J}/\text{mm}^2$ and a wavelength of 266nm. A method for seeding naphthalene into the TPC was detailed by Blum (1985).

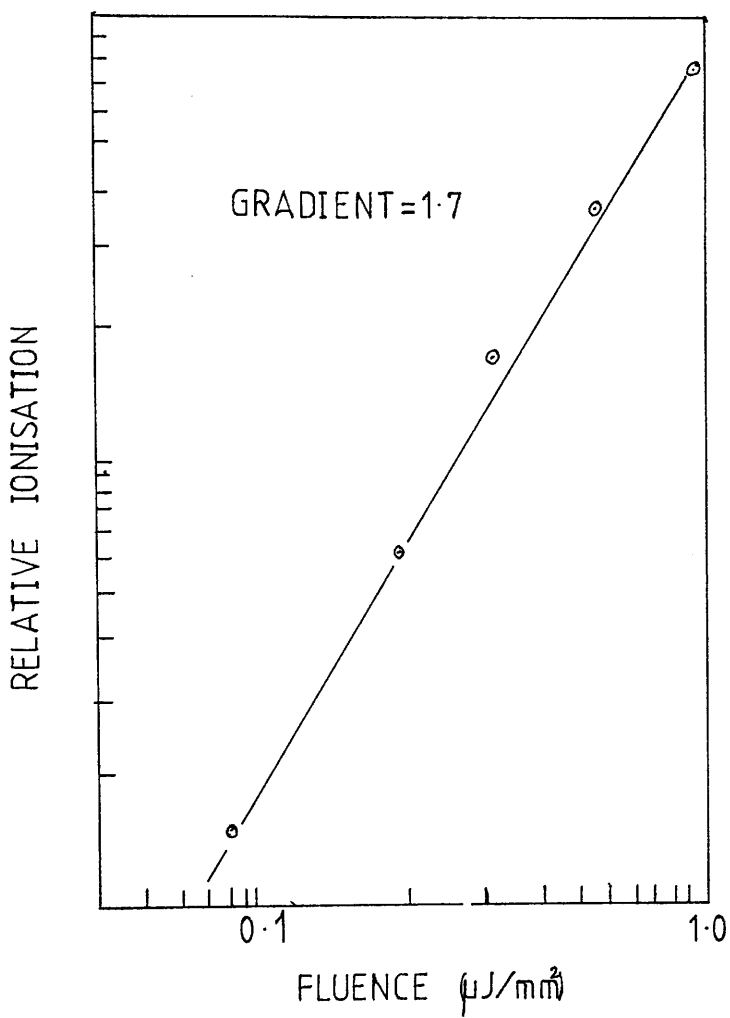
N,N,N',N'-TETRAMETHYL-P-PHENYLENE DIAMINE (TMPD).

P10 gas flowing at 250ml/min over a sample of solid TMPD at room temperature gave a concentration of not more than 3ppm in the gas. A $1 \mu\text{J}/\text{mm}^2$ laser pulse at 268.5nm gave 1.4×10^5 IP/cm at this concentration. The ionisation process was as expected two photon, as illustrated by the gradient of two in the log/log plot of ionisation versus laser fluence (figure 5-19).

Hubricht et al (1985) and Gushchin et al (1983) have both tried seeding TMPD. They observed ionisation of 6×10^4 IP/cm (1.3ppm and 266nm) and 7×10^4 IP/cm (1.3ppm and 337nm) respectively.

TMPD proved very difficult to flush out of the system after seeding by this method. For this reason it was considered no further.

Figure: 5-19 Attenuation curve for TMPD.



SECTION 5-3: CONCLUSIONS.

The most likely choice of lasers for calibration purposes are those with wavelengths between 340nm and 200nm. N₂ and Nd:YAG lasers have already been used for particle track simulation in MWPC's. A quadrupled Nd:YAG is to be used for the calibration of the ALEPH TPC. Additives to the gas in the ALEPH TPC would therefore have to produce appreciable enhancement in laser ionisation at 266nm.

Tables 5-1 to 5-3 give information on the properties of the additives tested. Table 5-3 lists the ionisation induced for each additive at dye laser wavelengths close to 337nm and 266nm, or by a N₂ laser at 337nm. All the additives except TMA and TEA produced ionisation at 337nm. The general trend was for an increase in ionisation as the wavelength was decreased. At 266nm all the additives, including TEA and TMA produced appreciable ionisation.

Along with an enhancement in ionisation additives also had to have the following properties before they could be considered 'safe' for introduction into large MWPC's: (1) Control of the concentration of the additive in the counter gas had to be quick and easy; (2) The additives had not be excessively sticky; (3) They had to have a negligible effect on the counter gain (for instance by not having a strong electron attachment cross-section); (4) The counter lifetime had to be reasonably unaffected by their introduction; (5) They had to be fairly safe and easy to handle and (6) The gas purification systems in the TPC had not to be inactivated by their introduction.

All except DMA, TMA and TEA fail on the first two counts. DMA could be introduced at concentrations up to its saturated vapour pressure at room temperature without affecting the counter gain. On the other hand TMA and TEA both produced gain increases at pressures of a few torr in the P10 gas, but at concentrations of <500ppm they had a

negligible effect on the gain.

At a concentration of 60ppm and a laser fluence of around $10\mu\text{J}/\text{mm}^2$ at 266nm wavelength, the ionisation of DMA appeared to saturate. This was attributed to space charge build up effects near the sense wire of the proportional counter.

Although DMA produced approximately 10 times more ionisation than TMA and TEA for the same concentration and laser fluence, it had the disadvantage of being the most sticky of the three additives. TMA proved to be the least sticky.

Long term effects (over several months) on the counter lifetime have not been carried out. DMA was tested over a week in a proportional counter with an Fe 55 source producing continuous irradiation of the gas. DMA had little measurable effect on the gain and resolution of the counter but the ionisation intensity did fall over this period.

Aging effects in a counter with TMA added at a concentration of 100ppm has been studied by Pollman at Dortmund University (the results are reported in an ALEPH note by Blum (1984)). A 3 fold increase in the counter lifetime was observed with TMA at a concentration of 100ppm in the counter gas.

Of the three additives TMA is the most promising, its major drawback being its extremely unpleasant smell. Even a low level of TMA in air (ppb) is very unpleasant. Since all three additives considered are dangerous at low concentrations in air (typically >5ppm is considered unsafe) the TMA signature may be a blessing in disguise.

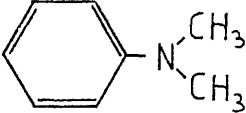
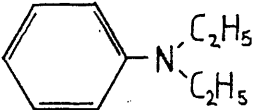
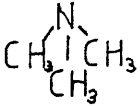
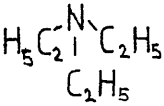
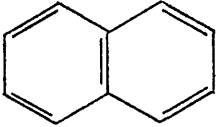
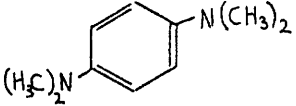
The study of additives for the artificial enhancement of ionisation could have continued in this vein, since thousands of low ionisation potential molecules exist. It was decided that a different approach to the problem might prove more fruitful.

Background laser ionisation in counters is caused by the presence of unknown impurities in the counter gas. It was thought that

identification of these impurities would lead to a greater understanding of the aging processes in MWPC's. Also, the 'background' impurities are at very low levels around 500ppb, (calculated from typical values of the ionisation cross-sections for molecules) and therefore seeding at these concentrations would probably be considered safe since the impurities are already present 'naturally' in the counters at these levels.

Two methods were used to try and identify the ionisable impurities. The first approach was to study the background 2-photon spectra of unseeded counter gas in various counters. The other was to study the ions produced by laser ionisation of the counter gas in a quadrupole mass spectrometer. Chapter 6 summarises the spectral analysis of the gas and chapter 8 the mass analysis.

TABLE 5-1: PROPERTIES OF ADDITIVES

NAME, CHEMICAL FORMULA & STRUCTURE	MOLECULAR WEIGHT, (AMU)	M.Pt. (°C)	B.Pt. (°C)	Density (g/L)	Ionisation Potential. (eV)
N,N Di-methylaniline (DMA) 	121.18	2.45	194.15	0.956	7.14 (1)
N,N Di-ethylaniline (DEA) 	149.24	-38.8	216.27	0.935	6.99 (2)
Tetrakis (dimethylamino) ethylene (TMAE) $(\text{CH}_3)_2\text{N}-\text{C}=\text{C}-\text{N}(\text{CH}_3)_2$	200.23	-11	59 #	0.86	5.36 (3)
Trimethylamine (TMA) 	59.11	-117.0	2.9	0.656	7.82 (1) 8.50 (4)
Triethylamine (TEA) 	101.19	-114.7	89.3	0.728	7.5 (1)
Naphthalene (Naphth.) 	128.19	80.55	218	1.0253	8.12 (6)
N,N,N',N'-Tetramethyl-p-phenylene diamine (TMPD) 	164.25	51	260	-	6.2 (5)

B.Pt. at 0.9 torr

- (1) Rosenstock et al (1977) (2) Franklin et al (1969)
 (3) Nakato et al (1974) (4) Lee & Bischel (1982)
 (5) Nakato (1971)
 (6) Handbook of Chemistry and Physics (1972)

TABLE 5-2: GENERAL PROPERTIES OF ADDITIVES.

NAME ABBREVIATED	VAPOUR PRESSURE DATA(FIGURE)	TOXICITY# (ppm)	SUPPLIER	COMMENTS
DMA	5-3	<5	BDH,KLL	Unpleasant odour even at very low concentrations. Avoid Contact with skin.
DEA	5-7	<5	BDH,KLL	Avoid contact with skin.
TMAE	5-10	--	ACC	Readily oxidised, must be handled in inert atmosphere. Avoid contact with skin.
TMA	GAS	<10	BDH	Very unpleasant odour which is extremely pervasive. Avoid contact with skin.
TEA	5-11	<10	KLL	Unpleasant odour. Avoid contact with skin.
Naphth.	ref (1)	<10		Avoid contact with skin.
TMPD	ref (2)	--	ACC	Irritant. Avoid contact with skin.

maximum concentration over a period of 8 hours.

BDH - BDH Chemicals Ltd.

KLL - Koch Light Laboratories Ltd.

ACC - Aldrich Chemicals Company Ltd.

(1) Handbook of Chemistry and Physics (1972).

(2) Guschin et al (1983).

TABLE 5-3: IONISATION OF ADDITIVES

NAME	IP/cm	CONC (ppm)	FLUENCE ($\mu\text{J}/\text{mm}^2$)	LASER TYPE	WAVELENGTH (nm)	REF.
DMA	1700	260	14	N	337	(1)
	3×10^7	260	12	DYE	266	(2)
DEA	1800	33	14	N	337	
TMAE	5000	1.3	1	N	337	(1)
TMA	NONE	1.3×10^4	1	DYE	300	(3)
	5.7×10^5	1.3×10^4	1	DYE	266	
TEA	NONE	1900	14	N	337	(2)
	1.3×10^7	1900	8	DYE	266	
Naph	2×10^5	60	4	DYE	300	
	2×10^7	60	4	DYE	274	
TMPD	1.4×10^5	3	1	DYE	268.5	
				N	337	

- (1) Ledingham et al (1984).
 (2) Ledingham et al (1985).
 (3) Raine et al (1983).

ANALYSIS OF THE BACKGROUND IONISATION IN PROPORTIONAL COUNTERS.

SECTION 6-1: INTRODUCTION.

Background 2-photon ionisation spectra produced for the type 1 counter were shown in chapter 5, figure 5-4. Fluctuations were observed in the ionisation intensities and these indicated the presence of resonant fine structure. Three processes which could account for the structure are: resonances into intermediate vibronic states of the system; resonances into vibronic states of the ionised molecule; resonant transitions into super-excited states, followed by preionisation. The ionisation could of course be a combination of all these processes.

If identification of the impurities in the counter gas were to be attempted by the comparison of the R2PI spectra with UV absorption spectra, then resonant transition into an intermediate level would have to be the dominant process. This chapter summarises the analysis of background R2PI spectra for three types of counter. It was assumed that the R2PI spectra would resemble, at least to first order, the UV (electronic) absorption spectra for the impurity. This assumption was justified for at least two of the impurities and could probably be applied to almost any molecule with intermediate resonant levels.

Results and discussion for the R2PI spectra of each type of proportional counter will be given in turn.

Experiments designed to identify the sources of the major contaminants will be outlined. The results and discussion of these experiments are given in section 3. The effects of the purification system (proposed for the ALEPH TPC) on the background ionisation are also discussed.

SECTION 6-2: WAVELENGTH DEPENDENCE OF IONISATION BETWEEN

260nm AND 337nm.

THE BACKGROUND IONISATION SPECTRUM FOR THE TYPE 1 COUNTER.

The background two photon ionisation spectrum was taken in 1nm increments between 260nm and 337nm. For each wavelength setting the data was collected, as described in chapter 3, and then binned into small increments for laser fluence. The laser fluence was kept lower than the saturation level of the two-photon process. The average ionisation intensity was expressed as ion pairs per cm (IP/cm) using Fe55 (227 IP.) as a calibration source. The data then could be normalised to $1\mu\text{J}/\text{mm}^2$.

The large dynamic range of the ionisation as a function of wavelength required the gain of the counter to be changed to keep the signal within the dynamic range of the analogue to digital converter (ADC).

The ionisation levels before and after the gain change, taken at a specific wavelength and laser fluence setting, were used to calculate the change in the counter gain.

The wavelength dependence of the background ionisation for the type 1 counter is shown in figure 6-1. The laser fluence was $8.1\mu\text{J}/\text{mm}^2$. Different symbols represent different dye regions of the laser covered by Coumarin 153 (+), Rhodamin 6G (\blacktriangle) and DCM (\circ) (See chapter 3-2). Differences in the levels of ionisation in the overlap regions of the dyes are possibly caused by variations in the spatial and temporal cross-sections of the laser beam. The beam cross-sections are affected by dye efficiency drops near the edges of its spectral range so that fewer modes of the pump laser are able to excite the dye. (Johnson et al (1976); Sorokin et al (1968))

Figure: 6-1 Wavelength dependence of the background ionisation in a type 1 counter.

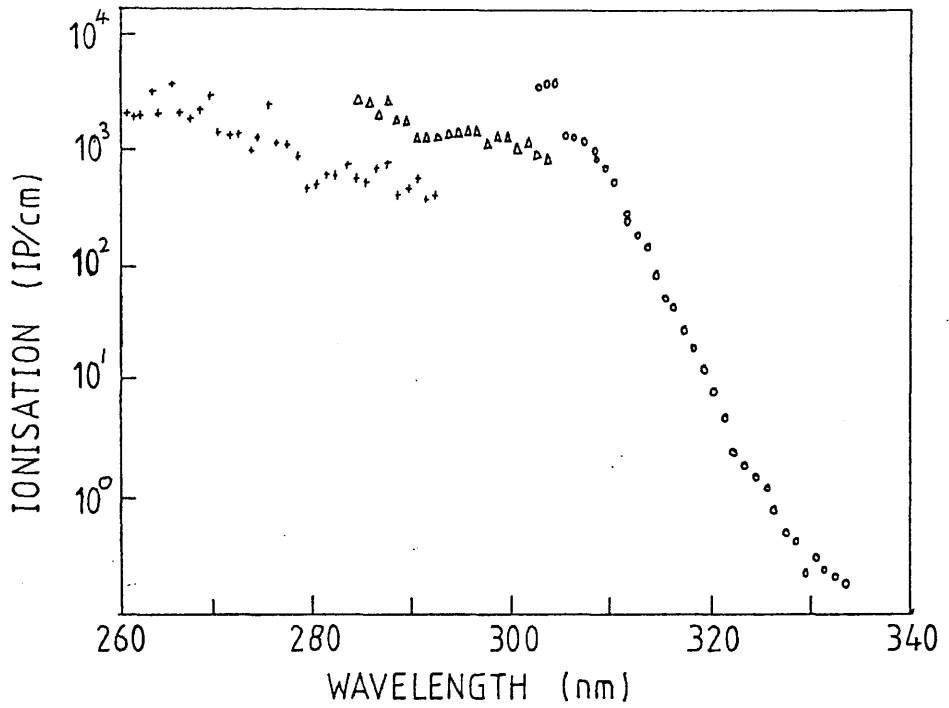
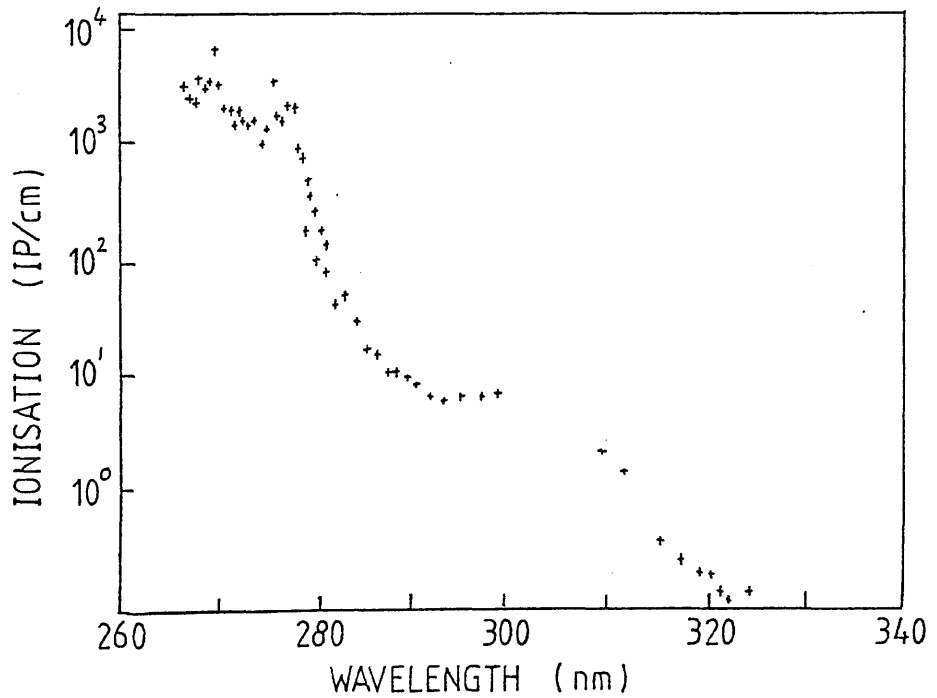


Figure: 6-2 Wavelength dependence of the background ionisation in a type 1 counter after cleaning and baking.



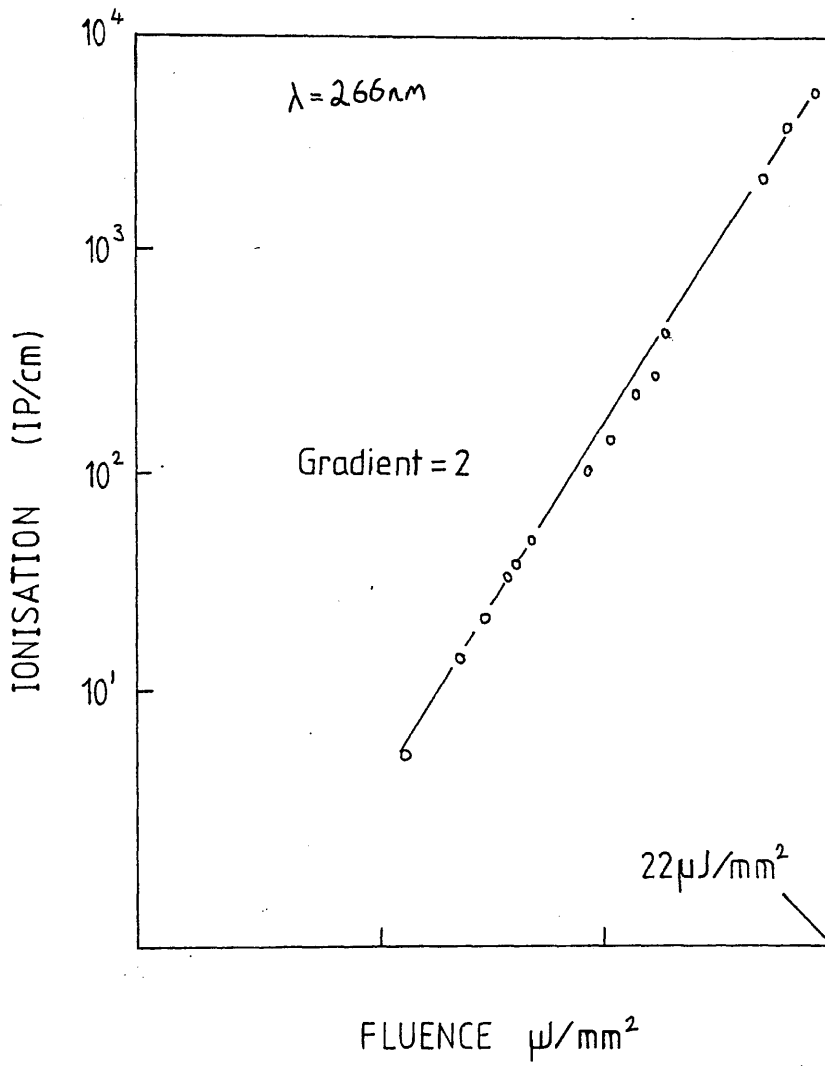
Between 260nm and 308nm the ionisation remains fairly constant at 2×10^3 IP/cm, but between 308nm and 337nm the ionisation decreases by about four orders of magnitude. The similarity between the spectrum in figure 6-1 and the R2PI spectrum for DMA in figure 5-4 was thought to be caused by contamination of the P10 gas by desorption of seeding compounds from the counter walls. Before the background spectrum had been taken, the counter had been used for seeding experiments with several molecules: DMA, DEA and TEA (Chapter 5). It was felt that some of these might still have been adsorbed on to the counter surfaces.

To remove any contaminant seeding agents the counter was completely dismantled and baked for several hours. A further spectrum over the same wavelength range was produced (See figure 6-2). This time the spectrum was noticeably different. At wavelengths below 279nm the ionisation was again found to be fairly constant at 2×10^3 IP/cm. Between 266nm and 308nm there was a drop in ionisation by over two orders of magnitude. The difference in the spectra (6-1 and 6-2) was attributed to the removal of some of the contaminating impurities (by baking the counter). This example proves that some of the seeding agents are persistent and may only be removed by very thorough cleaning of the counter system.

Figs 6-1 and 6-2 show evidence of fine structure between 266nm and 278nm. In order to resolve this fine structure the region was examined in greater detail. The data in figure 6-3 was taken with wavelength increments of 0.025nm and clearly shows resonant structure. To confirm that the order of the MPI process was $N=2$ the laser fluence was varied over a large dynamic range down to the detection limits of the apparatus. The results were plotted on a log/log scale (figure 6-4). Even at very low fluences the gradient of the curve is 2, indicating again a two-photon ionisation process.

The shortest wavelength of the spectrum is 266nm (4.66eV) and

Figure: 6-4 Attenuation curve for the background ionisation.



hence any impurities responsible for the production of the fine structure must have ionisation potentials $<9.32\text{eV}$.

THE ANALYSIS OF THE SPECTRA TAKEN BETWEEN 266nm AND 278nm.

The complexity of the two-photon ionisation spectrum in figure 6-3, and the low ionisation potential of the constituents responsible for it, suggest the presence of polyatomic molecular impurities, rather than atoms or small molecules. Although many of the metals used in the construction of the counter have low ionisation potentials in atomic form, they can be discounted as possible impurities because of their very low vapour pressures. Indium, used as a vacuum seal is an exception, but it does not exhibit electronic absorption resonances in this wavelength region. Small molecules likely to be present in the counter gas as impurities, such as O_2 , CO_2 , H_2O have ionisation potentials of greater than 9.32eV requiring at least 3-photons of wavelength 270nm , to ionise them.

The UV spectra of organic molecules are well documented (e.g. Murrell (1963) and UV Atlas of Organic Compounds (1966)). Two families of organic compounds that commonly absorb in the near UV are those with chromophoric groups and those with conjugated bonds. A chromophoric group contains an atom with a lone pair of electrons and generally will absorb at about 310nm (3.8eV). Conjugated molecules contain a chain of carbon atoms with alternate single and double bonds and generally will absorb at around 300nm (4.1eV). Many forms of conjugated systems are unstable and tend to undergo chemical reactions with their surroundings, effectively removing them as ionisable impurities from the counter gas. However, some are extremely stable, in particular aromatic ring systems like benzene and substituted benzenes. These exhibit electronic absorptions in the 260nm to 300nm wavelength region (See appendix 3).

Most benzene compounds have ionisation potentials of around 9eV and could therefore be ionised by two photons with wavelengths around 270nm. Two-photon resonant spectra for polyatomics at room temperature are scarce, hence identification of the unknown molecules had to be carried out by an alternative method.

In a R2PI process, the first step, from the ground state to an intermediate excited state is precisely that involved in electronic absorption spectroscopy. Therefore the R2PI spectrum of the molecule in the P10 counter gas will resemble the vapour phase absorption spectrum of the molecule in air. This assumes that either the first step in the two-photon process determines the rate of ionisation, or, that the cross-section for the transition from the intermediate state to the continuum is not strongly wavelength dependent (See chapter 1-5).

To test this, P10 gas was passed through the proportional counter flow system and its single photon electronic absorption spectrum taken. Using a quartz spectrometry cell the gas was analysed in a Beckman Spectrophotometer (Described in chapter 3-5). The P10 gas gave no absorption above background. This meant that either the impurities did not absorb in the wavelength region between 260nm and 300nm or that their concentrations were very low. For molecules with absorption cross-sections of the order $\sigma = 10^{-18} \text{ cm}^2$ (UV Atlas of Organic Molecules (1966)) typical of substituted benzenes, the lower limit of the sensitivity of the Beckman is about 10ppm.

A liquid nitrogen bath was used to trap impurities from the P10 gas. At these temperatures most contaminating organic compounds should be trapped. Careful gas flow regulation ensured that the levels of condensed methane and argon in the trap were kept constant. The trapped impurities were passed into a spectrometry cell by warming up the cold trap to room temperature and cooling the connected cell to -50° C . The UV spectrum for this sample exhibited several characteristics similar to

that of the background R2PI. Most noticeable was fine structure at similar wavelengths, an slight edge at 300nm and ^{some} _λ levelling off of absorption below 280nm (See figure 6-5a). This implied that the UV and R2PI spectra could be compared directly (As was expected from the similarity of the processes involved).

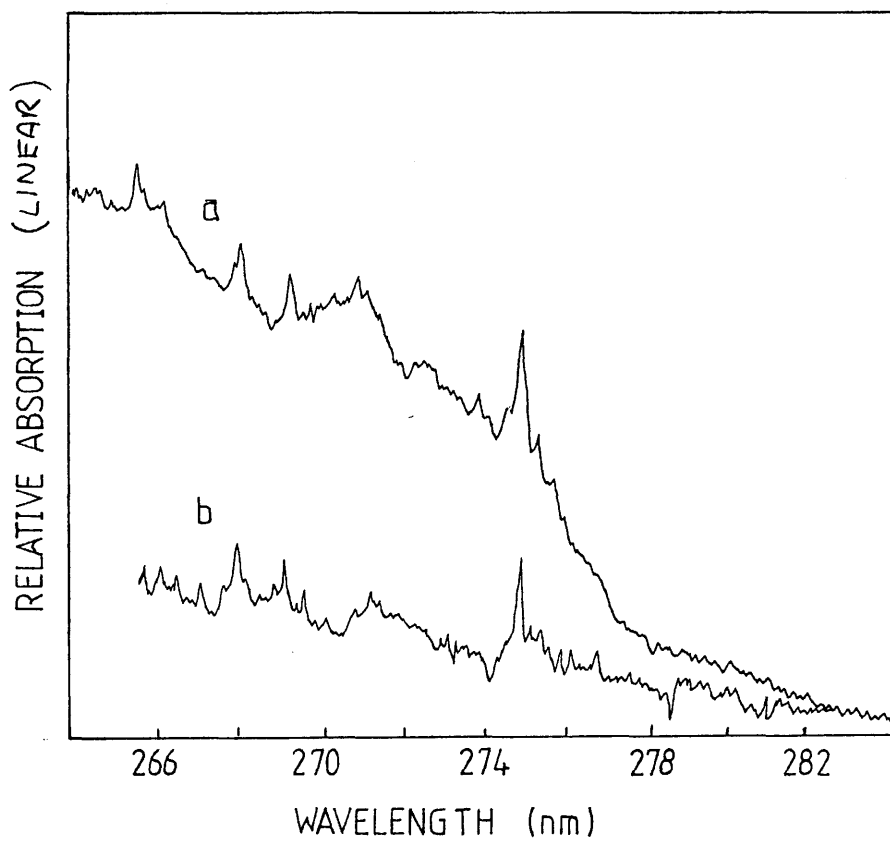
A second spectrum was obtained (See figure 6-5b) by the same method, except that the counter was removed from the gas flow line. The disappearance of the edge at 300nm indicated that it was produced by impurities in the counter.

Between 260nm and 280nm several substituted benzenes were identified (UV Atlas of Organic Compounds 1966) which, in methanol solution, produce electronic absorption spectra similar to the background R2PI spectrum

Absorption spectra for molecules are usually taken with the molecules dissolved in solvents. In solution the energy levels of molecules are shifted. For benzene type molecules the solvent causes a shift of the UV absorption spectrum to longer wavelengths. This occurs because benzene in an excited state tends to be more polar than in the ground state. Transition energies are reduced because dipole-dipole interactions lower the energies of the excited states more than that of the ground state. Also, the spectra are broadened by collisions between excited molecules and neutral solvent molecules (see chapter 1-4, Collision Broadening). Therefore, in solution, the absorption spectra are shifted to longer wavelengths and are collision broadened more than in the gas phase.

Since very little gas phase data exists for benzene type molecules, it was necessary to obtain it experimentally. A 10cm active length quartz spectrometer cell filled with substituted benzenes at room temperature vapour pressure was analysed using a Beckman Spectrophotometer. The differences between the solvent and gas phase

Figure: 6-5 UV spectrum of impurities in cold trap.



spectra are illustrated in figure 6-6.

The electronic absorption spectrum of the hydroxy-substituted benzene molecule (phenol) was found to be in agreement with work by Matsen et al (1945). The spectrum is identical to the R2PI structure in the wavelength range 266nm to 278nm, to first order (see figure 6-7).

Investigations revealed the source of the phenol in the type 1 counter to be from reinforced plastic gas flow pipes. Contamination occurred by phenol outgassing from the walls of the pipe into the counter gas as it flowed through into the counter.

THE BACKGROUND R2PI SPECTRUM IN THE TYPE 2 COUNTER.

The background ionisation (see figure 6-8) for the type 2 counter was measured in 1nm increments as described for the type 1 counter. The P10 gas flow through the counter was fixed at 25ml/min. Care was taken to ensure that none of the seeding agents used previously were allowed to contaminate the system. The plastic flow pipes were not used in this experiment. The ionisation was found to be at least an order of magnitude lower than that found for the type 1 counter and was without the resonant structure attributable to phenol (see figure 6-3).

With the removal of phenol, further R2PI fine structure was resolved at around 268nm. This suggested the presence of another benzene type impurity. A high resolution spectrum (of 0.01nm increments) was taken using a 'clean' type 2 counter with a static gas filling. The wavelength was scanned between 262nm and 269nm with increments steps of 0.01nm giving the spectrum shown in figure 6-9.

Identification of the impurity was simplified by the knowledge gained from the identification of phenol. Furthermore Boerner (1985) had reported the presence of a series of substituted benzenes in P10 gas used at CERN. In Boerner's work the impurities were trapped by passing

Figure: 6-6 Difference between solvent and gas phase UV spectra.

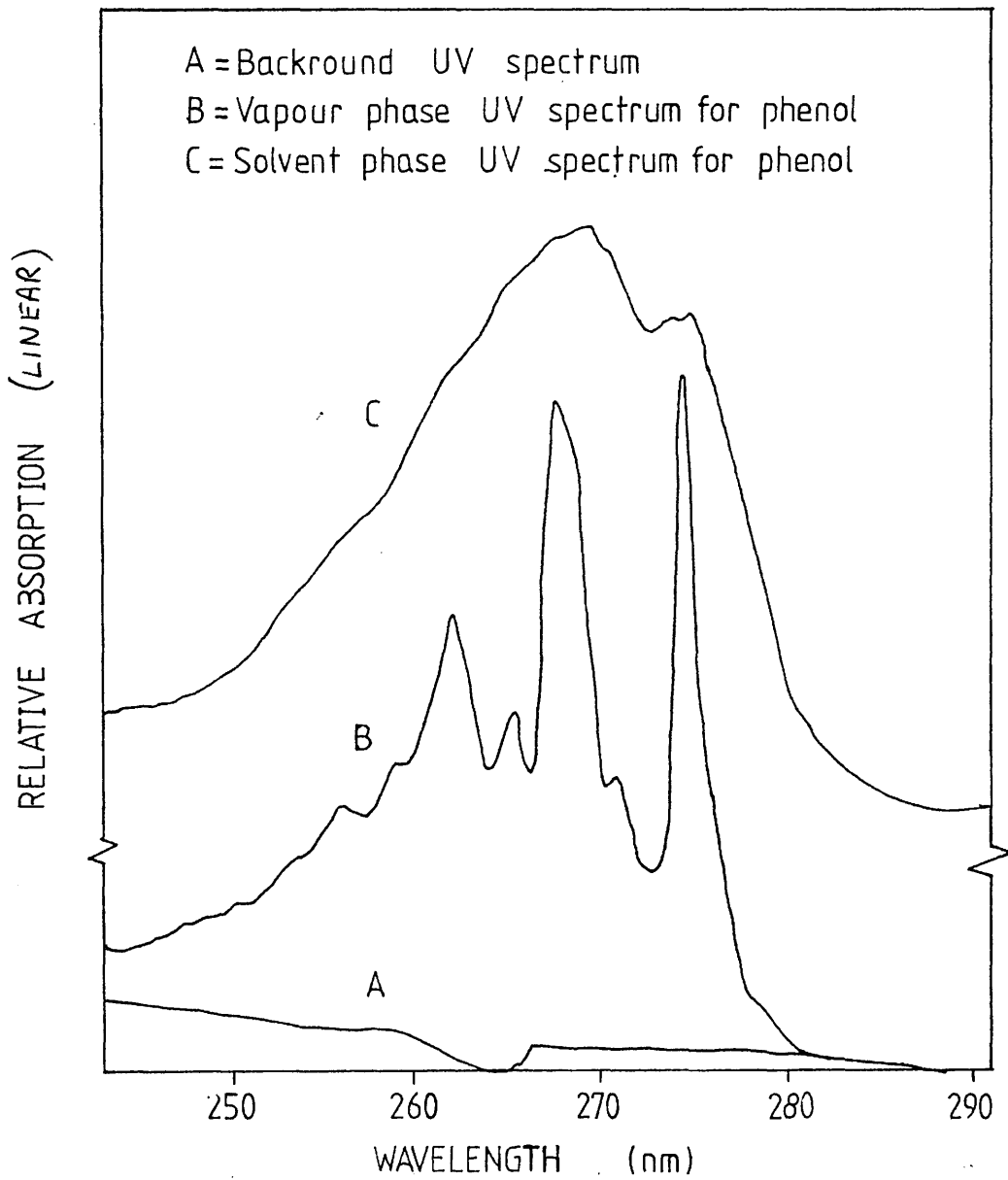


Figure: 6-7 Background R2PI and UV absorption spectra of phenol.

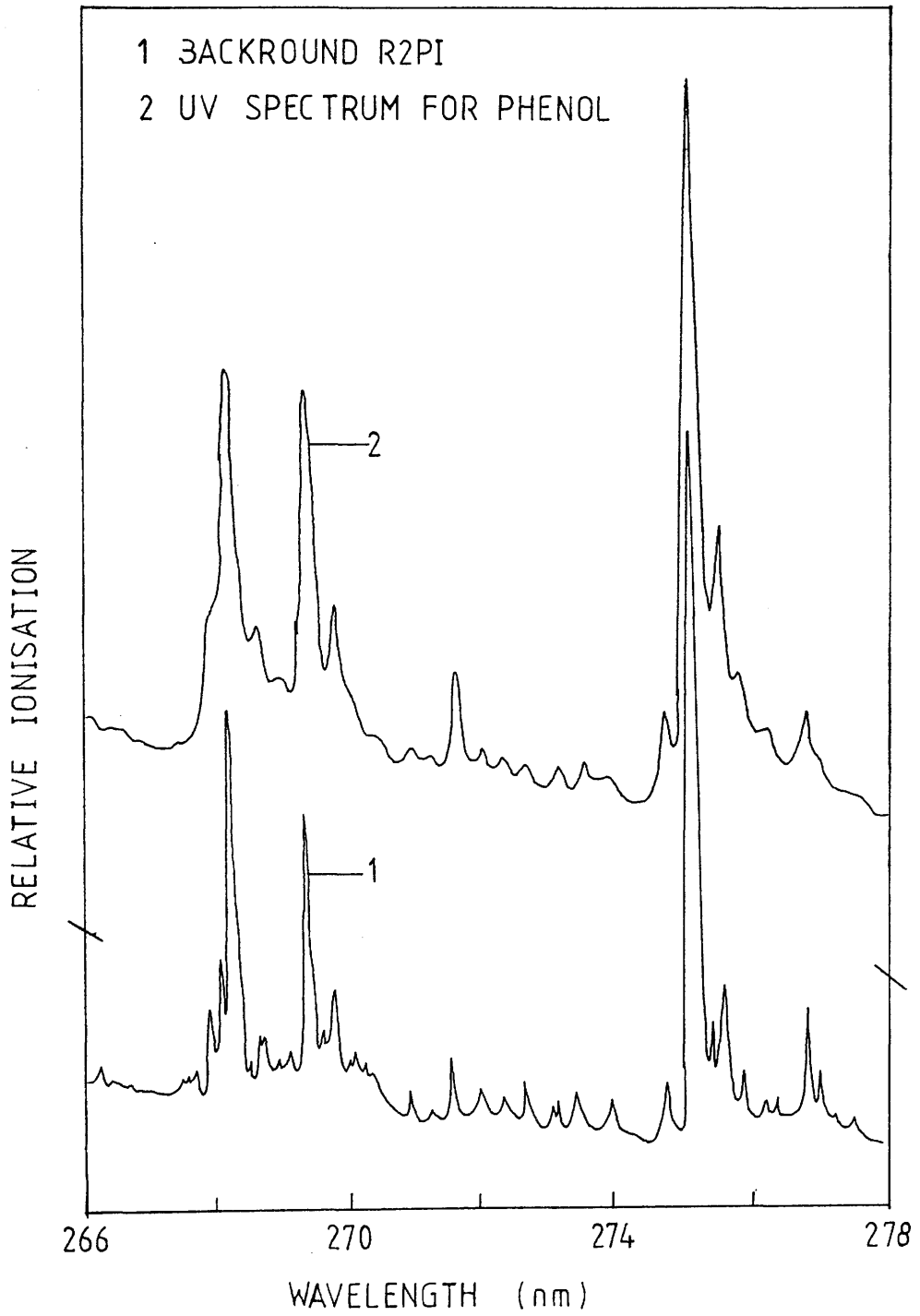


Figure: 6-8

Background ionisation of the type 2 counter.

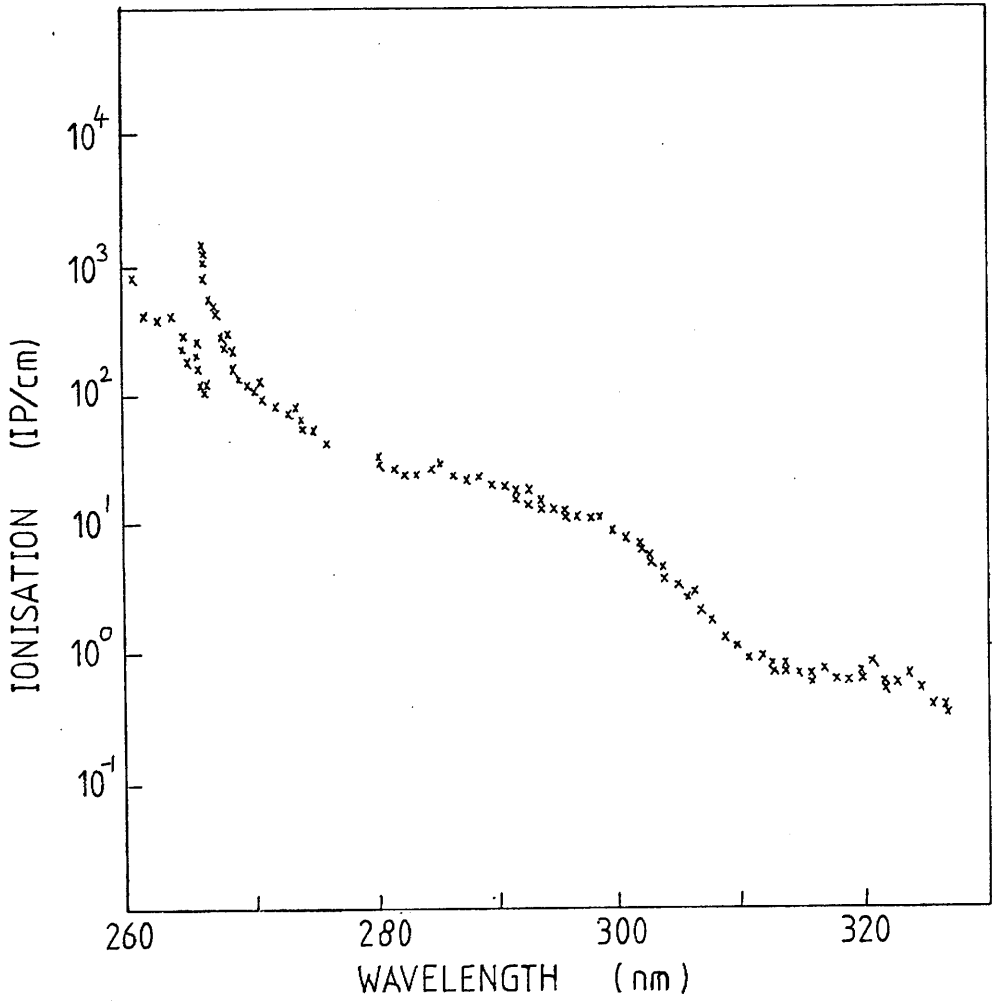
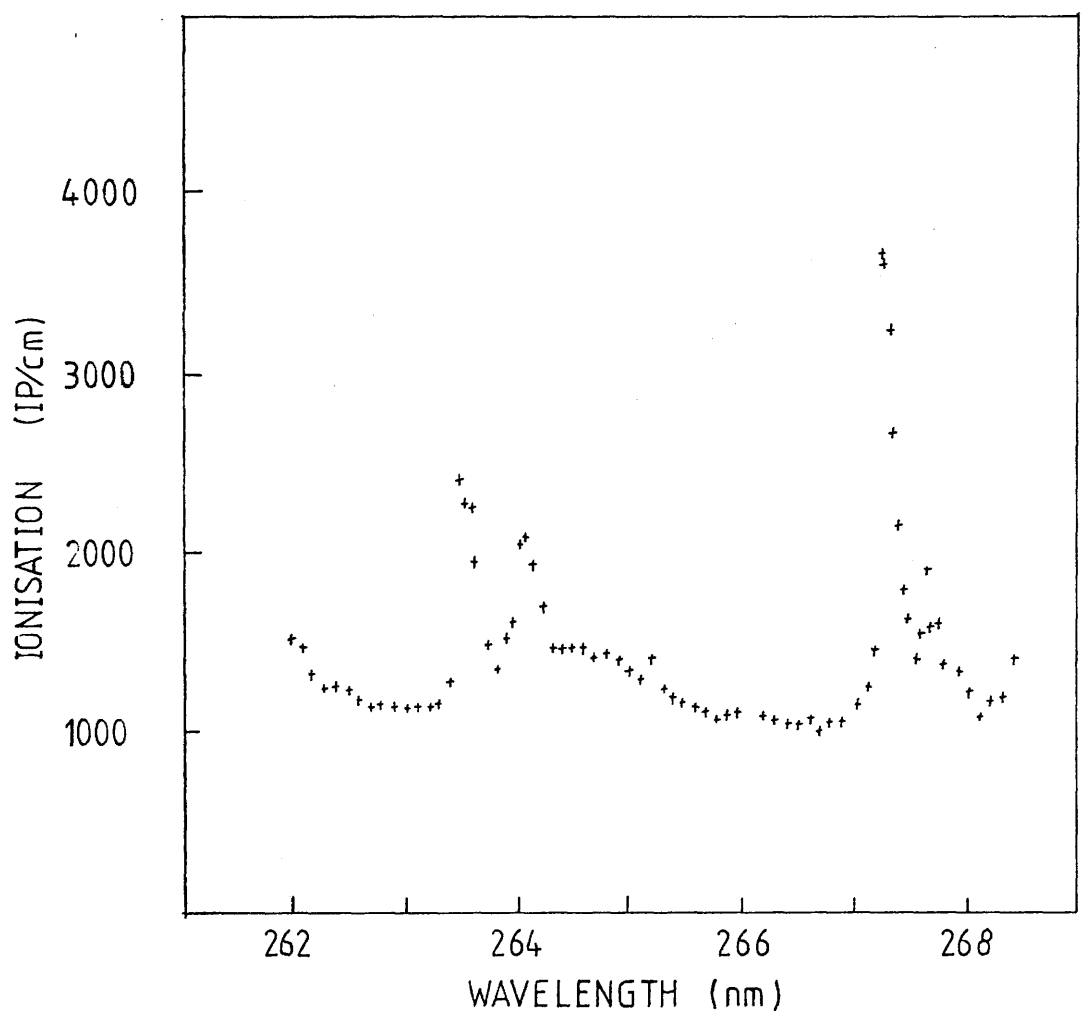


Figure: 6-9 Background R2PI spectrum between 262nm and 269nm for the type 2 counter.



a large volume of P10 gas through activated carbon and were then analysed using gas chromatography and mass spectrometry. Table 6-1 gives a list of the molecules trapped by this procedure. Vapour phase UV spectra of some of these molecules were taken for comparison with the R2PI spectrum. Some exhibited absorption in the 268nm wavelength region. One in particular, toluene, had an electronic absorption structure which closely matched the background R2PI structure (see figure 6-10). The R2PI spectrum of high purity toluene was investigated in the wavelength range 262nm to 269nm. P10 gas was passed at 50 ml/min over a sample of toluene held in a cold bath at a temperature of -80°C , (maintained by sublimating carbon dioxide). This procedure gave a toluene concentration of not more than 6ppm. The concentration was determined from the accepted vapour pressure for toluene of 5×10^{-3} torr at -80°C (Hand book of Chemistry and Physics (1972)). The R2PI spectrum, taken in 0.01nm increments, is plotted in figure 6-11a. The resonances are at the same wavelengths as those in the background R2PI (figure 6-11b). This confirms the presence of toluene as a contaminant in the P10 gas. By comparison of the relative peak to valley ratios of the background and toluene spectra, the concentration of the toluene in the counter was estimated to be 22ppb (Drysdales et al (1986a)).

Unlike phenol the source of toluene was not attributed to a single component in the apparatus. Toluene is a common impurity in methanol and ethanol which were used as cleaning agents for the counters. Also Boerner (1985) suggests that toluene is an inherent impurity in P10 gas.

Using the same type two counter in a static gas mode, two background R2PI spectra were taken ten hours apart showing an increase in the concentration of toluene with time (figure 6-12). Since the counter gas was static, this could only be explained by toluene outgassing from the counter surfaces into the P10 gas. Further experiments described in the next section corroborate this conclusion.

Figure: 6-10a UV absorption spectrum for toluene.

Figure: 6-10b R2PI spectrum of toluene.

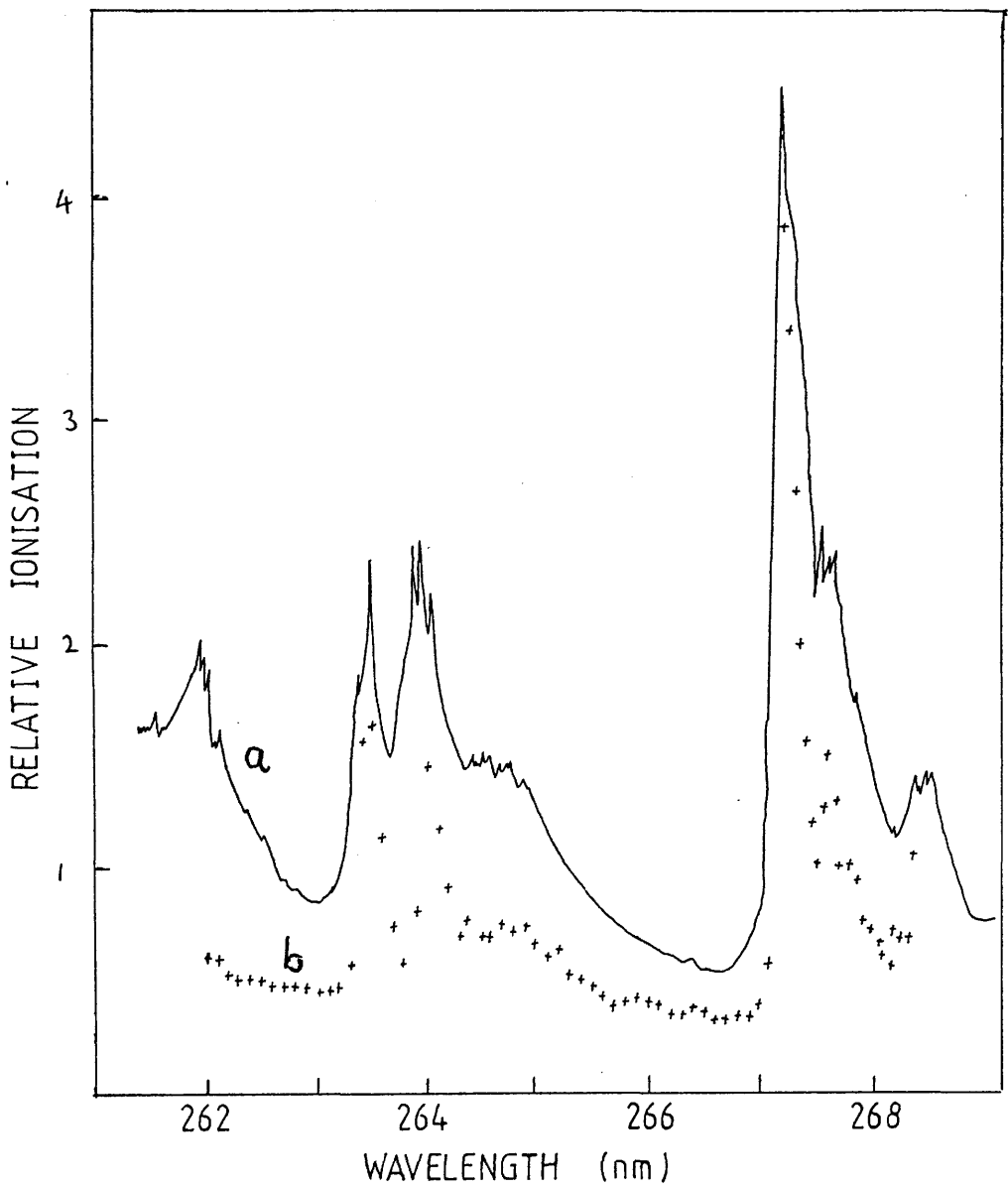


Figure 6-11 Background and toluene R2PI spectra.

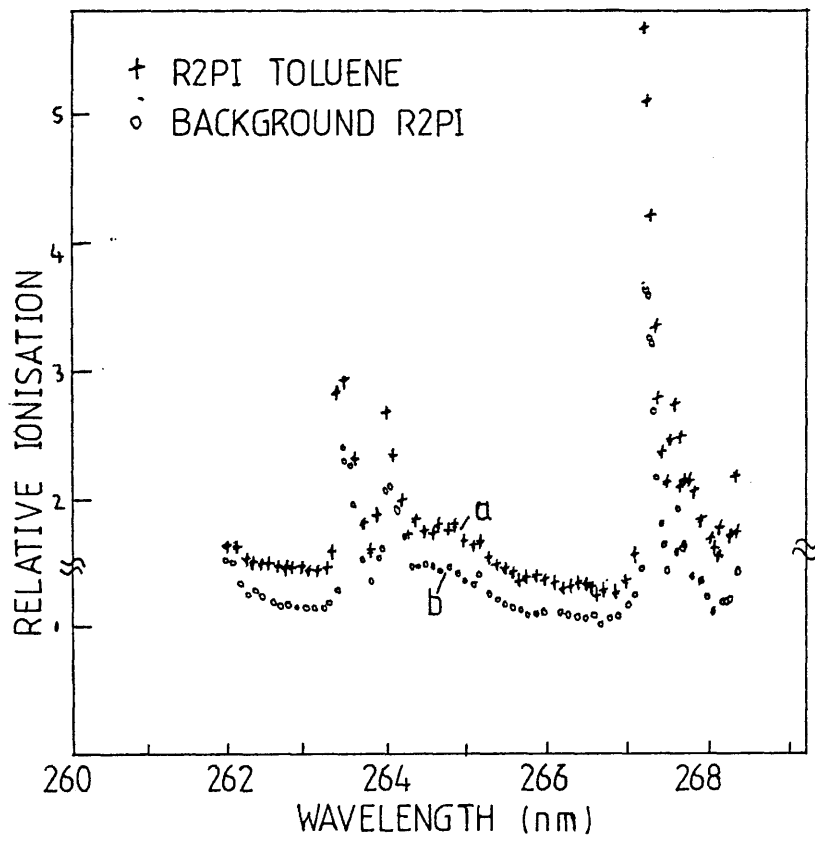
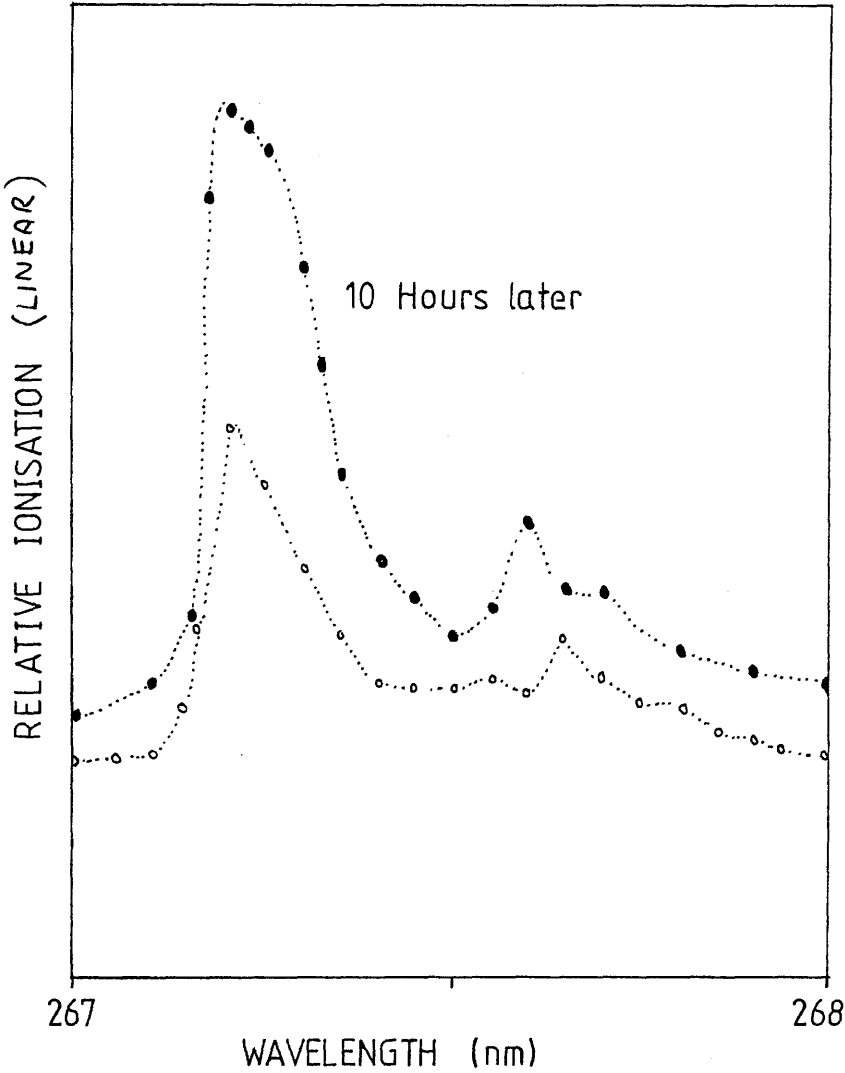


Figure: 6-12 Comparison between two R2PI spectra taken 10 hours apart.



The toluene spectrum was subtracted from the background spectrum using the known peak to valley ratios for toluene (figure 6-13). The remaining ionisation indicates the presence of other impurities in the P10 gas. Identification of these impurities would require the removal of much of the toluene impurity from the counter system. This has proven to be difficult. The problem is illustrated in the background R2PI spectra for the type 3 counter. Even after very thorough cleaning, fine structure associated with toluene contamination was observed.

THE BACKGROUND R2PI SPECTRUM OF THE TYPE 3 COUNTER.

The background R2PI spectrum for the type 3 counter was taken between 262nm and 330nm with the P10 gas in static mode (figure 6-14). This may be compared with the background R2PI spectrum for the type 2 counter over the same wavelength range (figure 6-8). Ionisation in the type 3 counter was approximately a factor of ten lower than in the type two counter. Since the same P10 gas was used in both counters, the difference must be attributable to different levels of impurities outgassing from the counter constituents. This indicates that the type 3 counter had cleaner surfaces than the type 2 counter, although the fine structure of toluene was still observed.

Figure: 6-13 Background subtracted R2PI spectrum.

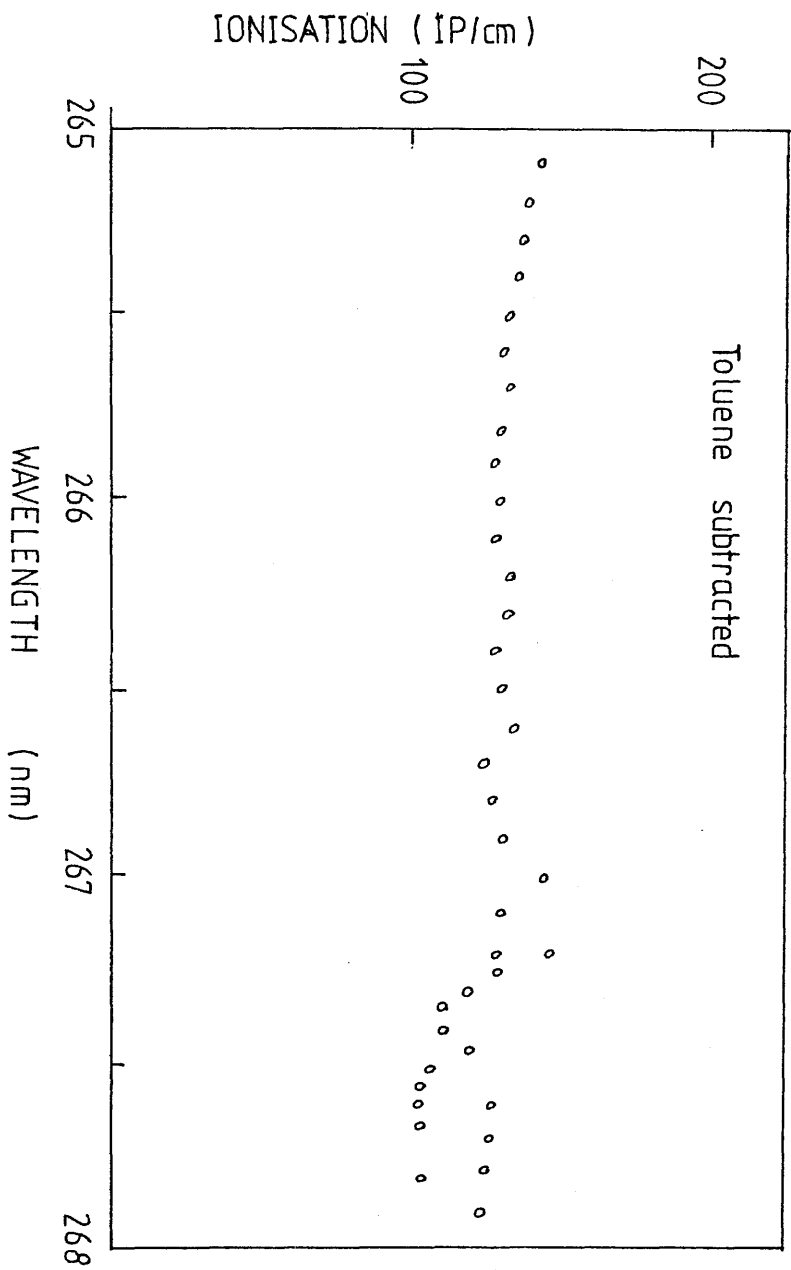
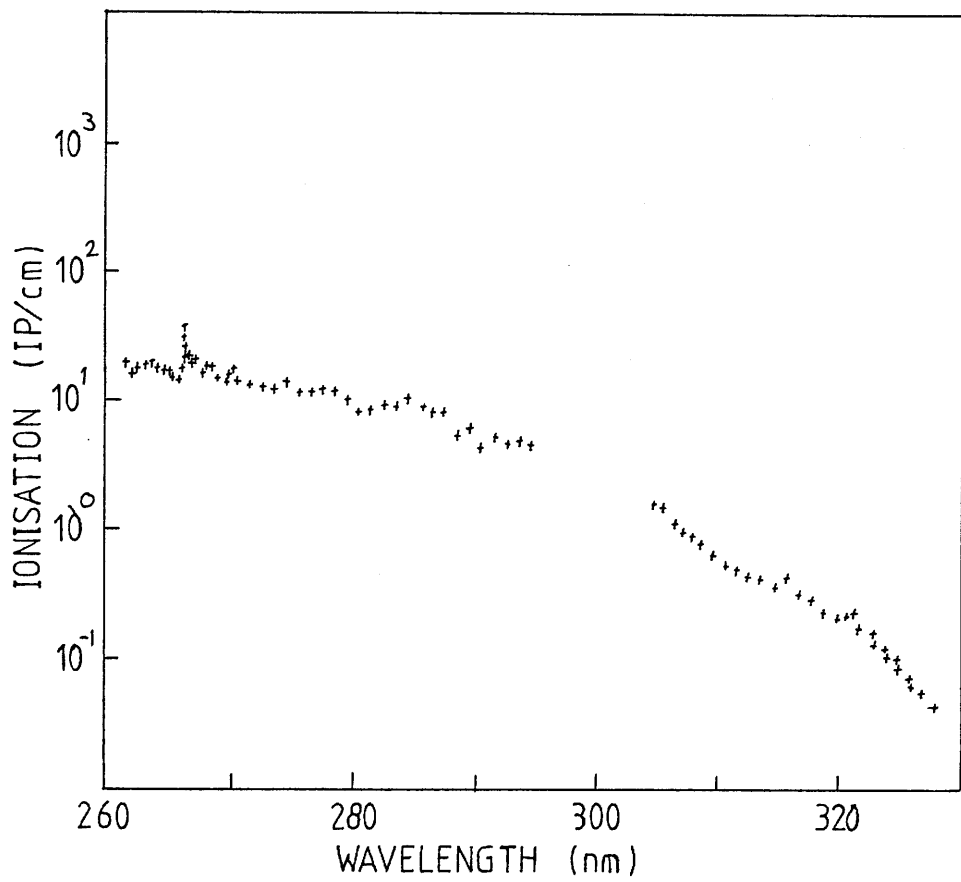


Figure: 6-14 Background R2PI spectrum for the type 3 counter.



SECTION 6-3: DESORPTION OF IMPURITIES FROM COUNTER SURFACES.

Outgassing has been shown to be a major source of impurities in the counter gas. Further evidence backing up this conclusion is given below.

A background spectrum for a type 2 counter was produced with P10 gas flowing through the counter at 50ml/min (figure 6-15). In figure 6-16 is the background R2PI spectrum for the type 2 counter with a static gas fill. The difference between the spectra can be explained if the source of the impurities is from the counter surfaces. Impurities outgassing from the counter surfaces increased in concentration in the static gas. This was observed as an increase in ionisation with time. Eventually the ionisation levelled off suggesting an equalisation in the rates at which the impurities were outgassing from and re-adsorbing back onto the counter surfaces. With P10 gas flowing through the counter the outgassed impurities were flushed from the counter. The result was a lowering in concentration of impurities in the gas and therefore a reduction in the ionisation.

Figure 6-16 shows the effect on the laser induced ionisation at 266nm in the type 3 counter when part of the counter was heated to around 100 °C. The ionisation increased by a factor of 6. The fluctuations in the rising part of the graph were thought to be the result of variations in the temperature of the heated area. When the heating was turned off the ionisation slowly fell again. These results clearly indicated that the impurities were outgassing from the counter surfaces. The fall in ionisation as the counter cooled must have been caused by the impurities re-adsorbing onto the counter surfaces.

Hubricht et al (1985) carried out a similar experiment with a very clean counter system. They studied the intensity of ionisation as a

Figure: 6-15 Static and Flow mode, R2PI spectra for the type 2 counter.

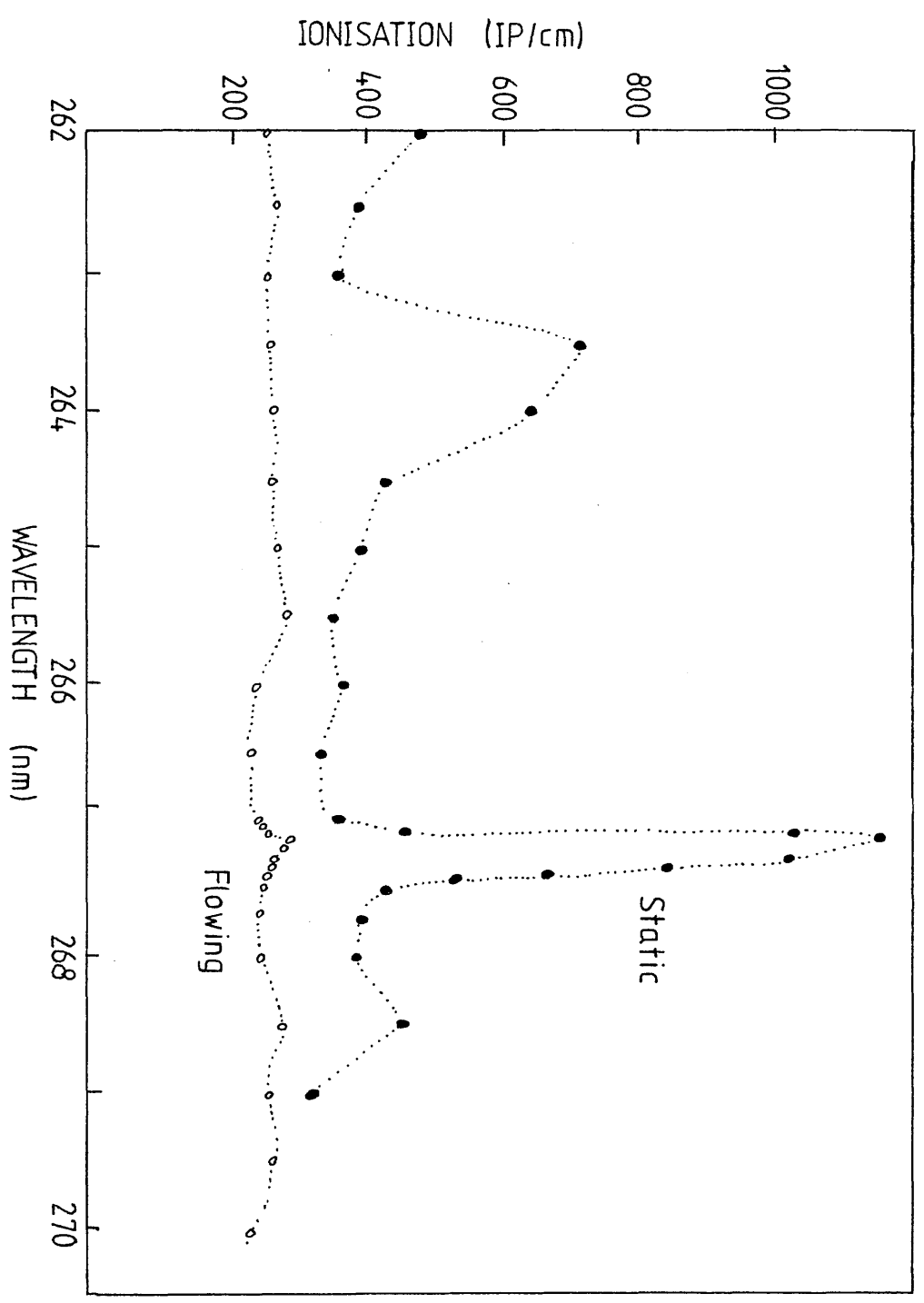
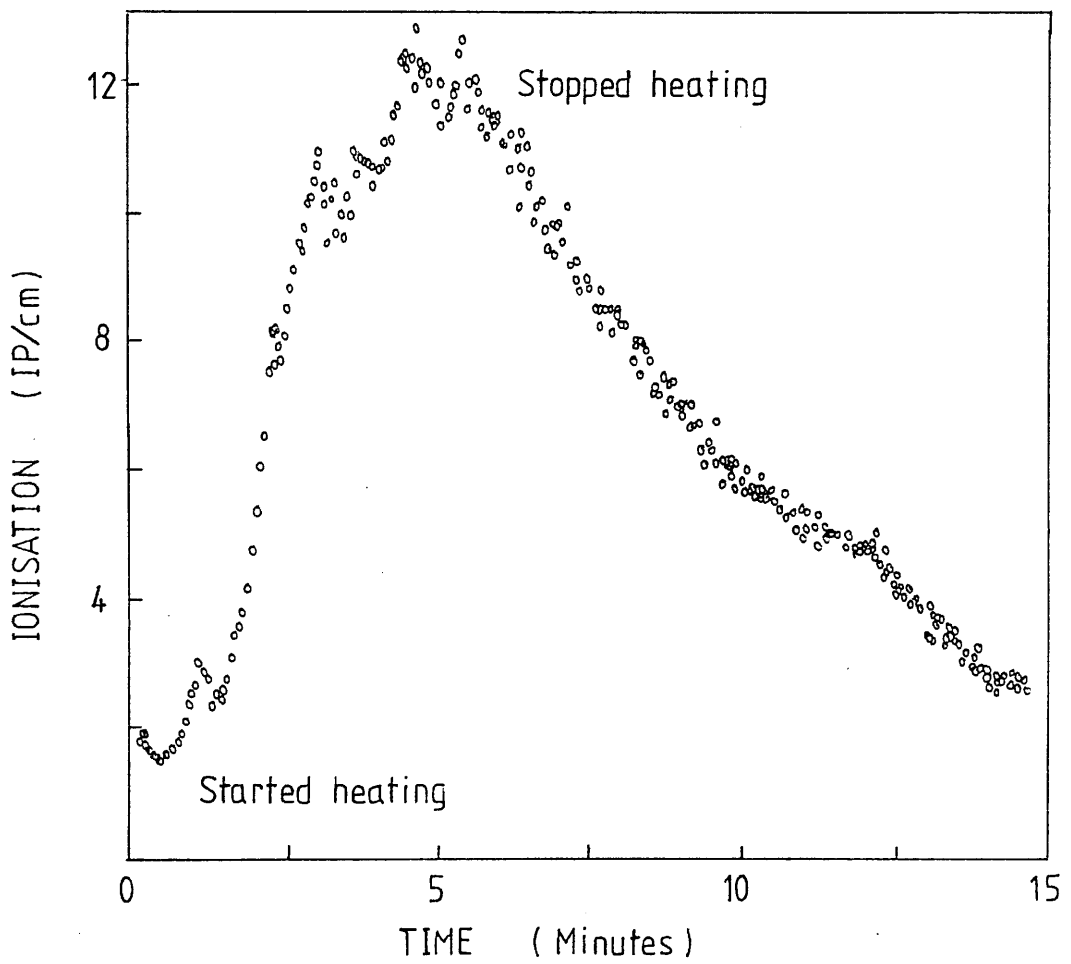


Figure: 6-16 Effect of heating the counter on the ionisation.



function of temperature and found that impurity levels in their system increased with temperature.

Argon/ethane (90/10%), argon/propane (90/10%), argon/isobutane (90/10%), argon/carbon dioxide (90/10%) and argon/ethane (50/50%) counter gases have all been used in a type 1 counter. The ionisation observed for each gas was independent of pressure and was approximately equal for each gas. The pressure independence would not have been observed if the impurities were inherent in the gas and must have been the result of outgassing.

Outgassing from and condensation onto the counter surfaces are caused by adsorption and desorption processes. There are two basic types of adsorption, physical (physisorption) and chemical (chemisorption). Physisorption is the result of a weak van der Waals interaction between the surface and the molecule. For example, random fluctuations in the electron distribution of a molecule can give it a transient dipole moment. The dipole can induce polarisation of a nearby system giving a brief coulombic attraction between the molecule and the system. The net effect is a weak attractive force between molecules in the gas and any surfaces the gas is in contact with. Chemisorption is the result of chemical bonding with the surface.

Desorption rates of molecules from surfaces depend on the strength of the attractive force holding the molecule to the surface (the stickiness of the molecule). Physisorbed molecules desorb rapidly, their typical lifetime on the surface is 10^{-5} secs. Chemisorbed molecules on the other hand may be very strongly bound to a surface. As a result their lifetimes on the surface may typically be many hours. This may explain how toluene could remain adsorbed onto the counter surfaces even after cleaning and baking.

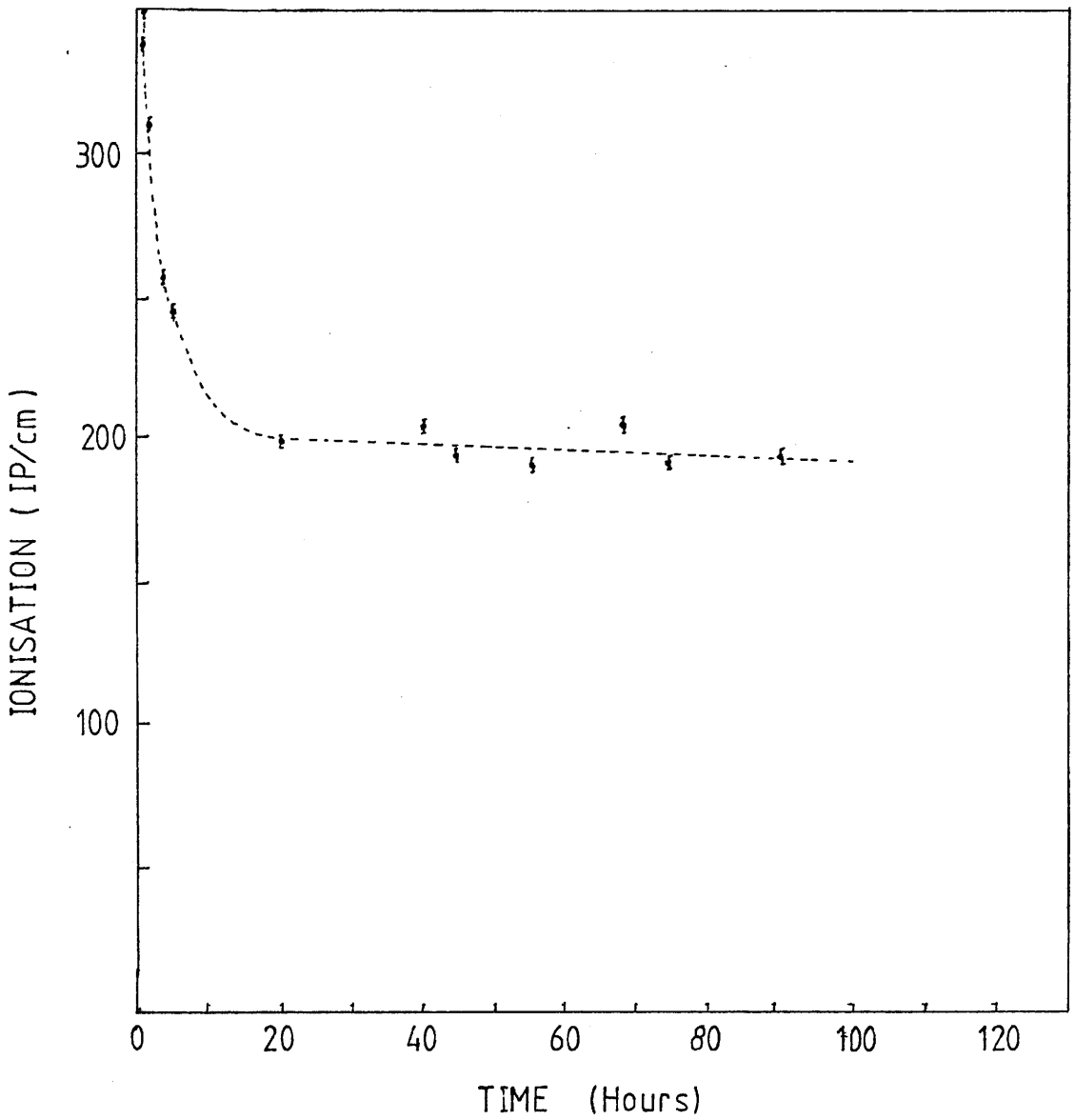
SECTION 6-4: INVESTIGATION OF THE EFFECT OF GAS PURIFICATION
ON THE BACKGROUND LASER IONISATION IN PROPORTIONAL
COUNTERS.

The effect on the ionisation of the purification of counter gases has been studied by Hubricht et al (1985). They flowed the gas in a closed circuit, trapping out impurities like oxygen and organic molecules in a titanium getter and an activated carbon cold trap. After several hours of gas cleaning in this way the ionisation fell below their detection limit of 0.4IP/cm. After about 80 hours they stopped cleaning the gas and the ionisation did not increase above the detection limit indicating that most of the ionisable impurities had been completely removed from the system.

In order to test the effect of the purification system on the ionisation a small test system (proposed for the ALEPH TPC) was built. (Drysdale et al (1986b)). A quadrupled Nd:YAG laser, with a 266nm output pulse of 10ns duration, was used to ionise the P10 counter gas. A quadratic behaviour was observed at all times during the experiment, indicating that the background ionisation was 2-photon ionisation of impurities in the gas.

Figure 6-17 shows the effect of the purification system on the ionisation over a period of 80 hours. Initially the ionisation drops very rapidly but after 40 hours the ionisation had reached a steady state at about half the original value. This indicates that the oxysorb at first adsorbs some of the ionisable impurities but that some of the impurities are affected little by the oxysorb.

Figure: 6-17 Effect of the gas purification system on the ionisation.



SECTION 6-5: CONCLUSIONS.

The background ionisation in the type 1 counter was thought to be due mainly to the desorption of seeding compounds introduced into the counter at an earlier date. After extensive cleaning and baking the background appeared different. This was credited to the removal of some of the adsorbed additives from the counter surfaces.

The 2-photon spectra for the type 1 counter exhibited fine structure at around 270nm. Comparing high resolution R2PI spectra with UV absorption spectra showed that the structure could be attributed to a resonant transition between the ${}^1A_{1g}$ state and a symmetry forbidden ${}^1B_{2u}$ state of the phenol molecule (see appendix 3). Desorption from plastic pipes (used to carry the P10 gas to the counter) was found to be the source of the phenol.

New R2PI spectra were taken for a type 2 counter with no previous history of seeding and with stainless steel gas flow pipes. The spectra again exhibited fine structure which was attributed this time to toluene. Toluene did not appear to have a definite source, although it was thought to be outgassing from the counter surfaces. Toluene is present as a trace impurity in most organic solvents (like methanol and ethanol). Organic solvents were used to clean all of the counters with the result that toluene may have been adsorbed, from the solvents, on to the counter walls. This would explain the presence of toluene in the 'super clean' type three counter.

The ionisation in an isolated counter was found to be temperature dependent, a definite indication that desorption of impurities from the counter walls was a major source of impurities.

TABLE 6-1: IMPURITIES IN COUNTER GAS AT CERN. (BOERNER (1985))

NAME	IONISATION POTENTIAL (eV)
ISOBUTANE	10.57 (1)
BENZENE	9.24 (1)
DIOXANE	9.13 (1)
TOLUENE	8.5 (1)
OCTANE	9.9 (1)
o-XYLENE	8.56 (1)
m-XYLENE	8.58 (1)
p-XYLENE	8.44 (1)
ETHYLBENZENE	8.76 (1)
NONANE	--
ISO-PARIFFIN C 10	--
BENZALDEHYDE	9.52 (1)
ALKYLBENZENE (ETHYLMETHYLBENZENE)	--
ALKYLBENZENES (WITH C ₃)	~ 8.70 (1)
ALKYLBENZENES (WITH C ₄)	~ 8.70 (1)
DICHLOROBENZENE	9.0 (1)
METHYL-ISOPROPENYLBENZENE	--
NAPHTHALENE	8.12 (1)
DODECANE	--
DIMETHYLPHTHALATE	6.9 (2)
DIETHYLPHTHALATE	--
DIOCTYLPHTHALATE	--

(1) HANDBOOK OF CHEMISTRY AND PHYSICS (1972).

(2) HANDBOOK OF CHEMISTRY AND PHYSICS (1986).

CHAPTER 7.

LASER IONISATION ENHANCEMENT WITH PHENOL, TOLUENE AND OTHER MOLECULES WITH UV RESONANCES AT AROUND 266NM WAVELENGTH.

SECTION 7-1: INTRODUCTION.

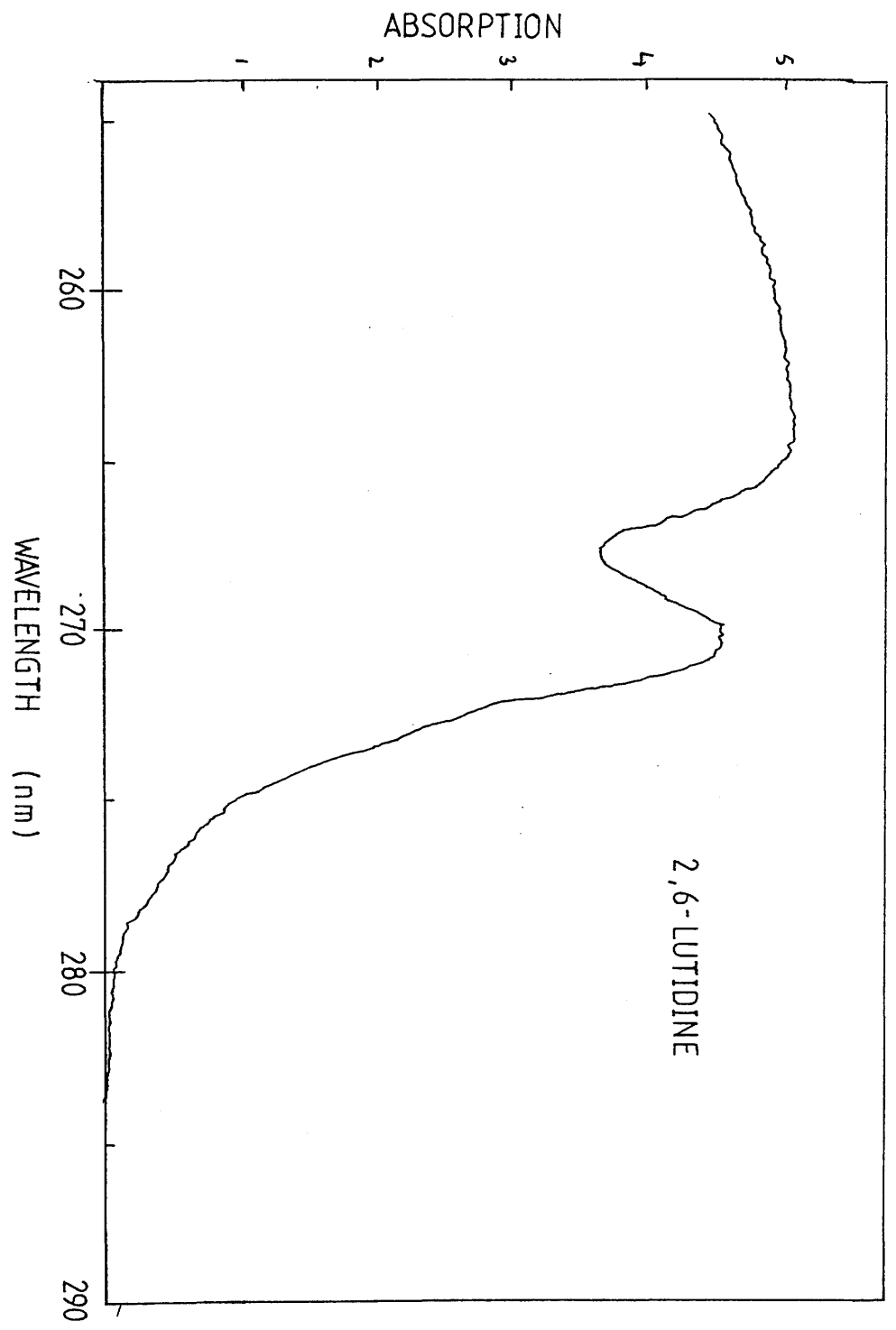
Phenol and toluene have both been identified as ionisable impurities. Their UV absorption spectra exhibit resonances attributable to a symmetry forbidden transition between ${}^1A_{1g}$ and ${}^1B_{2u}$ electronic states of the molecules (see appendix 3). Seeding experiments with these molecules are summarised in this chapter.

In addition, five other molecules were studied for reasons that are listed below.

(1) Diethyl- and dibutyl-phthalate: These molecules were two of several detected in a counter gas sample analysed by gas chromatography and mass spectrometry (Boerner (1985)). They are also known to be common impurities in rubbers.

(2) 2,6-Lutidine: A series of molecules with relatively large absorption coefficients and low ionisation potentials were found from the UV atlas of organic molecules (1966) and the Atlas of Spectral Data and Physical Constants for Organic compounds (1975). (A vapour phase absorption spectrum is given in figure 7-1) These, it was felt, would have large 2-photon ionisation cross-sections. Of these lutidine was chosen because of its very high vapour pressure at room temperature and its very strong, broad, resonances at around 266nm.

Figure: 7-1 Lutidine UV absorption spectrum.



(3) Mesitaldehyde: Mesitaldehyde also has strong resonances at around 266nm, but appears to have a low vapour pressure even at room temperature. The interesting thing about this molecule was its safeness. Mesitaldehyde, of all the molecules considered for seeding purposes, was the least toxic.

(4) Acetaldehyde: Acetaldehyde has an ionisation potential of 10.2eV and therefore cannot be ionised with 2-photons. It was chosen because it was known to have a 2-photon resonance close to 350nm, the wavelength of a tripled Nd:YAG. It was felt that if acetaldehyde could be ionised with 3-photons, without laser focussing, then ^{it} would have proven a useful seeding agent.

A summary of the results is given in table 7-1 at the end of the chapter. Also, in table 7-2 there is a summary of results for additives studied by other authors.

PHENOL SEEDING.

The presence of very low concentrations of phenol was detected in P10 gas by R2PI (Chapter 6). Outgassing from plastic flow lines was found to be the source.

It proved very difficult to introduce phenol at a known concentration into the counter gas. When seeded by the flow method the ionisation due to phenol steadily increased, indicating that phenol was very sticky. Once phenol had been introduced into a counter it proved very difficult to remove completely, even after cleaning with solvents and baking. Hubricht et al (1985) observed the same problem with phenol.

Eventually a known concentration of phenol was added to the P10 gas by placing a sample of phenol in a counter with a static gas fill. After a time its saturated room temperature vapour pressure of 0.28torr was reached (see figure 7-2).

Considerable absorption of the laser light was observed at wavelengths below 280nm. Therefore the intensity of the beam above the sense wire was estimated from the attenuation coefficient of phenol which was calculated from the relative intensity of the laser taken before and after the counter. After quadratic normalisation to a laser fluence of $1\mu\text{J}/\text{mm}^2$, the ionisation of phenol, on the 275nm resonance, was found to be approximately 4×10^7 IP/cm. At 266nm the ionisation fell to 8×10^5 IP/cm. Ionisation on the peak for the background of the type 1 counter was 3×10^4 IP/cm, which corresponds to a concentration of phenol of 0.26ppm.

Phenol was introduced at a concentration of approximately 2ppm into a type 2 counter with a static gas fill. Figure 7-3 shows the R2PI

Figure: 7-2 Vapour pressure curve for phenol.

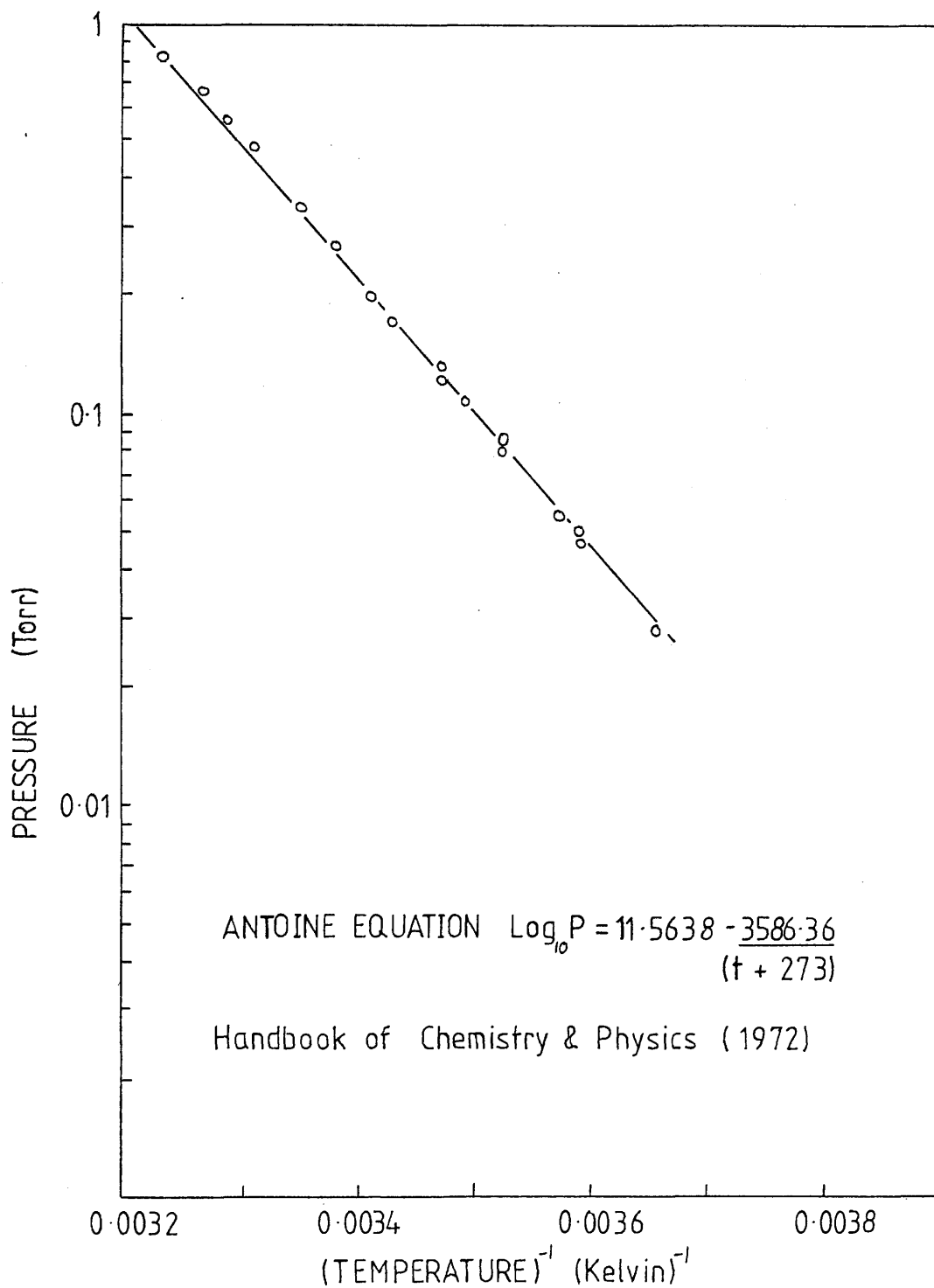
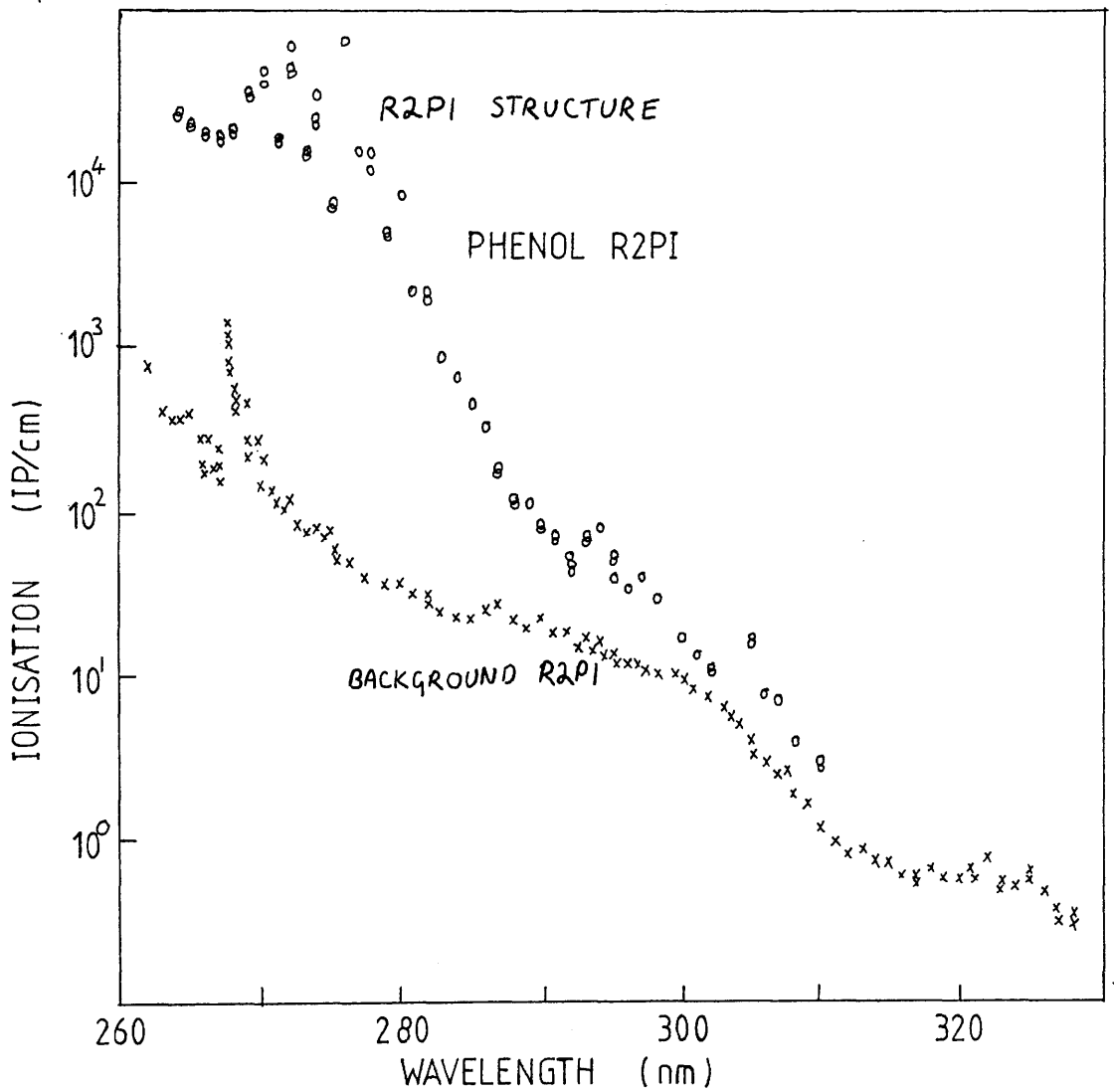


Figure: 7-3 R2PI spectrum of phenol.



spectrum for phenol taken in 1nm steps between 266nm and 312nm. The data was normalised pulse to pulse to a fluence of $1\mu\text{J}/\text{mm}^2$.

Above 290nm the ionisation falls rapidly with increasing wavelength. This is due to two effects; a steady drop in the absorption cross-section above 290nm and the proximity of the 2-photon ionisation edge at 290nm ($2 \times 4.25\text{eV}$). The ionisation at 312nm was very close to background and consequently phenol could not be considered as a seeding agent for systems which use lasers above this wavelength.

Phenol was known to outgas from plastic flow pipes. Passing P10 gas through various lengths of this pipe gave a method of introducing controllable levels of phenol at low concentration (0.4ppm) into the counter. Figure 7-4 shows R2PI spectra for a type 2 counter with and without a length of plastic flow piping added to the system.

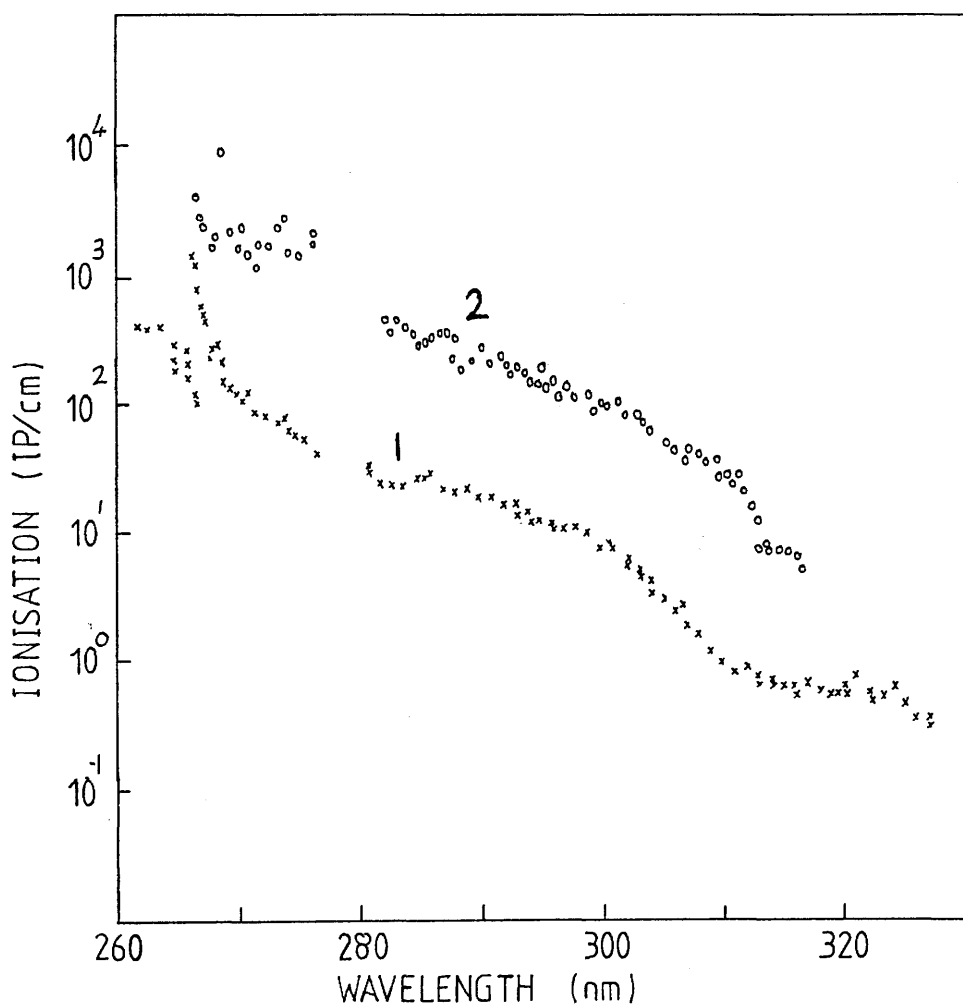
At a wavelength of 266nm and a fluence of $1\mu\text{J}/\text{mm}^2$, phenol, at a concentration of about 0.4ppm, gave 900IP/cm. Its stickiness made it a doubtful candidate for seeding into large MWPC's.

TOLUENE.

From background R2PI spectra taken for the type 2 and 3 counters a second impurity, toluene, was indentified. Toluene is chemically rather similar to phenol but it is a liquid with a high vapour pressure at room temperature. A seeding concentration of about 6ppm was maintained by flowing P10 gas over a sample of liquid toluene held in a bath of sublimating CO_2 at a temperature of -80°C .

Figure 6-11 shows the R2PI spectrum for toluene. At 266nm the ionisation was $10^4\text{IP}/\text{cm}$ for a laser fluence of $1\mu\text{J}/\text{mm}^2$. In addition to having a large 2-photon ionisation cross-section, toluene in low concentration does not appear to be sticky. P10 gas doped with 6ppm toluene was passed through a counter for 6 hours, after which time the

Figure: 7-4 R2PI spectra for a type 2 counter before, 1, and after, 2, introduction of a length of plastic pipe.



toluene sample was bypassed and the counter flushed with 'clean' P10 gas. The ionisation at 267.2nm rapidly fell to within a factor of two of the original background and thereafter continued to fall with time (figure 7-5).

Like most benzene molecules toluene is fairly toxic, but concentrations of a few ppm are not considered dangerous. Toluene unlike TMA, the only other favourable seeding agent, does not have an unpleasant smell. Even at concentrations of >100ppm it smells only vaguely of petroleum.

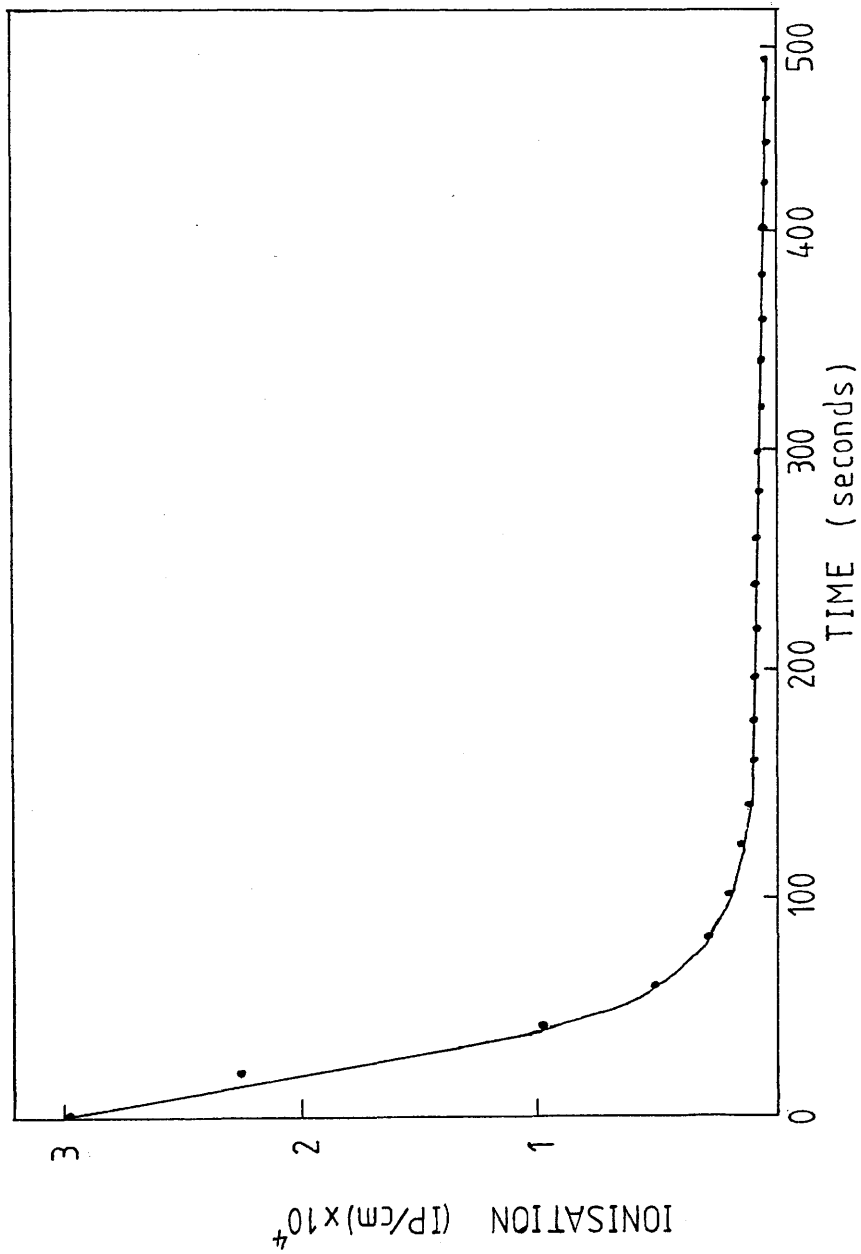
Tests have shown that at low concentrations of toluene around 5ppm, the performance of the counter is not affected with regard to its resolution and its useful lifetime (Pollman (1986)).

It has been shown (Drysdale et al (1986b)) that the impurities giving rise to the background ionisation are partially removed by the purification system proposed for the ALEPH TPC. The effect of toluene on the proposed purification system was investigated by Drysdale et al (to be published).

In this experiment a gas circulation system was filled to 760 torr with P10 gas which was slowly flowed over a sample of toluene held at -80°C . This produced concentration of 6ppm toluene in the gas. After 12 hours circulation the ionisation dropped from 10^4IP/cm to 500IP/cm, close to the background ionisation level. Heating the oxysorb cartridge (used to filter out oxygen and water) did not restore the ionisation, leading to the conclusion that the toluene had been adsorbed onto the molecular sieve which formed part of the filter.

After repeating the procedure 14 times the ionisation remained constant with time, at 10^4IP/cm , implying that the cartridge was saturated with toluene. The oxysorb system was then bypassed and the rest of the system refilled with 4 parts P10 gas and 1 part air (saturated with water vapour). No peak was observed for the Fe 55

Figure: 7-5 Flushing toluene from a counter.



calibration source, and a mass spectrometer showed strong O₂ and H₂O peaks.

The P10 counter gas was then circulated through the oxysorb cartridge (saturated with toluene) for 24 hours. After this time the pressure in the system had dropped and the Fe 55 gave a resolution of 25%, close to the usual 22%. The mass spectrometer indicated that O₂ and H₂O were present at less than 5ppm.

The conclusion drawn was that, at least in the short term, toluene did not impair the ability of oxysorb to remove O₂ and H₂O.

DIETHYL-PHTHALATE AND DIBUTYL-PHTHALATE.

Diethyl-phthalate and dibutyl-phthalate are commonly used in the manufacture of rubbers. They have been detected, along with dimethyl-, and dioctyl-phthalate, as impurities in counter gas (Boerner (1985)).

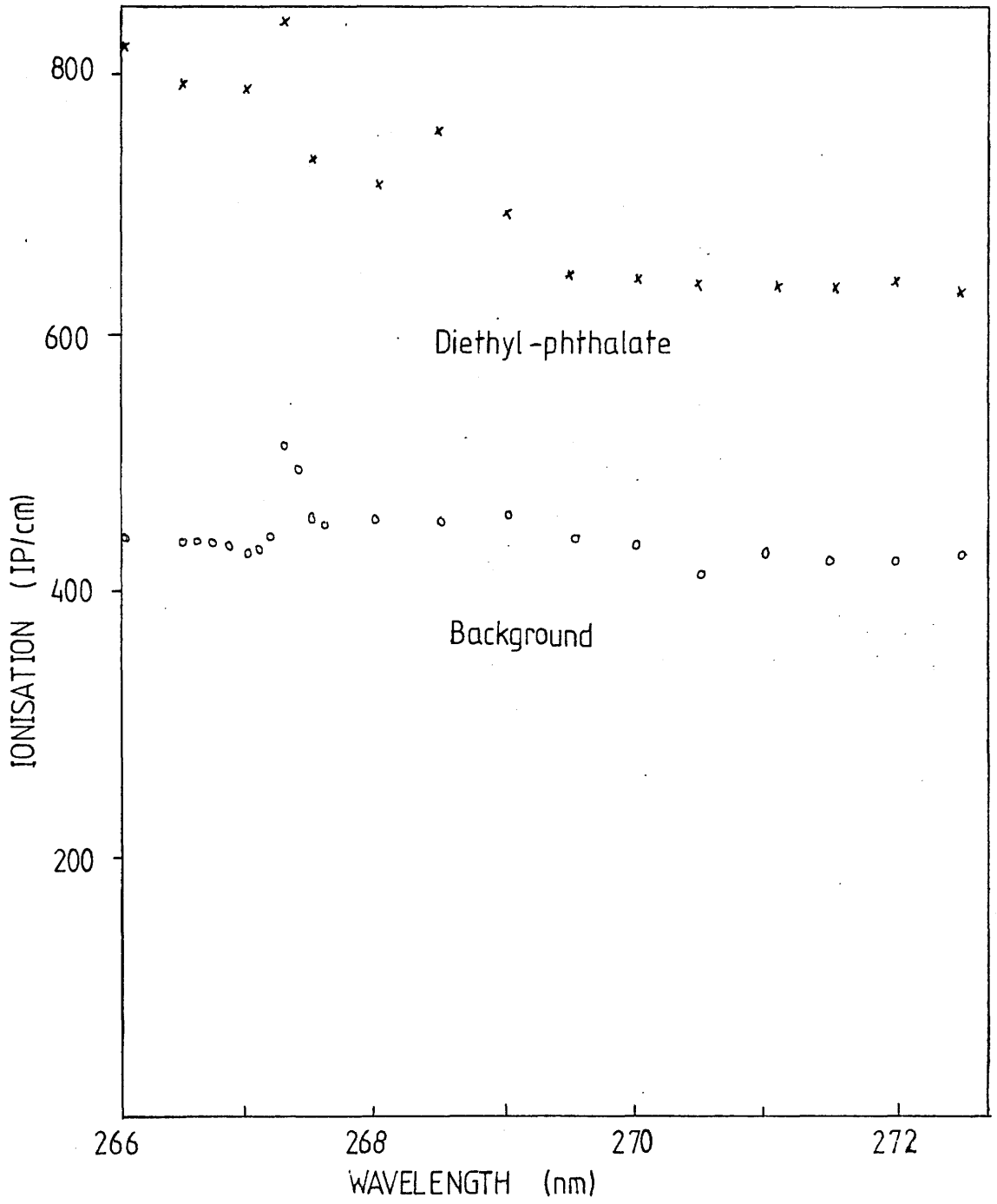
A concentration of about 0.4ppm was maintained by passing P10 gas at 100ml/min over a sample of Diethyl-phthalate held at room temperature. The concentration was found by extrapolation of vapour pressure data obtained by Small et al (1948).

Figure 7-6 shows the R2PI spectra of the gas before and after seeding with diethyl-phthalate. The wavelength was stepped in 0.5nm increments between 266nm and 278nm. The average laser fluence was 1μJ/mm² and each pulse was normalised to 1μJ/mm². An enhancement in ionisation by a factor of two was observed at a wavelength of 266nm. No obvious fine structure was apparent, but since the spectrum was taken at low resolution structure may not have been observed.

Dibutyl-phthalate was studied by the same method, it gave no measurable ionisation.

Diethyl-phthalate and dibutyl-phthalate have low 2-photon ionisation yields at around 266nm, which does not make them viable as seeding agents.

Figure: 7-6 R2PI of diethylphthalate.



2,6-LUTIDINE.

The concentration of lutidine was maintained at about 5000ppm by passing P10 over a sample held at 0°C in a cold bath. At this concentration 88% of the laser light was absorbed, as it passed through the counter, by the lutidine. The laser fluence at the centre of the counter (the active region) was calculated using the absorption equation.

$$I(L/2) = I_0 e^{(-\alpha L/2)}$$

where $L/2$ is the centre position of the counter with an absorption length L . The absorption cross-section of lutidine, α , was calculated from the fluence of the laser taken before and after passing through the counter. The fluence at the centre of the counter was calculated to be $0.7\mu\text{J}/\text{mm}^2$. At this fluence the observed ionisation was 2.3×10^4 IP/cm.

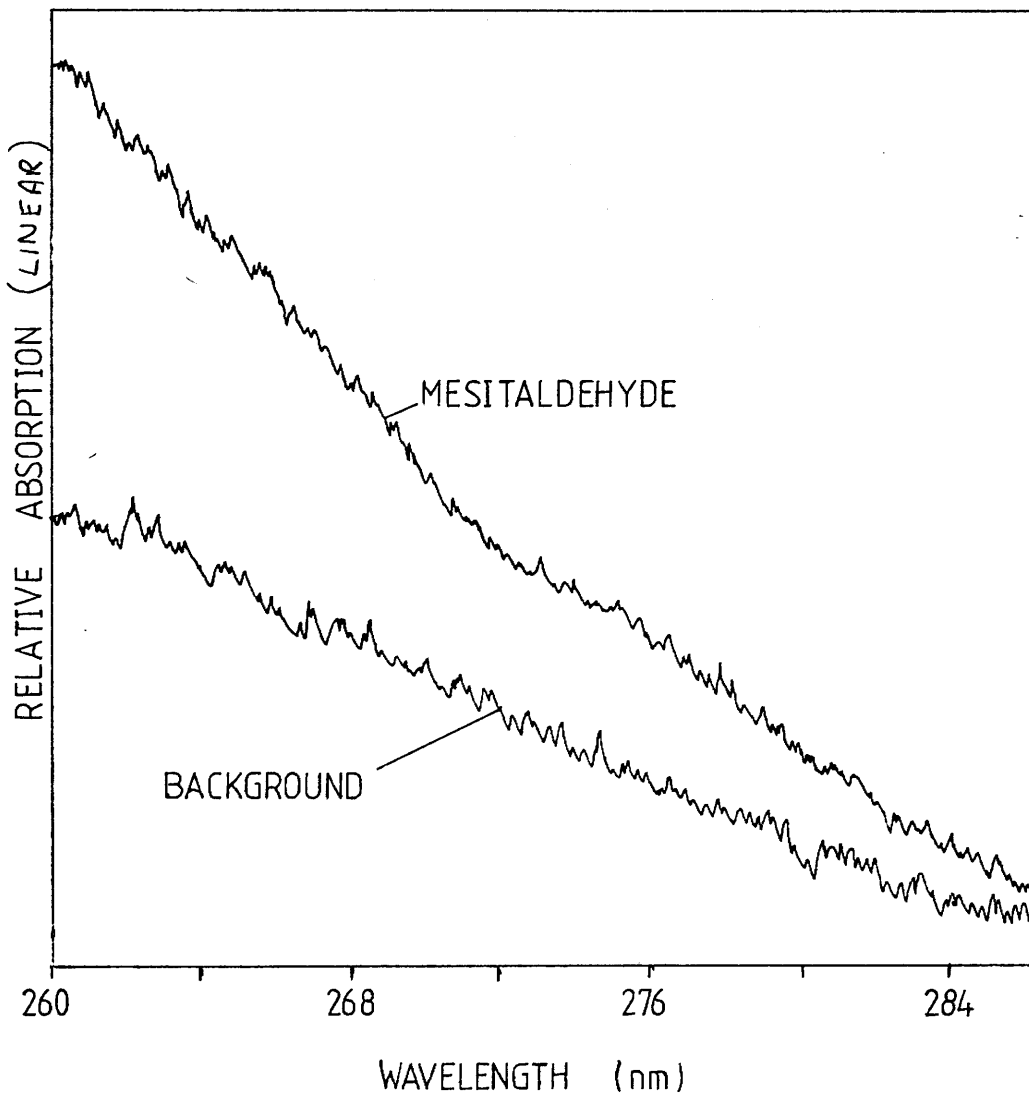
The estimated ionisation for a concentration of 60ppm lutidine is 560IP/cm at $1\mu\text{J}/\text{mm}^2$. This is 10 times less than TMA and 150 times less than DMA at the same concentration and laser fluence. To achieve ionisation at around 80IP/cm (as for a minimum ionising particle) a concentration of lutidine exceeding 20ppm would be required. At these concentrations linear absorption of light would be a problem.

MESITALDEHYDE.

Mesitaldehyde has a strong resonance at around 260nm but its vapour pressure appeared to be very low, since its vapour phase absorption spectrum was not well resolved. (see figure 7-7).

P10 gas was passed over a sample of mesitaldehyde held at room temperature. With a laser fluence of $1\mu\text{J}/\text{mm}^2$ at wavelength 266nm the

Figure: 7-7 Vapour phase UV spectra for Mesitaldehyde.



observed ionisation was about 10^4 IP/cm. Seeding at its room temperature vapour pressure resulted in mesitaldehyde sticking to the counter walls. No further tests were carried out with mesitaldehyde, but it was not positively excluded as a possible seeding agent.

ACETALDEHYDE.

Acetaldehyde is a volatile liquid at room temperature. It was reported to have R3PI structure at around 362nm (Heath et al (1980)). The ionisation process involved a 2-photon absorption through a virtual state into a resonant intermediate state with subsequent ionisation by a third photon.

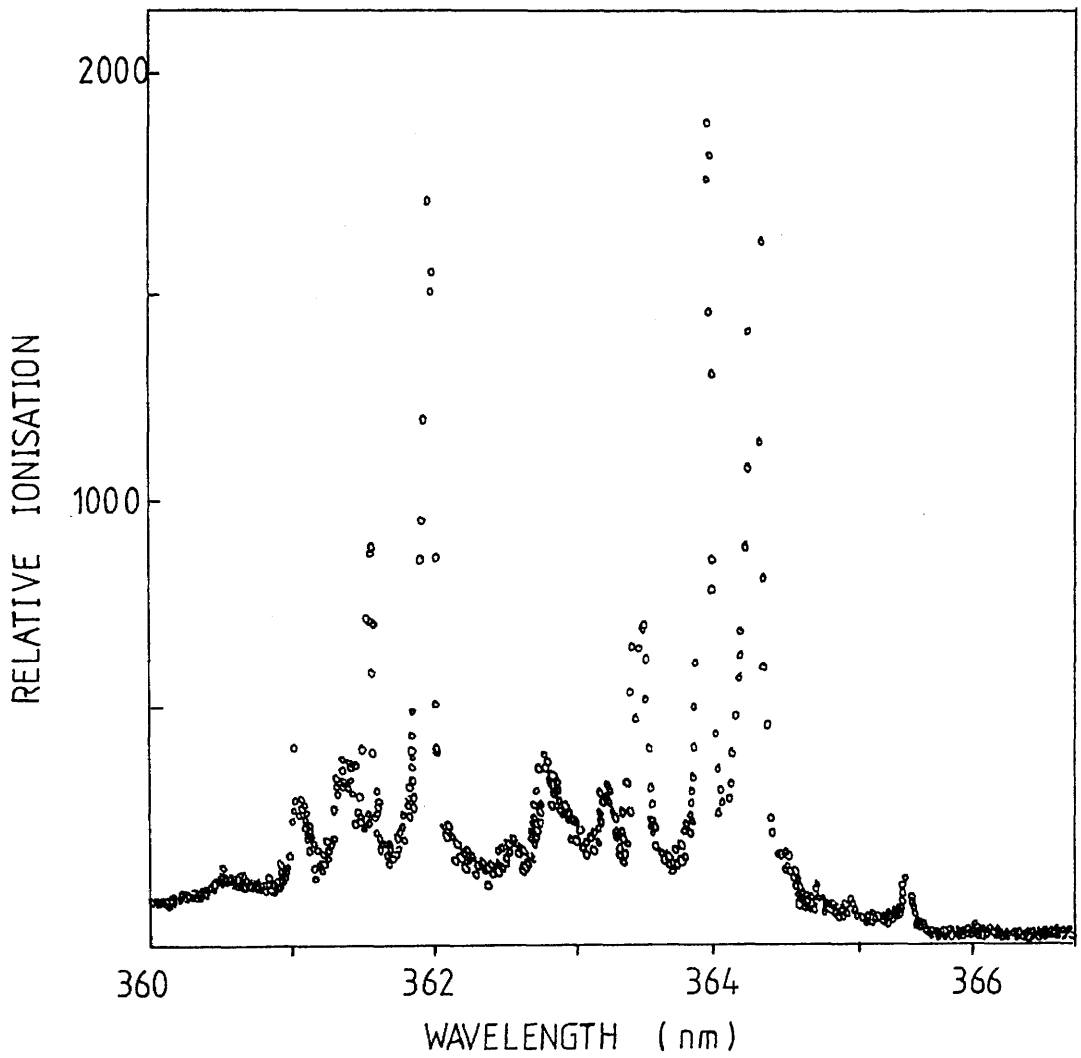
The resonances are near to the 350nm output wavelength of the tripled Nd:YAG. It was thought that acetaldehyde might provide a considerable enhancement in ionisation at this wavelength.

Acetaldehyde was held in a bath at 0°C and P10 gas was passed over it at 30ml/min. The concentration of acetaldehyde was found to be 4.3% (33torr) by careful measurement of the flow rate and the sample mass loss. At this pressure no effect on the gain of the counter was observed.

At 266nm and with a laser fluence of $8\mu\text{J}/\text{mm}^2$ acetaldehyde gave no appreciable ionisation. This was to be expected since at this wavelength acetaldehyde with its ionisation potential of 10.2eV would have to be ionised by a 3-photon non-resonant process (acetaldehyde does not absorb at 266nm).

The laser dye was changed to PBD which lases at around 365nm. No ionisation was observed with an unfocussed laser at 365nm and $100\mu\text{J}/\text{mm}^2$ fluence. After focussing, 6000IP/cm were observed, for a laser fluence of $1.6\text{mJ}/\text{mm}^2$. A continuous wavelength scan was produced between 360nm and 386nm at this laser fluence (see figure 7-8). Fine structure was

Figure: 7-8 R3PI spectrum of acetaldehyde.



observed which was very similar to that reported by Heath et al, except that a wavelength calibration error shifted the peaks 0.85nm to the red. At best the ionisation of acetaldehyde was 1.8×10^7 IP/cm for a laser fluence of 1.6mJ/mm^2 . A wavelength of 350nm could not be covered by the PBD dye but at this wavelength acetaldehyde is probably well off resonance and would not approach this level of ionisation.

Acetaldehyde at 33torr in a MWPC would probably not be considered 'safe'. Parts per million concentration may be acceptable, but then relatively large laser fluences would be required to produce significant ionisation. This leads to the problems of beam handling discussed earlier. In addition to this a large photoelectron background was observed when the laser was operated at these wavelengths and fluences. In conclusion acetaldehyde would appear to be an unlikely candidate for laser calibration purposes.

SECTION 7-3: CONCLUSIONS.

Phenol and toluene were identified as ionisable impurities in P10 counter gases (Cahill et al (1985) and Towrie et al (1985)). The suitability of these molecules as seeding agents for the ALEPH TPC was studied. Both had relatively large 2-photon ionisation cross-sections, but phenol proved to be very sticky. Toluene on the other hand could easily be removed from the counter by flushing with fresh P10 gas. Further tests with toluene (Pollman (1986)) showed that toluene had no obvious effect on the counter gain or lifetime when present in the gas at about 5ppm. Drysdale et al (1986b) found that toluene was adsorbed in a filter system similar to that proposed for the ALEPH TPC, but that it had a negligible effect on the ability of the system to remove O₂ and H₂O (at least in the short term). The filter consisted of a reduced chromium catalyst, which has an affinity for oxygen, and a zeolite molecular sieve.

Two photon ionisation of diethyl-phthalate and dibutyl-phthalate was studied at around 266nm. They are commonly used as plasticisers in rubbers, making them likely background impurities in counter systems. Their relatively low 2-photon ionisation yields and low vapour pressures make them unlikely seeding agents.

2,6-Lutidine, even with its large absorption coefficient at around 266nm produced a disappointingly low level of ionisation. One reason for this would be the proximity of its ionisation potential to the energy of 2 photons at 266nm (9.2eV). Chapter 1-5 has a description of the common ionisation channels available in a two photon process. The most probable scheme is an initial transition into a excited vibronic level followed by a rapid relaxation down to the vibronic ground state, a second photon subsequently ionising the molecule. 2,6-lutidine, with vibronic transitions around 266nm, probably ionises by this process. The ionisation potential of 2,6-lutidine is 8.85eV and the energy of

2-photons at 266nm is 9.2eV. Molecules will not be ionised if they relax to vibrational states lower than 4.6eV below the ionisation potential before the arrival of the second photon.

Predissociation or dissociation of lutidine may also be strongly competing with the ionisation process, which would effectively reduce the 2-photon ionisation yield.

In conclusion lutidine would not appear to be a suitable seeding agent.

Mesitaldehyde was not excluded as a possible seeding agent, although its only outstanding property was its low toxicity.

Acetaldehyde, could not be ionised at around 365nm without focussing of the dye laser beam. To be used as a seeding agent at 350nm, it would still have to be on resonance. At the $1.6\text{mJ}/\text{mm}^2$ fluence levels required at 365nm to give an adequate level of ionisation a large photoelectric background was observed. Background of this sort is undesirable in MWPC's, giving a further reason for avoiding the use of high intensity lasers for calibration.

Similarities between the magnitudes of the 2-photon ionisation cross-sections of phenol, toluene and some seeding agents (described in chapter 5), suggest that the latter also must be resonant. Vapour phase UV absorption spectra were produced for DMA, TMA, TEA and TMAE (see figures 7-9 to 7-12). All of them are resonant at around 266nm. Solvent UV absorption data for Naphthalene shows that it is also resonant (Atlas of Spectral Data and Physical Constants for Organic compounds (1975)). Figures 7-9 to 7-11 also show the R2PI spectra of DMA, TMA and TEA. In all cases the R2PI spectra follow the UV absorption spectra. None of them display resonant structure at $>266\text{nm}$.

Where possible, 2-photon ionisation cross-sections, UV absorption cross-sections and ionisation potentials were found for the seeding molecules described in chapters 5 and 7 (see table 7-3).

Figure: 7-9 R2PI and UV spectra of DMA.

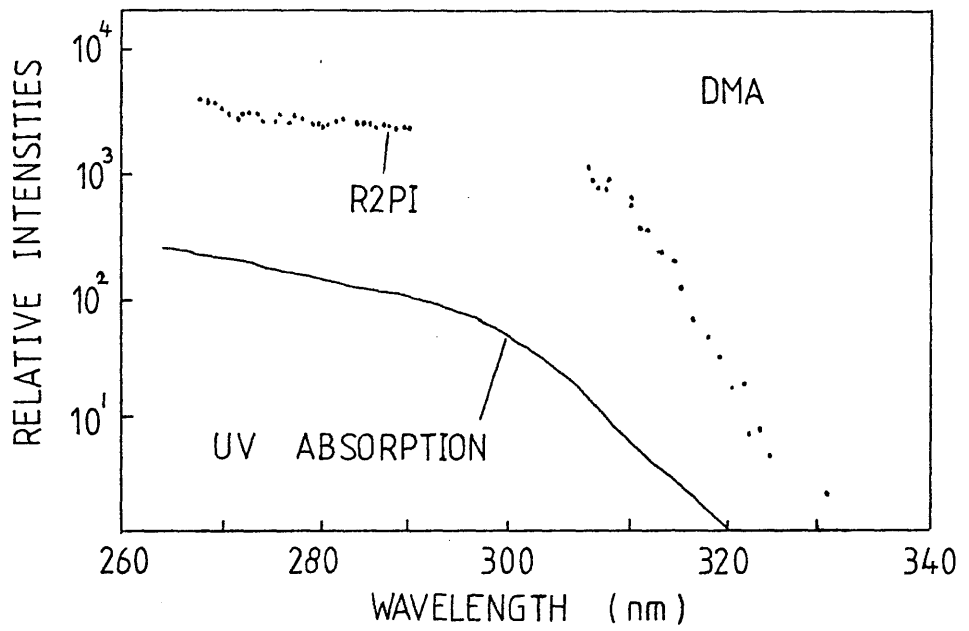


Figure: 7-10 R2PI and UV spectra of TEA.

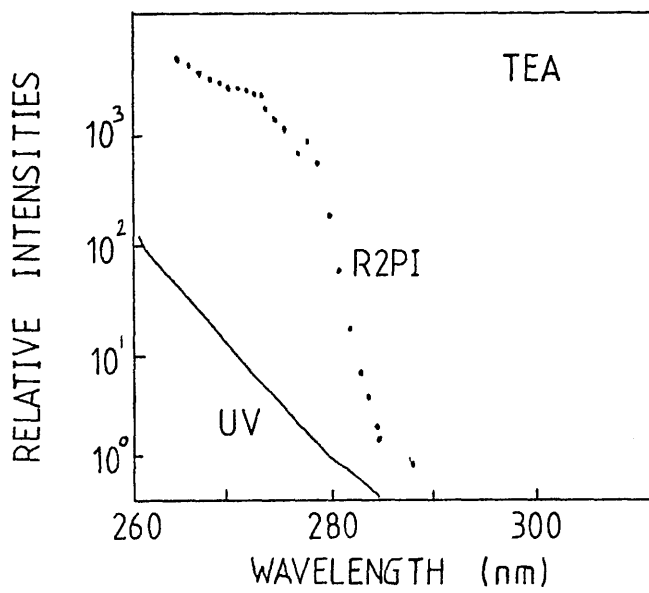


Figure: 7-11 R2PI and UV spectra of TMA.

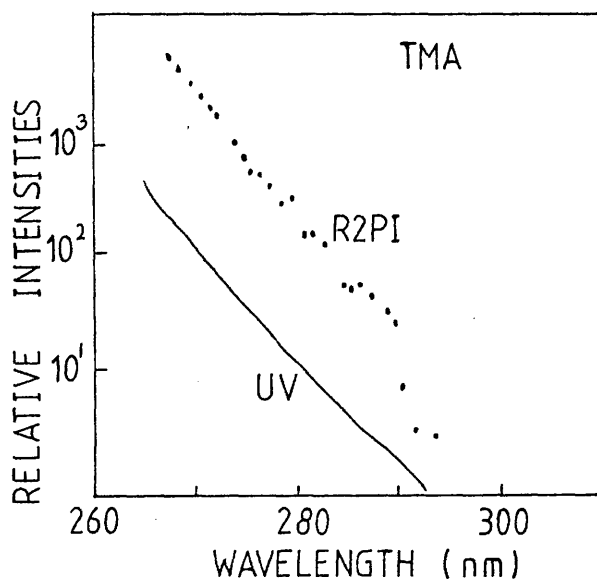


Figure: 7-12 UV absorption spectra of TMAE.

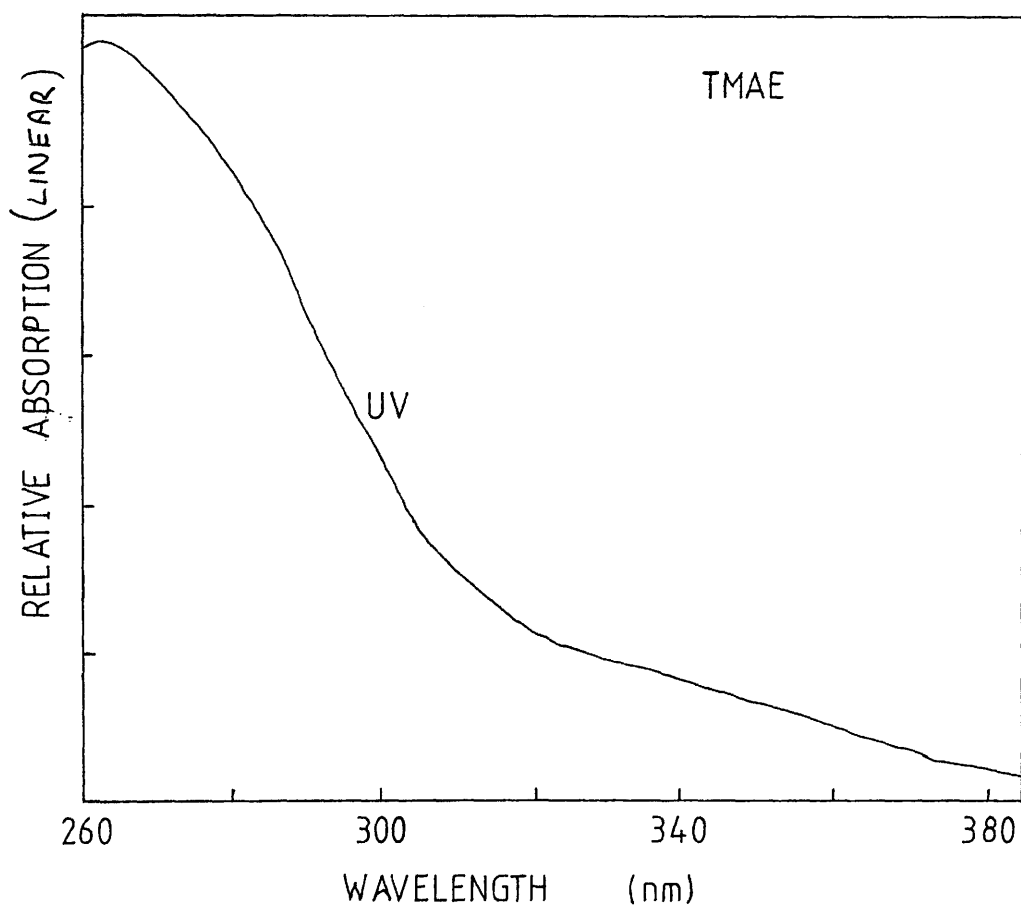


TABLE 7-1: SUMMARY OF ADDITIVES DISCUSSED IN CHAPTER 7.

ADDITIVE	IONISATION (IP/cm)	CONC. (ppm)	FLUENCE ($\mu\text{J}/\text{mm}^2$)	LASER TYPE	WAVELENGTH (nm)	TOXICITY (ppm)#
PHENOL	8×10^5	370	1	DYE	266	5
TOLUENE	10^4	6	1	DYE	266	100
DIETHYL- PHTHALATE	400	0.4	1	DYE	266	$5\text{mg}/\text{m}^3$
DIBUTYL- PHTHALATE.	NONE	--	1	DYE	266	--
2,6 LUTIDINE	2.3×10^4	5000	0.7	DYE	266	--
MESITALDEHYDE	10^4		1	DYE	266	--
ACETALDEHYDE	NONE	33Torr	8	DYE	266	200
	6000	33Torr	1.6×10^3	DYE	365	

Maximum concentration in air, for up to 8 hours.

TABLE 7-2: SUMMARY OF ADDITIVES STUDIED FOR LASER CALIBRATION.

ADDITIVE	IONISATION POTENTIAL (eV)	VAPOUR PRESSURE (Torr) 20°C(0°C)	MP/BP (°C)	IONISATION (IP/cm) REFERENCES. FOR 1μJ/mm ² AND 10 ⁻³ TORR ADDITIVE.
BENZENE	9.24	77	55/80	266:4x10 ³ (2)
CUMENE	8.69	3.8	-96/152	266:1.3x10 ⁴ (2)
n-BUTYL-BENZENE	8.69	1	-88/183	266:5.8x10 ⁴ (2)
m-XYLENE	8.56	6	-48/139	266: 4x10 ⁴ (2)
1,3,5, MES-ITYLENE	8.40	1.5	-45/165	266:2.6x10 ⁴ (2)
NAPH THYLAMINE	7.3	2.7x10 ⁻⁴	50/301	337:800 (at 2.7x10 ⁻⁴ Torr) (3)
DPA	7.1	1.2x10 ⁻²		337:90 (3)
DIACETYL-FERROCENE	7.08	1.2x10 ⁻⁶		337:10 (at 1.2x10 ⁻⁶ Torr) (3)
NICKEL-OCENE	6.5	1.1x10 ⁻³		337:>>bgr (6),(7)
DIETHYL-DIPHENYL MOLYBDENUM	5.5	5.4x10 ⁻⁶		337:120 (at 5.4x10 ⁻⁶ Torr) (3)
DEA	6.99	0.14	-39/216	337:>10 bgr. 0.07Torr (1) " 0.03Torr (9)
TMA	8.5	GAS	-117/2.9	266:80 (11)
NAPHTH-ALENE	8.12			266:4.9x10 ⁵ (4)
TMPD	6.18	2x10 ⁻³	51/260	266:5x10 ⁴ (11) 337:7x10 ⁴ (3)
TOLUENE	8.82	22	-95/110	266:6.5x10 ⁴ (2) 0.5x10 ⁴ (12)
PHENOL	8.51	0.28	43/	266: 3000 (10)
DMA	7.14	0.25 (0.065)	2.5/194	266:10 ⁴ (14) 337:2000 (at 0.25Torr and 14μJ/mm ²) (5)
TMAE	5.36	0.27 (0.06)	-10/59	337:>300 (5)

- (1) Bourotte & Sadoulet (1980)
 (2) Bamberger et al (1986).
 (3) Hilde (1986)
 (4) Hubricht et al (1985)
 (5) Raine et al (1984)
 (6) Anderhub et al (1979) & (1980).
 (7) Sadoulet (1982).
 (9) Guo et al (1982).
 (10) Present work.
 (11) Hubricht et al (1985).
 (12) Drysdale et al (1986).
 (13) Ledingham et al (1985).
 (14) Ledingham et al (1984).

TABLE 7-3 : IONISATION POTENTIALS, R2PI AND UV CROSS-SECTIONS AT 266NM FOR SEEDING COMPOUNDS.

COMPOUND	IONISATION POTENTIAL (eV)	IONISATION CROSS-SECTION σ_2 (cm ²) (From $\sigma_1 \sigma_2 F^2 = N_I/N_T$)	UV ABSORPTION CROSS-SECTION (cm ²) σ_1
DMA	7.14	$> 2 \times 10^{-20}$	9×10^{-18}
TMA	7.82	--	--
TEA	7.5	--	--
NAPHTH	8.12	$> 3 \times 10^{-18}$	2×10^{-17}
PHENOL	8.5	$\sim 3 \times 10^{-19}$	1×10^{-18}
TOLUENE	8.82	$\sim 8 \times 10^{-18}$	4×10^{-20}
LUTIDINE	8.85	$\sim 2 \times 10^{-23}$	5×10^{-17}
MESIT'DE	--	--	4×10^{-17}
ACET'DE	10.2	--	VIRTUAL
TMPD	6.2	--	--

IONISATION CROSS-SECTION IS DERIVED FROM

$$\sigma_1 \sigma_2 F^2 = N_I / N_T$$

$$\Rightarrow \sigma_2 = N_I / N_T \times \frac{1}{\sigma_1 F^2} \quad \text{cm}^2$$

$$N_I / N_T = \frac{\text{NO. OF MOLECULES IONISED IN BEAM VOLUME}}{\text{TOTAL NO. OF MOLECULES IN BEAM VOLUME}}$$

$$F = \text{LASER FLUENCE} \quad \text{PHOTONS SEC} / \text{cm}^2$$

CHAPTER 8

LASER IONISATION IN A QUADRUPOLE MASS SPECTROMETER.

SECTION 8-1: INTRODUCTION.

Detection of electrons formed in an R2PI process has led to the identification of phenol and toluene as background impurities in P10 gas. This method relied on the ability to draw comparisons between the R2PI spectra and the electronic absorption spectra of molecules. Uncertainties in this type of analysis arise for two situations:

(1) When the R2PI spectral structure is the result of contributions from many impurities and not just one.

(2) Where the R2PI spectrum has no fine structure at all (DMA, TMA and TEA being cases in point). Under these conditions it would be difficult to make positive identification of the impurities by comparison of the R2PI with the UV absorption spectra.

If ions, instead of electrons, are studied in the R2PI process, then ion mass analysis may be carried out. For case (1) molecules could be selectively ionised by tuning the laser wavelength on to one of the R2PI peaks. Case (2) may still be a problem since more than one species of molecule could be responsible for the ionisation. This would complicate the mass spectrum, making the assignment of the mass peaks to particular molecules more difficult.

After the removal of phenol as an impurity in the P10 gas, R2PI structure associated with toluene remained. Indications were that

toluene was not the sole impurity left in the system. A R2PI spectrum taken in a type 2 counter with gas flowing at 50ml/min showed toluene to be present at a very low level and that any other remaining ionisation had no obvious fine structure (see figure 6-13). This rules out the identification of any remaining impurities by the comparison of their R2PI and UV spectra.

Mass analysis of the ionisable impurities in P10 gas was carried out in a quadrupole mass spectrometer (see chapter 3 for a description of the mass spectrometer and experimental arrangement). It was hoped that this method would confirm the presence of phenol and toluene in the P10 gas, and that further impurities would be positively identified.

The following sections give results for and discussion of the experiments carried out in the quadrupole mass spectrometer.

A description of the apparatus used in these experiments is given in chapter 3. Ion production could be switched between electron bombardment and laser ionisation. Signals from the secondary electron multiplier (SEM) were passed through a current pre-amplifier before amplification in the mass spectrometer control unit. Mass spectra produced by electron bombardment were analysed by a microcomputer and plotted out as histograms. Unlike the electron bombardment signals, the laser ionisation signals were pulsed. Since it could not be triggered from the laser, the microcomputer could not be used to analyse the pulsed signals. Instead the amplified laser signals were connected to the y input of a D611 storage oscilloscope. An output from the mass spectrometer provided a 10V DC voltage ramp which was connected to the x input of the oscilloscope. The magnitude of the DC signal was proportional to the mass of the ions arriving at the SEM so the resultant trace on the scope was equivalent to a mass spectrum.

Frequency doubled laser light at 266.4nm was focussed with a 30cm lens into the centre of the ion source in the mass spectrometer. Prior to firing the laser the background pressure was measured to be 10^{-8} torr. The filament and electron energy volts were then switched off. No laser ionisation signals were detected when the quadrupole was scanned between mass 0 and 120AMU.

In an attempt to calibrate the system and to determine its sensitivity, TEA, was introduced up to a pressure of 10^{-6} torr into the mass spectrometer. Still no laser ionisation signal was observed.

TEA was introduced into the counter at a steady 7.5×10^{-7} torr. The intensity of the electron bombardment TEA mass spectrum was increased over 100 fold, by adjusting the ion focus, ion energy and SEM volts. This was achieved at some cost to the mass spectrometer resolution, but

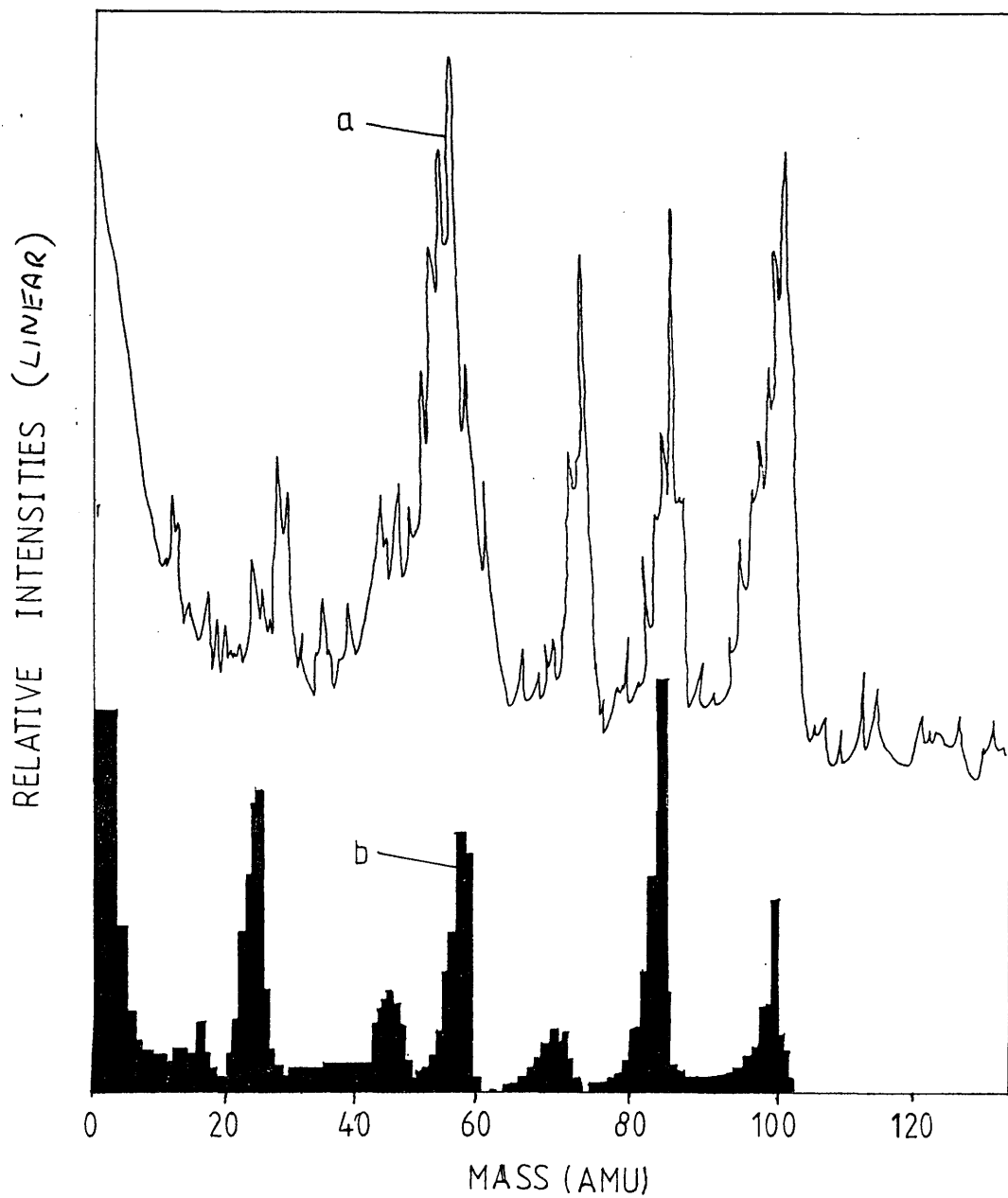
it was still capable of clearly resolving masses separated by 1AMU. The mass spectrometer was adjusted to give maximum sensitivity and again TEA was introduced at a pressure of 7.5×10^{-7} torr. This time a laser ionisation mass spectrum was produced. Figure 8-1a shows a trace of the spectrum taken from the D611 storage oscilloscope. Comparison of the relative magnitudes of the ion and noise signals, indicates that the minimum detectable pressure of TEA is around 10^{-8} torr. The sensitivity would be increased if the beam interaction volume and ionisation yield were increased. A $\times 500$ fold increase in the beam interaction volume was gained by removing the beam focussing, although this was at the cost of an equally large reduction in the laser fluence. The resultant effect was that no ionisation was detected with the unfocussed ionisation beam.

Figure 8-1b shows the electron bombardment mass spectrum for TEA. The spectrum was produced with the mass spectrometer parameters set to maximum sensitivity. Both the laser and electron induced spectra display fragmentation of the TEA molecule. Fragmentation of molecules in photoabsorption processes occurs by dissociation and predissociation of both the parent and ionic molecule. Ionisation and fragmentation of molecules can involve the absorption of many more photons than are necessary to simply ionise the molecule. A process of this type explains the presence of ion fragments that could not have been produced by a simple 2-photon absorption process.

An attempt was made to increase the sensitivity of the mass spectrometer by replacing the current pre-amplifier with a charge pre-amplifier. Ion signals from the charge pre-amplifier were first filtered through an Ortec amplifier (16 times gain) before being displayed on an oscilloscope. This should have produced signals of about 30mV for each detected ion. Laser ionisation signals were indeed detected with DMA introduced at 10^{-6} torr although the sensitivity of the system proved to be no greater than the previous experiment, with TEA,

Figure: 8-1a Laser induced mass spectrum for TEA.

Figure: 8-1b Electron bombardment mass spectrum for TEA.



using the current amplifier.

One of the main reasons for the lack of sensitivity was a large 400mV peak to peak AC pickup from the radio frequency generators in the mass spectrometer. Replacement of the spectrometer SEM high voltage supply with an independent supply reduced the pickup by a factor of 2. Electrical filtering of the AC pickup was not possible because its period was very close to the width of the ion signal. Eventually the AC pickup was removed by splitting the output signal in two and re-combining them 180° out of phase. A random, 40mv peak to peak, noise signal was left.

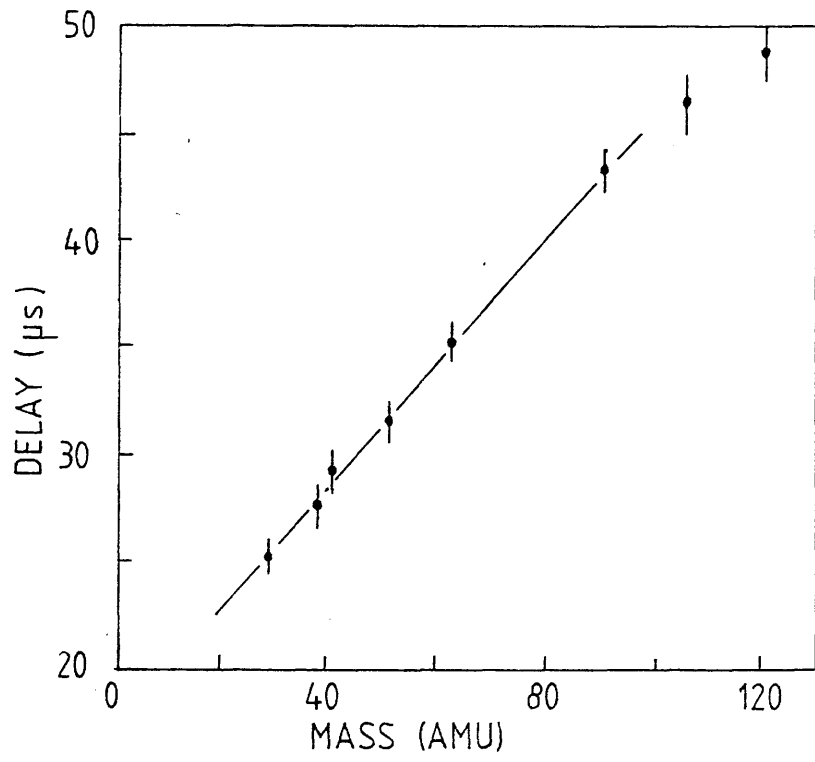
Laser ionisation signals were detected at mass 121 (the DMA parent peak). Double pulses were produced due to the technique adopted for the removal of the AC pick up. Little interference occurred between the pulses since they were both well resolved.

The minimum detectable pressure of DMA in the mass spectrometer was 3×10^{-9} torr. This was calculated from the ratio of the noise to DMA signal (at mass 121) multiplied by the ambient pressure of 10^{-6} torr DMA.

Signals from the charge amplifier were of a microsecond duration which proved too fast for the D611 storage oscilloscope. Instead the Camac system was used to record the data (as described in chapter 3). Triggered from the laser, the ADC gate was set to coincide with laser ionisation pulses produced at around 60AMU. At first the relative intensities of the peaks in the mass spectra were misrepresented due to the dependence of the ion arrival time at the SEM on mass. This resulted in the ion pulse peak moving off the 80ns ADC gate at masses above and below 60AMU. Figure 8-2 shows the dependence of the delay time with mass, measured for various fragments of phenol and DMA.

A pulse shaping amplifier provided the laser ion pulse with a slow rise and a very slow decay. The ADC gate was situated on the trailing edge of the ion pulse produced at mass 60. In this way the

Figure: 8-2 Signal delay time versus mass for the mass spectrometer.



signal recorded by the ADC was never less than 63% of the 'true' value for all masses in the range 1 to 120AMU,

The laser wavelength was set to the 275nm resonance of phenol and the beam focussed with a 50cm lens into the centre of the mass spectrometer ion source. The fluence at the interaction region was approximately $1\text{mJ}/\text{mm}^2$. Small quantities of phenol and DMA were introduced into the mass spectrometer. A quantitative evaluation of their pressure in the spectrometer could not be made at this time, due to damaged filaments in the ion source.

Ion signals were recorded pulse by pulse on a floppy disk. The mass spectrometer was set to scan at a rate of 0.1AMU/sec and the laser was pulsed at a repetition rate of 10pps. The ion masses were determined from the event number of their peak positions. Figure 8-3 shows the laser ionisation mass spectrum for phenol and DMA using a focussed laser. As with TEA, considerable molecular fragmentation occurred.

Phenol has a large 2-photon ionisation cross-section and this, along with the increased sensitivity of the mass spectrometer, meant that an ion signal could be detected with an unfocussed laser beam. Figure 8-4 shows the mass spectrum of phenol taken with an unfocussed laser at a fluence of $10\mu\text{J}/\text{mm}^2$. This time no fragmentation is observed.

A rough detection limit for phenol was determined to be 1.0×10^{-11} torr, for a beam of $2 \times 2\text{mm}^2$ cross-section and a fluence of $10 \mu\text{J}/\text{mm}^2$. This is equivalent to a detection limit of 2ppm phenol in P10 gas when introduced into the mass spectrometer at the maximum operable pressure of 5×10^{-6} torr. The concentrations of impurities in counter gas after flowing through a 'clean' type two counter would typically be less than 0.02ppm. Detection of impurities in P10 gas, introduced directly into the spectrometer, was therefore not feasible.

Figure: 8-3 Laser induced mass spectrum for phenol and DMA.

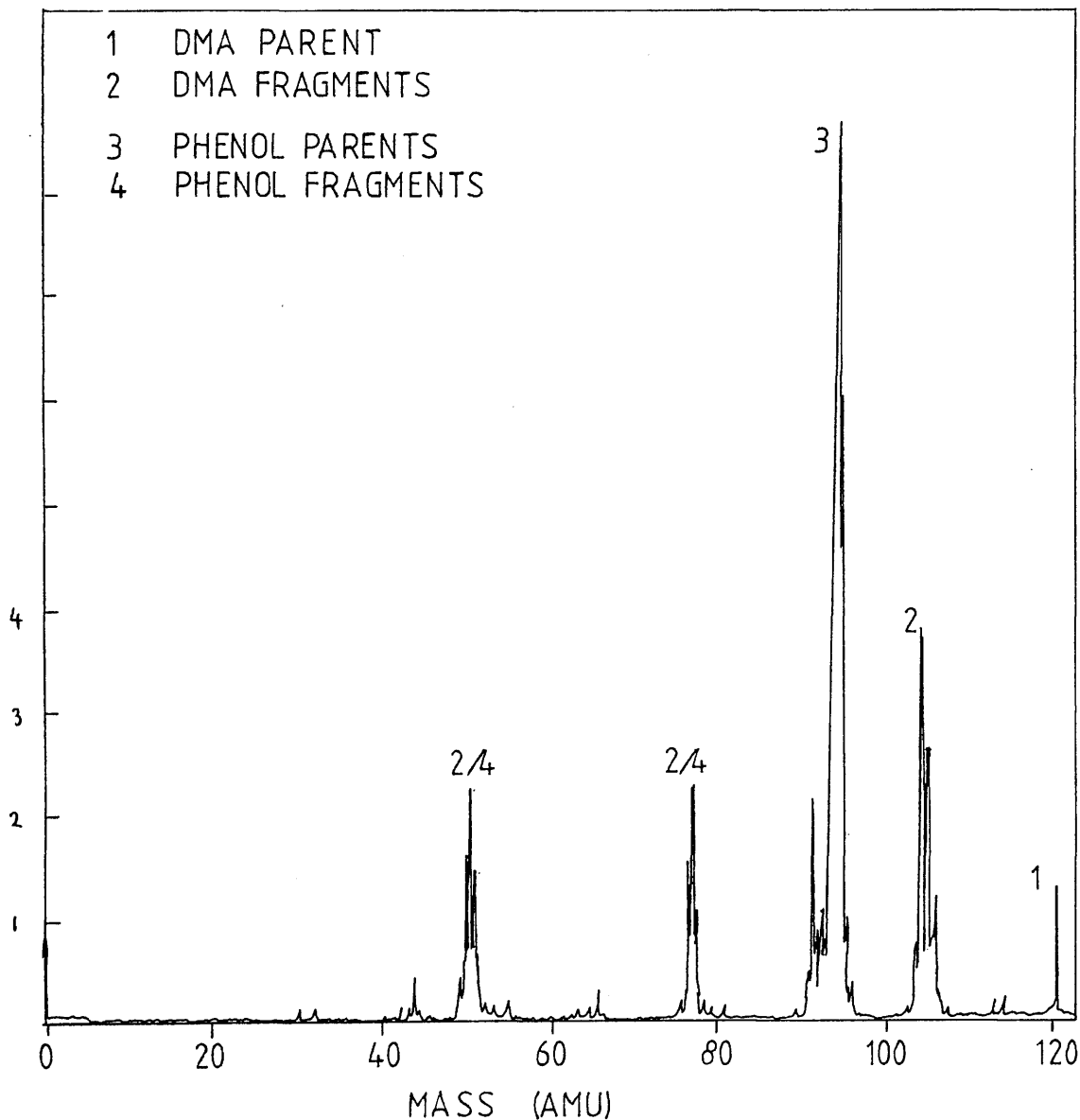
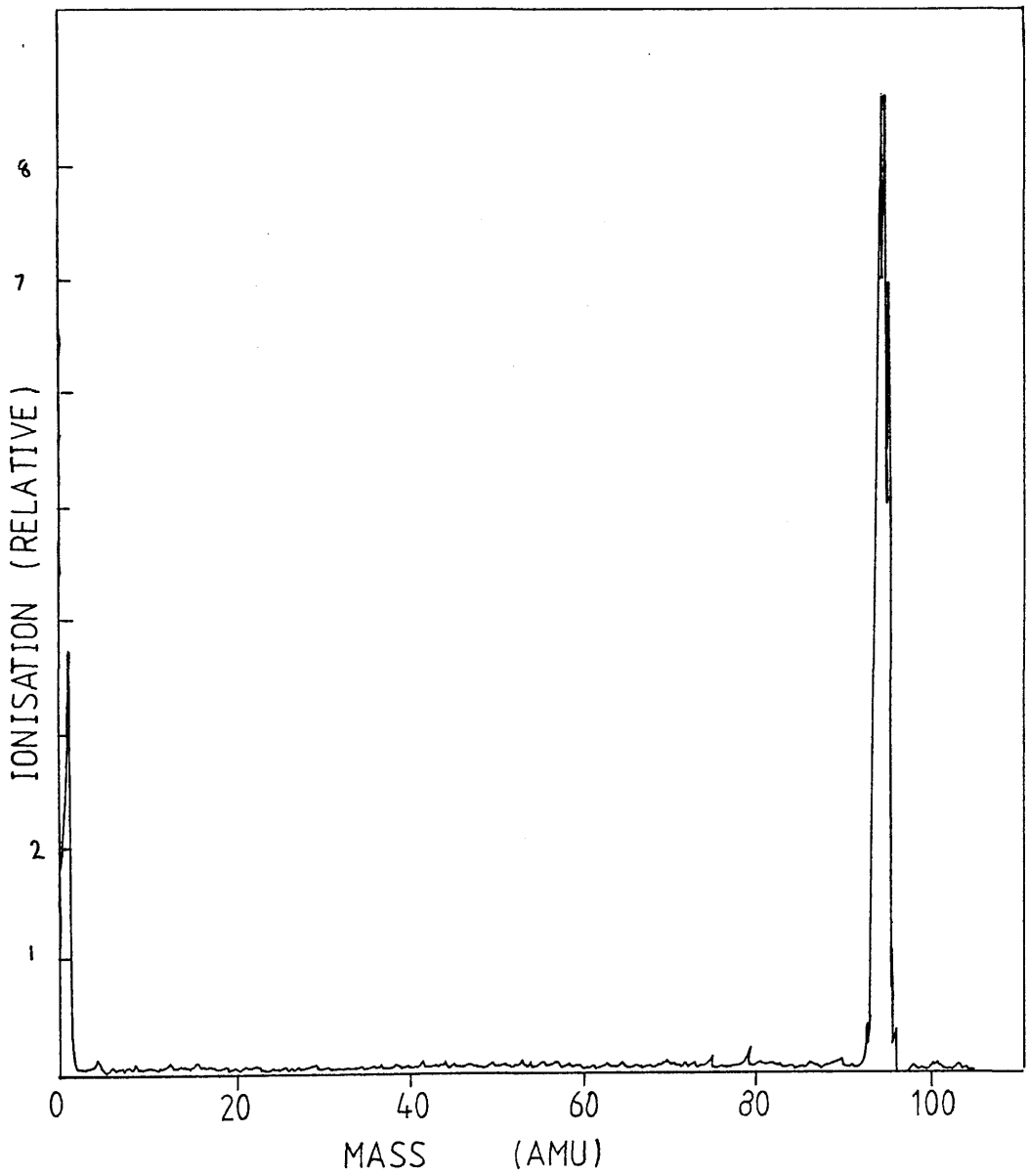


Figure: 8-4 Laser induced mass spectrum for phenol.



GAS INTRODUCTION THROUGH A FINE NOZZLE.

The sensitivity of the mass spectrometer was limited by the maximum allowable pressure of gas in the spectrometer. Above 5×10^{-6} torr the SEM efficiency was degraded, while prolonged exposure to this pressure could permanently damage the SEM's semiconductor properties.

Rather than fill the entire spectrometer with the sample it would be preferable to confine the sample to the locality of the ionisation region. A close approximation to this is met with a pulsed gas input synchronised to the laser pulse. By this method a pressure of 10^{-3} torr could be realised in the ion source, with the ambient pressure in the mass spectrometer remaining well below the 5×10^{-6} torr safety margin.

Another, less ideal solution, would be to introduce the sample gas through a fine nozzle placed inside the ion source.

Geometry considerations meant that the filaments could not be operated while the nozzle was in place. Ambient gas pressure inside the mass spectrometer was therefore monitored with a VG pirani-ion gauge. The pressure of the sample at the nozzle input could not be measured.

No major improvement in sensitivity was achieved using this method and detection limits remained at best 10^{-11} torr.

CONCENTRATION OF IMPURITIES IN A LIQUID NITROGEN COLD TRAP.

A pulsed gas input was not available therefore an alternative approach to the sensitivity problem was required. A greater pressure of impurities in the mass spectrometer could be achieved by concentrating them in the sample of P10 gas. A successful method for trapping ionisable impurities from the P10 gas was described in chapter 6. P10 gas was passed at 1000ml/min through a cold trap immersed in liquid

nitrogen (-197°C). Both argon and methane become liquid at this temperature, but after a short time the gas inflow and liquid evaporation rates equilibrate. By this method impurities were trapped from approximately 5000 litres of P10 gas passed directly from the cylinder via a regulator, into the trap.

A sample of the trapped impurities was attached to the input of the mass spectrometer. The sample was frozen by cooling down to $<-100^{\circ}\text{C}$. At these temperatures organic impurities are condensed out. The air in the sample holder was then pumped out. The sample was then brought up to room temperature. At an ambient pressure of 5×10^{-6} torr, the vapour above the sample was introduced into the spectrometer. A focussed laser beam of fluence $1\text{mJ}/\text{mm}^2$ at a wavelength of 266nm was positioned immediately below the output of the nozzle. No ion signal was detected at any mass. Analysis of the sample in a sensitive conventional magnetic sector mass spectrometer detected only water in the sample. Water is not ionisable by two-photon absorption at 266nm.

LASER IONISATION MASS SPECTRA OF PHENOL AND TOLUENE.

At the present the mass spectrometer is not sufficiently sensitive to detect impurities even from a cold trapped sample. In spite of this it was felt that laser ionisation mass spectra of phenol and toluene would prove useful for future reference.

Phenol was introduced through the nozzle into the mass spectrometer ion source. The ambient pressure in the mass spectrometer was 10^{-6} torr. RF pickup was removed (as described previously) from the SEM signals which were shaped and amplified. The output from the amplifier was passed directly into the Camac ADC. A 0-2V DC ramp signal whose magnitude was proportional to ion mass was provided from the mass spectrometer. The ramp signal was passed into a second input

of the ADC. Figure 8-5 shows the fragmentation spectrum produced for phenol ionised with a focussed beam of 266nm wavelength and $5\text{mJ}/\text{mm}^2$ fluence. Fragmentation of phenol was reduced when the ionising beam fluence was decreased to $50\mu\text{J}/\text{mm}^2$ (figure 8-6). Similar mass spectra were produced for toluene (figures 8-7 and 8-8).

Figure: 8-5 Fragmentation pattern of phenol.

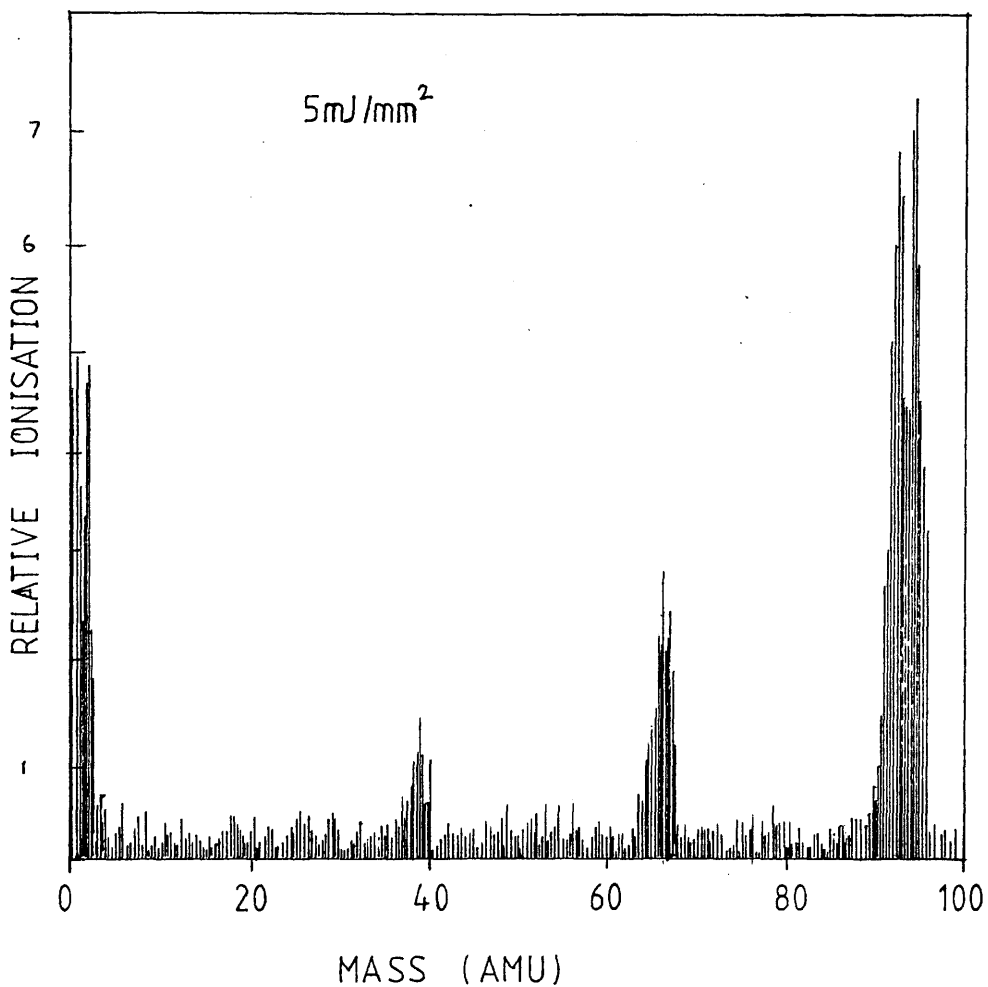


Figure: 8-6 Fragmentation pattern of phenol at lower laser fluence.

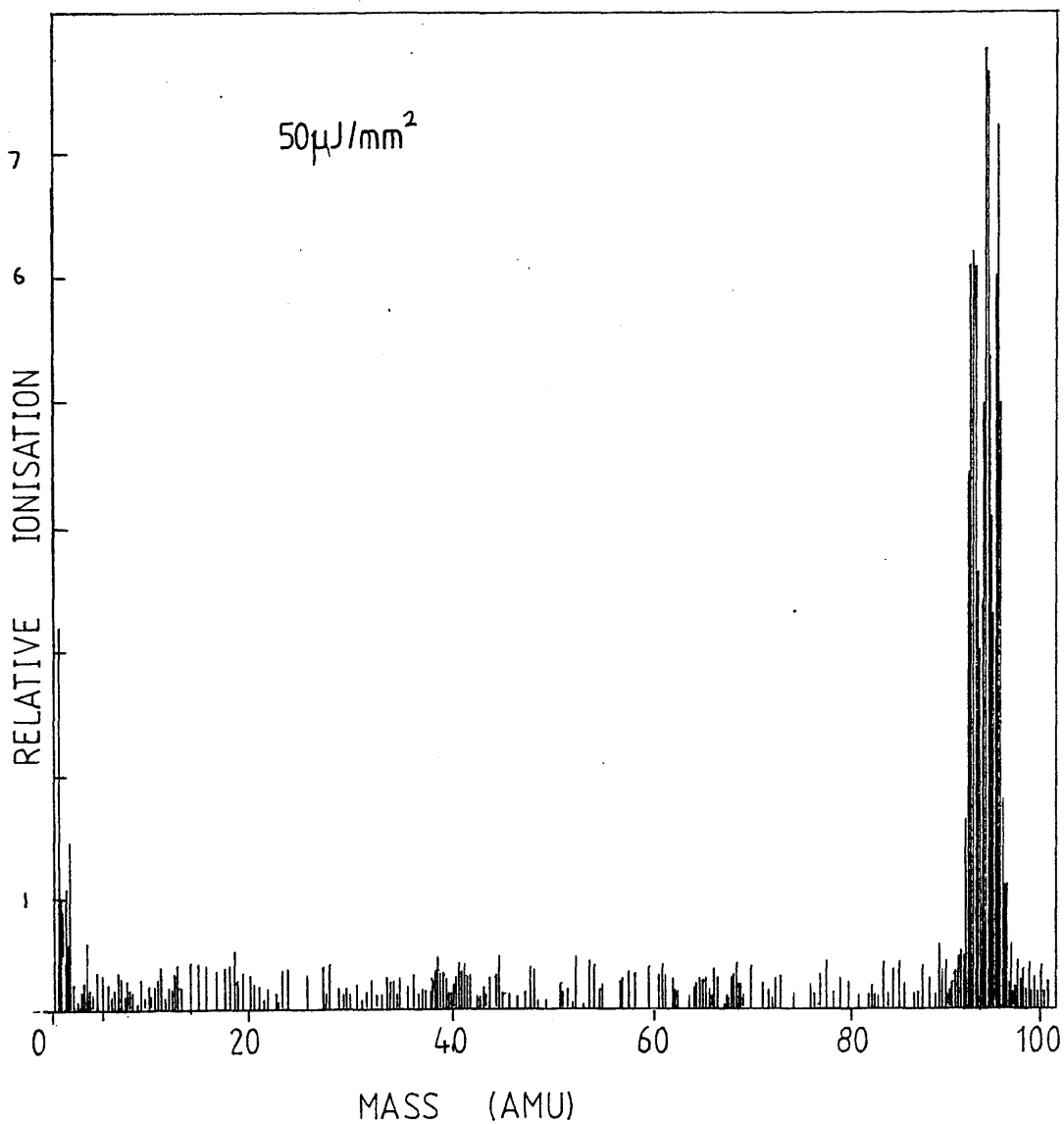


Figure: 8-7 Fragmentation pattern of toluene.

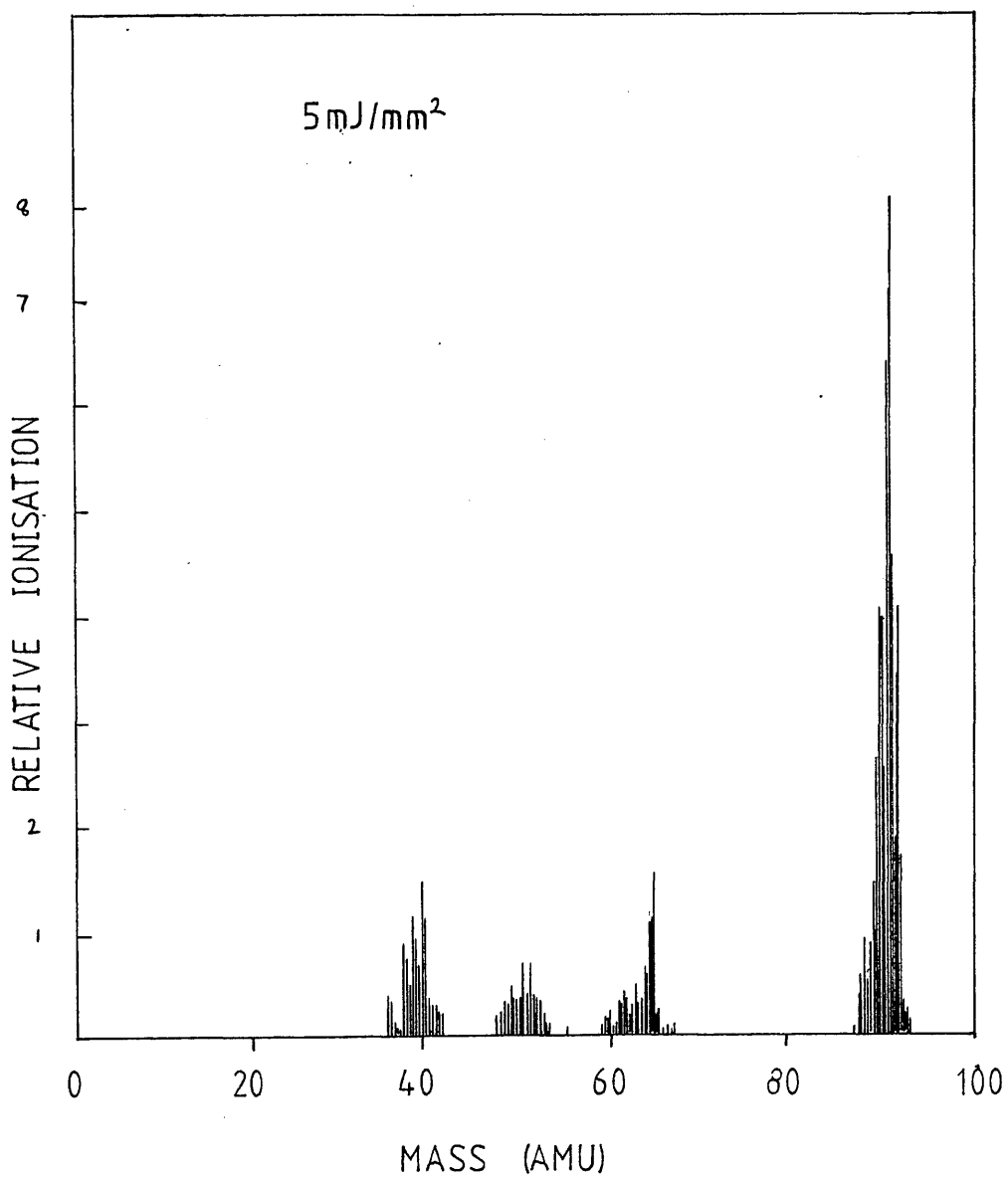
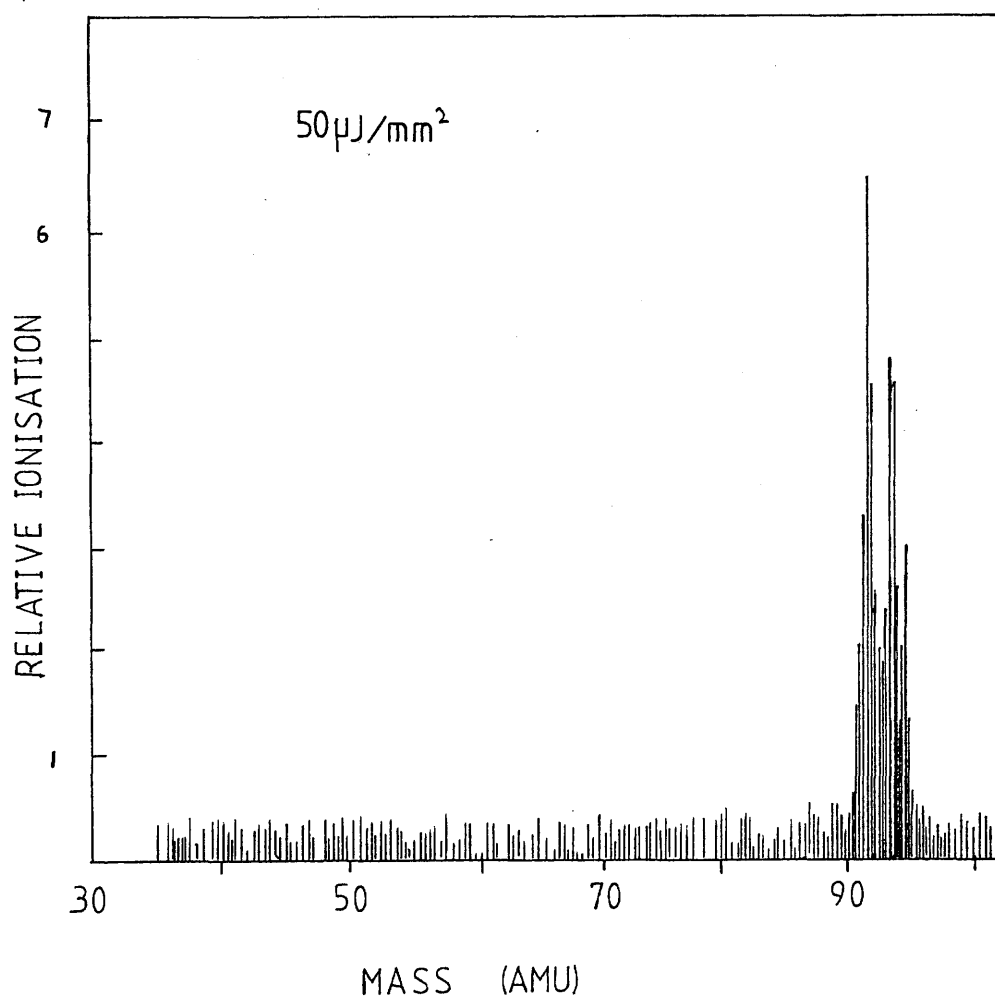


Figure: 8-8 Fragmentation pattern of toluene at lower laser fluence.



SECTION 8-3: CONCLUSIONS.

The maximum operating pressure of the mass spectrometer, imposes a limit of 2ppm to the concentration of the impurities in P10 gas which can be detected. Impurities in a clean counter are present at concentrations of about 0.02ppm. Detection of impurities in P10 gas passed directly into the mass spectrometer is not feasible by either electron bombardment or laser ionisation.

An attempt was made to increase the sample pressure by introduction of the gas through a fine nozzle directly into the ion source. No dramatic increase in sensitivity was observed.

Impurities from the P10 gas, concentrated in a cold trap, were introduced directly into the mass spectrometer. A focussed laser beam at 266nm produced no observable ionisation in this sample. The sample was analysed in a mass spectrometer, water was found to be the only detectable constituent in the cold trap sample.

Laser ionisation mass spectra were produced for phenol and toluene. Spectra were taken with strongly and weakly focussed laser light. As expected the fragmentation decreased with decreasing laser fluence.

CONCLUSIONS.

The purpose of the work, summarised in this thesis, was three fold:

1) To determine the most suitable laser type for the laser calibration of MWPC's with respect to both theoretical and experimental considerations.

2) To produce controllable and reproducible levels of laser ionisation in MWPC gas by the addition suitable seeding agents.

3) To identify the impurities responsible for the background laser ionisation in MWPC gases.

Calibration with lasers would be optimised by the production of narrow, well-defined laser induced ion tracks, with no variation in ion yield along the track, or from pulse to pulse. Generally the ion tracks must be a few metres in length. Ideal ion tracks would be produced by a non divergent laser with a short pulse duration ($<10\text{ns}$) and with no fluctuations in its output intensity.

In practice non divergent lasers cannot be produced. The lowest attainable divergence is obtained with single mode diffraction limited lasers. The divergence of a diffraction limited laser beam increases as a function of increasing wavelength. Variation in the spatial distribution and intensity of the laser beam, due to divergence, results in a variation in the ion yield along an ion track.

Ion yields are dependent on N, the order of the MPI process. With the exception of saturated MPI processes, the ionisation is proportional to the laser flux. Thus variation in the ion yield, due to divergence effects, increases very rapidly with increasing N. It would be desirable therefore to produce ionisation by laser beams with a low N dependence, or of sufficient intensity to saturate a higher order process. Saturation of MPI processes of order $N > 2$ would require very intense laser beams. Very expensive optics and stringent safety precautions are required to handle high intensity lasers, and thus for laser calibration low intensity lasers would be preferable.

Experiments have shown that appreciable 2-photon ionisation in counter gases can be achieved with unfocussed low intensity UV lasers at wavelengths between 193nm and 337nm. Divergence of diffraction limited laser beams between these wavelengths is between 17% and 42% over 10 metres, resulting in a decrease in the ion yield by factors of 1.35 to 2.

Divergence effects on the ion yield would be further reduced by using shorter wavelength lasers, but lasers with wavelength outputs below 200nm are rare. They tend to be excimer lasers which require frequent gas refills. Absorption of laser light in optics and air, also becomes a problem at wavelengths shorter than 200nm.

To minimise divergence effects it would be preferable to produce ion tracks by the single photon ionisation of low ionisation potential molecules. Lasers of $>200\text{nm}$ must be used to minimise absorption effects. Therefore the ionisation potentials of the molecules would have to be $<6.1\text{eV}$ and most molecules of this type are unstable.

Other properties required of a laser used for calibration are good pulse to pulse stability and a long lifetime. At best, the pulse to pulse stability of lasers with outputs between 200nm and 337nm is about 10% and lifetimes are about 10^8 pulses.

Ion yields are increased by using chaotic lasers (see chapter 1) instead of coherent lasers. This would allow a further decrease in the required intensity of the laser. Unfortunately, at best, only a decrease in intensity of a factor of two can be obtained in this way for a 2-photon MPI process. Effectively this means that there is little advantage in using chaotic lasers rather than coherent lasers.

Laser outputs may be multi-mode or single mode. Although in general multi-mode lasers are more intense than single mode lasers, they are also more divergent.

In conclusion, single mode lasers of short wavelength around 200nm and short pulse duration would be the best choice for laser calibration of MWPC's. For the calibration of the ALEPH TPC at CERN a frequency quadrupled Nd:YAG laser will be used. This has a single mode 266nm output of 5ns pulse duration, a pulse to pulse stability of $\pm 10\%$ and a lifetime of about 10^7 pulses.

As already stated, for laser calibration purposes it would be desirable to have controlled and reproducible ionisation yields along ion tracks. For this purpose it is better to use lasers with long lifetimes and good pulse to pulse stability. Experimentally, it was found that control of the output of the lasers was not sufficient to control the ionisation. Ionisation was found to vary hour by hour and from counter to counter. This was due to uncontrolled variations in the concentration of ionisable impurities in the counters. Control of the levels of laser induced ionisation was achieved by the addition of low ionisation potential vapours to the counter gas.

At first, the low ionisation potential molecules, DEA, DMA, TEA, TMA, TMPD, TMAE and Naphthalene were studied. These were chosen over many other similar molecules for a few reasons. They had either already been introduced into MWPC's, or had exceptionally high vapour pressures, or had very low ionisation potentials. Considerable enhancement in

ionisation over background was observed for all of these molecules using a laser with an output wavelength of 266nm. Unfortunately all, except TEA and TMA, proved either too sticky or too difficult to handle to be recommended as seeding agents. At a concentration of 100ppm in P10 gas, TMA was not sticky and appeared to have a beneficial effect on the lifetime of the counter with no apparent effect on the counter gain or resolution. TMA had one major fault. It gave off an extremely powerful and pervasive smell of rotting fish. For this reason alone it was not recommended as a seeding agent.

Later, phenol and toluene were also added, as seeding agents, to P10 counter gas. These were identified as impurities responsible for much of the background ionisation in counter gas. They were identified by comparing UV absorption spectra with background R2PI spectra of P10 counter gas. It was necessary therefore to add them to the counter gas in controlled concentrations so that their relative contributions to the background R2PI of the counter gas could be determined.

Phenol proved to be very sticky and difficult to control. Toluene on the other hand was not sticky. Its concentration could be maintained at a constant level, of about 6ppm, for several hours. At this concentration toluene had no noticeable effect on the resolution or the gain of the proportional counter. Ionisation of 10^4 IP/cm was produced by a laser beam of 1mm^2 cross-section, $1\mu\text{J}/\text{mm}^2$ fluence, 6ns pulse duration and at a wavelength of 266nm. Toluene does not have an unpleasant odour, although it is toxic at concentrations $>100\text{ppm}$ in air.

It was found that toluene had no short term effect on the purification systems proposed for the ALEPH TPC. Toluene, in P10 counter gas at 6ppm, was passed through the filters in a closed circuit flow system. At first it was removed from the P10 gas by adsorption onto the filter surfaces. After refilling the flow circuit several times with toluene at 6ppm the filters became saturated and no more

toluene was adsorbed. The ability of the filters to trap water and oxygen did not appear to be impaired.

All experiments so far suggest that toluene would make an ideal seeding agent. It is still necessary to determine the long term effects of toluene on the lifetime of a counter.

Both phenol and toluene are resonant at 266nm, and both have ion yields not very much different from the seeding agents described earlier. This indicated that the other seeding agents studied were also resonant at 266nm. A study of the UV absorption spectra of these molecules showed that this was indeed the case. It would seem therefore that 2-photon ionisation with laser fluences of around $1\mu\text{J}/\text{mm}^2$ requires not only that the ionisation potential of the molecule be less than the energy of 2 photons, but also that the ionisation process should be resonant.

It was thought that other organic molecules with strong resonances would prove useful as seeding agents. For this reason 2,6 lutidine and mesitaldehyde were chosen because they have very strong resonances at 266nm. In addition 2,6 lutidine has a very high vapour pressure and mesitaldehyde is not nearly as toxic as the molecules studied earlier. The ionisation yield of 2,6 lutidine proved to be very low. This was thought to be due to unfavourable competition between the ionisation and relaxation processes in the intermediate excited state of the molecule. Mesitaldehyde had a large ion yield. It has not been eliminated as a possible candidate for a seeding agent.

Dimethyl-phthalate and dibutyl-phthalate were studied since it was thought that they, or molecules like them, may be responsible for some of the remaining background ionisation observed in counter gases. The ion yield of dimethyl-phthalate was very low due to its low vapour pressure at room temperature. Dibutyl-phthalate produced no detectable ionisation at 266nm with a laser fluence of $1\mu\text{J}/\text{mm}^2$.

With acetaldehyde it was thought that three photon ionisation with the tripled Nd:YAG output (350nm) would be possible. Acetaldehyde has a 2-photon absorption resonance at about 350nm. Without laser focussing acetadehyde could not be ionised, even on the strong 2-photon resonance at 364nm.

Identification of the impurities responsible for the background ionisation of counter gases was important for reasons apart from their possible use as seeding agents. It was necessary, first of all, to form a better understanding of the ionisation processes involved in the interaction of the laser beam and secondly there was a need to identify the source of the impurities, with a mind to alternative methods of ionisation control.

It was already understood that the ionisation was due to the 2-photon ionisation of low ionisation potential impurities in the counter gas, but it was not clear whether the ionisation process was resonant or non-resonant. The presence of fine structure in the R2PI spectra of P10 counter gas indicated further that a resonant 2-photon process was involved. Comparison of the R2PI spectra with single photon electronic absorption spectra indicated that phenol and toluene were major contributors to the background ionisation. Phenol was found to be outgassing from plastic flow pipes used in the construction of the first counter flow systems. R2PI fine structure associated with phenol disappeared on removal of the plastic flow pipes from the system. R2PI structure associated with toluene was then identified. The source of the toluene did not appear to be from a single source in the counter or flow apparatus. Adsorption and subsequent desorption from the counter walls was the main mechanism by which toluene found its way into the counter gas. Toluene may have been introduced into the counter when cleaning the inner surfaces with solvents like methanol and ethanol, in which toluene is a common impurity.

By flushing clean gas through a counter a background R2PI spectrum was produced that indicated the presence of further, as yet unidentified, impurities.

Boerner (1985) reported the presence of several organic impurities in counter gas. Several of these were substituted benzenes with UV resonances at around 266nm. It seems likely that any of these molecules, or molecules similar to them, is responsible for the remainder of the R2PI background.

A positive identification of the remaining impurities could not be made using laser ionisation mass spectrometry, since the sensitivity of the quadrupole mass spectrometer was too low. At best the system could detect 10 ion pairs produced in the ion source. With the power levels available from the dye laser at 266nm it was calculated that partial pressures of an impurity in the spectrometer ion source would have to be of the order 10^{-10} torr. Direct introduction of the P10 gas into the counter meant that the impurities were present at pressures of about 10^{-13} torr. Several methods to increase the partial pressures of the impurities were attempted without success.

The mass spectrometer could not detect any impurities present in counter gases, but it was capable of detecting laser induced ions from pure samples of TEA, phenol and toluene. Pure samples of these molecules were introduced into the counter at partial pressures of around 10^{-6} torr. With focussing of the laser beam, extensive fragmentation of the parent molecules was observed.

Study of the R2PI of background impurities in counter gases is important in fields of study other than laser calibration. The presence of impurities like toluene is not confined to proportional counters and MWPC's. For instance materials used in, and methods used for, the construction of mass spectrometers are similar to those used for MWPC's. Therefore mass spectrometers are likely to contain traces of low

ionisation potential molecules. Trace levels would be at the ppb level, and therefore for all but the most sensitive mass spectrometers they would not be detected. Where the presence of minute traces of low ionisation potential molecules may become a problem is in Resonant Ionisation Mass Spectrometers (RIMS). For many applications RIMS systems must be very sensitive (ie capable of detecting single ions). Their sensitivity often depends on an ability to selectively ionise an atom or molecule by resonant MPI. If the absorption resonance coincides with one of the broad resonances of an ionisable impurity then many unwanted ions may be produced. The problem may be exacerbated by fragmentation of the impurities, thus producing ions of indeterminate mass over a wide mass range. Therefore it would be better for RIMS if wavelengths of greater than 350nm were used. This would reduce the R2PI background by several orders of magnitude.

LASER CALIBRATION.

Toluene appears to be a very strong candidate as the seeding agent in the ALEPH TPC. It is not sticky, it has a large ion yield and in the short term it has no effect on the properties of the counter or on the filters used to remove oxygen and water from the counter gas. However, the long term effects of toluene seeding on the properties of counters have still to be studied.

In the future, work at Glasgow, related to the laser calibration of MWPC's will decline. The process of laser ionisation in counter gases is now better understood and toluene has been found to be a useful seeding agent. From this work R2PI spectroscopy has shown itself to be a very promising technique for the detection of trace levels of certain organic impurities.

The emphasis of work at Glasgow has now shifted to resonant ionisation mass spectroscopy and we hope that this technique will have sufficient sensitivity to identify further low ionisation potential molecules in counter gases.

RESONANT IONISATION MASS SPECTROSCOPY.

In future the RIS group at Glasgow will concentrate on the development of laser mass spectrometer systems for the analysis of trace elements in bulk samples. At present there exists a quadrupole mass spectrometer with both electron bombardment and laser ionisation facilities. Although, as already explained in chapter 8, this system could not be used for sensitive analysis, it has been useful for determining fragmentation patterns of organic impurities known to be

present in proportional counter gas. This spectrometer will continue to be used for resonant ionisation spectroscopy and mass spectroscopy.

Several types of mass spectrometer exist that can be used for laser ionisation mass spectroscopy, for example, quadrupole, magnetic sector and time of flight (TOF) mass spectrometers. For analysis of trace elements, the mass spectrometer must have a very high ion collection efficiency. The best ion collection efficiencies are obtained with TOF mass spectrometers. Quadrupole and magnetic sector mass spectrometers are less efficient because the ion optics used only transmit those ions that are travelling almost parallel to the longitudinal axis of the mass filter. The filter in turn separates out an individual mass. TOF mass spectrometers, on the other hand, can transmit most ions produced in the ion source and do not filter out individual masses.

Ions produced by laser ionisation in a TOFMS, are first accelerated in an electric field. The velocity of an ion, after acceleration, will be related to its mass (a lighter ion will have a greater velocity than a heavier ion). Mass separation is achieved by drifting the ions down a region of field free space, where they are detected by a secondary electron multiplier or a channeletron. The arrival time, t , of the ions is related to their mass, m , by the following equation:

$$t = \sqrt{d^2 m / 2Ve}$$

where d is the drift length, V is the accelerating potential and e is the charge of an electron. TOF systems do not have particularly good mass resolution, although they can easily resolve masses separated by 1AMU. Therefore they are suitable for elemental and isotopic analysis, where single element selection is achieved in the ion source by resonant ionisation.

Where the low resolution of TOF systems may become a problem is in molecular analysis, or where molecular ions contribute to background signals in elemental analysis.

Two types of time of flight (TOF) mass spectrometer are being built. A schematic diagram of these is shown in figure 9-1. The first TOF system uses a laser to ablate the surface of the sample to be ionised, producing a plume of neutral atoms just above the surface. (A N_2 laser is to be used for the ablation of the sample). The atoms in the plume are then interrogated by the tunable output of a Spectron Nd:YAG pumped dye laser with a pulse length of 15ns and a maximum repetition rate of 20Hz. (Due to be installed shortly is a second dye laser which will allow multi-laser and Doppler free experiments to be carried out). The ions are accelerated in an electric field and focussed with ion optics. They then pass down a 1m field free region onto a secondary electron multiplier. Signals from the multiplier are digitised in a transient recorder. Data is collected by an IBM personal computer via a GPIB/IEEE-488 communications bus.

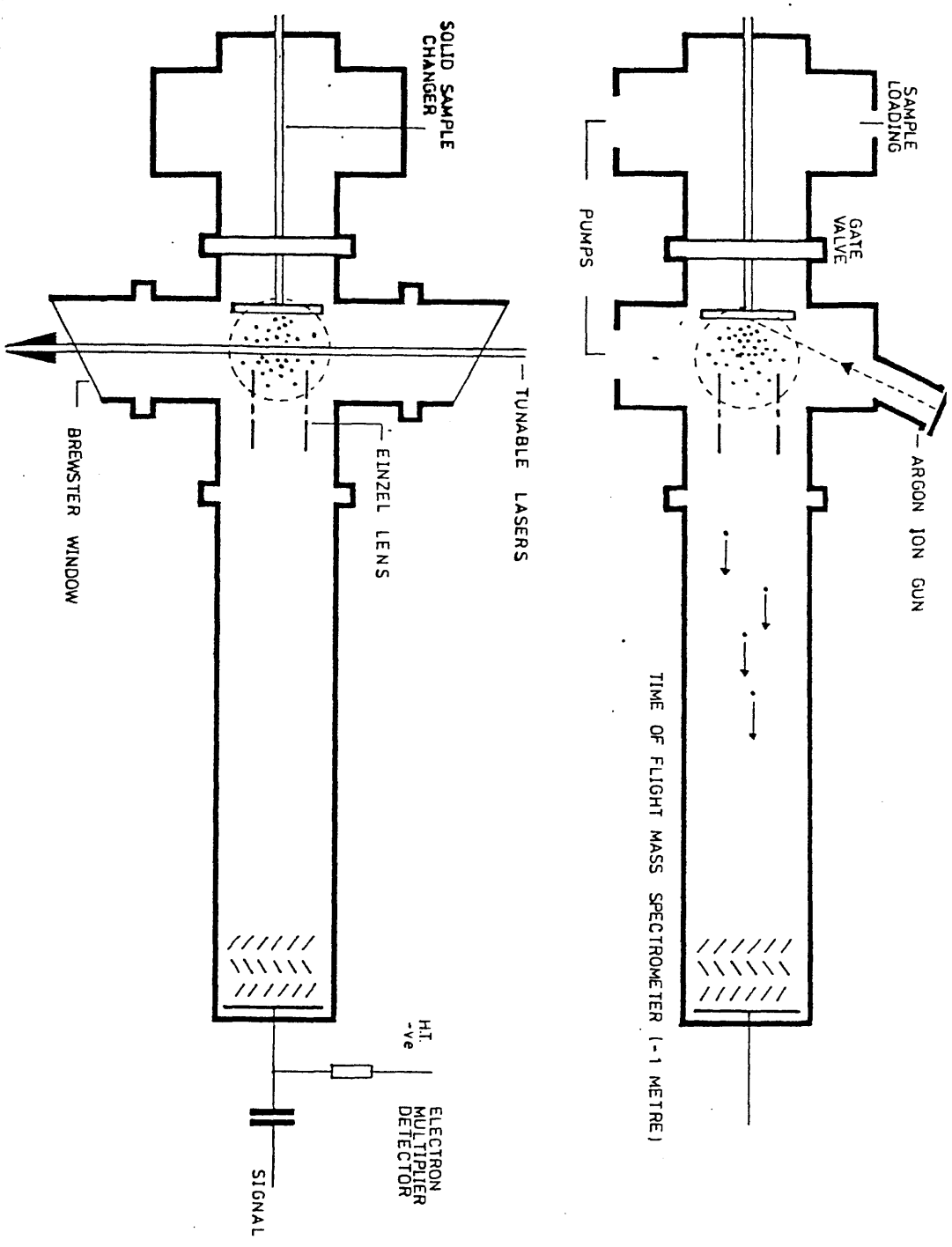
The second TOF system will use a pulsed argon ion gun to ablate the surface of the sample. The argon ion gun has the facility to raster the surface allowing a topographical analysis of trace elements.

The mass spectrometers will be used for various studies.

a) The sensitivity of a spectrometer may be impaired by the ionisation of low ionisation potential molecular impurities. Studies are to be carried out on the effects of these impurities on spectrometer sensitivity. It is hoped that other low ionisation potential impurities in P10 gas may be identified.

a) Another study will determine the suitability of RIMS for nuclear waste monitoring, especially low energy β^- emitters like Caesium.

Figure: 9-1 The Time of Flight Mass Spectrometer .



b) Determination of the half lives of long lived β^- emitters will also be attempted. Initially Technetium (99), with a half life of 10^6 years, will be studied.

c) A more sensitive technique for trace analysis of impurities in semiconductor materials. Using the argon ion gun it is hoped that depth profiling of the semiconductor sample may be possible.

d) As a method for the detection of trace levels of explosive materials in air. Replacement of the current technique used for detecting explosives with laser ionisation may give greater sensitivity. The TOF spectrometers will be used to determine the optimum wavelength for the ionisation of explosive molecules.

SENSITIVITY OF TOF SPECTROMETERS.

At present it is estimated that the TOF mass spectrometers at Glasgow will have a sensitivity of the order of parts per billion ($1:10^9$) for most elements. This compares well with the best sensitivity of secondary ionisation mass spectrometers (SIMS), which are already used commercially for elemental analysis. SIMS relies on the detection of ions produced by an ablating ion beam. The yield of ions produced in this way is very matrix dependent and only in certain favourable cases can ppb sensitivity be attained (Kimock et al (1984)). RIS will also use ion ablation but, unlike SIMS, it will analyse the neutral atoms sputtered from the surface of the sample. This has two advantages over SIMS: 1) Sputtering neutral atoms from solid samples is not strongly matrix dependent and 2) The ratio of neutral to ionic species sputtered from the surface of a sample is generally better than

100:1.

The current sensitivity of RIMS systems is limited by the following considerations:

- a) The efficiency with which neutral atoms, in their electronic ground states, can be removed from the surface of the sample.
- b) The efficiency with which the interrogating laser can ionise the selected neutral atoms. This is related to the geometric overlap of the laser beam with the neutral atoms removed from the sample and to the intensity and repetition rate of the laser.
- c) The transmission efficiency of the TOF system.

Each of these considerations will be dealt with in turn.

- a) Ablation: TOF systems require a pulsed ion source. Continuous ablation of the sample would be very inefficient, and hence ablation is pulsed by using a pulsed ion gun or laser.

The number of neutral atoms ablated from the sample surface by laser ablation is dependent upon the wavelength and intensity of the light and its angle of incidence to the sample surface.

The number of neutral atoms ablated from the sample surface by ion ablation is dependent on the primary ion energy (which determines the sputter yield, see figure 9-2), the ion current, the angle of incidence of the ion beam to the sample surface (optimal at between 45° and 60° from the normal to the surface (Kimock et al (1984))) and the ion species used to ablate the surface. Noble gas ion beams produce a greater proportion of neutrals than other ion beams that are available. Figure 9-3 shows the variation of sputter yield with different noble gas ion beams.

The system at Glasgow will use an argon ion gun. This has an ion current of $15\mu\text{A}$ ($9.4 \times 10^{13} \text{Ar}^+/\text{sec}$) with a pulse length of $3\mu\text{s}$ and a pulse rate of 20Hz (limited by the Nd:YAG repetition rate). The ions will

Figure: 9-2 Dependence of sputter yields on primary ion energy.

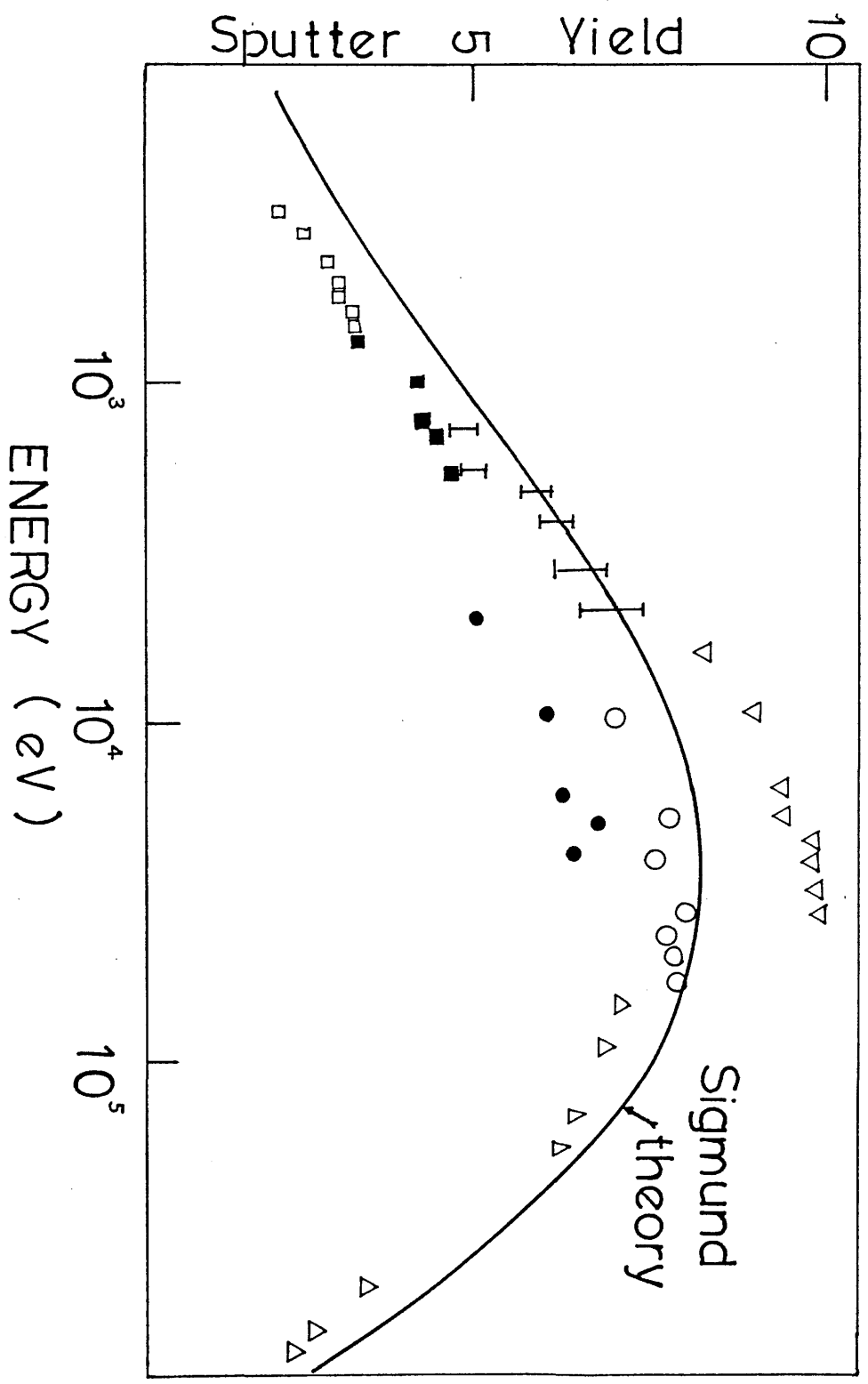
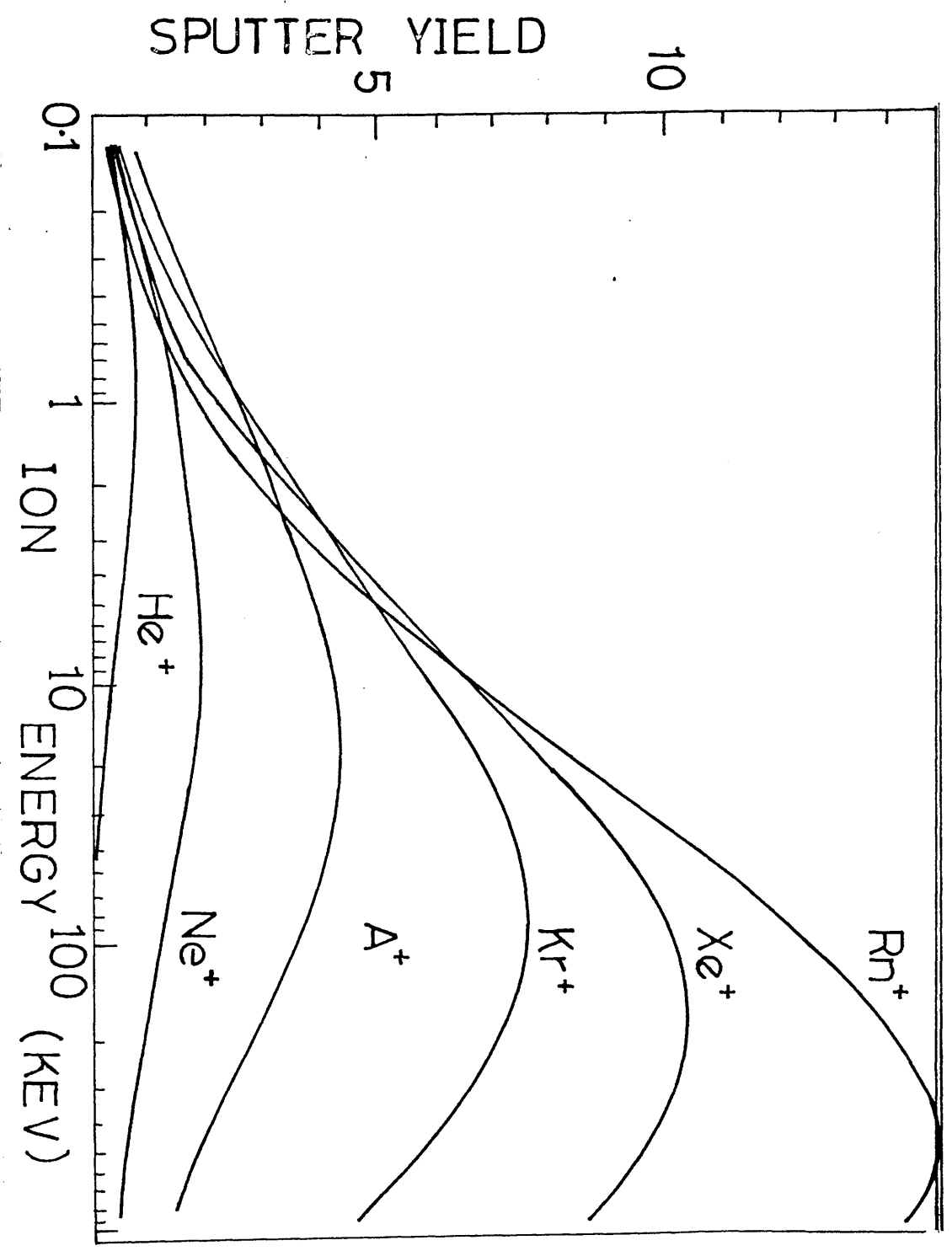


Figure: 9-3 Variation of sputter yields on different noble gases.



have a typical sputter yield of 5 neutrals per argon ion. therefore the number of atoms ablated from the surface will be about 3×10^{10} /sec.

b) Laser ionisation: Maximum ionisation efficiency is approached when there is a 100% geometric overlap between the laser beam and the sputter plume and when the laser ionisation process is saturated. Even under these conditions not every atom will be ionised since some have been excited into electronic states from which they cannot be resonantly ionised by the same laser wavelength as that to ionise those in the ground state. It has been estimated that the number of atoms in unsuitable electronic configurations may be as high as 50%, which means that 1.4×10^{10} atoms/sec ground state atoms will be produced. The sputter plume produced by a $3 \mu\text{s}$ argon ion beam pulse will extend some 6mm over the duration of the pulse. At present the Nd:YAG system cannot produce a saturation fluence for a beam 6mm in diameter. It is estimated that with the fluence currently available 30% of the plume will be ionised, meaning that for the typical argon ion beam 4×10^9 IP/sec will be produced.

By using techniques complementary to resonant MPI it is hoped that the ionisation efficiency may be improved. Figures 9-4a,b and c show three possible techniques. Figure 9-4a depicts ionisation by resonant excitation into a high lying Rydberg level followed by collisional ionisation. Collision induced ionisation from the Rydberg levels is easily saturated. Collisional ionisation is more efficient than R2PI because the absorption cross-sections of transitions into Rydberg states are generally greater than for transitions into states in the continuum. Appendix 3 summarises studies carried out on the collisional ionisation of caesium and in the near future similar experiments will be carried out on rubidium.

Figure 9-4b depicts field ionisation. As in collisional

Figure: 9-4a Collision induced ionisation.

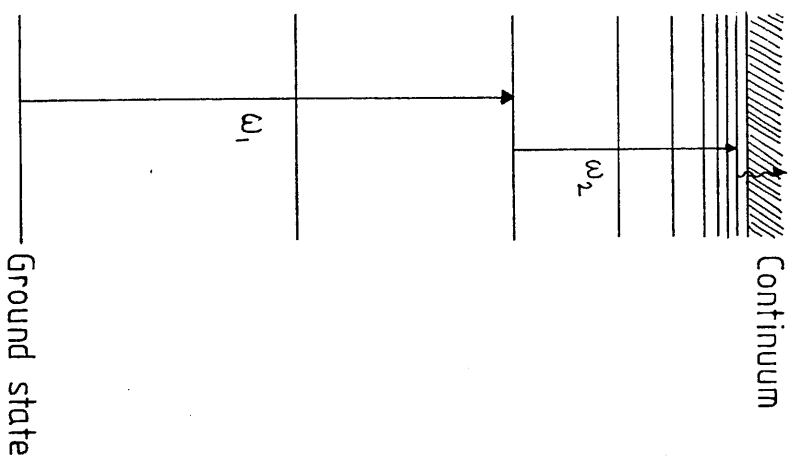


Figure: 9-4b Field induced ionisation.

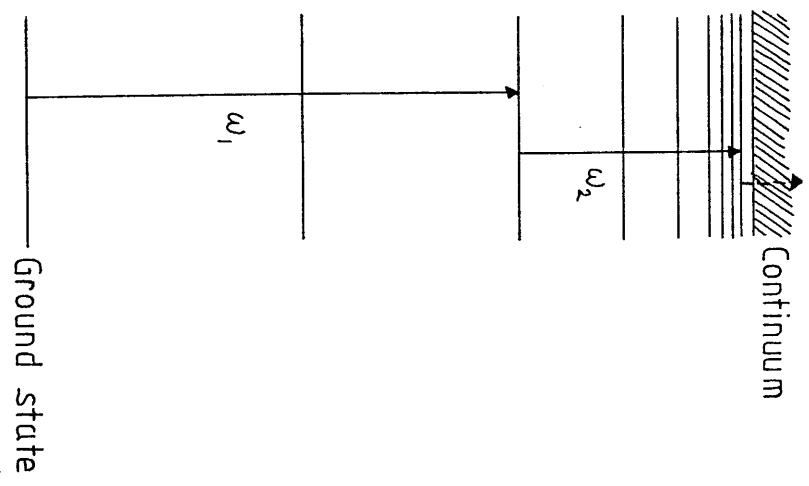
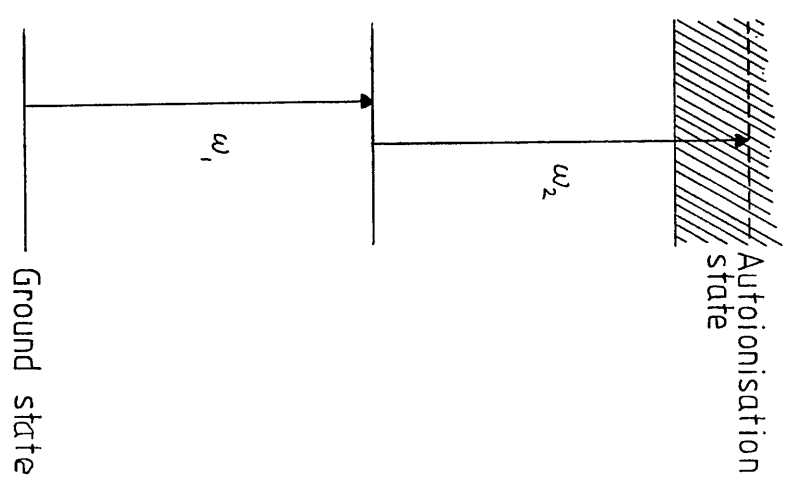


Figure: 9-4c Autoionisation.



ionisation this involves excitation of the atom into high lying Rydberg levels. Ionisation is then induced by a pulsed electric field. The third technique involves autoionisation (see chapter 1-4: Autoionisation). Essentially autoionisation produces apparent resonances above the continuum level of the atom (see figure 9-4c). By tuning the laser to one of these resonances, ionisation can be enhanced considerably.

c) Transmission efficiency: Typical transmission efficiencies for a TOF system are 50%, but with careful construction they can approach 100%. Assuming 50% transmission, 2×10^9 ion/sec will be detected by the RIMS system which is consistent with detection of about 1ppb of impurity in a bulk sample (current systems can detect single ions impinging on the detector).

As mentioned above, laser or ion ablation can be used to remove neutral atoms from the surface of a sample. For rapid analysis of bulk materials laser ablation is favoured. It can sputter large numbers of neutrals from a sample surface in a very short time ($< \mu\text{s}$). The main drawback of laser ablation is that it cannot easily be adapted for continuous depth profiling. Argon ion beams are seen as a more gentle method of ablation and are currently used for depth profiling of solid samples. The accuracy of depth profiling by ion ablation is limited by a process called Cascade Mixing. This effect is caused by atoms in surface layers of the sample receiving sufficient energy from the ion beam to be implanted in lower layers of the sample. Their movement can then confuse the results for the subsequent analysis of the lower layers.

The resolution of conventional RIMS systems is limited by the temporal, spatial and kinetic energy distributions of the ions leaving

the ion source. Lasers produce very a narrow temporal distribution because their pulse length is very short. The spatial resolution is related to the spatial cross section of the probe laser. A laser beam of about 6mm diameter would be required to efficiently ionise neutrals sputtered from a sample by an argon ion beam. Laser ionisation beams with smaller diameters could be used for if the ablation was carried out with lasers because of the narrower spatial distribution of sputtered neutrals.

Kinetic energy distributions for laser sputtered neutrals follow a Maxwell-Boltzmann distribution around a temperature value which would typically be 1000K ($\sim 0.1\text{eV}$). The typical energy spread of sputtered neutrals produced by an ion gun range from a few eV to KeV but are sharply peaked around 5eV.

High resolution high transmittance TOFMS are available and may be acquired for RIMS experiments at Glasgow. Two such systems are the reflectron (Boesl et al (1982) and Schlag and Neusser (1983). and poschenrieder (Poschenrieder and Oetjen (1971) TOF mass spectrometers. In both of these systems the effect of the initial kinetic energy spread on the resolution is reduced by increasing the distance travelled by the higher energy ions relative to the lower energy ions.

There is no doubt that the sensitivity of the RIMS technique will be improved in the near future. This will be achieved by the development of more powerful tunable lasers with very high repetition rates and by the development of more efficient high resolution mass spectrometers. Even at present RIMS competes well with conventional analytical techniques (such as SIMS) and for some applications proves to have a greater sensitivity.

RIMS will find important applications in the fields of fundamental and applied sciences. In fundamental physics it may be applied to experiments concerning magnetic monopole searches, double

beta decay, solar neutrino experiments and baryon conservation. It may also be used for the detection of quark atoms and superheavy atoms.

In applied science RIMS can detect trace impurities in semiconductor materials. These impurities restrict the performance of high speed, high density integrated circuits. Present detection limits for these impurities should be extended considerably with RIMS. In the medical field the technique can be used as a non invasive method of measuring trace element concentrations in body tissues. This may help in the early diagnosis of certain diseases. At present there is a great deal of concern over the possible detrimental effects on the environment of the nuclear industry. RIMS can be used to monitor nuclides emanating from nuclear plants and may assist in selecting sites for the safe disposal of nuclear waste.

POPULATION RATE EQUATION MODELLING.

Only for very simple systems does quantum theory give exact quantitative predictions for MPI processes. More complicated multi-electron and molecular systems are generally modelled using perturbation theory. By this method, the real solutions to the Schrödinger wave equation for the system, are approximated by the combination of a set of exactly solvable solutions. Approximation to the real solutions for complex systems leads to more qualitative predictions for the MPI of the system.

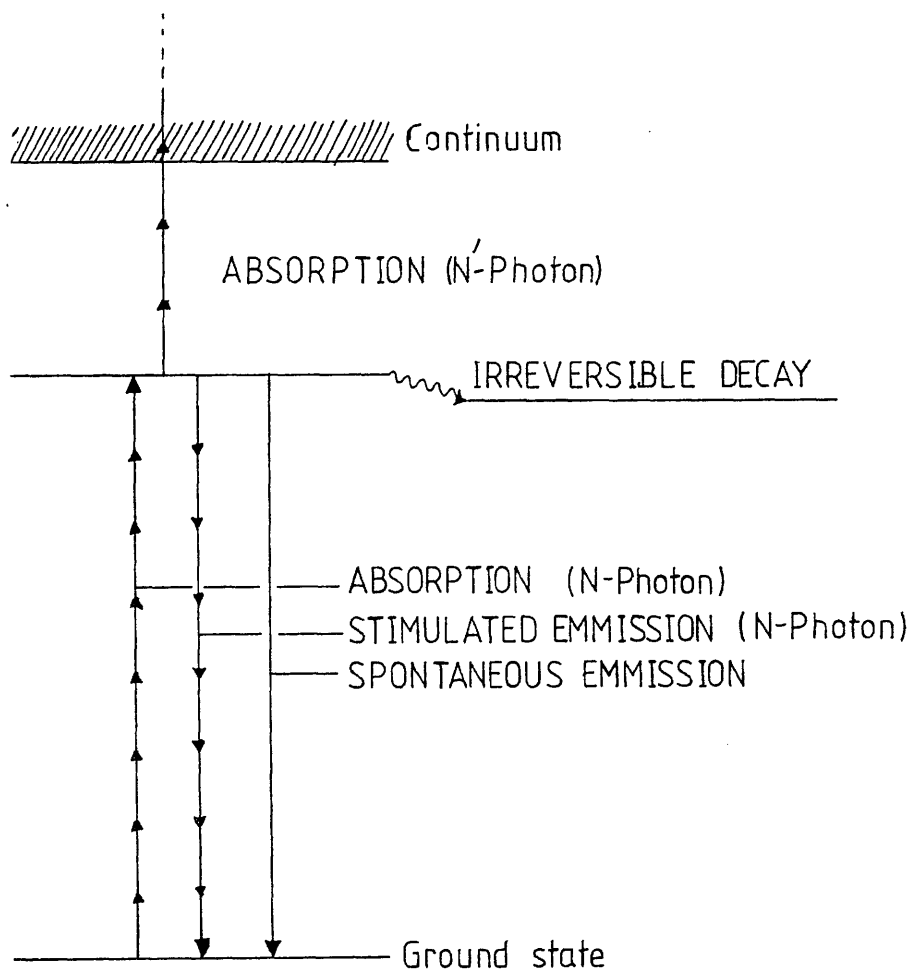
Adequate quantitative modelling of MPI processes can be achieved by using the quite simple population rate equations (PRE). The PRE method incorporates some of the basic predictions of perturbation theory. For example, multiphoton absorption transition rates through virtual states are given by perturbation theory as:

$$W_{fg} = \sigma_{fg} I^N$$

and is also used to describe a similar transition, using the PRE model. PRE modelling is applicable only for MPI processes where coherence effects of the light play an insignificant role in the absorption process.

Figure A1-1 shows schematically a MPI process through a single real intermediate state. It shows a N-photon absorption into the real state followed by an N'-photon absorption into the ionisation continuum. Also depicted on the figure are various competing processes often observed in molecular systems. These are spontaneous, stimulated and irreversible decay processes. Irreversible decay often occurs as the result of level

Figure: A1-1 Schematic diagram of $N+N'$ -photon ionisation of molecules.



crossing and collisional processes (see chapter 1).

The rate of change of population, in the radiation field, for each molecular state is first calculated. Equations A1, A2 and A3 give the rate equations for each of states S_0 , S_1 and C respectively.

$$\dot{S}_0(t) = -\alpha S_0(t) + (\alpha + k_0) S_1(t) \quad A1$$

$$\dot{S}_1(t) = \alpha S_0(t) - (k_0 + k_p + \alpha + \beta) S_1(t) \quad A2$$

$$\dot{C}(t) = \beta S_1(t) \quad A3$$

where $S_0(t)$, $S_1(t)$ and $C(t)$ are the ground, intermediate and continuum state populations. k_0 and k_p are the spontaneous and irreversible decay rates and α and β are the stimulated absorption-emission and ionisation rates respectively, given by:

$$\alpha = \sigma_1 I^N$$

$$\beta = \sigma_2 I^N$$

respectively. Using a top hat approximation to the laser temporal profile and assuming that at $t=0$, only the ground state is populated ($S_0(0)$), then the rate equations can be solved for C to give:

$$C = \beta S_0(0) (\beta + k_p) \left[1 + (L/(K-L))e^{-KT} - (K/(K-L))e^{-LT} \right] \quad A4$$

$$P = k_0 + k_p + \alpha + \beta$$

where T is the pulse duration and

$$+ \begin{pmatrix} K \\ L \end{pmatrix} = (P + \alpha)^{1/2} \begin{pmatrix} + \\ - \end{pmatrix} \left[(P + \alpha)^2 - 4\alpha(\beta + k_p) \right]^{1/2} / 2$$

and when $k_p \ll T^{-1}$

At low laser flux ΛKT and LT become $\ll 1$. The exponentials can then be replaced by their Maclaurin expansions:

$$e^x = 1 + x + x^2/2 + x^3/6 + \dots$$

The ionisation yield C then simplifies to:

$$C = \alpha \beta S_0^2 I^{(N+N')} = \sigma_1 \sigma_2 I^{(N+N')} S_0^2$$

Therefore, with T constant, the ionisation yield varies as the $N+N'$ th power of the laser flux. Under these conditions the MPI process is unsaturated. Log/log plots of ionisation versus flux would yield a straight line with a gradient of $N+N'$.

As the flux is increased KT and LT eventually become $\gg 1$ and the exponentials in equation A4 approach zero, leaving:

$$C = \beta S_0 / (\beta + k_p)$$

and

$$C = S_0 \quad \text{when } \beta \gg k_p$$

These equations represent saturation of the MPI process.

Calculations for the resonant two-photon ionisation (R2PI) of molecules are given below. R2PI is the most simple of the MPI mechanisms described above, since N and N' are both set to 1.

Typical values for the absorption decay parameters in molecular R2PI processes are :

$$\sigma_1 = 10^{-17} \text{ cm}^2 \quad \sigma_2 = 10^{-18} \text{ cm}^2 \quad k_0 = 10^8 \text{ sec}^{-1} \quad k_p = 0 - 10^{13} \text{ sec}^{-1}$$

A typical laser pulse duration is 6×10^{-9} sec. Figure A1-2 shows the calculated value of the proportion of molecules ionised in the interaction region against laser flux, using the parameter values listed above.

For example, phenol has an UV cross-section of $\sigma_1 = 10^{-18} \text{ cm}^2$. With a "laser fluence" of $1 \mu\text{J}/\text{mm}^2$ at 266nm only 1 in 2×10^8 molecules of phenol is ionised. Using these values the ionisation cross-section is calculated to be about 10^{-18} cm^2

Figures A1-3 to A1-9 show the effect of varying the parameters in equation A4. Listed below are brief explanations for each graph. Unless otherwise stated the parameters are as above, with k_p set to a value of 10^8 sec^{-1}

Figure A1-3: σ_1 the UV absorption cross-section was varied in multiples of 500 between $2.5 \times 10^{-33} \text{ cm}^2$ and 10^{-11} cm^2 . Ionisation yield dependence on laser flux for each is numbered in order of decreasing cross-section.

Figure A1-4: σ_2 the ionisation cross-section was varied between $2.5 \times 10^{-34} \text{ cm}^2$ and 10^{-12} cm^2 in multiples of 500. Ionisation yield dependence on laser flux for each is numbered in order of decreasing cross-section.

Figure A1-5: k_p the irreversible decay rate was varied between 10^{14} sec^{-1} and $4 \times 10^{25} \text{ sec}^{-1}$ in multiples of 500. Ionisation yield for each k_p is numbered in order of increasing k_p .

Figure A1-6: k_o the spontaneous decay rate was varied between 10^{14} sec^{-1} and $4 \times 10^{25} \text{ sec}^{-1}$ in multiples of 500. Curves are numbered by increasing values of k_o .

Figure A1-7: T the pulse duration was varied between 6×10^{-14} sec to 6×10^{-2} sec in multiples of 100. The curves are numbered by increasing T.

Figures A1-8 and A1-9: Show the effect on the ionisation of varying the laser flux but keeping fluence constant. The separate horizontal lines in figures A1-8 and A1-9 represent variations in UV absorption and ionisation cross-sections respectively. Over a wide range of flux the ionisation is constant.

CONCLUSIONS.

PRE's can be used to model MPI processes in complex systems. Analytical solutions to a general MPI process through an intermediate real state were calculated. Using typical cross-sections and state lifetime values for molecules the PRE model predicts that in a 6×10^{-9} sec pulse of fluence $1 \mu\text{J}/\text{mm}^2$ about 1 in 2×10^8 of the molecules in the interaction region should be ionised. For phenol the experimental value was calculated to be $1 \text{ in } 1.8 \times 10^8$ (assuming an irreversible decay rate of 10^4 sec). The curve in figure A1-4 indicates that saturation of the R2PI process begins at a laser flux of around 10^{25} photons/cm²/sec. This is equivalent to a fluence of about $400 \mu\text{J}/\text{mm}^2$ for a laser pulse duration of 6×10^{-9} sec and wavelength of 266nm. Fluences of this order can be achieved by the use of high power UV lasers or by focussing lower power lasers.

It should be noted that for irreversible decay rates between 10^4 and 2.5×10^8 sec⁻¹, the PRE model predicts very little change in the total ion yield. For values of $k_p > 10^9$ sec⁻¹ the ion yield falls rapidly. Lutidine (chapter 7) gave unexpectedly low ion yields this may be the result of a large irreversible decay rate.

For typical parameters in the PRE equation the ion yield is constant with constant fluence (flux x pulse duration = constant). Only

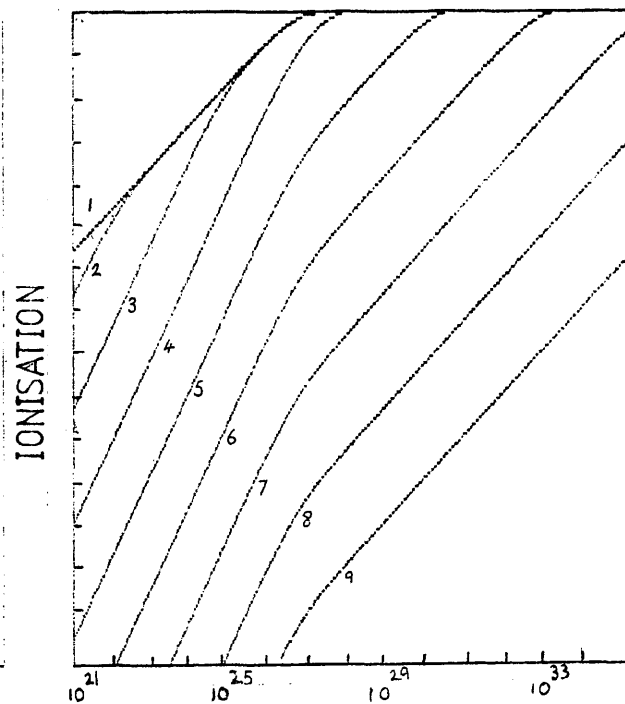
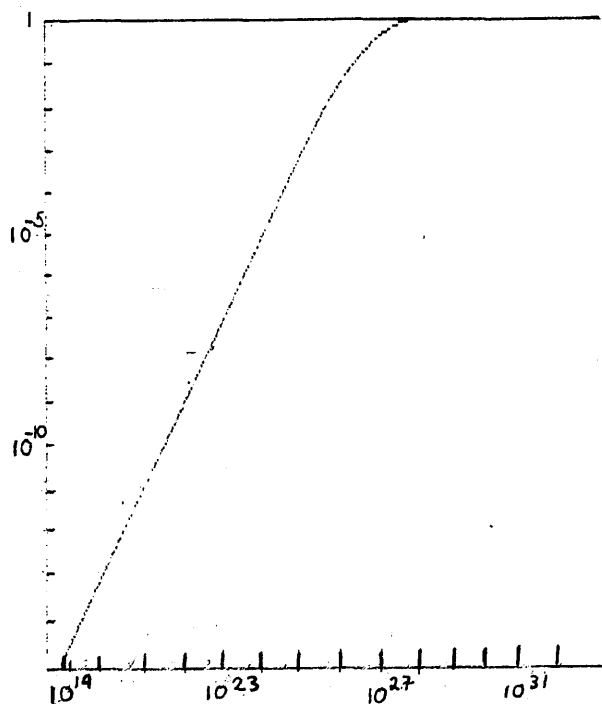
at extreme parameter values does it deviate from this behaviour. This deviation may have been caused by a computer underflow.

PRE modelling can be extended to multi-step, multi-laser MPI processes. The rate equations for these more complicated processes often have no analytical solutions, and must be solved numerically. PRE modelling of 2-laser, 3-photon resonant ionisation of atoms is described by Singhal et al (1987).

Figure A1-2: PRE model calculation

Figure A1-3: Variation of σ_1 .

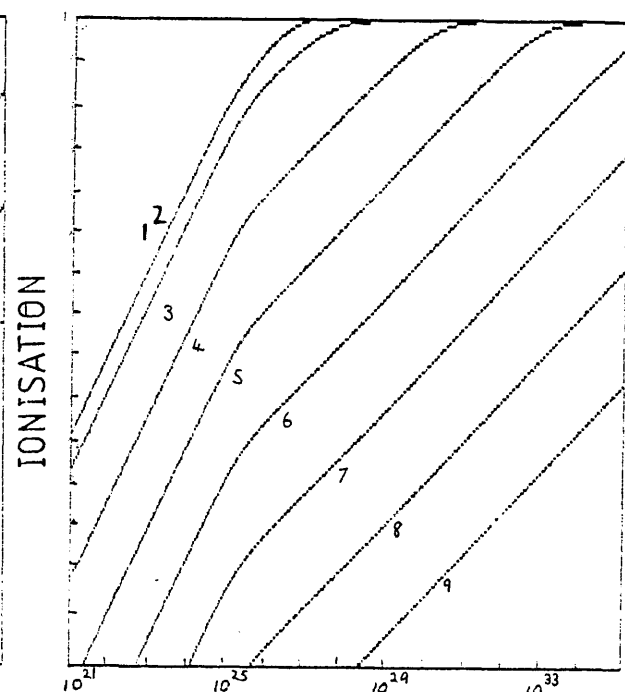
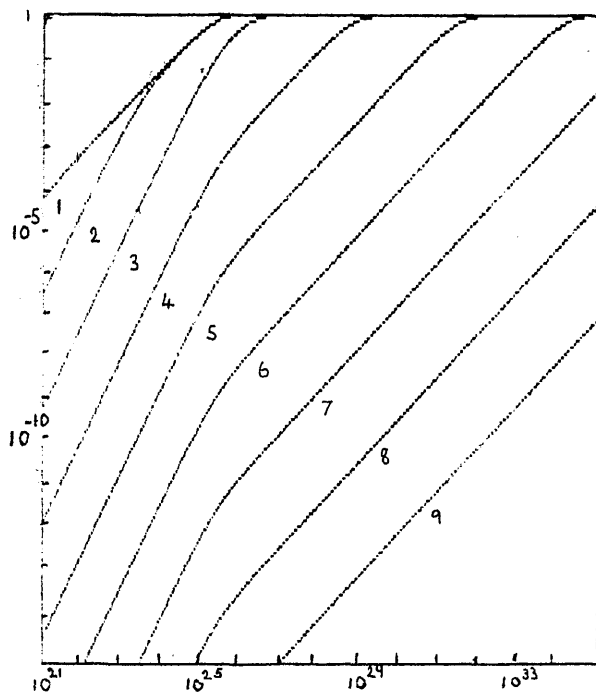
for MPI of a typical molecule.



FLUX (photons/cm²/sec)

Figure A1-4: Variation of σ_2 .

Figure A1-5: Variation of k_p .



FLUX (photons/cm²/sec)

Figure A1-6: Variation of k_0 .

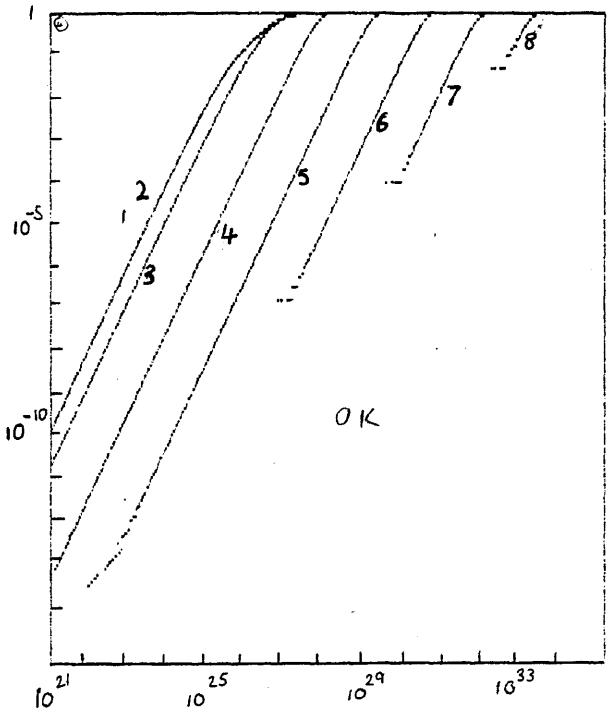
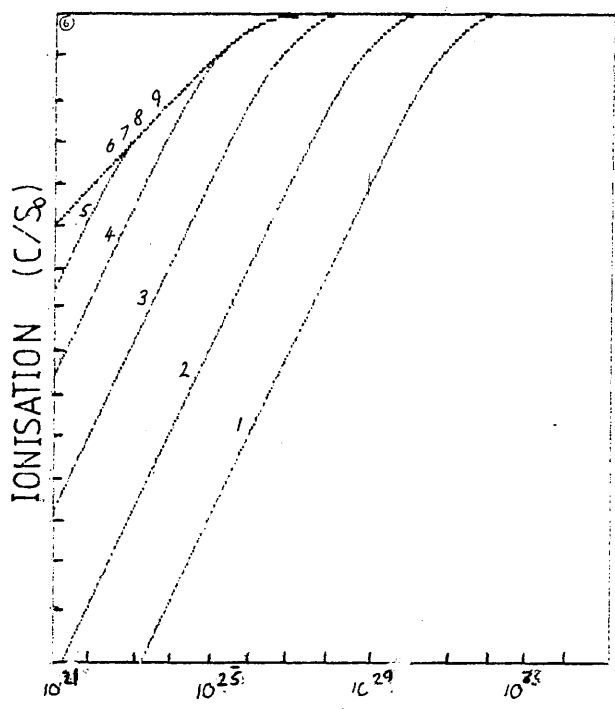


Figure A1-7: Variation of T.



FLUX (photons/cm²/sec)

Figure A1-8: Constant fluence with, σ_1 , variant.

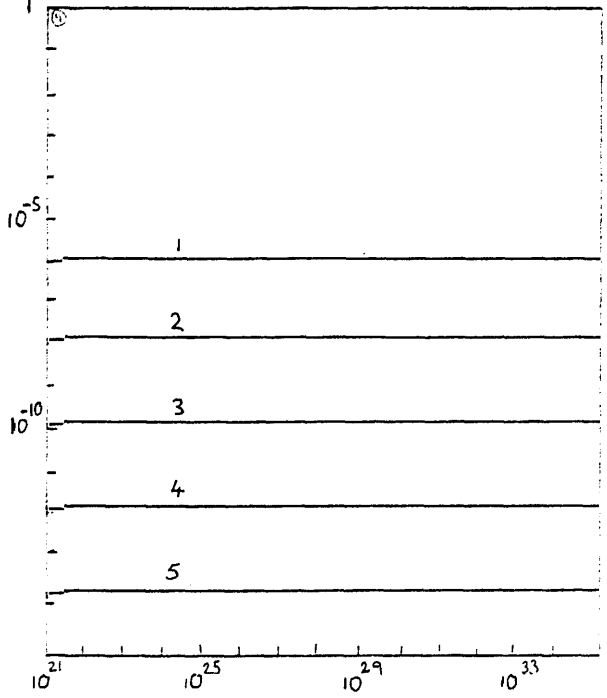
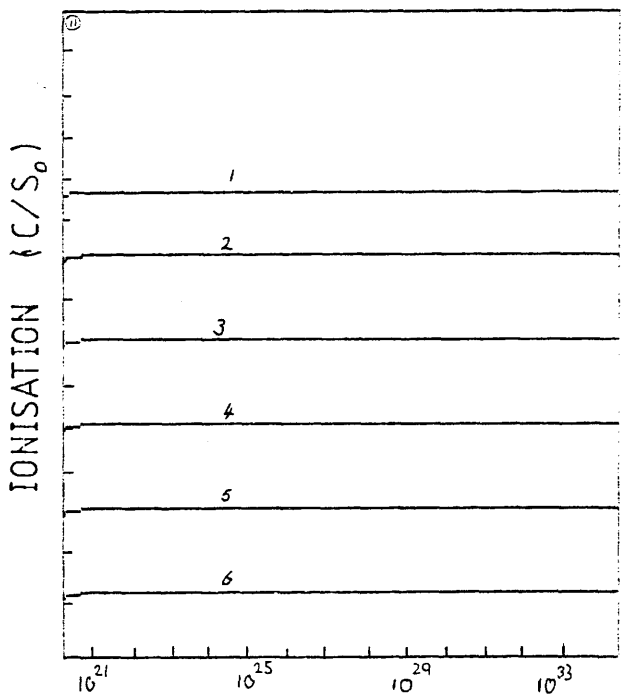


Figure A1-9: Constant fluence with, σ_2 , variant.



FLUX (photons/cm²/sec)

APPENDIX 2

THE ALEPH TPC.

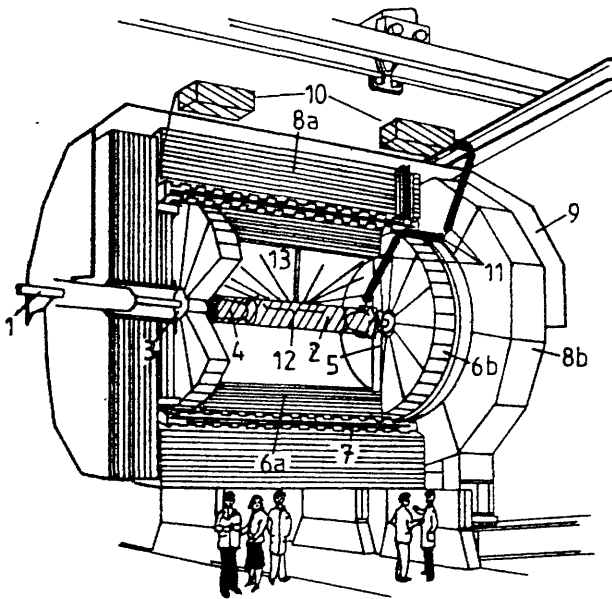
The ALEPH Time Projection Chamber (TPC) forms the centre of the particle detector being built at CERN. The TPC will be situated at an interaction point of the large electron-positron collider.

Figure A2-1 shows a cutaway view of the ALEPH detector. The TPC will have a cylindrical geometry of 4.4m length, split into two 2.2m drift regions by a central high voltage membrane. Plates at the ends of the chamber will have an outer radius of 1.77m and inner radius of 0.33m. A 90-10% or 80-20% argon/methane mixture at atmospheric pressure will be used as the electron drift gas medium.

Electrons produced by a particle event or by laser ionisation will drift towards the end plates in an electric field of about 200v/cm parallel to the chamber axis. Their arrival at the end plates will be recorded by grids of proportional wires and also by signals from an array of rectangular metallic plates called pads. Signals from the pads are induced by the charge avalanche produced close to the proportional sense wires. In the $r-\phi$ plane the position of the track is determined by the pulse height ratios induced from adjacent pads. The distance, z , above the pad plane is calculated from the arrival time of the signals on the pads and on the drift velocity of the electrons in the gas.

An end plate will have 21 pad rows, with a total of 22000 pads. Four millimetres above the pad plane are the field and sense wires. A further grid plane 8mm above the pad plane provides an earth, maintaining the electric drift field between the detectors and the high voltage membrane. Electric field inhomogeneities in the drift region are reduced by outer and inner field cages supporting ringed conductors

Figure: A2-1 Cutaway view of the ALEPH TPC.



1. BEAM PIPE
2. INNER TRACKING CHAMBER
3. LUMINOSITY MONITOR
4. BEAM PIPE CONE
5. TPC
- 6a. e- γ CALORIMETER (BARREL)
- 6b. e- γ CALORIMETER (END CAP)
7. SUPERCONDUCTING SOLENOID
- 8a. HADRON CALORIMETER (BARREL)
- 8b. HADRON CALORIMETER (END CAP)
9. MUON CHAMBERS
10. YAG LASER (265nm)
11. MIRRORS
12. MIRRORS ATTACHED TO INNER FIELD CAGE.
13. LASER TRACKS INSIDE THE TPC VOLUME

held at suitable potentials.

Space charge near the sense wires produced by the amplification of unwanted background ion tracks, can drift into the electron drift region introducing inhomogeneities in the electric field. The ions are prevented from doing this by placing a gating grid of wires 12mm above the pad plane. Figure A2-2 and A2-3 show diagrams of the pad geometry and the wire plane configuration for the ALEPH TPC.

THE ACCURACY OF THE ALEPH TPC.

The diffusion of electrons, as they drift towards the detector plane, sets the limit to the accuracy that can be achieved in a gas filled MWPC. The inherent accuracy of the ALEPH TPC in the $r-\phi$ plane has been calculated to be about $\sigma_0 = 160\mu\text{m}$ (Blum 1984). Further effects defining the accuracy of the TPC are given below, and in more detail by Blum (1984). All of these effects can be studied with laser induced ion tracks.

ANGULAR AND E X B EFFECTS.

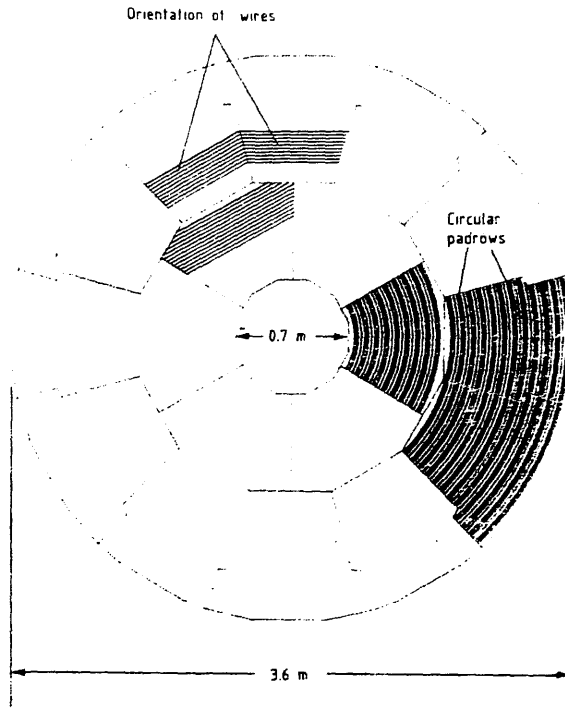
The distribution of electron avalanches on a wire, with no magnetic field present is given by:

$$\sigma_d = \sigma_0 (D/D_0) \sin \theta / \cos \alpha \quad D_0 = 1m$$

where D is the distance of electron drift, θ is the polar angle of the track and α is the angle between the normal to the wire and the projection of the track in the wire plane (see figure A2-4).

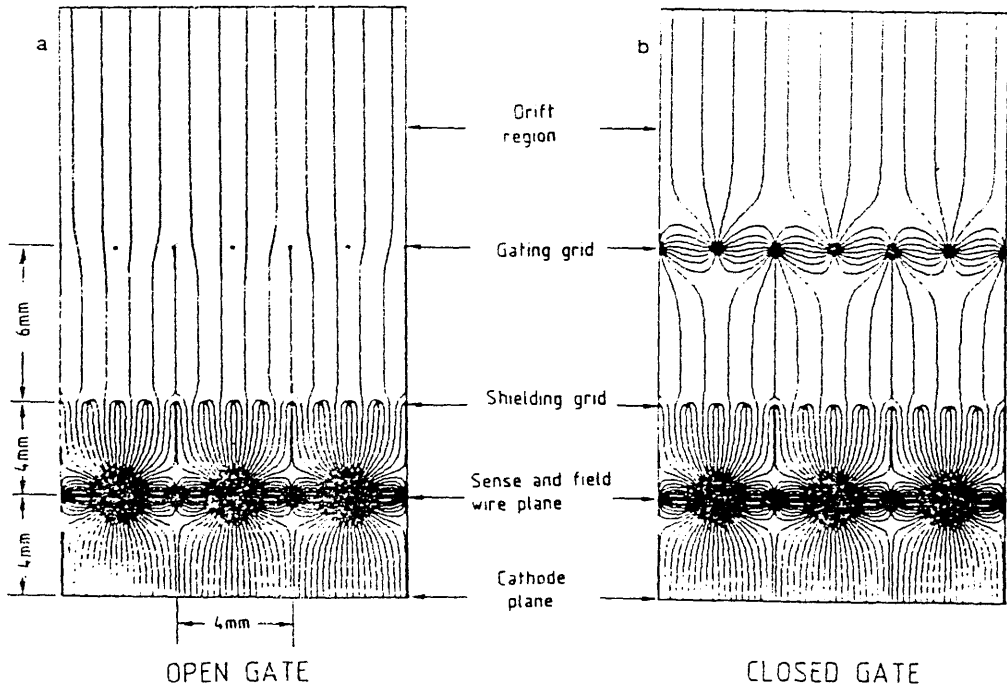
Clustering of electrons along the track from fluctuations in the primary ionisation distribution, and changes in the drift direction due

Figure: A2-2 Pad geometry of the ALEPH TPC.



Division of one ALEPH TPC endplate into 18 sectors.

Figure: A2-3 Wire plane configuration of the ALEPH TPC.



Grid configuration and field map for (a) gating grid open and (b) gating grid closed.

Figure: A2-4 Projection of track on wire plane.

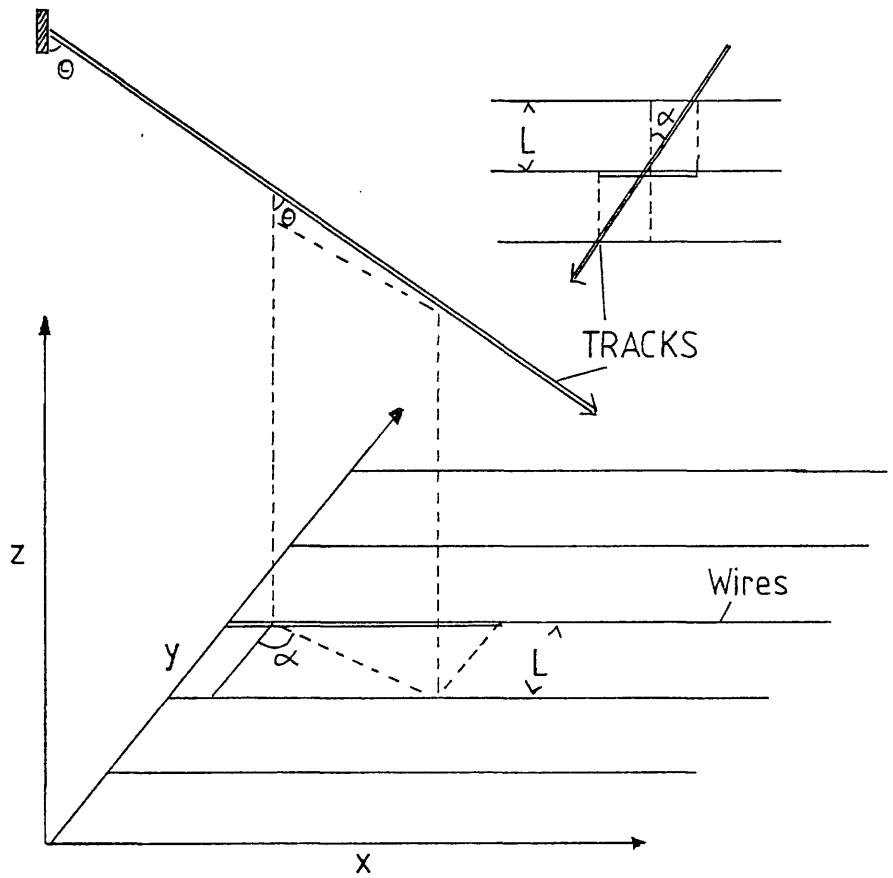
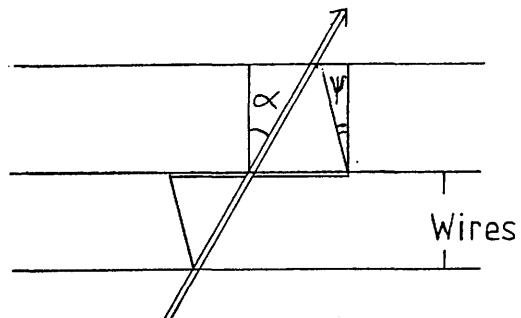


Figure: A2-5 Projection of track on wire plane with $\underline{E} \times \underline{B}$ effect.



to $\underline{E} \times \underline{B}$ effects near the sense wires, produce further uncertainties. The $\underline{E} \times \underline{B}$ effect can be characterised by an angle Ψ (see figure A2-5). The length, l , of the wire affected by the charge from the track is then given by:

$$l = L |\tan \alpha - \tan \psi|$$

The number of clusters along l is then:

$$n_c = N_c L / C \cos \alpha \sin \theta$$

where N_c is the number of primary charge clusters along the track per unit length. L, α and θ are as before. The mean square displacement of the mean avalanche position along the track is given by the relation:

$$\sigma_c^2 = \sigma_1^2 (\cos \alpha \sin \theta) (\tan \alpha - \tan \psi)$$

and

$$\sigma_1^2 = K_1^2 L / 12 N_c$$

K_1 is a factor which takes into account fluctuations in the cluster sizes. Positional accuracy σ_w of the avalanches on the wire is then given by:

$$\sigma_w^2 = \sigma_d^2 + \sigma_c^2$$

PAD ACCURACY.

The accuracy in the determination of the x-coordinate from the

pulse height measurements from the pads has been calculated to be:

$$\sigma_x^2 = (\sigma_0^2 / n_{\text{eff}})(D / D_0) \cos^2 \gamma \sin \theta / \cos \alpha + (\sigma_1^2 / n_{\text{eff}}) \cos^2 \gamma \cos \alpha \sin \theta x$$

$$(\tan \alpha - \tan \psi)^2 + (\sigma_2^2 / n_{\text{eff}}) \sin^2 \beta / \cos^2 \alpha + \sigma_N^2$$

where σ , θ , ϕ , ψ and α are as before. n_{eff} is the number of wires over one pad, γ is the angle between the wires and the x-axis and β is the angle of the projection of the track onto the pad plane and the y-axis (see figure A2-6). The term:

$$(\sigma_2^2 / n_{\text{eff}}) \sin^2 \beta / \cos^2 \alpha$$

reflects uncertainties in the signal due to amplifier noise and other effects. σ_N^2 represents the uncertainty due to the electrical pulse height measurement and to angle dependent effects.

MOMENTUM RESOLUTION.

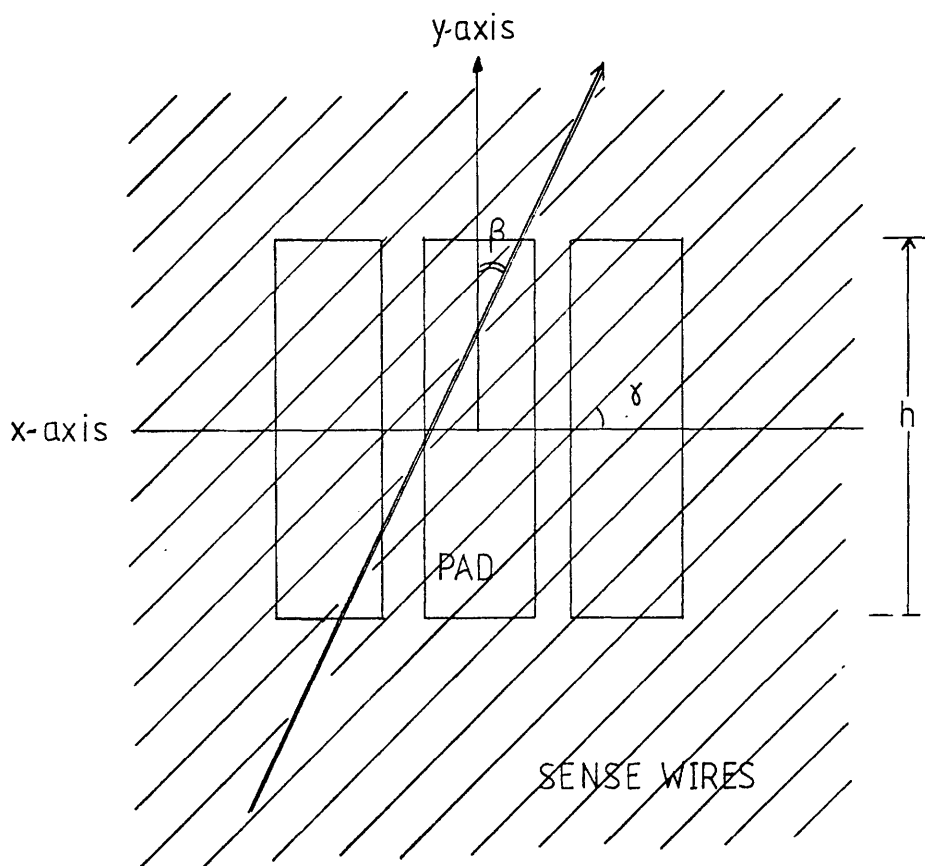
The momentum, P_T , of particles in the counter is determined from the sagitta measurements for the laser ion track. For the ALEPH TPC the momentum resolution is given by $\Delta P_T / P_T^2$ and is calculated to be 0.9×10^{-3} (GeV/c)⁻¹ for stiff tracks. Further losses in momentum resolution occur due to the bending of the track in a magnetic field.

DOUBLE TRACK RESOLUTION.

The double track resolution is given by the minimum distance between two points on different tracks that can be separated. In the r - ϕ plane the minimum separation $r\phi$ is about 2 pad widths (12mm).

Separation in the z direction is determined by the pad length h , the polar angle, θ , of the track and on the integration time of the

Figure: A2-6 Projection of track on pad plane.



electronic amplifiers. i.e.

$$\Delta z = (h / \tan \theta)^2 + (\Delta z)_{\text{electrical}}^2$$

The separation in the polar angle is given by:

$$\Delta \theta = \Delta z / r_1 \sin^2 \theta$$

A further limit to the accuracy of the z coordinate calculation is the rate at which the analogue to digital converters (ADC's) can analyse the pulse data. The ALEPH TPC will record the height of the amplified signal from the pads about every 80ns (a frequency of 125MHz). A gaussian fit to the pulse heights of three successive time bins covering the peak of the pulse is used to calculate the centroid of the pulse distribution.

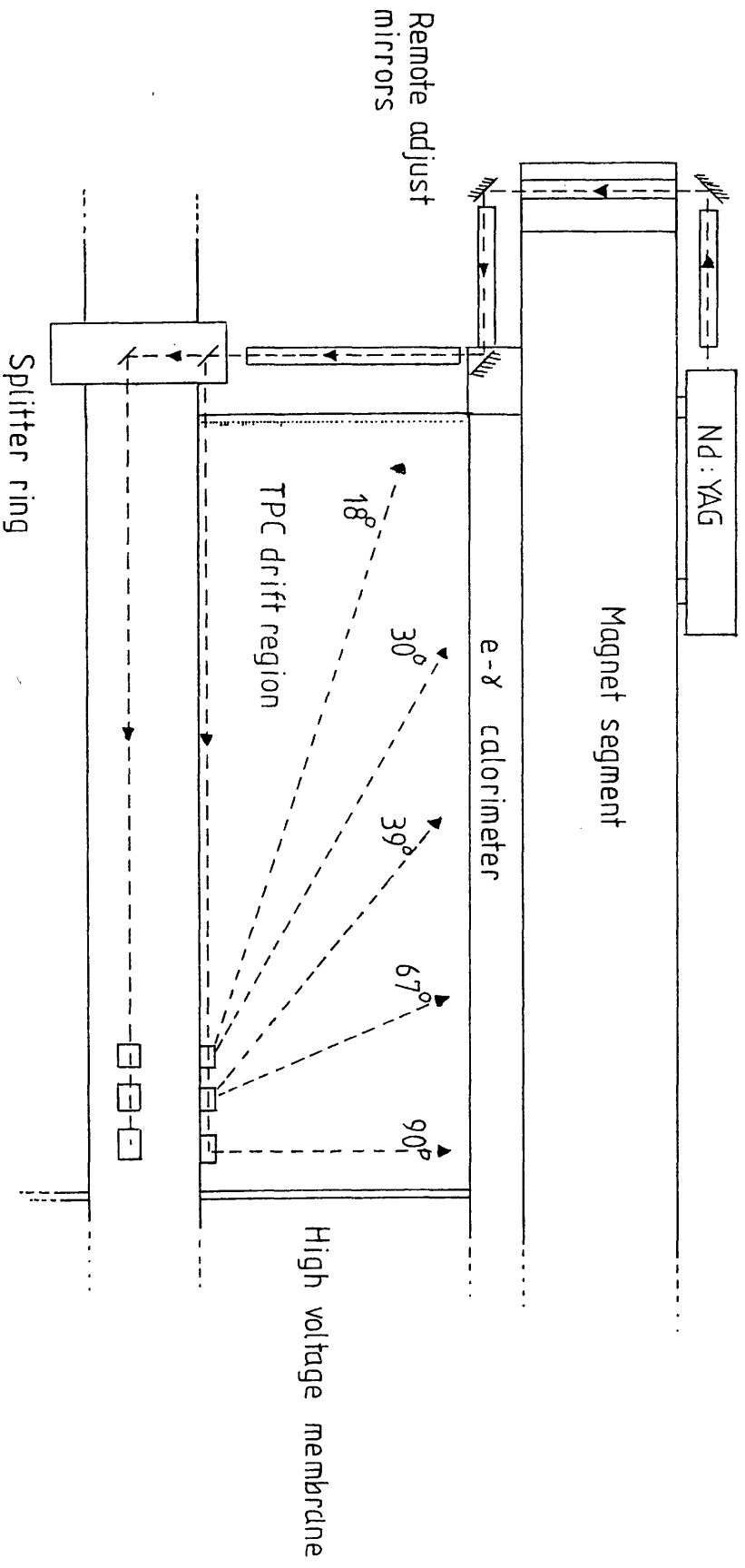
The position of the track in the z direction is then calculated from the time separation of the centroid of the pulse and a reference trigger. Calculation of the centroid has a maximum accuracy of about 25ns (equivalent to about 1.5mm in the z-axis) (Richter (1984)).

All of these effects on the accuracy of the TPC can be studied by laser induced ion tracks, but the most important use for laser calibration is the determination of global distortions in the MWPC and for real time calibration of the chamber during particle experiments.

THE ALEPH TPC LASER CALIBRATION SYSTEM.

A laser calibration system will be incorporated into the ALEPH TPC. Two single mode quadrupled Nd:YAG lasers will produce a total of 30 tracks per 'shot' in the TPC, 15 in each half of the chamber. Figure A2-7 shows a schematic picture of the laser beam transport system.

Figure: A2-7 ALEPH TPC beam transport system.



Laser beams are directed by a series of high quality mirrors into the centre of the TPC. It is then split into 3 beams of equal intensity parallel to the chamber axis at angles of $\phi = 0^\circ, 120^\circ$ and 240° . 5 partially reflecting mirrors close to the particle interaction region split the beams further. The beams produce ion tracks which simulate high momentum stiff particle tracks emanating from the interaction region at polar angles of $\theta = 18^\circ, 30^\circ, 39^\circ, 67^\circ$ and 90° . The quadrupled Nd:YAG is diffraction limited, and its divergence is given by the equation:

$$w(x) = w(0) [1 + (\lambda x / \pi w(0)^2)^2]^{1/2}$$

Where $w(0)$ is the beam waist diameter (typically 2×10^{-3} m), x is the length of the beam (about 10m) and λ is the wavelength (266nm for the quadrupled Nd:YAG). Typical values for the parameters in the above equation give a spread of only 30% over 10m.

Correction for global long-range distortions in the ALEPH TPC will be made by the measurement of the deviation from straightness of the laser track, and by apparent sagitta measurements (Wells et al 1986).

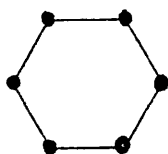
Earlier factors limiting the accuracy of the ALEPH TPC were outlined. To test these calculations and to determine the feasibility of using this type of detector on a large scale, a test TPC, the TPC 90, was constructed.

APPENDIX 3.

ELECTRONIC ABSORPTION IN BENZENE AND ITS SUBSTITUTES.

The benzene molecule absorbs light in the near UV in three wavelength regions: there is a strong absorption at 185nm, and two weaker absorptions at about 200nm and 260nm. The strong absorption is attributed to an allowed transition between two electronic states of benzene. The weaker absorptions are attributed to symmetry forbidden electronic states of the benzene. Appearance of these resonances has been explained by quantum mechanical and group theoretical considerations, and are described briefly, for benzene, below.

A benzene molecule consists of 6 carbon atoms and hydrogen atoms arranged in an hexagonal configuration shown below:



● = Carbon nuclei

Bonding between the carbon atoms occurs because the s and p orbitals of neighbouring carbon atoms overlap. The bonds are of two forms: s to s (σ) bonds and p to p (π) bonds. (π bonds in the ring system dominate the spectroscopy of benzene in the near UV). Delocalisation of the electrons in each of the bonding p states leads to the formation of molecular orbitals, which are characterised by linear combinations of the *i* orbital for each individual carbon atom ($\pi_1, \pi_2, \pi_3, \pi_4, \pi_5, \pi_6$).

Figure A3-1 shows a schematic diagram of the 6 p orbitals in an hexagonal arrangement. Since the benzene molecule is symmetric, calculations of the orbital wavefunctions are simplified by applying a group theoretical approach. The benzene molecule has D_{6h} symmetry (table A3-1 gives the D_{6h} group table), but the more simple subgroup C_{6v}

Figure: A3-1 Schematic diagram of the benzene molecule.

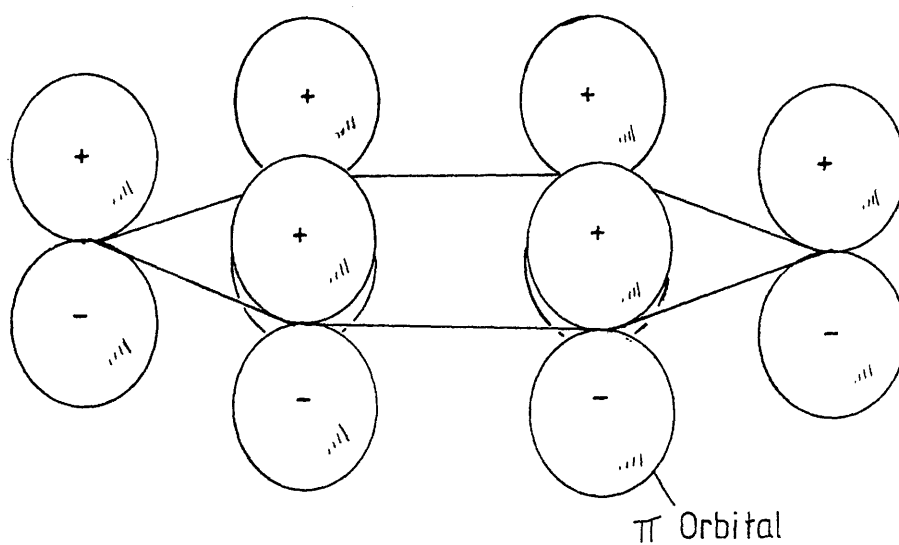
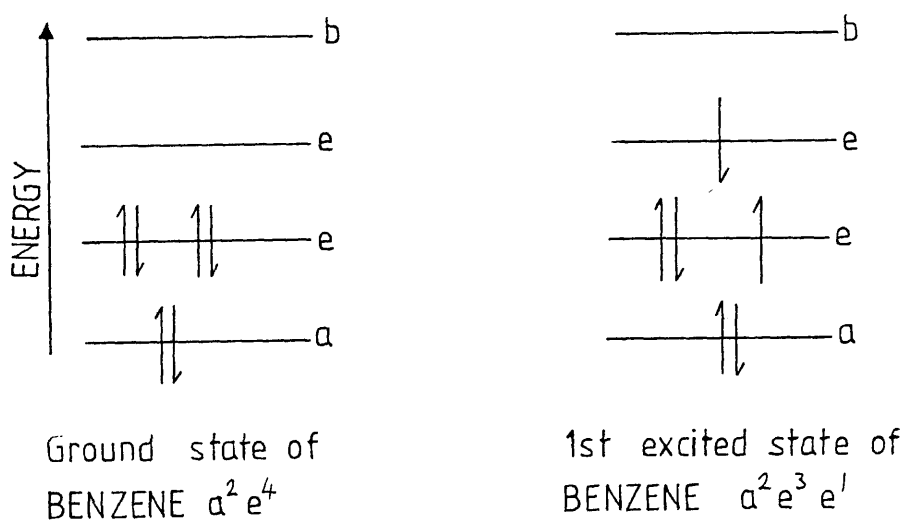


Figure: A3-2 Energy levels of the benzene molecule.



(table A3-2) suffices for the initial calculations of the molecular wavefunctions and their energies.

By group theoretical methods the six molecular wavefunctions, spanned by ($\pi_1, \pi_2, \pi_3, \pi_4, \pi_5, \pi_6$) are found. The six functions are (Bishop (1973)):

$$\text{Symmetry } A_1 : a = (1/6)^{1/2} (\pi_1 + \pi_2 + \pi_3 + \pi_4 + \pi_5 + \pi_6)$$

$$\text{Symmetry } B_1 : b = (1/6)^{1/2} (\pi_1 - \pi_2 + \pi_3 - \pi_4 + \pi_5 - \pi_6)$$

$$\text{Symmetry } E_1 : e = (1/12)^{1/2} (2\pi_1 - \pi_2 - \pi_3 + 2\pi_4 - \pi_5 - \pi_6)$$

$$\text{Symmetry } E_1 : e = (1/12)^{1/2} (\pi_2 - \pi_3 + \pi_5 - \pi_6)$$

$$\text{Symmetry } E_2 : e = (1/12)^{1/2} (2\pi_1 + \pi_2 - \pi_3 - 2\pi_4 - \pi_5 + \pi_6)$$

$$\text{Symmetry } E_2 : e = (1/12)^{1/2} (\pi_2 + \pi_3 - \pi_5 - \pi_6)$$

The energies of the orbitals are calculated from the equation below,

$$E = \int \Psi \hat{H} \Psi d\tau$$

where Ψ is the orbital wavefunction and \hat{H} is the Hamiltonian (energy operator) for the system. The following integrals are introduced;

$$\alpha_i = \int \pi_i \hat{H} \pi_i d\tau$$

$$\beta_{ij} = \int \pi_i \hat{H} \pi_j d\tau = \beta \quad (i, j \text{ are neighbours})$$

$$= 0 \quad (i, j \text{ are not neighbours})$$

Where α is a Coulomb integral and β is a resonance integral. From these integrals the energies of the states are found to be,

$$E(A_1) = \alpha + 2\beta$$

$$E(B_1) = \alpha - 2\beta$$

$$E(E_1) = \alpha - \beta \quad \text{doubly degenerate.}$$

$$E(E_2) = \alpha + \beta \quad \text{doubly degenerate.}$$

This gives the energy level diagram for the molecular orbitals of benzene shown in figure A3-2. Each of the p orbitals of the atoms

contributes one electron to the bonding; these are placed into each orbital according to the Pauli principle. The benzene ground state is therefore of the form $a_{2u}^2 e_{1u}^4$. Molecular orbitals a_1 and e_1 all contain 2 electrons, and are called closed orbitals. Molecules with closed orbitals are called totally symmetric, (i.e. they span the totally symmetric representation for the group). For benzene this is the ${}^1A_{1g}$ representation of the D_{6h} group

Now, for an allowed electronic transition the transition dipole integral must be non-zero, i.e.

$$\langle g | \underline{d} | e \rangle = \int \Psi_g \underline{d} \Psi_e \, d\tau \neq 0$$

where Ψ_g and Ψ_e are the ground and excited state wavefunctions for the molecule and \underline{d} is the electric dipole operator. Group theory may again be used to determine the electronically allowed transitions for benzene.

The transition dipole integral will be zero unless its irreducible representation contains the totally symmetric irreducible representation of the group. The irreducible representation is found by taking the products of the irreducible representations for the ground state, excited state and dipole operator. The ground state has ${}^1A_{1g}$ symmetry, the dipole operator transforms as space coordinates x, y and z and its irreducible representation is the sum of the irreducible representations for the x, y and z coordinates which are given in each group table (see table A3-1). The first excited state of benzene is $a_{2u}^2 e_{1g}^3 e_{2u}^1$ (see figure A3-2) this gives a state symmetry of ${}^1B_{1u} + {}^1B_{2u} + {}^1E_{1u}$.

The dipole operator spans ${}^1A_{2u}$ and ${}^1E_{1u}$ in D_{6h} so the allowed transitions for benzene are calculated to be ${}^1E_{1u}$ and ${}^1A_{2u}$, since the cross products:

$${}^1A_{1g} \times {}^1E_{1u} \times {}^1E_{1u} = {}^1A_{1g} + {}^1A_{2g} + {}^1E_{2g}$$

$${}^1A_{1g} \times {}^1A_{2u} \times {}^1A_{2u} = {}^1A_{1g}$$

contain the totally symmetric irreducible representation ${}^1A_{1g}$.

The 185nm absorption observed in benzene has been ascribed to the symmetry allowed transition between the the ground state with ${}^1A_{1g}$ symmetry and the excited electronic states with ${}^1E_{1u}$ symmetry (the transition is written as ${}^1A_{1g} \rightarrow {}^1E_{1u}$). The 260nm absorption has been ascribed to a symmetry forbidden ${}^1A_{1g} \rightarrow {}^1B_{2u}$ transition. It is not yet clear, but the 200nm absorption is thought to be the forbidden ${}^1A_{1g} \rightarrow {}^1B_{1u}$ transition. (Atkins (1978)). Why these transitions are observed at all is explained below.

VIBRATIONAL/ELECTRONIC (VIBRONIC) TRANSITIONS.

A symmetry forbidden ${}^1A_{1g} \rightarrow {}^1B_{2u}$ transition is observed at around 260nm in benzene. A general theory accounting for the appearance of the transition using perturbation and group theory is given below.

The potential energy of an electron in a molecular orbital is dependent on the configuration of the nuclei of the molecule, so, therefore is the Hamiltonian (the energy operator) for the electron. The Hamiltonian for the electron can then be written as the Taylor expansion of the potential, V , with respect to the nuclear framework of the molecule in normal coordinates, Q_i , i.e.

$$H_e = H_e^0 + \sum_i (\delta V / \delta Q_i)_0 Q_i + \dots$$

The kinetic energy operator of the electrons is independent of Q_i ; so the equation can be written:

$$H_e = H_e^0 + \sum_i (\delta H_e / \delta Q_i)_0 Q_i + \dots$$

where $\hat{H}_e^0 \psi_e = E_e^0 \psi_e$ and E_e^0 is the energy of the unperturbed system. The presence of the terms dependent on Q_i in the Hamiltonian constitute a

perturbation to the molecular system. This causes a mixing of the wavefunctions of the molecule. The wavefunction for a state is then taken as the unperturbed wavefunction plus the sum of contributions from all the other states of the molecule i.e.

$$\Psi_g = \Psi_g^{(0)} + \sum C_u \Psi_u^{(0)}$$

where C_u is given by the equation;

$$C_u = \sum_i Q_i \int \Psi_u^{(0)*} (\delta H_e / \delta Q_i)_0 \Psi_g^{(0)} (E_g^{(0)} - E_u^{(0)}) d\tau$$

$E_k^{(0)}$ are the energies of the states.

Now supposing that only the upper excited state of the molecule is perturbed then;

$$\Psi_g = \Psi_g^{(0)}$$

and

$$\Psi_u = \Psi_u^{(0)} + \sum_{u'} C_{u'} \Psi_{u'}^{(0)}$$

Therefore the transition dipole is:

$$\begin{aligned} \langle g | \underline{d} | u \rangle &= \int \Psi_g^{(0)*} \underline{d} \Psi_u d\tau \\ &= \int \Psi_g^{(0)*} \underline{d} \Psi_u^{(0)} d\tau + \sum_u C_u^* \int \Psi_u^{(0)*} \underline{d} \Psi_u^{(0)} d\tau \end{aligned}$$

If the $\Psi_g \rightarrow \Psi_u$ transition is forbidden (like the ${}^1A_{1g} \rightarrow {}^1B_{2u}$ transition for benzene) then the first term on the right hand side of the equation is zero, so the equation becomes ;

$$\langle g | \underline{d} | u \rangle = \sum_u C_u^* \int \Psi_u^{(0)*} \underline{d} \Psi_u^{(0)} d\tau$$

The integral will be non-zero if the product of the irreducible representations for $\Psi_{u'}, \Psi_u$ and \underline{d} contains the totally symmetric irreducible representation for the group. The coefficient C_u will be non-zero if the product of the irreducible representations for Ψ_u, Ψ_g and $(\delta H_e / \delta Q_i)_0$ contain the totally symmetric irreducible representation for the group. The Hamiltonian of a system always transforms as the

totally symmetric representation of the group and therefore so must $Q(\partial \hat{H}_e / \partial Q_i)_0$. The coordinates will span representations Γ_i^i which need not be totally symmetric, so $(\partial H_e / \partial Q)_0$ must span the same representation Γ^i . Therefore C_u will be non-vanishing if the product of the representations, $\Gamma^u \times \Gamma^i \times \Gamma^g$ contains the totally symmetric irreducible representation of the group. This means that through the mixing of states, caused by a perturbation to the system, it is possible to obtain transitions between electronically forbidden states.

The appearance of Q_i , the coordinates of the nuclei, in the perturbation implies a mixing between vibrational and electronic states (vibronic states) so the wavefunction for the system should probably be written;

$$\Psi_{gn} = \Psi_g \Psi_n = \Psi_g^{(0)} \Psi_n^{(0)} + \sum_{\lambda} \sum_u C_{\lambda u} \Psi_u^{(0)} \Psi_n^{(0)}$$

where

$$C_{\lambda u} = \sum_i \int \Psi_n^{(0)*} Q_i \Psi_n \, d\tau \int \Psi_u^{(0)*} (\partial H_e / \partial Q_i)_0 \Psi_g (E_{gn}^{(0)} - E_{\lambda u}^{(0)})^{-1}$$

and Ψ_n are the vibrational wavefunctions of the system.

The break in the symmetry rules observed for the ${}^1A_{1g} \rightarrow {}^1B_{2u}$ transition for benzene can then be explained. Symmetry selection rules must be applied to the vibronic states of benzene and not just to the electronic states. Then the overall symmetry of the system should be taken into account.

In benzene for instance if a vibration of ${}^1E_{2g}$ symmetry can be excited then the dipole transition integral will be non-zero and the transition will be allowed. The symmetry of the ${}^1B_{2u}$ excited state when vibrating with a symmetry ${}^1E_{2g}$ is found by taking the product of the irreducible representations ${}^1B_{2u} \times {}^1E_{2g}$

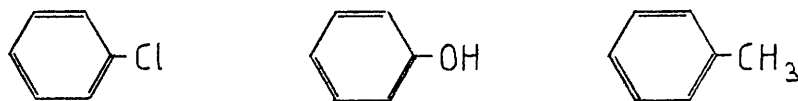
$${}^1B_{2u} \times {}^1E_{2g} = {}^1E_{1u}$$

as already stated the ${}^1A_{1g} \rightarrow {}^1E_{1u}$ transition is symmetry allowed.

Accounting for the appearance of the spectrum at 260nm.

NEAR UV ABSORPTION IN MONOSUBSTITUTED BENZENES.

The near UV absorption at around 260nm for benzene has been shown to be allowed through weak interactions with vibrations that remove some of its symmetry. The symmetry of benzene can also be reduced by the substitution of one of the hydrogen atoms on the molecule with a radical or a group of atoms i.e.



The extent of the intensification of the transition is dependent on the extent of the interaction between the electrons in the substituent and the benzene ring system. Sklar (1939) showed that the intensification of the ${}^1A_{1g} \rightarrow {}^1B_{2u}$ transition in benzene could be explained satisfactorily by the migration of electrons from the substituent into the ring system. Larger migrations result in a more intense absorption. For example Phenol is observed to absorb about 20x more than toluene which in turn absorbs about 10x more than benzene. The -OH group contains a lone pair of electrons which can both migrate into the ring giving a large intensification of the ${}^1A_{1g} \rightarrow {}^1B_{2u}$ transition. The -CH₃ group has only tightly bound electrons, and so contribute little to the ring.

In addition to the intensification of the absorption due to substitutions, a shifting of the wavelength of the absorption is observed. Herzfeld (1947), by similar methods as Sklar, showed that the wavelength shifts were also dependent on the extent of electron migration into the ring system. Toluene and phenol are both shifted about 9nm and 15nm respectively above the 260nm absorption for benzene.

TABLE A3-1

THE D_{6h} GROUP TABLE.

D_{6h}	E	$2C_6$	$2C_3$	C	$3C_2'$	$3C_2''$	i	$2S_3$	$2S_6$	σ_h	$3\sigma_d$	$3\sigma_v$	
A_{1g}	1	1	1	1	1	1	1	1	1	1	1	1	$x^2 + y^2, z^2$
A_{2g}	1	1	1	1	-1	-1	1	1	1	1	-1	-1	R_z
B_{1g}	1	-1	1	-1	1	-1	1	-1	1	-1	1	-1	
B_{2g}	1	-1	1	-1	-1	1	1	-1	1	-1	-1	1	
E_{1g}	2	1	-1	-2	0	0	2	1	-1	-2	0	0	$(R_x, R_y)(xz, yz)$
E_{2g}	2	-1	-1	2	0	0	2	-1	-1	2	0	0	$(x^2 - y^2, xy)$
A_{1u}	1	1	1	1	1	1	-1	-1	-1	-1	-1	-1	
A_{2u}	1	1	1	1	-1	-1	-1	-1	-1	-1	1	1	z
B_{1u}	1	-1	1	-1	1	-1	-1	1	-1	1	-1	1	
B_{2u}	1	-1	1	-1	-1	1	-1	1	-1	1	1	-1	
E_{1u}	2	1	-1	-2	0	0	-2	-1	1	2	0	0	(x, y)
E_{2u}	2	-1	-1	2	0	0	-2	1	1	-2	0	0	

TABLE A3-2 THE C_{6v} GROUP TABLE.

C_{6v}	E	$2C_6$	$2C_3$	C_2	$3C_2'$	$3C_2''$	
A_1	1	1	1	1	1	1	z $x^2 + y^2, z^2$
A_2	1	1	1	1	-1	-1	R_z
B_1	1	-1	1	-1	1	-1	
B_2	1	-1	1	-1	-1	1	
E_1	2	1	-1	-2	0	0	(x, y) (R_x, R_y) (xz, yz)
E_2	2	-1	-1	2	0	0	$(x^2 - y^2, xy)$

APPENDIX 4.

MPI SPECTROSCOPY OF CAESIUM ATOMS.

SECTION A4-1: INTRODUCTION.

Of current interest to the RIS Group at Glasgow is the development of an analytical tool for monitoring low level nuclear waste materials in the environment. A time of flight mass spectrometer is to be adapted to detect atoms ionised by MPI.

Resonant ionisation mass spectroscopy will provide an alternative method for monitoring trace levels of low energy, β^- active nuclides since conventional counting techniques are unsuitable for their detection at levels $<1\text{pCi/g}$ of material.

One such nuclide, Caesium 137 ($^{137}_{55}\text{Cs}$), was thought to be of particular environmental interest. Therefore a study was made of its R2PI and R3PI (2-photon resonant) spectra (scheme 1 and 5 on figure 1-19) to identify the most efficient method of ionising the atoms.

Caesium atoms were ionised inside proportional counters filled with a 70% argon 30% methane gas mix at low pressure. A liquid sample of caesium was placed inside the proportional counter close to the laser interaction region. A dye laser was used to resonantly ionise caesium emanating from the solid sample. Preliminary experiments using a small brass counter failed to detect any caesium. The reason for this was thought to be because of reactions between caesium with organic impurities desorbed from the counter walls, and with air leaking into the counter.

Glass counters were built to reduce the level of background impurities in the counter gas. Some R2PI spectra of caesium were taken

with the glass counters but eventually oxide layers formed on the surface of the caesium sample. This layer prevented evaporation of caesium into the counter gas.

Finally, the type 3 counter was designed and built. High vacuum components were used to minimise leakage of air into the counter. A probe connected to a linear drive was used to extract small samples of caesium from a caesium reservoir at the base of the counter. With this design it was found that the number of ion pairs produced in a saturated R2PI process was two orders of magnitude lower than the value expected for caesium at its saturated vapour pressure. Therefore even in the type 3 counter atomic caesium is removed by reaction with impurities in the counter gas, or possibly adsorption onto the counter walls.

SECTION A4-2: SUMMARY OF RESULTS.

THE GLASS COUNTER.

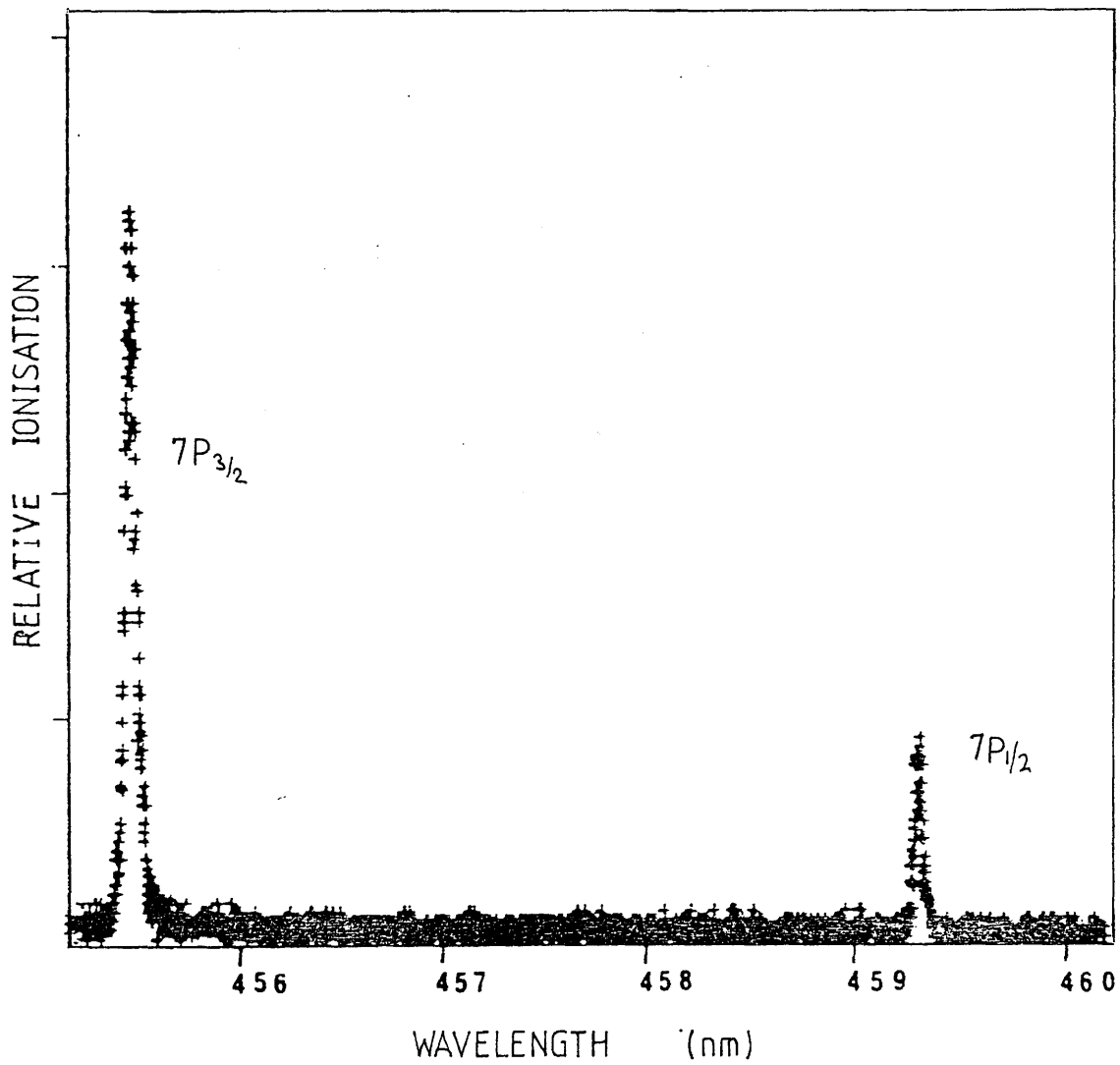
Figure 4A-1 show a R2PI spectrum for caesium taken between 455nm and 460nm at a laser fluence of $7.2\mu\text{J}/\text{mm}^2$. It shows well resolved $6s \rightarrow 7p$ transitions. The $6s_{1/2} \rightarrow 7p_{3/2}$ and $6s_{1/2} \rightarrow 7p_{1/2}$ transitions have intensities 17 times and 4.5 times background respectively. (The background is attributed to the production of photoelectrons from the interaction of scattered light with caesium adsorbed onto the counter walls. The same effect was observed in the type 3 counter). The ratio of the peak intensities is 3.3:1 which is close to the value of 3.4:1 quoted by Hurst et al (1977). At a laser fluence of around $7\mu\text{J}/\text{mm}^2$ some saturation of the R2PI of caesium at 455.5 and 459.3nm was observed.

Laser line broadening was observed (chapter 1:laser line broadening). Figure A4-2 shows the effect of increasing laser fluence on the line width of the resonance at 455.5nm. The laser fluences were $7.2\mu\text{J}/\text{mm}^2$, A; $8.9\mu\text{J}/\text{mm}^2$, B; and $520\mu\text{J}/\text{mm}^2$, C; with respective FWHM line widths of 0.06, 0.07 and 0.1nm.

The line widths of the caesium resonances are greater than the natural line widths of the transitions (derived in chapter 1). This is due to a combination of Doppler, collisional and laser induced line broadening effects. The resolution (bandwidth) of the laser is a major contributor to the line width.

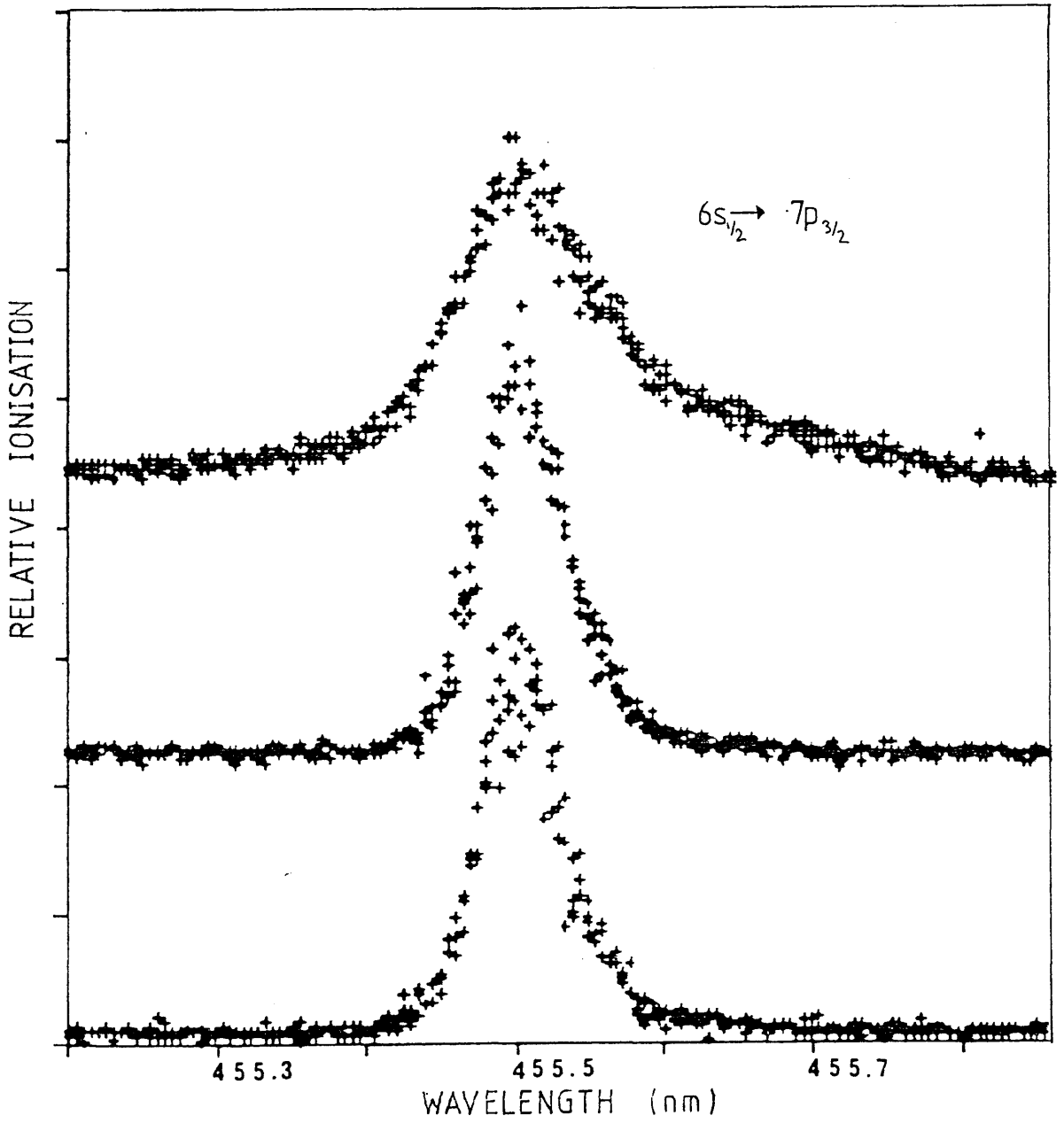
TYPE 3 COUNTER RESULTS.

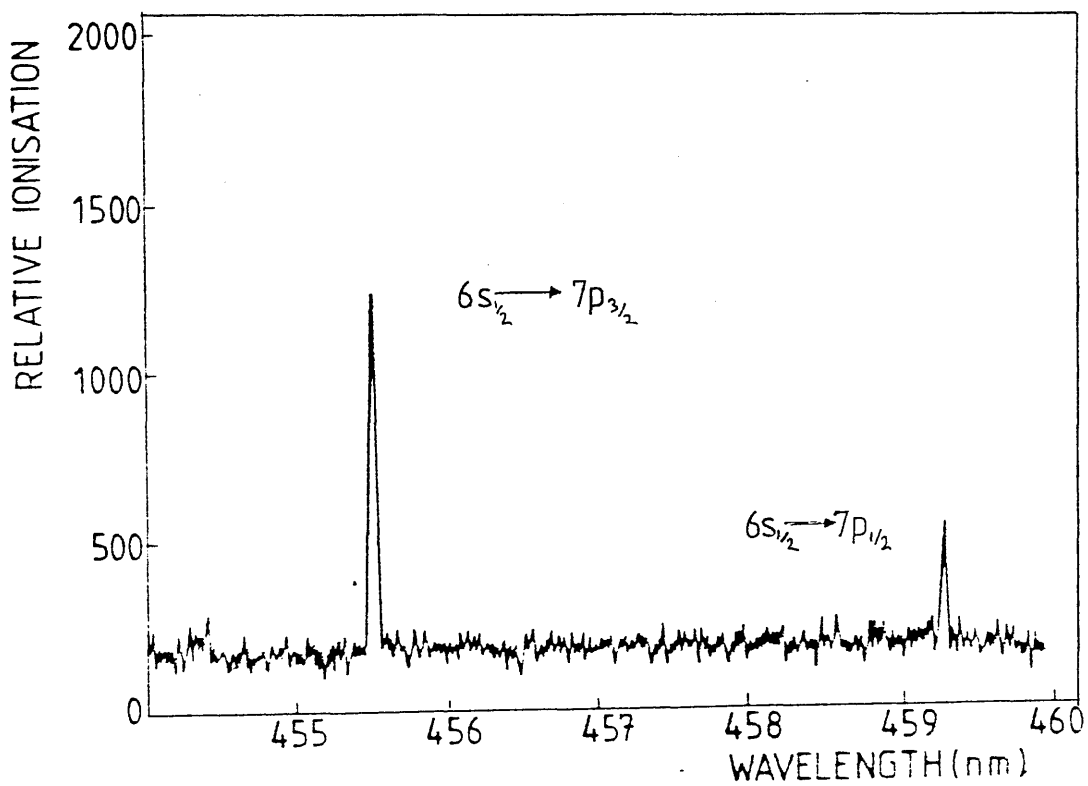
R2PI spectra at wavelengths between 450nm and 460nm were taken at different laser fluences. Figure 4A-3 shows the 455.5nm and 459.3nm resonances. These have peak intensity ratios of about 3.1:1. The



4A-2 Effect of increasing laser fluence on linewidth.

- A) Laser fluence of $7.2\mu\text{J}/\text{mm}^2$
- B) Laser fluence of $8.9\mu\text{J}/\text{mm}^2$
- C) Laser fluence of $520\mu\text{J}/\text{mm}^2$





fluence of the laser was $0.8\mu\text{J}/\text{mm}$ and log/log plots of ionisation versus laser fluence indicated that the R2PI process was not saturated.

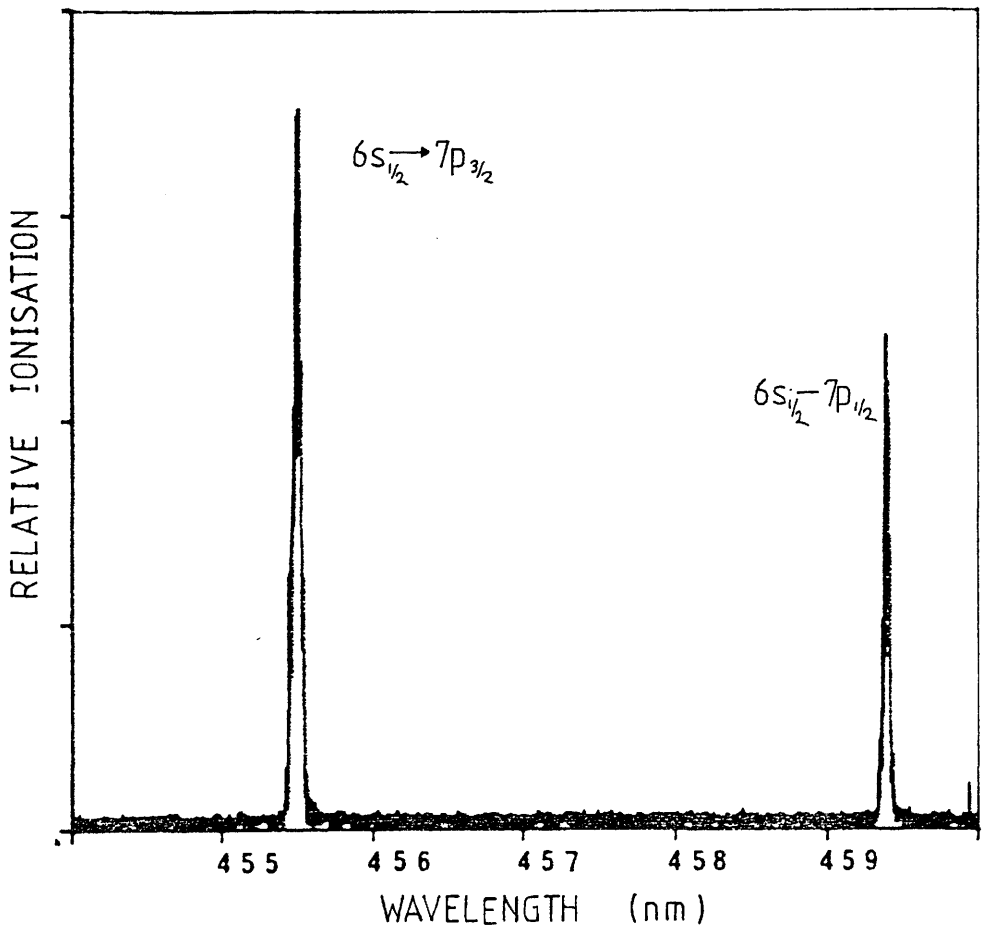
As for the glass counter, laser line broadening and R2PI saturation effects were studied. At a fluence of $8\mu\text{J}/\text{mm}^2$ the ratio of the peak intensities had reduced to about 3:2 (see figure 4A-4). At a laser fluence of $1.18\text{mJ}/\text{mm}^2$ both peaks displayed considerable broadening and the ratio of their heights was 1:1 (see figure 4A-5). This was in agreement with Hurst et al (1979), who reported that the R2PI process via the 7p levels was 90% saturated at a laser fluence of $1.0\text{mJ}/\text{mm}^2$.

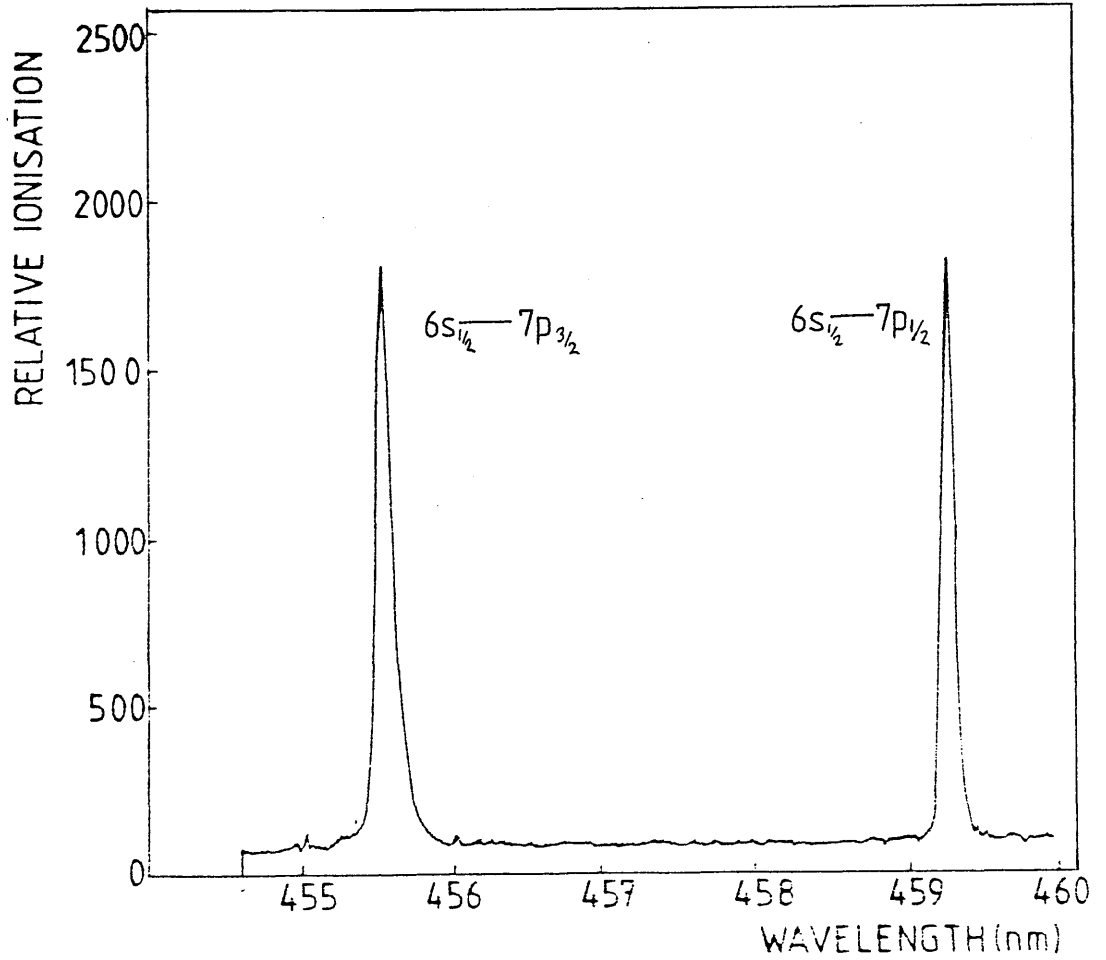
Figure 4A-6 further illustrates laser line broadening effects. The laser fluence was $8\mu\text{J}/\text{mm}^2$, A; $32\mu\text{J}/\text{mm}^2$, B; and $400\mu\text{J}/\text{mm}^2$, C; with respective FWHM widths of 0.05nm, 0.1nm and 0.13nm. Shoulders are observed on the blue wings of the peaks. Their appearance may be the result of distortions of the caesium 7p levels by argon atoms of the counter gas. Such structure has been observed by Nayfeh et al (1978) in a similar gas system, but he observed satellite peaks 0.4nm from the line centre.

6s - 8p AND 9p TRANSITIONS.

R2PI through 8p and 9p states were studied using different laser dyes. The $6s_{1/2} \rightarrow 8p_{3/2}$, $6s_{1/2} \rightarrow 8p_{1/2}$, $6s_{1/2} \rightarrow 9p_{3/2}$ and $6s_{1/2} \rightarrow 9p_{1/2}$ transitions, were observed at the expected wavelengths of 387.7nm, 388.9nm, 361.2nm and 361.9nm (Moore (1952)).

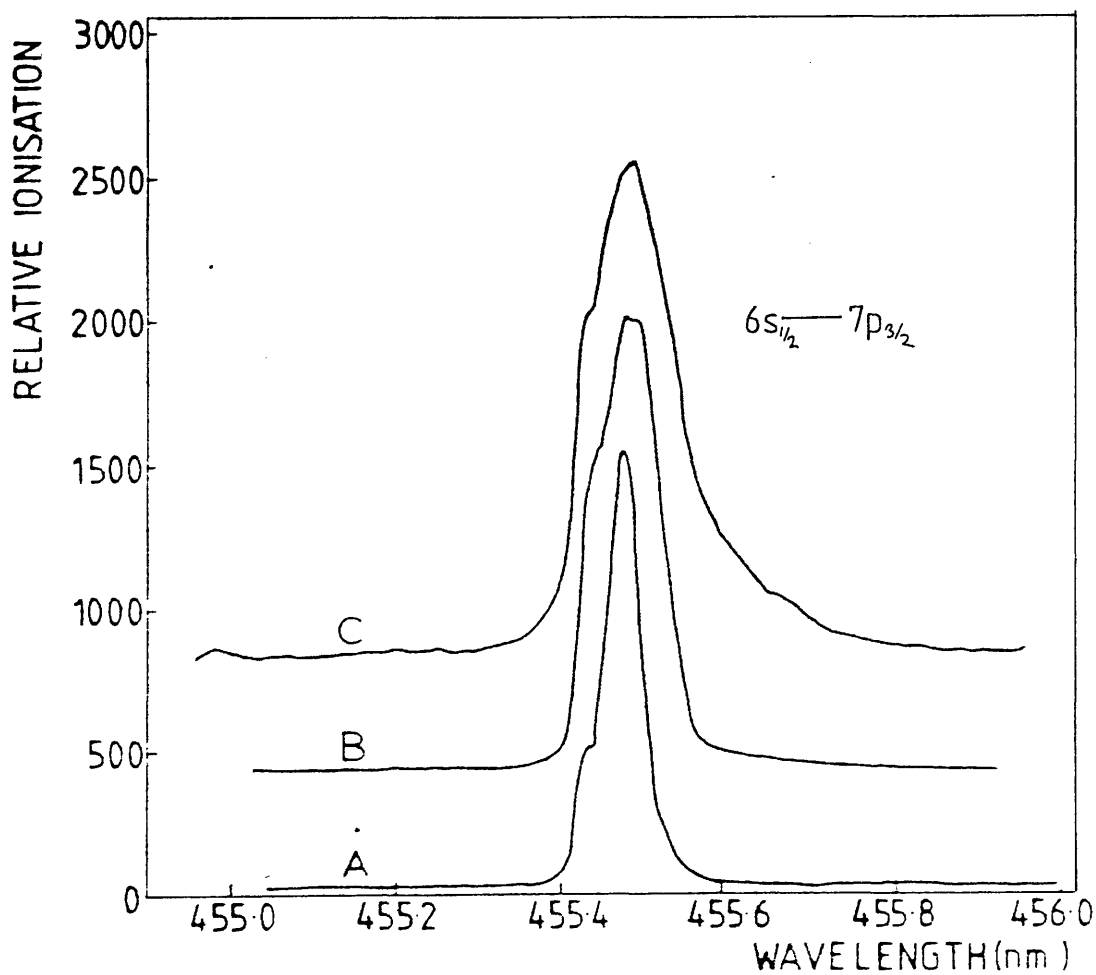
Again the dependence of the ionisation yield and peak width on laser fluence was studied (see figures 4A-7 to 4A-11) Literature values for the relative peak intensities do not appear to exist, so the experimental values obtained could not be ratified, although the bound-bound transitions are known. Total saturation of the R2PI process did not occur even at laser fluences around $7\text{mJ}/\text{mm}^2$.

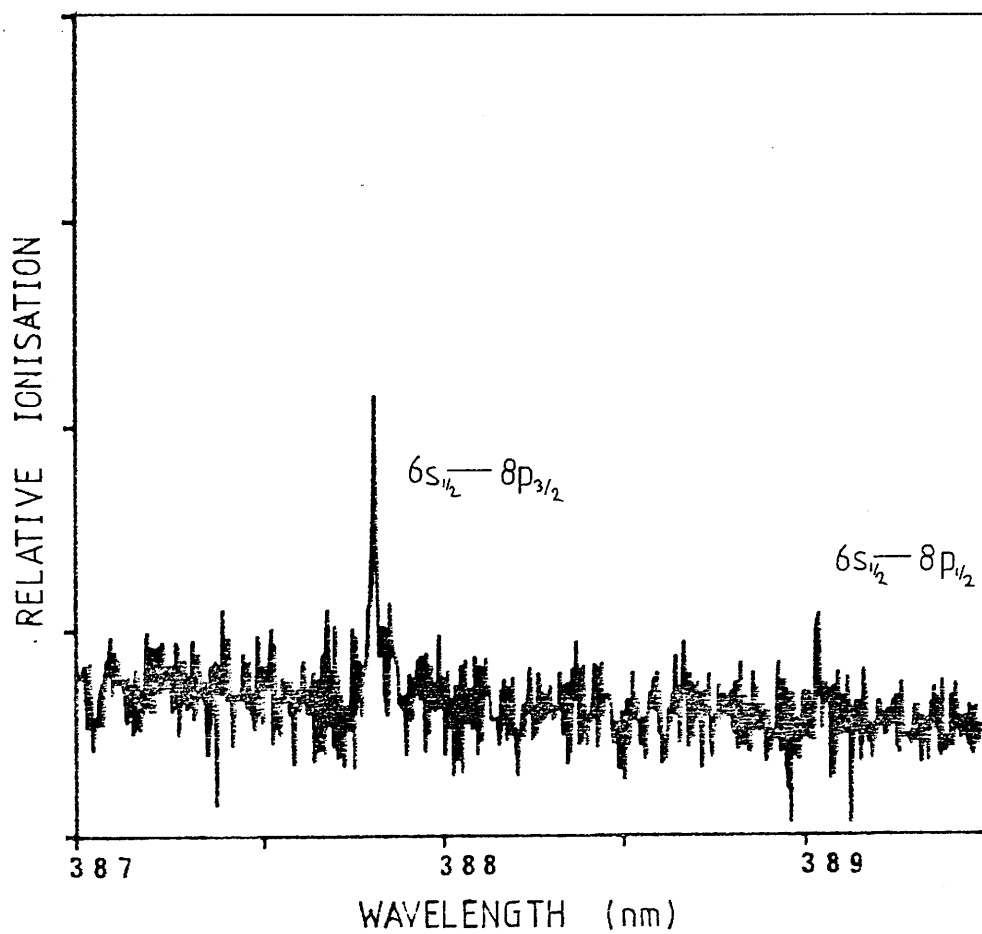


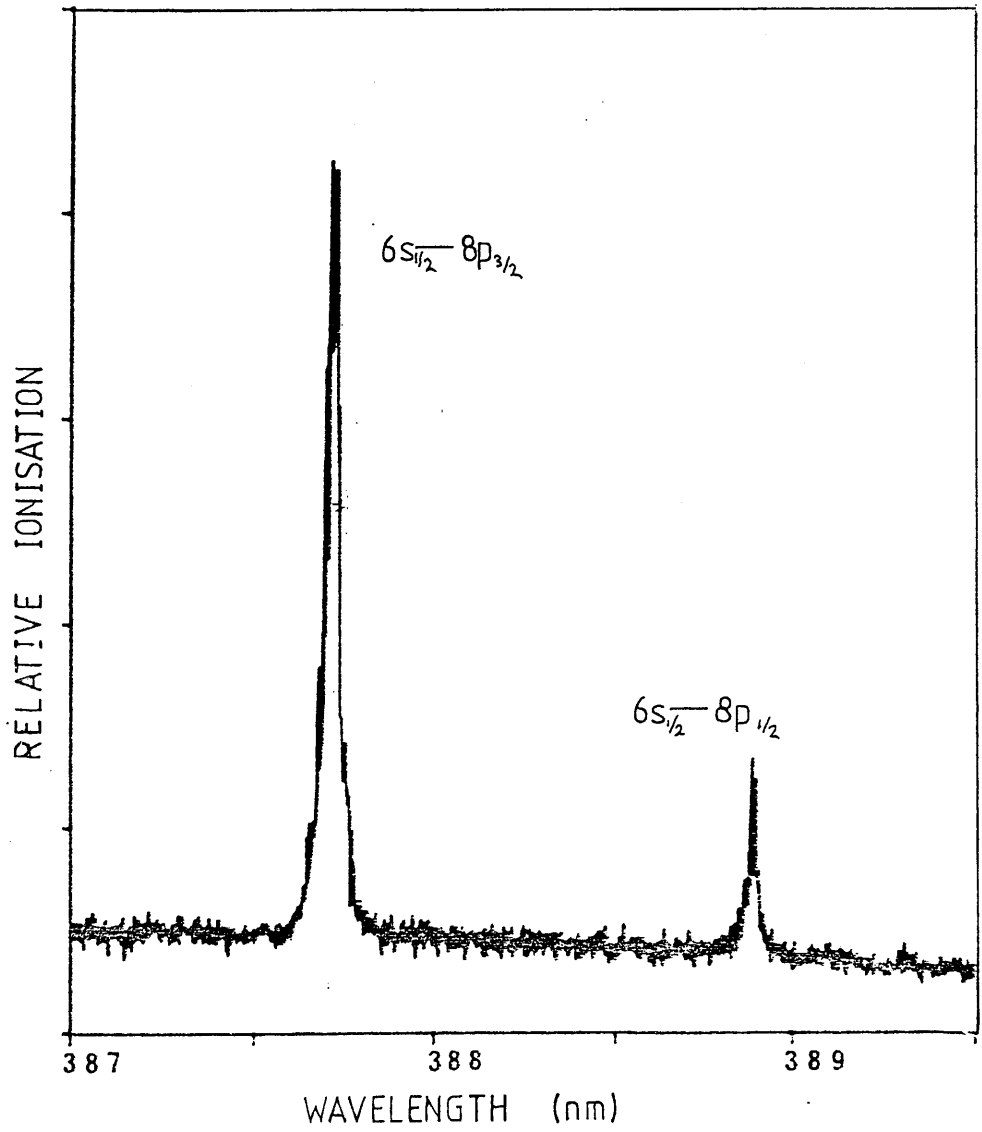


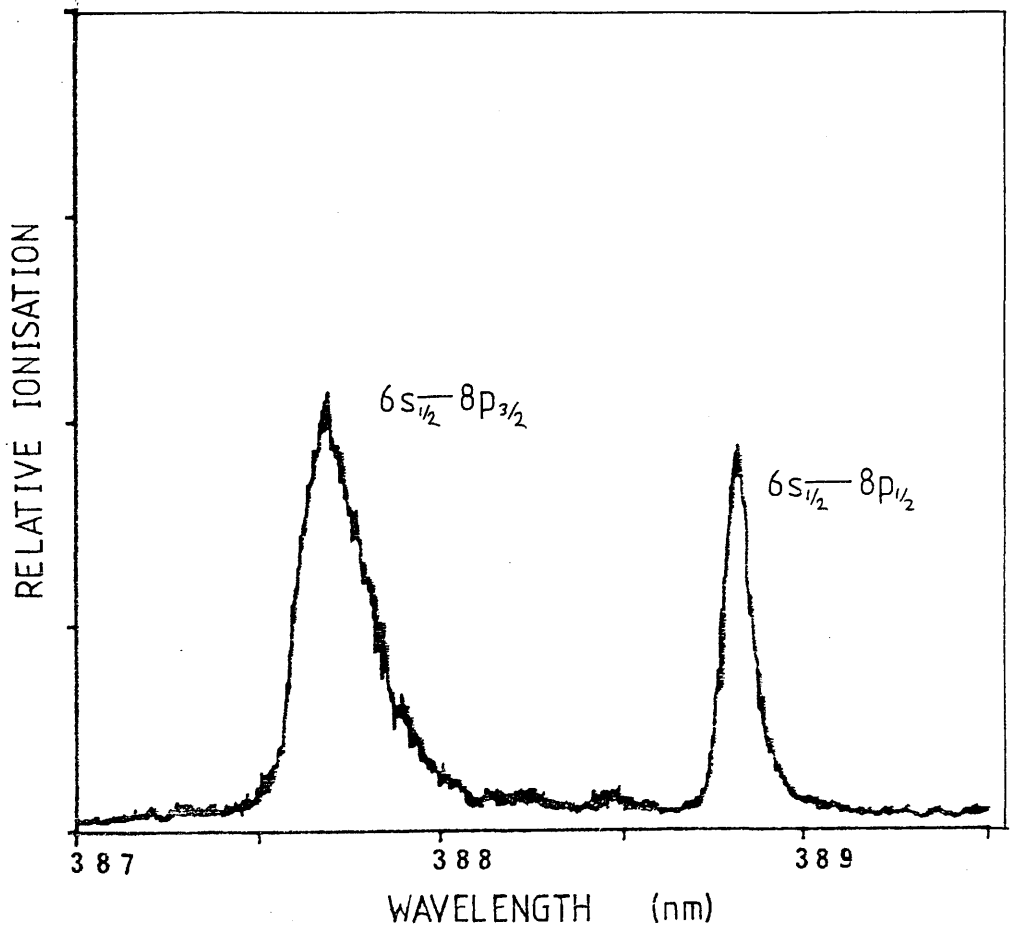
4A-6 Laser line broadening effects.

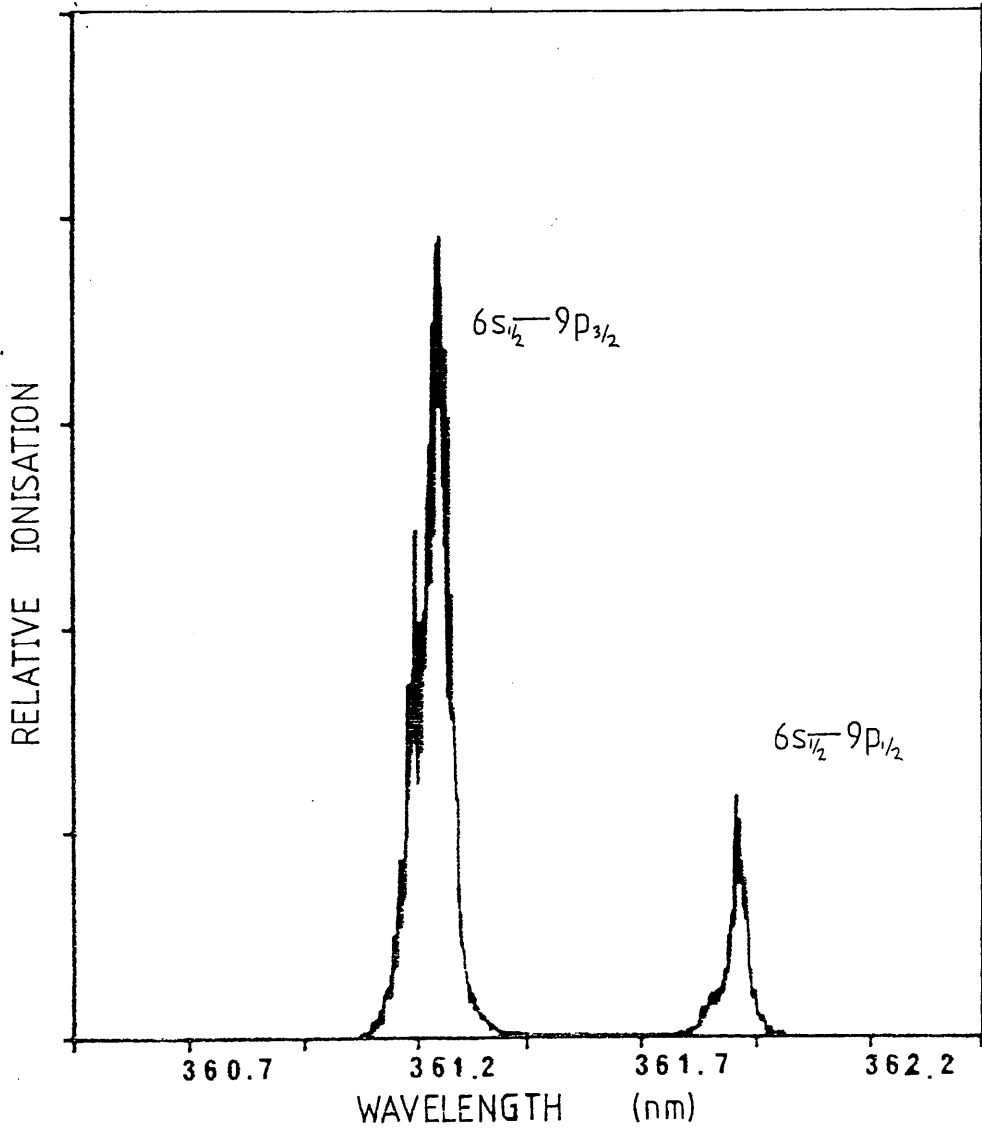
- A) Laser fluence of $8\mu\text{J}/\text{mm}^2$.
- B) Laser fluence of $32\mu\text{J}/\text{mm}^2$.
- C) Laser fluence of $400\mu\text{J}/\text{mm}^2$.

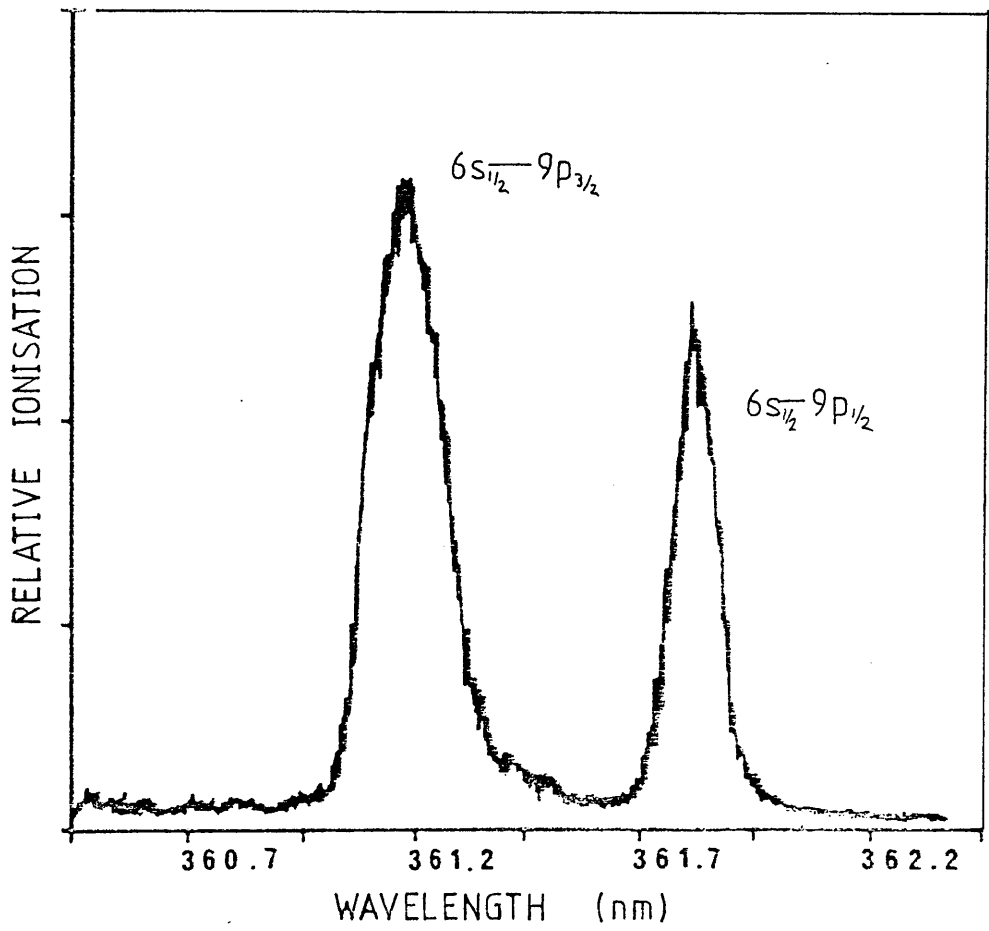












Saturation of the $6s \rightarrow np$ ($n = 7, 8$ and 9) transition requires greater laser power as the value of n increases. This is directly related to the transition probabilities for these transitions which decrease with increasing n , requiring a greater laser fluence to saturate the bound-bound transition in the R2PI process.

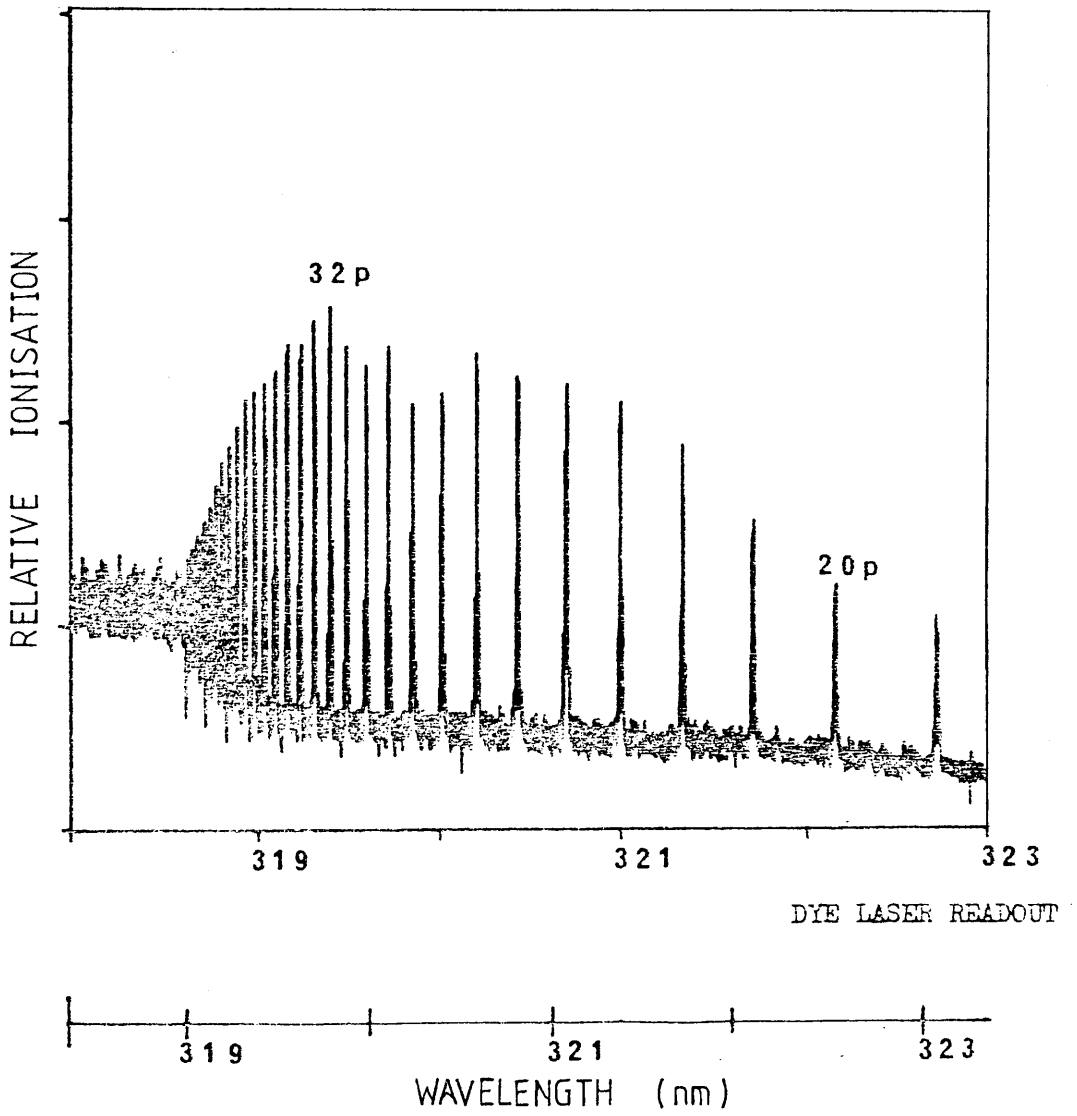
6s - RYDBERG TRANSITIONS.

Atomic states, close to the caesium single photon ionisation edge at 318.4nm (Compton et al (1984)), were studied. R2PI spectra were taken between the wavelengths of 318nm and 332nm using the frequency doubled output of the DCM dye. Continuous spectra could be obtained, since at the time these experiments were carried out the INRAD automatic tracking system was operative.

Resonant structure in the R2PI spectra, at wavelengths close to the ionisation edge, is attributed to ionisation via Rydberg states. Rydberg states are high energy orbitals close to the continuum. Cross-sections for the transition into the intermediate excited state have a $1/n^3$ dependence. (n is the principle quantum number). Compton et al (1984) reported a $1/n^5$ dependence of the intermediate state to continuum cross-section. A $1/n^8$ dependence would therefore be expected for the R2PI cross-section (assuming the R2PI process is unsaturated).

Figure 4A-12 shows the R2PI spectrum for caesium taken between 318nm and 323nm at a laser fluence of $1\text{mJ}/\text{mm}^2$. Instead of a decrease in the ionisation yield with increasing n values, an increase in the ion yield occurs up to values of $n=32$. At values of $n>32$ the ion yield falls at a rate which is approximately $1/n^3$ dependent.

Rydberg levels are long lived and have large orbitals (Letokhov (1983)). Therefore depopulation of the Rydberg states by collisional processes will be common. An atom in an excited Rydberg state may



receive sufficient energy in a collision process to ionise it. The probability of ionisation by this process is related to the number of atoms or molecules in the counter gas with sufficient energy to raise the excited caesium above its ionisation potential. As n increases the additional energy required to ionise the atom decreases and a larger proportion of the atoms or molecules in the Maxwell-Boltzmann distribution can ionise the caesium atom. Eventually a state is reached where every atom reaching the Rydberg level will be ionised. This is called collisional saturation. Beyond this point the ion yield is expected to fall as $1/n^3$ (the dependence of ground to intermediate cross-section on n).

Collisional ionisation and collisional saturation explain the increase in ion yield from $n=20$ to $n=32$ and the subsequent fall in ion yield for $n>32$. Plots of ion yield versus n for $n>38$ gave a $1/n^3$ dependence, confirming theoretical predictions. A similar behaviour was observed for data obtained for rubidium (Bushaw and Whitaker (1981)).

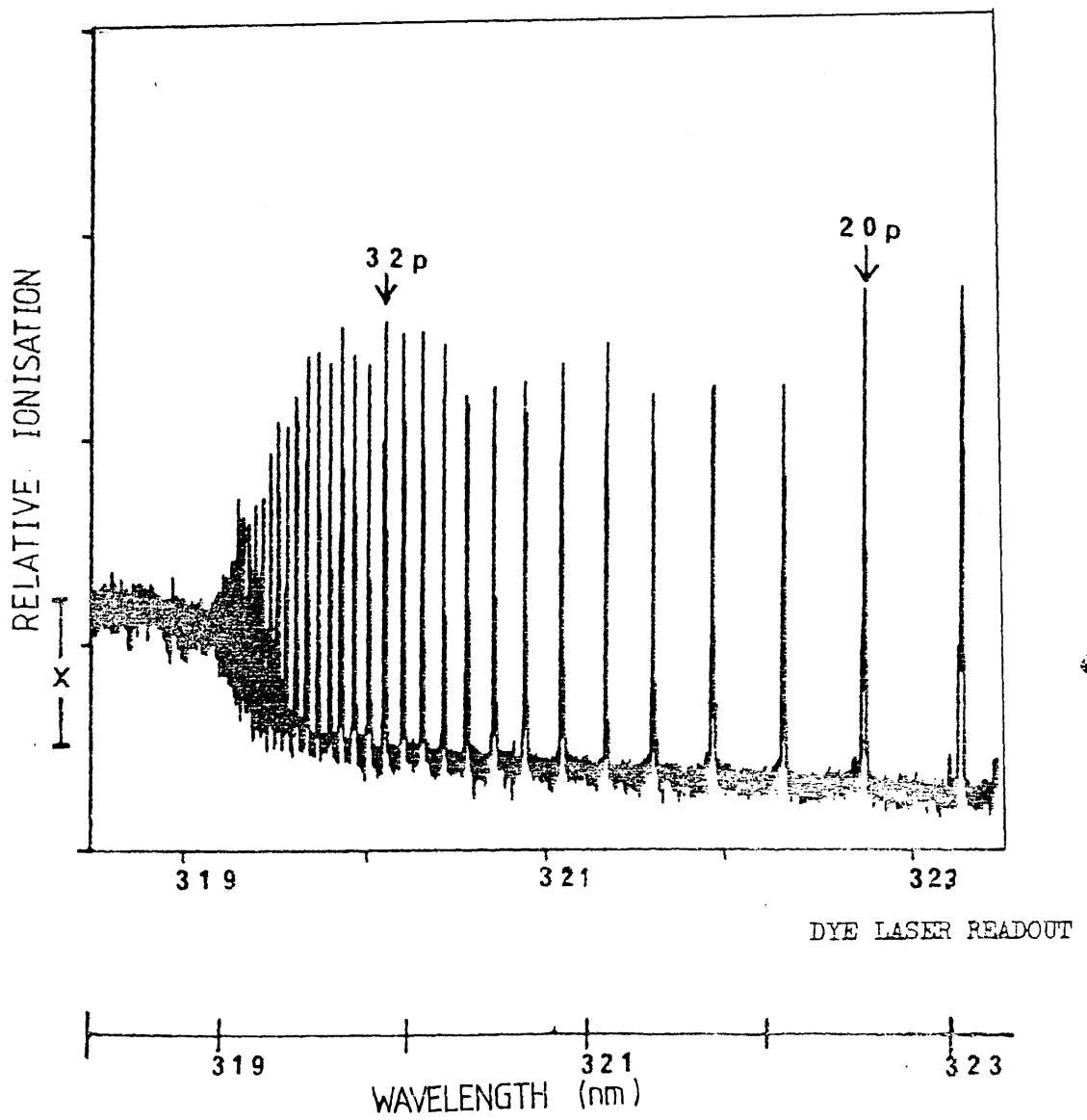
The experiment was conducted in an electric field. Stark effects induced by the electric field in the proportional counter were thought to be responsible for shifts from the expected values of peak positions and single photon ionisation edge.

Figure 4A-13 shows the R2PI spectrum of caesium taken between 319-323nm at a laser fluence of 6.3mJ/mm^2 . Fundamental light at a fluence of 18.3mJ/mm^2 was passed through at the same time. Due to the increased laser intensity the ion yields of the peaks around 20p are similar to the collisionally enhanced peaks at around 32p. The immediate fall off in ion yield beyond $n=32$ is not as pronounced as in figure 4A-12, this is probably due to some saturation of the rydberg states at these n values.

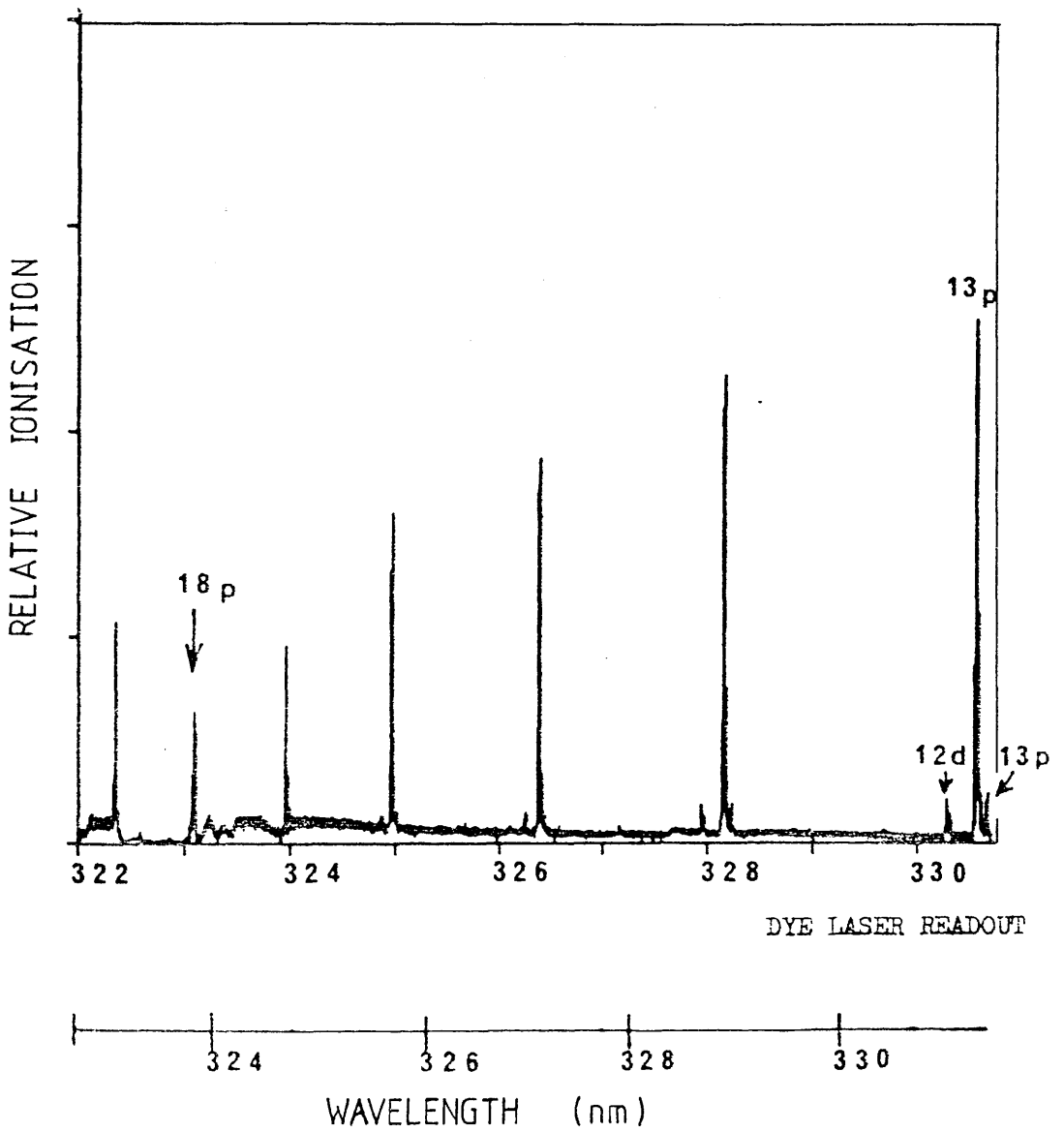
Figure 4A-14 shows the R2PI spectrum for caesium between 322nm and 332nm at a laser fluence of 2.8mJ/mm^2 UV light and 12.7mJ/mm^2 red

4A-13 R2PI spectrum of caesium at a laser fluence of 6.3mJ/mm^2 .

UV and 18.3mJ/mm fundamental.



4A-14 MPI spectrum of caesium at laser fluences of $2.8\text{mJ/mm}^2\text{UV}$ and 12.7mJ/mm^2 fundamental.



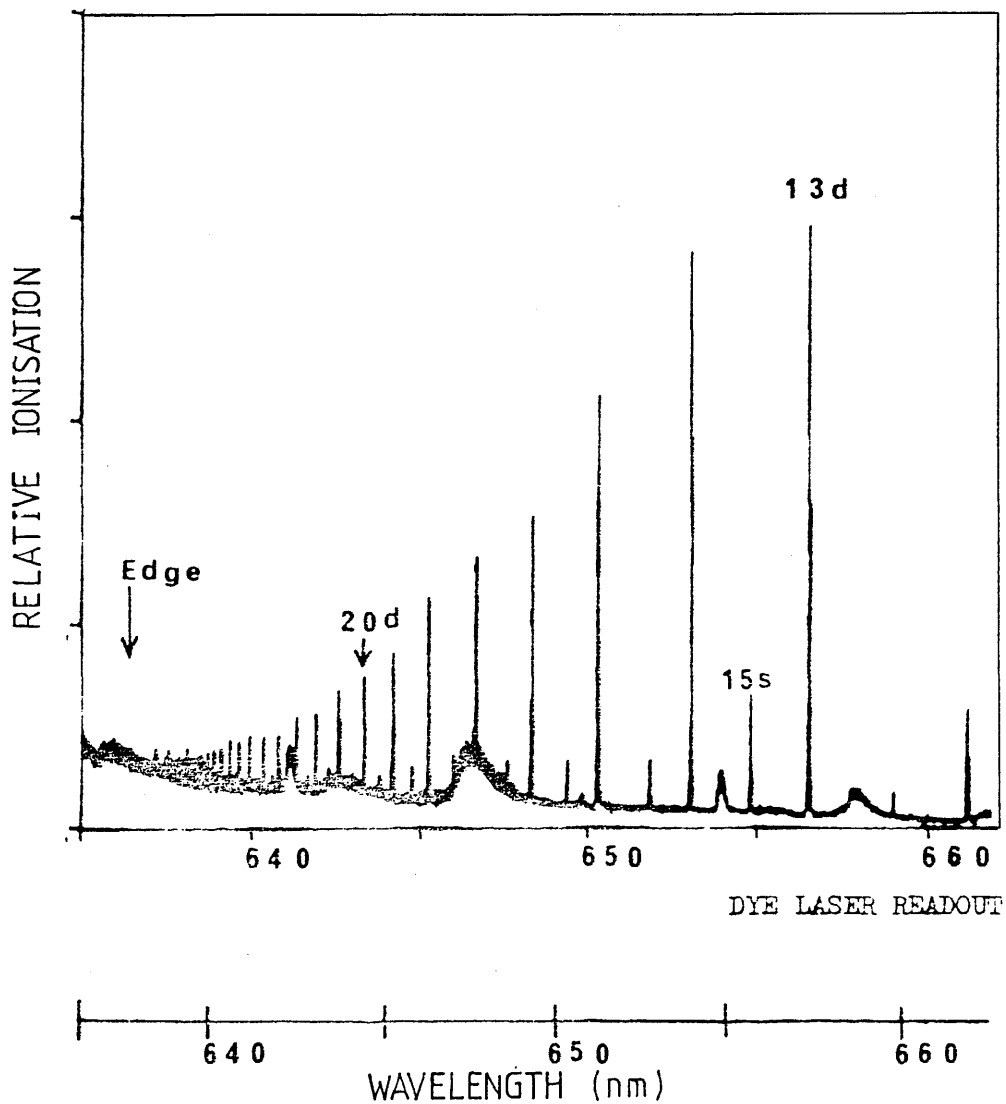
light. It shows that collisional effects reverse the downward trend of the ion yield for values of $n > 18$.

6s - ns AND 6s - nd TRANSITIONS.

As mentioned in chapter 1, single photon transitions between s-s and s-d states are forbidden. In a 2-photon absorption process they are allowed. Some evidence of s - d and s - s transitions can be seen in figure 4A-14 where both the doubled and fundamental light from the laser were used to ionise caesium.

A focussed laser beam was necessary to observe 2-photon absorption 3-photon ionisation resonances between 635nm and 665nm. A typical spectrum obtained in this wavelength range is shown in figure 4A-15. The laser fluence was 53mJ/mm^2 . Two series of peaks were observed one set 6 times more intense than the other. The more intense series are s-d transitions and the other s-s transitions. The difference in intensity between both series of peaks is attributed to dissimilar intermediate excited state to continuum cross-sections from d and s levels (Compton et al (1984)).

Broad resonant structure observed in the R3PI spectra are tentatively attributed to resonant ionisation of caesium dimers or polymers. They were not visible in the background spectrum and only appeared when caesium vapour was present.



SECTION 4A-3: CONCLUSIONS.

For maximum detection efficiency of caesium in a time of flight mass spectrometer, saturation of the MPI process is desirable. Saturation of the R3PI of caesium could not be obtained, even with focussing, which gave a laser fluence of $53\text{mJ}/\text{mm}^2$. The advantages of R2PI processes over higher order MPI processes have already been discussed in chapter 1 (R2PI of molecules).

An interesting alternative to R2PI could be the ionisation of caesium by excitation into a Rydberg state with subsequent collisional ionisation. UV light is required to excite these levels, leading to possible problems due to R2PI of background impurities. Since the fluence of the laser however, need only be sufficient to saturate the ground to Rydberg state transition, the laser fluence may be too low to produce significant ionisation of background impurities.

Sanguinetti,G., Schlatter,W.D., Sedgebeer,J., Settles,R., Sinnis,G.,
Smith,K.M., Stefanini,G., Stierlin,U., Takashima,M., Tejessy,W.,
Thomas,J., Vayaki,A., Wells,J., Wicklund,E., Witzeling,W., Wu,S.L. and
Wu,W.M.

Nucl. Instr. & Meth. A252 (1986b) 392.

'TPC 90, a test model for the ALEPH Time Projection Chamber'.

Anderhub,M., Devereux,M.J., and Seiler,P.G.

Nucl. Instr. & Meth. 166 (1979) 581.

'On a new method for testing and calibrating ionizing particle
detectors'

Anderhub,M., Devereux,M.J. and Seiler,P.G.

Nucl. Instr. & Meth. 176 (1980) 323.

'On a new method for testing and calibrating wire chambers'.

Anderson,D.F.

IEEE Trans. Nucl. Sci., NS-28 (1981) 842

Anderson,J. and Fenn,J.

Phys. Fluids. 8 (1965) 780.

Andreyev,S.V., Antonov,V.S., Knyazev,I.N. and Letokhov,V.S.

Chem. Phys. Lett. 45 (1977) 166.

Antonov,V.S., Letokhov,V.S. and Shibanov,A.N.

Usp. Fiz. Nauk. 142 (1984) 177.

Antonov,V.S., Knyazev,I.N., Letokhov,V.S. and Movshev,V.G.

Sov. Phys. JETP 46 (1977) 6971.

Antonov, V.S., Knyazev, I.N., Letokhov, V.S., Matiuk, V.M., Movshev, V.G. and Potapov, V.K.

Opt. Lett. 3 (1978) 37.

Antonov, V.S. and Shibanov, A.N.

Opt. Spectrosc. 52 (1982) 234.

Arnous, E., Klarsfeld, S. and Wane, S.

Phys. Rev. A 7 (1973) 1559.

Atkins, P.W.

Clarendon Press, Oxford (1978). 'Molecular Quantum Mechanics', Part III.

'An introduction to Quantum Mechanics'.

'Atlas of Spectral Data and Physical Constants for Organic Molecules'.

Editors Grasselli and Ritchey, 2nd Edition, CRC Press (1975).

Baggott, J.E.

Royal Society of Chemistry, Photochemistry. 17 (1985)

'Gas phase photoprocesses'.

Bamberger, A., Isele, R., Schlüpmann, J. and Stegle, M.

Nucl. Instr. & Meth. A252 (1986) 517.

'Aromatic Seeding Agents for Laser Ionisation in Counting Gases'.

Bakos, J.S., Kanter, J. and Kiss, A.

Sov. Phys. JETP Lett. 12 (1970) 255.

Bebb, H.B. and Gold, A.

Phys. Rev. 143 (1966) 1.

Becker,U., Capell,M., Chen,M., White,M., Yee,C.H. and Yee,K.

Nucl. Instr. & Meth. 214 (1983) 525.

'Special gas mixtures with very small drift angles at low drift velocities'.

Benetta,M. Froberger,J.P., Lehraus,I., May,J., Price,M., Schlatter,D.

Tejessi,W., Matherson,R., Witzeling,W., Vayaki,A., Weimin Wu.,

Kleinknecht,K., Pollmann,D., Richstein,J., Wells,J., Sedgbeer,J.,

Blum,W., Milotti,E., Peisert,A., Richter,R., Settles,R., Stierlin,U.,

Amendolia,S.R., Fidercaro,F., Marrocchesi,P.S., Liello,F., Ragusa,F.,

Rolandi,L., Caldwell,A., Cherney,M., Izen,J., Jared,R.C., Mermikides,M.,

Meyer,T.C., Takashima,M., Wicklund,E. and Wu,S.L.

IEEE Trans. on Nuclear Science Vol NS-32 No.1 (1985). (ALEPH-PUB 85-13).

'Measurement of magnetic and electric field inhomogenities in a time projection chamber using laser tracks'.

Berg,J.O., Parker,D.H. and El-Sayed,M.A.

Chem. Phys. Lett. 56 (1978) 411.

Bethke,G.W.

J. Chem. Phys. 31 (1959) 669.

Biagi,S. and Booth,P.

Wire Chamber Conference (1986)

Bishop,D.M.

Clarendon Press, Oxford (1973).

'Group Theory in Chemistry'

Bjorkholm, J.E. and Liao, P.F.

Phys. Rev. Lett. 33 (1974) 128.

Blum, W.

ALEPH-PUB 84/2 (Invited talk at the 2nd PISA meeting on advanced detectors, Castiglione, Italy, June 1983).

'The time projection chamber for the ALEPH-Experiment'.

Blum, W.

ALEPH TPCCAL 84/54 13th July 1984.

Blum, W.

CERN 11th July 1984.

'Notes on doping'.

Blum, W.

ALEPH-TPCDET 85-52 25/9/85 (1985).

'ALEPH TPC: Admixture of Naphthalene'.

Blum, W., Steigler, U., Gondolo, P. and Rolandi, L.

Nucl. Instr. & Meth. A252 (1986) 407

'Measurement of avalanche broadening caused by the wire ExB effects'.

Boerner, H.

Private communication (1985).

Boesl, U., Neusser, H.J. and Schlag, E.W.

Chem. Phys. 55 (1981) 193.

Boesl, U., Nuesser, H.J. and Schlag, E.W.

J. Chem. Phys. 72 (1980) 4327.

Boesl, U., Neusser, H.J. and Schlag, E.W.

Chem. Phys. 55 (1981) 193.

Boesl, U., Neusser, H.J., Weinkauff, R. and Schlag, E.W.

J. Phys. Chem. 86 (1982) 4857.

Bourotte, J. and Sadoulet, B.

Nucl. Instr. & Meth. 173 (1980) 463-470.

'Ionization of multiwire proportional chamber gas by double photon absorption'.

Brody, S.S.

Rev. Sci. Instrum. 28 (1957) 1021.

Brophy, J.H. and Rettner, C.T.

Chem. Phys. Lett. 67 (1979) 351.

Brozzi, D., Chesi, E., Cochet, C., Desalvo, R., Dumps, L., Lecoœur, G., Markiewicz, T., Maurin, G., Queru, P., Raynaud, J., Rubbia, C., Sadoulet, B., Sumarok, K., and Timmer, J.

p \bar{p} UA-1 Collaboration. Pub #TN 82/14 April 1, 1982.

'Central detector calibration with U.V. lasers'.

Bunkin, F.V. and Prokurov, A.M.

Sov. Phys. JETP 19 (1964) 739.

Bushaw, B.A. and Whitaker, T.S.

J. Chem. Phys. 74 (1981) 6519.

Cahill, J.W., Houston, C.M., Ledingham, K.W.D., Raine, R., Smith, K.M.
Smyth, M.H.C., Stewart, D.T., and Towrie, M.
CERN-EP/85-198 (Dec) 1985
'Detection of phenol in proportional counter gas by two-photon
ionisation spectroscopy'.

Carusotto, S., Giulietta, A. and Vasetta, M.
Lett. Nuovo. Cimento. 4 (1970) 1243.

Chang, C.S. and Stehle, P.
Phys. Rev. Lett. 30 (1973) 1283.

Charpak, G., Bouclier, R., Bressani, T., Favier, J. and Zupancic, C.
Nucl. Instr. & Meth. 62 (1968) 235.

Charpak, G. and Sauli, F.
Nucl. Instr. & Meth. 225 (1984) 627.
'Use of TMAE in a multistep proportional chamber for Čerenkov ray
imaging and other applications.

Chin, S.L.
Phys. Rev. A 4 (1971) 992.

Chin, S.L., Isenor, N.R. and Young, M.
Phys. Rev. 188 (1969) 7

Chin, S.L. and Lambropoulos, P.
Academic Press Inc., London (1984).
'Multi-photon ionization of atoms'.

Cochet,C., Desalvo,R., Markiewicz,T., Sadoulet,B., Sumorok,K., and
Timmer,J.

p̄ UA-1 Collaboration. Pub #TN 82/17 October 8, 1982.

'Measurement of the ionisation density induced in an Argon/Ethane gas
mixture by a N₂ laser'.

Collins,C.B., Johnson,B.W., Popescu,D. Musa,G., Pascu,M.L. and
Popescu,I.

Phys. Rev. A 8 (1973) 2197.

Compton,R.N., Klots,C.E., Stockdale,J.A.D. and Cooper,C.D.

American Institute of Physics Conference Proceedings (1984a).

'Multiphoton Ionisation of Caesium in Laser Techniques in the extreme
Ultraviolet'.

Compton,R.N., Stockdale,J.A.D. and Cooper,C.D.

Phys. Rev. A 30 (1984b) 1766.

Condon,E.U.

Phys. Rev. 32 (1928) 858.

Dalby,F.W., Petty-Sil,G., Pryce,M.H.L. and Tai,C.

Can. J. Phys. 55 (1977) 1033.

Delone,G.A., Delone,N.B. and Piskova,G.K.

Sov. Phys. JETP 35 (1972) 672.

Desalvo,M. and Desalvo,R.

Nucl. Instr. & Meth. 201 (1982) 357.

'Measurement of Laser Induced Ionisation in Argon-Ethane Gas Mixture'.

Desalvo,R.

CERN SPS/83-6 (ELE) 1983.

'Laser calibration of drift chambers'.

Donahue,D.L., Smith,D.H., Young,J.P., McKown,H.S. and Pritchard,C.A.

Anal. Chem. 56 (1984) 379.

Drysdale,S.L.T., Houston,C.M., Ledingham,K.W.D., Raine,C., Smith,K.M.,
Smyth,M.H.C., Stewart,D.T., Towrie,M. and Houston,C.M.

Nucl. Instr. & Meth. A252 (1986a) 521.

'Detection of toluene in proportional counter gas by resonant two photon
ionisation spectroscopy'.

Drysdale,S.L.T., Land,A.P., Ledingham,K.W.D., Raine,C., Smith,K.M.,
Smyth,M.H.C., Stewart,D.T., Towrie, M. and Houston,C.M.

ALEPH 86-30 (distr. TPC-CAL) (1986b).

'Investigation of the Effect of Gas Purification on the Background
Ionisation in Proportional Chambers'.

Drysdale,S.L.T., Ledingham,K.W.D., Raine,C., Smith,K.M., Smyth,M.H.C.,
Stewart,D.T., Towrie,M. and Houston,C.M.

(To be published)

'Investigation of the Effect of Toluene on the Gas Purification system
Proposed for the ALEPH TPC'.

Duncanson,J., Lingard,A., Strand,M. and Berry,R.S.

ICPEAC, 9th Seattle, Washington, Vol.1 of Abstracts, p.571. (1975).

Evans,R.G. and Thonemann,P.C.

Phys. Lett. A39 (1972) 133.

Fisanick, G.J., Eichelberger IV, T.S., Heath, B.A. and Robin, M.B.

J. Chem. Phys. 72 (1980) 5571.

Fox, R.A., Kogan, R.M. and Robinson, E.J.

Phys. Rev. Lett. 26 (1971) 1416.

Franck, J.

Trans. Faraday. Soc. 21 (1926) 536.

Franken, P.A., Hill, A.E., Peters, C.W. and Weinreich, G.

Phys. Rev. Lett. 7 (1961) 118.

Franklin, J.L., Dillard, J.G., Rosenstock, H.M., Herron, J.T., Draxl, K. and Field, F.H.

N.S.R.D.S. N.B.S. 26 (June 1969).

Frueholz, R., Wessel, J. and Wheatley, E.

Anal. Chem. 52 (1980) 281.

Geltman, S. and Leuchs, G.

Phys. Rev. A 31(3) (1985) 1463.

Glasgow group.

ALEPH-TPC CAL 84-34 (1984).

'Excimer laser studies in the TPC 90'.

Glownia, J.H., Romero, R. and Sander, R.K.

Chem. Phys. Lett. 88 (1980) 292.

Gobeli, D.A., Yang, J.J. and El-Sayed, M.A.

Chem. Rev. 85 (1985) 529.

Goldberger, M.L. and Watson, K.M.

Wiley, New York (1964).

'Collision Theory'.

Gontier, Y. and Trahin, M.

Phys. Rev. A 7 (1973) 2069.

Gontier, Y., Rahman, N.K. and Trahin, M.

Phys. Rev. Lett. 34 (1975a) 779.

Gontier, Y., Rahman, N.K. and Trahin, M.

J. Phys. B 8 (1975b) L179.

Gontier, Y., Rahman, N.K. and Trahin, M.

Phys. Lett. A 54 (1975c) 341.

Gopert-Mayer, M.

Ann. Phys. (Leipzig) 9 (1931) 273.

Granneman, E.H.A., Kleuar, M., Nygaard, K.J. and Van der Wiel, M.J.

J. Phys. B9 (1976) 865.

Granneman, E.H.A. and Van der Weil, M.J.

J. Phys. B 8 (1975) 1617.

Guo, J.C., Hartjes, F.G. and Konijn, J.

Nucl. Instr. & Meth. 204 (1982) 77.

'The use of N₂ laser induced clusters for drift chamber tests'.

Gushchin, E.M., Lebedev, A.N. and Somov, S.V.

Preprint, Inst. of Physical Engineering, Moscow (1983), unpublished.

'Two-photon ionisation of composite molecules as a method of imitation of particle tracks by means of N_2 laser radiation'.

Haissinski et al.

DELPHI; LAL/84-38, (1984).

Handbook of Chemistry and Physics.

53rd Edition, (1972/1973), CRC Press, (A division of the Chemical Rubber Company).

Handbook of Chemistry and Physics.

67th Edition, (1986), CRC Press, (A division of the Chemical Rubber Company).

Heath, B.A., Robin, M.B., Kuebler, N.A., Fisanick, G.J. and Eichelberger, T.S.

J. Chem. Phys. 72 (1980) 5565.

Heitler, W.

Oxford Univ. Press, London and New York (1954).

'The Quantum Theory of Radiation'.

Held, B., Mainfray, G. and Morellec, J.

Phys. Lett. A39 (1972a) 57.

Held, B., Mainfray, G., Manus, C. and Morellec, J.

Phys. Lett. A 35 (1971) 257.

Held, B., Mainfray, G., Manus, C. and Morellec, J.

Phys. Rev. Lett. 28 (1972b) 130.

Held, B., Mainfray, G., Manus, C., Morellec, J. and Sanchez, F.

Phys. Rev. Lett. 30 (1973) 423.

Heldman, D.L., Lengel, R.K. and Zare, R.N.

Chem. Phys. Lett. 52 (1977) 413.

Hepburn, J.W., Trevor, D., Pollard, J., Shirley, D. and Lee, Y.T.

J. Chem. Phys. 76 (1982) 4287.

Herrman, A., Leutwyler, S., Schumacher, I. and Woste, L.

Chem. Phys. Lett. 52 (1977) 418.

Hertzfeld, K.F.

Chem. Rev. 41 (1947) 233.

Hilke, H.J.

Nucl. Instr. & Meth. 174 (1980) 145.

'On Formation and Application of Laser Induced Ionization Tracks in Gases'.

Hilke, H.J.

Nucl. Instr. & Meth. A252 (1986) 169.

'Detector Calibration with Lasers- A Review'.

Hopkins, J.B., Powers, D.E. and Smalley, R.E.

J. Phys. Chem. 85 (1981) 3731.

Hubricht,G.K., Kleinknecht,E., Muller,E., Pollmann,D. and Teupe,E.

Nucl. Instr. & Meth. 228 (1985) 327.

'Ionization of counting gases and ionizable gaseous additives in proportional chambers by UV lasers'.

Hubricht,G.K., Klienkecht,E., Muller,E., Pollmann,D., Schmitz,K. and Sturzl,C.

ALEPH-NOTE 154 26/11/85. (b1985)

'Investigations of UV laser ionisation in Naphthalene and Phenol vapours added to proportional chamber gases'.

Hundley,L., Coburn,T., Garwin,E. and Stryer,L.

Rev. Sci. Instrum. 38 (1967) 488.

Hurst,G.S., Nayfeh,M.H. and Young,J.P.

Phys. Rev. A 15 (1977) 2283.

Hurst,G.S., Payne,M.G., Kramer,S.D. and Young,J.P.

Rev. of Modern Physics 51 (1979) 767.

Jacobs,V.L.

J. Phys. B 6 (1973) 1461.

Johnson,P.M.

J. Chem. Phys. 64 (1976) 4638.

Johnson,P.M., Berman,M.R. and Zakheim,D.

J. Chem. Phys. 62 (1975) 2500.

Jungen,C. and Dill,D.

J. Chem. Phys. 73 (1980) 3338.

Kantrowitz, A. and Grey, J.

Rev. Sci. Instrm. 22 (1951) 328.

Kimock, F.M., Baxter, J.P., and Winograd, N.

Surface Science, 124 (1983) L41.

Klarsfeld, S. and Maquet, A.

Phys. Rev. Lett. 29 (1972) 79.

Klarsfeld, S. and Maquet, A.

J. Phys. B 7 (1974) L228.

Kliger, D.S.

Quantum Electronics Principles & Applications, Academic Press (1983)

'Ultra Sensitive Laser Spectroscopy'.

Kobetich, E.J. and Katz, R.

Phys. Rev. 170 (1968) 391.

Kogan, R.M., Fox, R.A., Burnham, G.T. and Robinson, E.J.

Bull. Am. Phys. Soc. 16 (1971) 1411.

Konijn, J. and Hartjes, F.

Nucl. Instr. & Meth. 217 (1983) 311.

'Laser Track Alignment Calibration of Drift Chamber Systems Over Four Metres'.

Krasinski, J., Chudzynski, S., Majewski, W. and Glodz, M.

Opt. Commun. 12 (1974) 304.

Krichevski, J.R., Khazanova, N.E., Svetlova, G.M., and Panina, R.S.

Russ. J. Phys. Chem. 34 (1960) 1027.

Lambropoulos, M. and Berry, R.S.

Phys. Rev. A 8 (1973) 855.

Lambropoulos, M., Moody, S.E., Smith, S.J. and Lineberger, W.

Bull. Am. Phys. Soc. 18 (1973) 1514.

Lambropoulos, P.

Adv. At. Mol. Phys. 12 (1976) 87.

Lambropoulos, P.

Phys. Rev. A 9 (1974) 1992.

Lambropoulos, P.

Phys. Rev. Lett. 28 (1972a) 585.

Lambropoulos, P.

Phys. Rev. Lett. 29 (1972b) 453.

Lambropoulos, P. and Teague, M.R.

J. Phys. B 9 (1976) 587.

Lambropoulos, P. and Zoller, P.

Academic Press, Canada, (1984).

'Multiphoton Ionisation of Atoms'.

'Nonlinear Laser Chemistry'.

Leuchs, G. and Walther, H.

Academic Press (Edited by Chin, S.L. and Lambropoulos, P.) (1984)

'Multiphoton Ionization of Atoms'.

Lin, S.H. and Fujimura, Y.

Excited States. 4 (1979) 237.

Lin, S.H., Fujimura, Y., Neusser, H.J. and Schlag, E.W.

Quantum Electronics Principles & Applications, Academic Press (1984)

'Multi Photon Spectroscopy of Molecules'.

Long, S., Meek, J., Harrington, P. and Reilly, J.

J. Chem. Phys. 78 (1983) 3341.

Louisell, W.H.

Wiley (Interscience), New York (1973).

'Quantum Statistical Properties of Radiation'.

Lubman, D.M., Naaman, R. and Zare, R.N.

J. Chem. Phys. 72 (1980) 3034.

Maeda, M.

Academic Press, New York (1984).

'Laser Dyes: Properties of organic compounds for dye lasers'.

Mainfray, G. and Manus, C.

Academic Press (Edited by Chin, S.L. and Lambropoulos, P.) (1984)

'Multiphoton Ionization of Atoms'.

Maker, P.D., Terhune, R.W. and Savage, C.M.

Columbia Univ. Press, New York (1964) p1559

'Quantum Electronics'

Markiewicz, T., Sadoulet, B., Sumarok, K. and Timmer, J.

UA1/TN83-05 (1983)

'Tests of laser on Central Detector'.

Mathur, B.P., Rothe, B.W., Reck, G.P. and Lightman, A.J.

Chem. Phys. Lett. 56 (1978) 336.

Matsen, F.A., Ginsburg, N., Robertson, W.W.

J. Chem. Phys. 13 (1945) 309

May, J., Richstein, J. and Rolandi, L.

ALEPH-TPC Note 84-37 (1984).

'Systematic displacements of the measured coordinates of a laser beam in
TPC 90'.

Meek, J., Jones, R. and Reilly, J.

J. Chem. Phys. 73 (1980) 3503.

Melton, C.E., Hurst, G.S. and Bortner, T.E.

Phys. Rev. 96 (1954) 643.

Messiah, A.

Wiley, New York Vol.2 (1965).

'Quantum Mechanics'.

Mizuno, J.

J. Phys. B 6 (1973) 314.

Moore, C.E.

NBS Publication 467, U.S. Gov. Printing Office, Washington (1952).

'Atomic Energy Levels'.

Moore, L.J., Fassett, J.D. and Travis, J.C.

Anal. Chem. 56 (1984) 2770.

Mower, L.

Phys. Rev. 142 (1966) 799.

Murakami, J., Ito, M. and Kaya, K.

Chem. Phys. Lett. 80 (1981) 203.

Murrell, J.N.

Mathuen and Co. London (1963).

'The Theory of the Electronic Spectra of Organic Molecules'.

Nakato, Y.

Chem. Phys. Lett. 9 (1971) 615.

Nayfeh, M.H., Hurst, G.S., Payne, M.G. and Young, J.P.

Phys. Rev. Lett. 41 (1978) 302.

Nakato, Y., Chiyoda, T. and Tsubomura, H.

Bull. Chem. Soc. Japan 47 (1974) 3001.

Neiman, G.C. and Colson, S.D.

J. Chem. Phys. 68 (1978) 5656.

Otis, C.E. and Johnson, P.M.

Chem. Phys. Lett. 83(1) (1981) 73.

Parker, D.H. and Avouris, P.

Chem. Phys. Lett. 53 (1978) 515.

Parker, D.H., Sheng, S.L. and El-Sayed, M.A.

J. Chem. Phys. 65 (1976) 5534.

Peisert, Anna.

N-TPC Note #85-16 (1985).

'Preliminary results of the two track resolution in TPC90'.

Petty, G., Tai, C. and Dalby, F.W.

Phys. Rev. Lett. 34 (1975) 1207

Pollmann, D.

(Private communication) (1986).

Poschenrieder, W.P. and Oetjen, G.H.

J. Vacuum Science and Technology. 9 (1971) 212.

Price, M.J.

ALEPH-TPC Note 84-16 Feb 1984.

'Electric field distortions in the TPC 90'.

Raine, C., Ledingham, K.W.D. and Smith, K.M.

Nucl. Instr. & Meth. 217 (1983) 305.

'Laser Induced Ionisation in Proportional Counters'.

Raine, C.

Glasgow Workshop (1984).

Reilly, J.P. and Kompa, K.L.

J. Chem. Phys. 73 (1980) 5468.

Reiss, H.R.

Phys. Rev. Lett. 29 (1972) 1129.

Richstein, J.

ALEPH 86-13. (1986).

'A measurement of $\omega T(E)$ with laser beams in different counter gases'.

Richstein, J. and Rolandi, L.

ALEPH-TPC Note 84-20 (1984).

'Behaviour of Pad Responce Function (PRF) with magnetic field and drift length'.

Richter, R.

ALEPH TPC 84-80 12th November 1984.

'A flash ADC system for TPC readout'.

Robin, M.B. and Kuebler, N.A.

J. Chem. Phys. 69 (1978) 806.

Rockwood, S., Reilly, J.P., Hohla, K. and Kompa, K.L.

Opt. Commun. 28 (1979) 175.

Rolandi, L.

ALEPH-TPC Note 84-21 (1984).

'Statistics in laser ionisation'.

Rosenstock, H.M., Draxl, K., Steiner, B.W. and Herron, J.T.

J. Phys. Chem., Ref. DATA 6 (1977), Suppl. No.1.

Rothberg, L.J., Gerrity, D.P. and Vaida, V.

J. Chem. Phys. 75 (1981) 4403.

Teich, M.R. and Lambropoulos, P.

J. Phys. B 9 (1976) 1251.

Turner, R.B., Vaida, V., Molini, C.A., Berg, J.O. and Parker, D.H.

Chem. Phys. 28 (1978) 47.

Sadoulet, B.

CERN-EP/80-138. CERN/UA1/p \bar{p} /Note 63 1 August 1980.

'Fundamental processes in drift chambers'.

Sadoulet, B.

p \bar{p} UA-1 Collaboration, Pub #TN 81/21 May 3 1981.

'Note on diffraction limitation on a calibration laser beam'

Sadoulet, B.

CERN/EP 82-41.

Sakurai, J.J.

Addison-Wesley, Reading, Massachusetts (1967).

'Advanced Quantum Mechanics'.

Sansonetti, C.J. and Lorenzen, C.J.

Phys. Rev. A 30 (1984) 1805.

Sargent, M., III, Scully, M.O. and Lamb, W.E., Jr.

Addison-Wesley, Reading, Massachusetts (1974).

'Laser-Physics'.

Sauli, F.

Lectures given in the Academic training program of CERN 1975-76, Geneva
1977.

'Principles of operation of multiwire proportional and drift chambers'.

Sauli, F.

Nucl. Instr. & Meth. A248 (1986) 143-149.

'Ultraviolet photon detection and localisation with multiwire chambers'.

Schiff, L.I.

McGraw-Hill, New York (1955).

'Quantum Mechanics'.

Schlag, E.W. and Neusser, H.J.

Acc. Chem. Res. 16 (1983) 355.

Schlüpmann, J.

Diplomarbeit, Freiburg (1986)

Singhal, R., Land, A.P., Ledingham, K.W.D. and Towrie, M.

(To be published) (1987).

Sklar, A.L. J. Chem. Phys. 7 (1939) 984.

Small, P.A., Small, K.W. and Cowley, P.

Trans. Faraday Soc. 40 (1948) 810

Smalley, R.E., Wharton, L. and Levy, D.H.

Acc. Chem. Res. 10 (1977) 139.

Sobelmann, I.I.

Springer series in Chemical Physics, Springer-Verlag, Berlin, Heidelberg, New York (1979).

'Atomic Spectra and Radiative Transitions'.

Sorokin, P.P., Lambard, J.R., Moruzzi, V.L. and Hammond, E.C.

J. Chem. Phys. 48 (1968) 4726.

Steinfeld, J.I. and Houston, P.

Plenum, New York (ed. Steinfeld), p.1, (1978).

'Laser and Coherence Spectroscopy'.

Sworrford, R.L. and McClain, W.M.

Chem. Phys. Lett. 34 (1975) 455.

Tagaki, H. and Nakamura, H.

J. Chem. Phys. 74 (1981) 5808.

Teague, M.R. and Lambropoulos, P.

Phys. Lett. 56A (1976a) 285.

Teague, M.R. and Lambropoulos, P.

J. Phys. B 9 (1976b) 1251.

Towrie, M., Drysdale, S.L.T., Houston, C.M., Ledingham, K.W.D., Raine, C.,
Smith, K.M., Smyth, M.H.C. and Stewart, D.T.

J. Phys. B: At. Mol. Phys. 19 (1986) 1989.

'Detection of phenol in proportional counter gas by resonant two photon
ionisation spectroscopy'.

Turner, R.E., Vaida, V., Molini, C., Berg, J.O. and Parker, D.H.

Chem. Phys. 28 (1978) 47

UV Atlas of Organic compounds.

ed. Photoelectric Spectrometry Group, London, and Institut für
Spectrochemie und Angewandte Spektroskopie, Dortmund. (London:
Butterworths; Weinheim: Verlag Chemie) (1966).

Vaida, V., Turner, R.E., Casey, J.L. and Colson, D.S.

Chem. phys. Lett. 54 (1978) 25.

Vapour pressures and critical points of liquids.

Vol.12 aromatic nitrogen compounds, Engineering Sciences Data Unit Item
Number 78011 (Institute of Chemical Engineers, London, (1981)).

Va'Vra, J.

SLAC-PUB-2984 October 1982.

'The use of a nitrogen laser for the observation of space charge effects
in drift chambers.

Voronov, C.S. and Delone, N.B.

Sov. Phys. JEPT Eng. Trans. 23 (1966) 54.

Wells, J.

ALEPH 83-64 (Distribution TPCCAL) 14th May 1986.

'ALEPH TPC Laser Calibration of drift chambers'.

Williams, M.W., Beekman, D.W., Swan, J.B. and Arakawa, E.T.

Anal. Chem. 56 (1984) 1348.

Zacharius, H., Rottke, H. and Welge, K.H.

Appl. Phys. 24 (1981) 23.

Zakheim, D.S. and Johnson, P.M.

Chem. Phys. 46 (1980) 263.

Zandee, L., Bernstein, R.B. and Lichtin, D.A.

J. Chem. Phys. 69 (1978) 3427.

Zandee, L. and Bernstein, R.B.

J. Chem. Phys. 70 (1979a) 2574.

Zandee, L. and Bernstein, R.B.

J. Chem. Phys. 71 (1979b) 1359.

